UNIVERSIDADE DE SÃO PAULO

ESCOLA POLITÉCNICA

PROGRAMA DE PÓS-GRADUAÇÃO EM ENGENHARIA CIVIL

MARTINA PACIFICI

Urban Morphology and Climate:
field assessment and numerical modeling of interactions

São Paulo

2019

MARTINA PACIFICI

Urban Morphology and Climate:
field assessment and numerical modeling of interactions

Tese apresentada à Escola Politécnica da Universidade de São Paulo para obtenção do título de Doutora em Ciências pelo Programa de Pós-graduação em Engenharia Civil

Área de Concentração: Engenharia de Construção Civil e Urbana

Versão corrigida contendo as alterações solicitadas pela comissão julgadora em 15 de maio de 2019. A versão original encontra-se na unidade que aloja o Programa de Pós-graduação.

Orientadora: Prof. Dra. Karin Regina de Castro Marins

São Paulo
2019

Este exemplar foi revisado e corrigido em relação à versão original, sob responsabilidade única do autor e com a anuência de seu orientador.

São Paulo, 8 de Julho de 2019

Assinatura do autor: *Martina Pacifici*

Assinatura do orientador: _____

Catalogação-na-publicação

Tese de autoria de Martina Pacifici, sob o título "**Urban Morphology and Climate: field assessment and numerical modeling of interactions**", apresentada à Escola Politécnica da Universidade de São Paulo, para obtenção do título de Doutora em Ciências pelo Programa de Pós-graduação em Engenharia Civil, na área de concentração Engenharia de Construção Civil e Urbana, aprovada em 15 de maio de 2019 pela comissão julgadora constituída pelos doutores:

_____

Profa. Dra. Karin Regina de Castro Marins

Universidade de São Paulo – Escola Politécnica

Presidente

_____

Profa. Dra. Eleonora Sad de Assis

Universidade Federal Minas Gerais (UFMG) – Escola de Arquitetura

_____

Profa. Dra. Denise Helena Silva Duarte

Universidade de São Paulo (USP) – Faculdade de Arquitetura

_____

Prof. Dr. João Roberto Gomes de Faria

Universidade Estadual Paulista (UNESP) – Faculdade de Arquitetura, Artes, Comunicação

_____

Prof. Dr. Fernando Akira Kurokawa

Universidade de São Paulo (USP) – Escola Politécnica

A Fabrizio
e i misteriosi disegni del Cielo
che hanno intrecciato il nostro Incontro.

Acknowledgements

"There is one path in the world that none can walk but you.
Where does it lead? Don't ask, walk!"
(Friedrich Nietzsche)

Abstract

PACIFICI, Martina. **Urban Morphology and Climate: field assessment and numerical modeling of interactions**. 2019. 225 p. Dissertation (PhD of Science) – Engineering School, University of São Paulo, São Paulo, 2019.

In last decades, the increase of megacities in many regions and particularly in developing countries, contributed to deplete rural landscape enhancing the urbanization impacts. Such urban settlements result in high greenhouse gas emissions and negative energy balances. By gathering millions of people, they develop a complex network of infrastructures, services, housings and factories. Climate impacts of metropolitan areas are universally recognized in the *urban heat island* (UHI) effect that entails the increase of average night temperatures relative to rural surroundings. New global challenges for urban agendas involve the restraint of urban sprawl, the enhancement of urban density and the mitigation of urban climate changes. Densification strategies had risen as key planning tools to be inserted in the urban development practice. Nevertheless, the integration of compact city pattern into the existing urban structure lead to dense arrangements of urban forms, changes transport models, raises human and energy exchanges, shaping new outdoor environments. In the framework of these transformations, the present work explored the interaction between morphological and climate urban variables in urban lands affected by on-going densification and verticalization processes. An integrated research procedure was developed and applied to a case study in the municipality of São Paulo, characterized by high-rise and low-rise zones under development subjected to a subtropical climate. The proposed procedure integrated field data collections, analysis of database and modeling techniques, addressing multiple scales of analysis. Climate and morphological features were gained by available city database, meteorological stations, *Local Climate Zone* (LCZ) maps, and further integrated by fieldworks. Numerical models were implemented as interpretation data tools to investigate the physical processes and to build the conceptual model of the interactions between urban morphology and climate. ENVI-met and Grasshopper computational codes were used to simulate the existing case study area, as well as to implement numerical experiments (scenarios) in which different densification patterns were tested and compared. The calibration process of the ENVI-met model relied on prior sensitivity tests of input parameters in a smaller domain. Main findings underlined the high-rise buildings shading as the main climate driving force at subtropical latitudes, inducing different microclimates in the outdoor spaces. Compact low-rise areas were found highly affected by high temperatures, low-albedo materials and absence of vegetation. High-rise buildings arrangements were discussed focusing on the effects of buildings heights and spacing variability. Finally, results were summarized in urban design precepts helping climate-sensitive practices and understanding of urban lands in which densification and verticalization processes are in action. Design percepts included suggestions on building height and arrangement, materials and green infrastructure. The importance of a local-scale planning was also highlighted.

Keywords: Urban Morphology. Urban Climate. Outdoor Spaces. Density. Numerical Modelling. ENVI-met. Grasshopper.

Resumo

Nas últimas décadas, o aumento das megacidades em muitas regiões do mundo e particularmente nos países em desenvolvimento, contribuiu para recuo do ambiente rural, aumentando os impactos da urbanização. Grandes assentamentos urbanos resultam em altas emissões de gases de efeito estufa e balanços energéticos negativos. Ao reunir milhões de pessoas, as cidades contemporâneas desenvolvem uma complexa rede de infraestruturas, serviços, moradias e centros produtivos. Os impactos climáticos relacionados são universalmente reconhecidos no efeito de ilha de calor urbana (ICU), que implica o aumento das temperaturas médias noturnas em relação ao entorno rural. Novos desafios globais para as agendas urbanas envolvem a contenção da expansão urbana, o aumento da densidade populacional e a mitigação das mudanças climáticas. Assim, estratégias de densificação surgiram como ferramentas-chave de planejamento a serem inseridas na prática urbana. No entanto, a integração do padrão de cidade compacta na estrutura urbana existente leva a arranjos densos de formas urbanas, requerendo modificações nos modelos de transporte, aumenta as trocas de pessoas e de energia, moldando novos ambientes externos. No âmbito dessas transformações, o presente trabalho explorou a interação entre variáveis urbanas morfológicas e climáticas em áreas urbanas afetadas por processos de densificação e verticalização presentes e futuros. Um procedimento integrado de pesquisa foi desenvolvido e aplicado a um estudo de caso no município de São Paulo, caracterizado por zonas de grande e baixa altura em desenvolvimento, sujeitas a um clima subtropical. O procedimento proposto integrou coletas de campo, análise de conjuntos de dados e técnicas de modelagem, abordando múltiplas escalas de análise. Aspectos climáticos e morfológicos foram obtidos por meio de *database* disponibilizados pela Prefeitura, estações meteorológicas, mapas de Zonas Climáticas Locais (LCZs) e posteriormente integrados por trabalhos de campo. Modelos numéricos foram implementados como ferramentas de interpretação de dados para investigar os processos físicos e construir o modelo conceitual das interações entre morfologia urbana e clima. Os códigos computacionais *ENVI-met* e *Grasshopper* foram usados para simular a área de estudo, bem como para implementar experimentos numéricos (cenários) nos quais diferentes padrões de densificação foram testados e comparados. O processo de calibração do modelo *ENVI-met* baseou-se em testes de sensibilidade prévios, realizados sobre parâmetros de *input* em um domínio menor. Os principais resultados ressaltaram o sombreamento causado por grandes objetos construídos como a principal forçante climática nas cidades de latitude subtropical, induzindo diferentes microclimas nos espaços externos ao redor. Tecidos urbanos baixos e compactos foram encontrados afetados por altas temperaturas, materiais de baixo albedo e ausência de vegetação. Arranjos de edifícios altos foram investigados focando nos efeitos das alturas dos edifícios e na variabilidade do espaçamento entre eles. Por fim, os resultados foram resumidos em preceitos de desenho urbano que suportassem uma abordagem de projeto mais sensível ao clima, assim como a compreensão das áreas da cidade onde os processos de densificação e verticalização encontram-se ativos. Os preceitos de desenho urbano incluíam sugestões sobre a altura e disposição dos edifícios, materiais e infraestrutura verde. A importância de um planejamento em escala local também foi destacada.

Palavras-chave: Morfologia Urbana. Clima Urbano. Espaços abertos. Densidade. Modelagem numerica. ENVI-met. Grasshopper.

Index of figures

Index of Tables

Index of abbreviations and acronyms

API	Application Programming Interface
BCA	Building Coverage Area
BES	Building Energy Simulations
CDF	Cumulative Distribution Function
CETESB	Sao Paulo State Environmental Sanitation Technology Company
CFD	Computational Fluid Dynamics
CGE	Emergency Management Center - São Paulo
COE	Municipal Buildings Code
COST	Cooperation in Science and Technical Development
DEM	Digital Elevation Model
DP_CET	Meteorological station Dom Pedro CETESB
EPW	Energy plus weather file
EETU	Structuring Axes of the Urban Transformation
FAR	Floor Area Ratio
FDM	Finite - Difference Method
GHG	Greenhouse gases
GIS	Geographical information systems
H/W	Height to width
IAG	Institute of Astronomy, Geophysics and Atmospheric Sciences
IMM	Integrated Modification Methodology
INPE	National Institute of Spatial Research
INMET	National Institute of Meteorology (Brazil)
IPTU	Urban Land and Territorial Tax
LAD	Leaf Area Density
LBD	Lateral Boundary Condition
LAI	Leaf Area Index
Lat	Latitude
Long	Longitude
LCZ	Local Climate Zone
LPUOS	Law of Land Parceling, Use and Occupation (Zoning)
MAF	Moving Average Filter
MS_INM	Meteorological station Mirante Santana INMET

MUHI	Micro-Urban Heat Islands
N, S, E, W	North, South, East, West
PDE	Plano Diretor Estratégico (Masterplan)
PDF	Probability Density Function
PET	Physiological Equivalent Temperature
Pe_CGE	Meteorological station Penha CGE
PITU	Integrated Urban Transport Plan
RANS	Reynolds-averaged Navier–Stokes
RSM	Rural Station Model
Se_CGE	Meteorological station Sé CGE
SVF	Sky View Factor
TOD	Transit-Oriented Development
UC-BEM	Urban Canopy and Building Energy Model
UBL	Urban Boundary Layer
UCL	Urban Canopy Layer
UHI	Urban Heat Island
USP	University of São Paulo
UTCI	Universal Thermal Comfort Index
UWG	Urban Weather Generator
VDM	Vertical Diffusion Model
VM_CGE	Meteorological station Vila Mariana CGE
VP_CGE	Meteorological station Vila Prudente CGE
WMO	World Meteorological organization
WUDAPT	World Urban Database and Access Portal Tool
ZEU	Structuration Zone of Urban Transformation
ZEUP	Forecasted Structuration Zone of Urban Transformation

Index of Symbols

CO_2	Carbon dioxide
CH_4	Methane
N_2O	Nitrous oxide
K_m, K_h, K_q	Turbulent exchange coefficients
f	Coriolis parameter
p'	Local pressure perturbation
θ	Potential temperature at level z *or* azimuth
θref	Reference potential Temperature
Su, Sv and *Sw*	Wind speed losses due to drag forces
ui	Three-dimensional advection term
xi	Three-dimensional diffusion term
MRT	Mean radiant Temperature
T_s	Surface Temperature
T_a, T	Air Temperature
RH	Relative Humidity
T_{gs}	Ground Surface Temperature
T_g	Globe Temperature
ε	Emissivity or Dissipation rate
$ε_g$	Globe emissivity
D	Diameter
w_s	Wind speed
w_d	Wind direction
v_a	Air velocity
γ	Solar access angle
α	Obstruction angle or albedo or level of significance
p-value	Probability value
ß	Sun Elevation angle
dx, dy, dz	Grid point spacing in each Cartesian direction
$η_s$	Water content at saturation
$η_{fc}$	Water content at field capacity
H_{wilt}	Water content at wilting point
MatPot	Matrix potential

$K_{\mu s}$	Hydraulic conductivity
CP	Volumetric heat capacity
b	Clapp and Hornberger constant
HCN	Heat conductivity
A	Absorption
T	Trasmission
R	Reflection or Receptor
C	Specific Heat
HCN	Thermal conductivity
q	Specific humidity
Q	Internal sources/sinks
K	Kelvin
D_{bor}	Distance between building and lot border
D_{bld}	Distance between buildings within the lot
x,y,z	Cartesian axes
S	Scale
r_s	Spearman correlation coefficient
RADG	Global Solar Radiation
z_0	Roughness length
w_{dir}	Wind direction
NG	Nested Grids
T_h	Dissipation of turbulent energy
c1, c2, c3	Constant values used to calibrate the ε-equation
ρ	Density
t_{ck}	Thickness
E	Kinetic energy
E_r	Energy radiated
σ	Stefan–Boltzmann constant
LW	Long-waves radiant flux

Glossary

Absorptivity: is an optical property of a material, describing the ratio between the wall absorbed radiation to the wall incident radiation. It falls between 0 and 1.

Accuracy (instrument): represents the capability of the instrument to faithfully indicate the value of the measured signal

Building coverage area (BCA): $\frac{\text{Total First Floor Area (B+D)}}{\text{Site Area (A)}} \times 100$
It can also be called "site coverage". In Portuguese: *taxa de ocupação*.

Floor Area Ratio (FAR): $\frac{\text{Total Floor Area (B+C+D+F)}}{\text{Site Area (A)}}$
In Portuguese: *coeficiente de aproveitamento*.

Example of BCA and FAR concepts
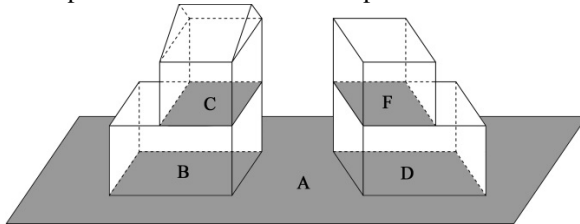
Source: Martina Pacifici, 2019

Calibration (modeling): comparison between field and modeled values.

CDF: acronym indicating *Cumulative Density Functions*. The cumulative density function $F(x)$ means the probability that the variable will have a value less than or equal to x (TRAUTH, 2015).

H/W: height to width ratio, defining the geometrical relationship between the main buildings' height and the street width of an Urban Canyon.

Kurtosis: measures whether the data are peaked or flat relative to a normal distribution. A high kurtosis describes a distribution with a distinct peak near the mean. A distribution characterized by a low kurtosis displays a flat top close the mean and broad tails (TRAUTH, 2015).

Multiplicity: the multiplicity of a design element means the number of times it repeats. The multiplicity concept presupposes the existence of distinct levels of scale. The multiplicity rule depends upon repeating elements of the same size.

Podium: is a concrete platform raised from street level, above which towers are implanted. Its height can vary from some centimeters to few meters. It can accommodate green areas and trees. Often it stands above underground garages.

Precision (instrument): represents the stability of the instrument to result in the same measurement over and over again for the same input signal.

PDF: acronym indicating *Probability Density Function.* The probability density function $f(x)$ means the probability that the variable has a value equal to x (TRAUTH, 2015).

Skewness: is a measure of the asymmetry of the tails of a distribution. Distributions with positive skewness have large tails extending towards the right-side. A negative skewness describes distributions which tail spreads out more to the left of the mean value (TRAUTH, 2015).

Urban morphology: can be referred to the study field that investigates the urban forms making up the urban environment. In addition, the term can indicate the own urban forms and their physical attributes.

Thermal admittance (W/m²K): indicates the material ability to absorb and release heat. It is calculated as the heat transfer (W/m²) through the material divided by the temperature difference (K) between the surface of the material and the air.

Thermal inertia: is the resistance/slowness of a body/system in its current state to temperature change, given by the delay in temperature variations during a full heating/cooling cycle.

ZEU: Structuration Zone of Urban Transformation, defined by the Law of Land Parceling, Use and Occupation (LPUOS) (SÃO PAULO MUNICIPALITY, 2016). ZEU includes urban territories under transformation in which built and people densification is encouraged and oriented to the public transport. In Portuguese: *Zona Eixo de Estruturação da Transformação Urbana*.

ZEUP: Forecasted Structuration Zone of Urban Transformation, defined by the Law of Land Parceling, Use and Occupation (LPUOS) (SÃO PAULO MUNICIPALITY, 2016). ZEUP are ZEU that will be densified in the future, since the collective transport system still had not been implanted. In Portuguese: *Zona Eixo de Estruturação da Transformação Urbana Previsto*.

Index

1   Introduction

Cities are hybrid spaces, in which the natural landscape blends with the built form produced by man. The interaction of environmental processes and human activities introduces complexity in urban settlements, leading to the landscape transformation and the emergence of a new form of "anthropic diversity". Natural and human interconnected landscapes are dynamic: their shapes live, change and die, as a result of inner natural phenomena and human vision (LYLE, 1991). The way in which built spaces are organized and fit into the original geographical context is of great importance. Among the mosaic of urban forms, the geographical context embeds a great amount of elements, including soils and topography, flora and fauna, green spaces and water resources, as well as the climate of the city. Cities' inhabitants both shape and are shaped by this complex arrangement of interactions. According to Soleymanpour, Parsaee and Banaei (2015), people's comfort and satisfaction strongly depend on the accommodation of urban forms within the local climate.

Due to their hybrid nature, urban environments are characterized by an own climate that stands out from countryside. In a city environment, the alteration of natural climate variables was mainly due to five factors (LOWRY, 1967): (1) predominance of highly conductive materials, (2) variety of urban structure in interaction with solar energy, (3) abundance of heat sources, (4) a reduced opportunity for evaporation, (5) presence of particulates in the air. Evidences of warmer urban areas and cooler countryside had been observed since 1818 by Luke Howard in the city of London.

Despite contemporary trends, the balance between natural and human-made elements has changed profoundly throughout history. Traditional cities, falling in the first urbanization period (1750 – 1950) and mainly diffused in the Global North (UN ENVIRONMENT, 2018), were organized in small and medium settlements, sometime enclosed by defensive walls and entirely accessible on foot. Motor vehicles were limited and open spaces were much lived. Inhabitants developed appropriate construction techniques to take advantage of local topography and climate conditions. Exemplary solutions of bioclimatic architecture are scattered to the North and South of the world. Historical cities, ranging from Siena to *San Gimignano*, from *Suzhou* and *Beijing* to *Tunis* and *Jerusalem*, were considered reference due to the successful relation connecting people, climate and their urban environment (SALAT; BOURDIC, 2011). Today, cities expanded, attracting a large amount of population. Alexander (1977) said: "The big city is a magnet. It is terribly hard for small towns to stay alive and healthy in the face of central urban growth". The large size of these cities, the

multiplication of heat sources and motor vehicles damaged the bond to the natural environment, modifying urban climates.

The industrial revolution (XVIII century) is a significant step that brands the transition from small urban centers to great modern cities (HARVEY, 2005). Since then, new patterns of urban growth have emerged; they diverge from the historical urban fabric and modify the spatial proportionality between built forms. New borderless cities sprawled, enhancing real estate investments and gathering people (BERTOLINI, 2000; HARVEY, 2011). The traditional pattern (in retrospect recognizable as resilient and focused on microclimate benefits) was replaced by the modern architecture plans, disconnected from the original environmental context (BARAU et al., 2014). The increasing of sizes implied greater infrastructures, longer connections and new spatial structures, resulting in urban mega-objects and fragmented land uses (HARVEY, 2005; SUAU; BUGARIČ; FIKFAK, 2015). Contemporary cities became complex objects: dynamic, disputed and decentralized. Services, housings and employments are readily accessible only for a part of population.

Therefore, in many cities, people live far from their places of interest and main connections. Consequently, the integration of land use policy and transport lines is one of most relevant topics on the agenda of municipalities. These goals were usually condensed in an urban strategy know as Transit-Oriented Development (TOD), which spread from North America across many cities abroad (CURTIS; RENNE; BERTOLINI, 2009, p.3). Such strategy intends discouraging the use of car "to promote public transit and human-powered transportation modes through high density, mixed use, environmentally-friendly developments within areas of walking distance from transit centers" (SUNG; OH, 2011, p.75).

Many American and European cities have incorporated TOD concepts in their planning by inducing high-density developments along the transportation lines (UN-HABITAT CORE TEAM, 2016). In their master plans, the morphological transformation of certain urban fabrics of city is proposed by means of specific land use policies (SUZUKI; CERVERO; IUCHI, 2013) that encourage the maximum exploitation of the land value, favoring a high plot ratio with low site coverage (ZHU, 2012). These intense urban interventions raise doubts on climatic consequences of TOD strategies in the target areas. On one hand, TOD areas optimize traffic and reduce private transport dependence. On the other hand, they modify interactions of urban morphology and climate environment by replacing low density areas with high-rise and verticalized plots. Given the recent implementation of this strategy, climate impact assessments are still rare in TOD areas. Its realization is an

ongoing process and, sometimes, the proposed land use change has only been foreseen. In addition, beyond the TOD common principles, each city chooses its own parameters and tools to make compactness feasible along transport corridors. Thus, specific studies are required in the different realities.

Despite the impact of city development on urban climate was addressed in many field studies, limited attention has been given towards TOD areas. Hsieh and Wu (2012) examined the pedestrian wind environment around high-rise and close buildings in the surroundings of a rail station in Taiwan, showing as land-control measures can improve ventilation. According to Yuan and Ng (2012), street-level ventilation can be enhanced by increasing pedestrian-level building porosity. This is obtained by decreasing the site coverage, favoring wind permeability in the podium layer, opening air passages at the ground level, planning building setback and spacing blocks. Conversely, uniform and tall building heights at limited distance, combined with large podium structures, decrease wind permeability affecting people comfort at pedestrian level (NG, 2009). The dispersion of atmospheric pollutants is also affected by compact urban morphologies. High densities favor pollution concentration, along with "uniformity" of canyon geometries. Conversely, non-uniformly roof heights provide better ventilation (ERELL; PEARLMUTTER; WILLIAMSON, 2011). Air motion and pollutant dispersion in the canyon are influenced by variations in solar heating that leads to strong buoyancy effects close to urban surfaces (XIE et al., 2005). Moreover, the increase of physical obstructions retains longwave radiative heat loss while the anthropogenic activities favor heat excess release in the air, both contributing to UHI effect (UNGER, 2004). Simultaneously, by increasing the plot ratio, the daylight availability on building facades and the openness of sky view at the ground level would decrease (CHENG et al., 2006). Complementary, the increase of the built mass would entail a greater amount of surfaces, roofing and other urban furniture exposed to the sun, mainly covered with man-made materials different from natural surfaces. For Erell et al. (2011), the absorptivity ($0 \leq \alpha \leq 1$) and thermal admittance (W/m^2K) of these surface materials have a significant impact on the thermal and hydrological balance of a city. At the pedestrian scale, the materials switch radiant exchanges with people, affecting their thermal comfort.

Driven by buildings and open spaces distribution, the balance of daylight and shadows was showed as a main stress of local and micro-climate variations (MORAKINYO et al., 2017; LOBACCARO, 2013; SHASHUA-BAR; PEARLMUTTER; ERELL, 2009; ARNFIELD, 1990). Compact building structures could cause solar obstruction towards the surrounding lower-rise fabrics, favoring the reduction of surface and air temperature around.

Consequences of such phenomena were desirable or undesirable according to the daily hour, the season, the latitude. In this regard, Knowles and Berry (1980) were concerned with the Los Angeles new developments which cast long shadows over the northern single family houses by means of high-rise buildings. These actions restricted the right to solar access, impacting the neighborhood quality of life, as well as compromising their potential of energy conversion (KNOWLES; BERRY, 1980). For tropical climates, Emmanuel, Rosenlund and Johansson (2007) claimed the importance of shading by developing "shadow umbrella" areas to promote cooler open spaces. However, this approach compromised the solar potential for energy conversion (BRANDÃO, 2004). Duarte, Brandão and Prata (2004) developed a building code proposal in the context of the metropolitan area of São Paulo, Brazil, to implement a setback regulation as a function of solar orientation, guaranteeing a minimum solar access for buildings.

In a nutshell, the insertion of highly densified and verticalized areas in the city is a controversial operation. Much attention has to be addressed integrating new buildings in existing neighborhoods, to avoid undesired impacts to the urban climate. In general, climate sensitive urban practices can be introduced into TOD strategies to enhance more livable and comfortable climatic environment. However, municipalities usually disregard environmental studies or modeling techniques to plan TOD areas.

The city of São Paulo is one of the most polluted mega cities in the world (WORLD HEALT ORGANIZATION, 2016), with a large part of pollutants caused by motor vehicles (JACOBI; MACEDO, 2001). This reason, along with many people living at the city edges, resulted in a reviewed Masterplan (PDE) (SÃO PAULO MUNICIPALITY, 2014) that incorporated TOD concepts, optimizing transport lines, urban density and land use. In 2016, these guidelines became effective by means of Law of land parceling, use and occupation (LPUOS) (SÃO PAULO MUNICIPALITY, 2016). LPUOS demarcated the urban zones in which TOD concepts had to be applied. In such zones, law regulations are defined at the plot-scale, without considering several lots interferences and blocks performance. Specific norms are required in terms of floor area ratio (FAR) and building coverage area (BCA) (also called site coverage), while setback regulations are similar to other parts of the cities. No limits to buildings heights are imposed, except for environmental preserved areas and a minority of other territories. Attractive facades e walls permeability at the ground floor are encouraged, while no environmental considerations dealing with climate were integrated into the master plan. Because of the weakness of the legislative structure, great freedom is allowed to builders planning built and open areas. Consequently, profit-oriented urban design is expected instead

of climate-sensitive solutions. Under these circumstances, the distribution of open spaces risks to be highly damaged at the expense of badly designed and placed towers.

In the last years, numerical tools have been developed in scientific research to promote sustainability, focusing on city and climate interactions. Given the great amount of variables involved, the use of numerical models is becoming common to investigate the environmental performance of urban fabrics or blocks arrangements. From building scale, the "art of modeling" is expanding towards larger domains of study, exploring the complexity of urban environment. Numerical models constitute a simplified way to represent the urban interactions, focusing on selected aspects of the urban system (WALLOTH et al. 2016). Through a modeling approach, the real system is converted in a mathematical formulation that can be fixed by approximated solutions (ANDERSON; WOESSNER; HUNT, 2015). Numerical representations of reality are used to predict future impacts. Moreover, models are suitable to integrate missing information and incomplete field data, consolidating the observations directly measured on the site. The increase of computer efficiency and availability of massive databases results in holistic and fully-integrated codes that favor the understanding of complex urban dynamics at different scales. Notwithstanding, urban modeling is not included in the daily practice of urban design and municipal planning, which do not require climate predictions in support of construction activities.

In this framework, the present research combines numerical models and field monitoring in an integrated procedure for the morphological and climate investigation of a TOD area in São Paulo. Taking into account the current city agenda, the proposed research procedure delve into the implications that future strategies of urban transformation can produce. In particular, the thesis focuses on the effects of densification of existing urban fabrics supported by TOD theories, proposing an in-depth investigation of low-rise areas. The city of São Paulo was considered as a representative context in which such dynamics occur and express their contradictions. In this context, Belenzinho neighborhood (*Mooca* district) was selected as the case study. Being close to the metro station and railways, such selected urban area is part of the TOD strategy and classified as ZEU (Structuration Zone of Urban Transformation) according to the land use policy. In addition, within this region, a verticalization process had been occurred in the past decade, scattering towers in the middle of low-rise housings. Thus, it was possible to analyze the effects of an in-action densification, as well as develop numerical simulations to predict the variation of climate characteristics related to the insertion of new dense high-rise buildings in the domain.

Main strengths concern the interdisciplinary approach to urban issues with a climate focus, along with the exploration of physical processes affecting high- and low-rise built-up areas in the development of a conceptual model. Moreover, the proposed integrated procedure, combining data analysis and modeling techniques, allowed the development of a research framework in which the investigation of morphological urban features is deeply embedded in the climate analyses. For the city of São Paulo, findings confirm the importance of building features over the variation of climate patterns, as well as a need for more detailed legislative guidelines to guarantee the quality and effectiveness of new dense urban environments. At the end, climate-sensitive design practices in TOD areas under subtropical climate are suggested. Therefore, based on extended analyses, the study aims to provide practical tools to connect academic perspective with the current urban issues.

1.1 Main questions

- Which climate impacts are associated with the increasing of density and building heights in a low-rise urban area?
- Is TOD regulation enough defined to guarantee a climate-sensitive urban design in São Paulo?
- Which urban design strategies and rules could enhance the implementation of high densities in São Paulo?

1.2 Hypothesis

Local and micro climate variations are expected within the urban open spaces when morphological and density variations are introduced on the existing urban fabrics. Moreover, consequences for pedestrian comfort are hypothesized in increasing built density within a city. Thus, urban master plans should implement climate analyses and forecasting tools to the traditional planning instruments to enhance the physical understanding of their existing fabrics and to forecast environmental smart solutions for the evolution of these urban lands. Within this general framework, it is hypothesized that São Paulo municipality has not suitable municipal tools to take into account the climate implications of its current planning strategies. In the context of TOD (Transit-Oriented Development) areas, Prefecture is assumed to not provide a climate-sensitive built densification pattern. For this reason, research fieldworks,

analyses and modeling activities could enhance the comprehension of these areas, really supporting an environmental friendly future urban design.

1.3 Objective

The main objective of this work is to develop an integrated procedure to explore the interactions between urban forms and climate features within the outdoor urban environment, focusing on thermal fluxes and solar availability of urban spaces affected by buildings, surfaces and vegetation. Such procedure aspires to be a tool for the deep understanding of the existing urban reality. Moreover, it should be suitable to evaluate the climate implications of future urban densifications by implementing modeling techniques. In this sense, the implementation of such full procedure allows to discuss the adequacy of the municipal regulations to the built density increase. The investigated open spaces are selected from on-transformation low-rise urban fabrics in which dense and verticalized built-up areas are being introduced accordingly to the TOD strategy.

Specific objectives are:

1. Developing and applying a set of analytical procedures to a TOD urban area under the way of densification. Highlighting the main climate processes and the urban morphology typologies which describe the current physical condition of the area and outlining its conceptual model;

2. Developing, applying and integrating numerical models to reproduce the interactions between urban morphology and climate variables in the studied area on the basis of collected field information;

3. Developing numerical simulations (scenarios) to investigate the effects related to alternative built densification patterns, highlighting the limitations of municipal regulation from a climate point of view and recommending urban design precepts to enhance TOD application in São Paulo.

1.4   Research methods

To face the proposed objectives, an integrated method was developed, involving three main procedures: field data collection, data analysis and numerical modeling. Results were valid for the urban area under analysis and for similar urban contexts at comparable latitudes, on which densification strategies are ongoing. Moreover, the whole method and single procedures are rather well general to be applicable to different urban situations, providing an effective tool-guide for the morphological and climatic investigation of cities.

The entire procedure combines the investigation of multiple scales making up the urban environment: the mesoscale, the local scale, the microscale. On the mesoscale, a wide point of view is adopted to look at the mosaic of urban fabrics and climates characterizing a large portion of São Paulo city region. On the local scale (case study), the urban morphology of the neighborhood is analyzed in detail and long-term climate surveys were carried on. On the microscale, specific studies were implemented focusing on the close interaction between street elements, pedestrians and microclimates.

The characterization of the case study was based on available database and field collections carried out between May, 2016 and December, 2018. The entire dataset included both climate variables and morphological features on which procedures of multi-scale data analysis and modeling were applied. Great emphasis was dedicated to the study of interferences between buildings size and shading.

The field climate collection was conducted by means of measurement equipment provided by the Laboratory of Environment and Energy Studies (LABAUT) of the Faculty of Architecture and Urbanism (FAU) of the São Paulo University (USP). Climate investigations were conducted outdoor, within public and private open spaces of the neighborhood. In the public spaces, transect-strategies were applied, in order to preserve the security of climate stations. In the private open spaces, long-term climate measurements had been possible. Meso-scale data were obtained from the main meteorological stations of the city. The collection of morphological features relied on online-available database and field collections using equipment provided by the Transport Engineering Department of Polytechnic School of USP.

Techniques of data analysis were applied to explore the entire database. Climate time-series were processed by procedures of data consolidation to obtain consistent data and remove noise (meaningless information from low-level data errors) caused by equipment bias and variable atmospheric conditions. Relationships between variables were brought out by

means of correlations, probability and cumulative density functions, scatter plot analyses. Most of the treated data were used as data-entry into the modeling processes.

The use of different numerical codes was proposed. A numerical model of the urban area under analysis was developed on *ENVI-met* code (Bruse, 1995) and displayed by the visualization interface *Leonardo*. Supplementary modeling activities were carried out on Grasshopper to investigate solar access, thermal comfort and UHI effect in the domain, using *Diva*, *Honeybee*, *Ladybug* and *Dragonfly* plug-ins. To compute the leaf area index (LAI) of tree canopies, the software *CanEye* was selected. The calculation of the sky view factor (SVF) and the Physiological Equivalent Temperature (PET) index were achieved by *Rayman* code. The reading of thermographic photos was made on *Flir Tools* software.

1.5   Research overview

- Background: introduces and explores a collection of key-topics from literature, useful to understand the research subject. Urban morphology and climate studies are presented and a further effort was dedicated to integrate these two fields. The section also introduces technical vocabulary.

- Case study: leads to the urban region in which the research will be conducted. The case study is introduced from general to particular. At the large scale, the city of São Paulo is described as a whole entity; at the smaller scale more detailed landscape characteristics are highlighted.

- Material and methods: describes the integrated method proposed, highlighting the procedures of data collection, steps of modeling and the development of the conceptual model. The set of techniques, equipment, specifications and softwares implemented along with the process are detailed.

- Results: the exposition and interpretation of all findings is raised. With regard to field assessment, the relationships between climate variables and morphologic features are in-depth explored. Modeling findings include sensitivity tests, calibration and numerical experiments (scenarios).

- Summary: intersects the field analysis with the modeling findings, summarizing contents in urban design precepts, useful to be applied in urban areas affected by land use changes. Law regulations from São Paulo master plan will be reviewed and discussed.

- <u>Conclusion:</u> detaches the highlights of the present research, as well as its limitations. Recommendations for the continuity of research are raised and future works appointed.

2   Background

Goal: The background chapter discusses the main theoretical aspects that sustained the whole research process of this Thesis. Due to the wide range of issues faced, the chapter introduces a sequence of key-topics that go through different fields including city planning, urban morphology, urban climate, data analysis and modeling. Each topic provides an overview of the proposed issue, introduces a technical vocabulary and informs on the specific state of art. Therefore, the research problem is split in a chain of theoretical key-points, whose understanding is relevant for structuring and develop the next chapters.

2.1   City as a living body

Human societies strongly depend on the geographical position in which they settle and grow. The distance from the Equator (latitude) especially affects their living conditions in essential aspects, such as climate, vegetation and people density (KUMMU; VARIS, 2011). However, within each climate region, metropolitan areas grow as great living beings, developing their own urban climate, drastically modifying the geographical environment in which they are inserted. The urban heat island (UHI) is the most evident product of this man-caused urban distortion; its profile embeds the whole city landscape and its magnitude is proportional to the city size (OKE, 1987; ERELL; PEARLMUTTER; WILLIAMSON, 2011). Nonetheless, the urban climate within large cities is not homogenously spread (ANIELLO et al., 1995; GIRIDHARAN et al., 2007); cities are living bodies constituted of recognizable parts with distinct shape and function, at colder or warmer temperatures. Generally, the compact high-rise districts are warmer, covered by impervious surfaces and *traffic-choked*; intermediary neighborhoods mitigate these effects, while the peripheral areas are cooler, low-rise, characterized by single-family homes, fewer cars, sometimes factories and greener.

The urban morphology of these noticeable zones is discernable from the surroundings due to the similarity of its urban forms (WHITEHAND, 2001); the specific climate regimes characterizing each zone were widely investigated by the literature and many e□orts were made to classify them universally (AUER JR., 1978; ELLEFSEN, 1991; STEWART; OKE, 2012; STEWART; OKE; KRAYENHOFF, 2014). According to the last and widely accepted classification developed by Stewart and Oke (2012), seventeen (17) classes, called Local Climate Zones (LCZ) define the urban landscape; classes are homogeneous in land cover, urban form, materials, and function; their extent ranges between hundreds of meters and

various kilometers. The World Urban Database and Access Portal Tool (WUDAPT) applies this classification to discriminate cities' LCZs across the world. WUDAPT maps are based on remote sensing analysis (MILLS et al., 2015); their quality is being constantly improved and many eorts have been made to raise their accuracy. Recent applications show low accuracy to detect high and midrise built zones (LCZ-1, LCZ-2, LCZ-4, LCZ-5), while low-rise zones (LCZ-3, LCZ-6) are better extracted (REN; WANG; CAI, 2016). Ferreira et al. (2017) highlight zones improperly classified for the São Paulo city LCZ map using the WUDAPT Methodology. Wang et al. (2018) states that the inaccuracies can be explained by the heterogeneity of urban morphology; when mixed and irregular urban fabrics are selected, LCZ classification aggregates multiple zones into a single dominant zone.

In addition, even within homogeneous local areas, the assortment of different physical forms enhances "pockets of urban microclimates" in the city environment (GOLANY, 1996). The open spaces and the built forms mutually interact, shaping one another (MOUDON, 1997). Every built element induces its own microclimate around it; thus, air and surface temperature differences can be observed in the outdoor spaces between objects, even at a short distance (OKE, 2006). Temperature variations at micro-scale are strongly influenced by building density, building height and green plot ratio (WONG et al., 2011). Building height, above all, plays an important role, because of the shading effect. Within an urban canyon in a tropical city, Johansson and Emmanuel (2006) find that high ratios between canyon height and width (H/W) decrease nighttime building cooling and ventilation while lower daytime temperatures are favored; consequently, the improvement of the outdoor thermal comfort can be achieved by raising the H/W ratio that enhances shadows (EMMANUEL; ROSENLUND; JOHANSSON, 2007). Conversely, the lack of sun access affects the light quality inside the shaded houses, as well as the energy conservation and the time-space perception (KNOWLES, 1980, 2003). Therefore, from the larger to the smaller scale, distinct thermal environments shape the city climate, accumulating the influence of the geographical latitude, the heat island, the effect of local fabrics, the urban canyon, including single buildings and their shadows. Despite the difference in magnitude, these factors are concurrent and not disjointed; their interaction shapes unique climate environments and enhances temperature contrasts in outdoor spaces.

2.2   Density and TOD theory

The concept of density in urban planning describes the relationship between a reference area and the amount of entities contained in that area, such as people, buildings, services, or open spaces (BERGHAUSER PONT; HAUPT, 2010, p.15). The need for increasing density arises in opposition to the spread of cities across the countryside (NEUMAN, 2005) that led to the progressive disappearance of unbuilt lands. Conversely, the idea of compact cities livened up the international debate encouraging the search for more sustainable urban forms and developments. According to Jenks, Burton, Williams et al., 2003, the pattern of "densely developed cores" of many historic European cities has for a long time conditioned the vision of the compact city, whereas other authors highlighted that the concept of sustainable cities could not be rooted on an idealized experiences of past settlements (HAUGHTON; HUNTER, 1994, p. 311). In the early 1990's Peter Calthorpe theorized a new model of compact city based on the concept of Transit-Oriented Development (TOD). This novel pattern of growth was focused on pedestrians, human-scaled communities, diversification of use and population. The proposal provided an alternative to sprawl and encouraged transit investments supported by land use patterns that provided jobs and housing at easy walk distance from station. Afterwards, the evolution of the TOD theory led to the real first implementations in American Cities and around the world. Today, the Transit Oriented Development Institute displays on its official webpage (http://www.tod.org/projects.html) a dense network of transit-oriented projects actives in Washington D.C. and U.S. Also in European cities, the dismantlement of industrial buildings, the privatization and expansion of railways, as well as the new spatial dynamics of contemporary society have driven the redevelopment of railway stations and surroundings for more than two decades (BERTOLINI; CURTIS; RENNE, 2012). In São Paulo municipality, the TOD theory was implemented by means of two urban planning instruments (PDE of 2014 and LPUOS of 2016).

2.3   Urban Form

The etymology of "morphology" comes from Greek (morphé + lógos + ía) that means "the study of form". In the city context, urban morphology indicates the investigation of urban forms in its physical attributes that make up the Human habitat. Among the main interests of this science, buildings analysis and ground plan (land use) assessment are highlighted (ARAGÃO, 2006; STEINER, 2008, p.71; MOUDON, 1997, p.3). The study of a city urban

morphology has to deal with a complex set of urban objects in mutual relationship and in strong or weak connection with the whole (OLIVEIRA, 2016). Batty (2008) considers the urban morphology as a hierarchy of clusters across many scales, from the entire city to neighborhoods. To enhance the understanding of such urban clusters hierarchal organized, key-urban forms including *LCZs* or *Urban Fabric*, *Urban Block*, and *Urban Canyon* were further explained.

At a general level, city morphology is composed of urban fabrics (OLIVEIRA, 2016). Urban fabrics (from a morphological point of view) or local climate zones (from a climate point of view) indicate recognizable and homogenous parts of the urban structure. Urban fabrics are characterized by a close relationship between roads shape and buildings. The structure of road network (grid, organic, irregular) and the grain (thin, medium, large) are between the most important attributes, indicating the distribution and the size of continuous urban forms (MATTOGNO, 2014, pp.289). Within the urban fabric, sets of urban blocks can be recognized. According to Oikonomou (2014) the urban blocks are three-dimensional urban forms made up of buildings and contiguous plots, meanwhile surrounded by streets. The proximity of their functions makes them interconnected systems of social and spatial relationships. Between two urban blocks, the urban canyon takes places. The urban canyon corresponds to the road section delimited by buildings and is internationally defined by the *H/W* parameter, the ratio between the height of buildings (H) and the width (W) of street (Marins, 2010). According to Oke (1987) the street canyon is the basic geometric unit, described by two dimensional cross-sections, with the predominant airflow direction normal to the street axis.

Whereas the previous definitions were based on geometry concepts, other morphological entities surpass the physical meaning, embedding historical, social and cultural evidences, enclosed by indefinite boundaries. In this regard, *Urban Neighborhoods* and *Communities* are morphological urban wholes, recognizable for a robust social identity, not always coincident with the character of their shape. Despite similarities between the two terms, a distinction can be drafted. According to Chaskin (1997), the concept of communities implies "connection", networks among individuals sharing common interests, concerns, beliefs. Communities provide collective actions, often are place based but cannot be seen as mere geographical units. Otherwise, neighborhoods are "spatial constructions" within the broader urban landscape, where people share closeness and interact. Such geographical entities are more strongly related with the territory in which they are integrated; their "power" does not lie in their sociological construction but in the complexity that merge elements of

connections with the geographical circumstance. In this thesis, the term "neighborhood scale" will be considered coincident to the "local scale" term. Communities and Neighborhoods can be distinctive areas into which larger urban fabrics can be subdivided; conversely, different urban fabrics can be part of larger neighborhoods or communities.

2.4 Outdoor Urban Spaces

Urban spaces could be seen as the complementary part of the urban forms. In this work, *outdoor* or *open* urban spaces indicate the whole of no built public and private urban areas enclosed between buildings. Under an historical perspective, urban spaces were born to carry out three important functions, implying the meeting and exchange of social information (1), the offer of good and services (2), the connection between all the functions and the access to their benefits (3). In the Twentieth century, the key-role of traditional open spaces lose centrality and vitality, due to a complex set of reasons including the growing of urban population, the transformation of economic and social exchanges and the increased use of motor vehicles (THOMPSON; TRAVLOU, 2007).

Beside these changes, the urban spaces still host functions and activities that determine the quality of life for its inhabitants. By occupying about two-thirds (2/3) of the total urban area, outdoor urban spaces are an active part of urban living, providing meeting places and encouraging the development of human skills (SHASHUA-BAR; TZAMIR; HOFFMAN, 2004). The public space performs a structuring role in the urban form system, affecting forms of mobility, accessibility and circulation, parceling and urban land ownership (MACEDO et al., 2012). Hence, the planning and design of successful urban open spaces is crucially important for promoting the urban outdoor living (GHAFFARIANHOSEINI et al., 2017). Alexander (1977) in *Pattern Language* discerned positive open spaces from negative ones, taking into account how much the spaces were successfully used and lived by its inhabitants. "Negative" are generally residual and shapeless spaces, accidentally resulting from the construction of buildings. Conversely, positive urban spaces are open air *rooms* with distinct shapes. Outdoor urban spaces also play an important role in the city climate. Geometric proportions and materials are key-conditioning elements affecting microclimates and space functionality, with social, economic and environmental consequences (CHATZIDIMITRIOU; YONNAS, 2016).

In tropical latitudes, critical temperatures compromise outdoor thermal comfort, therefore shading factors become important mitigating solutions (EMMANUEL, 1993; 2018).

However, in the contemporary urban landscape, strong real estate building activities deeply increase the shading conditions in open spaces. Benefits or disadvantages of these circumstances are not obvious. According to Costa (2003) and Ribeiro, De Carvalho and Dos Santos et al. (2010), excessive shading between buildings leads to require greater artificial lighting; meanwhile, the increase of built surfaces exposed to solar radiation prevents the dispersion of stored thermal energy.

2.5   Urban Climate and Scales

Urban environment is an ecosystem under incessant modification due to the evolution of city form, spaces and all living things. According to Oke et al. (2017, p.3) the study of urban climates deals with the interactions among urban morphology, urban function and the overlying atmosphere. Such climates are created and reshaped along the process of urban development, enhancing every time their diversity. The availability of environmental resources within urban areas greatly affects the physical quality of the city, as well the urban energy balance in which natural irradiation, illumination and ventilation are of great importance (ASSIS, 2002). For a long time, Earth inhabitants transformed landscapes through the implementation of several land uses including agriculture, livestock, reforestation and urbanization. The effect of these activities is seen in temperature and precipitation changes, concentrations of carbon dioxide (CO_2), methane (CH_4), and nitrous oxide (N_2O) in the atmosphere and in the laying of atmospheric pollutants on the land (BONAN, 2016, p.14). Meanwhile all ages produced changes; downtowns of modern cities have contributed to make local climates worse, consigning the quality of outdoor climates to the oblivion. Modern buildings around world were built similarly in form and spacing, notwithstanding the diversity of climates in which they were embedded (BOSSELMANN et al. 1995). City and countryside came towards distinct thermal behaviors. Relevant temperature differences between urban and rural atmospheres were observed since long time under clear skies and low wind speeds (BORNSTEIN, 1968), resulting in the Urban Heat Island (UHI) effect. Today, with the increase of megalopolis, UHI phenomena were noted all over the globe. The *Global Surface UHI Explorer* is a global database (https://yceo.users.earthengine.app/view/uhimap) displaying urban heat islands intensities into cities around world, in a time interval ranging between 2003 and 2017. UHI is particularly problematic at tropical latitudes, where UHI effect has to be add to a generally hot climate, with serious implications to energy

consumption, green gas emissions (GHG) and human health (GIRIDHARAN; EMMANUEL, 2018).

Given the complexity of climate phenomena affecting the urban environment at different layers, the adoption of multiple scales of climate investigation favors the understanding of the urban climate as a whole and of the interactions between its single parts. Horizontally, most of urban climate phenomena occur in microscale, local scale and mesoscale regions. Microscale (extended from 10^{-2} to 10^3 m) involves street elements and the pedestrian condition, local scale (extended from 10^2 to $5{\times}10^4$ m) deal with neighborhoods while mesoscale (extended from 10^4 to $2{\times}10^5$ m) includes large parts of an urbanized region and the geographical features (OKE, 1987 to 2017). Thus, it would be noted the range between 10^2 and 10^3 is a transition interval since the attribution to 'micro' or 'local' category leaves space to the scientist's interpretation. For the case of São Paulo, Tarifa and Armani (2000) proposed a similar tripartition by defining the meso, topo (local) and micro scales. For these authors, within the space of a topoclimatic unit, many microclimatic environments should be redefined. They considered the micro-scale as the level of dwelling, living and working; it included internal or external microclimatic environments in which alterations of atmospheric states had been proven.

Vertically, the complex atmospheric structure overlaps several layers, here summarized into the urban boundary layer (UBL) and urban canopy layer (UCL). UBL is an urban modified layer with a variable height (100 m – 2km) depending on the strength of thermal mixing occurring at night and during the day. Under no wind conditions, UBL takes the form of an urban dome, whereas has a plume shape when winds blow carrying on for kilometers the pollutants, the thermal and the moisture effects coming from city. The lower part of UBL delimited by the top of urban elements is called UCL. UCL is strongly affected by human activities, energy exchanges, roughness and turbulences caused by buildings. It takes account of the external environments and the internal living spaces, as well as the transmission between them through walls and windows. Both horizontal and vertical scales are not discrete and isolated systems; turbulences drive their interactions merging one scale with the other in an atmospheric continuum, from the smaller microclimate up to the boundary layer (OKE, 1987, p.4; MILLS, 1997; OKE, 2006, p.2; OKE, 2017, p.30).

The spatial definition of the horizontal and vertical climatic scales is crucial for understanding the interaction between atmosphere layers and urban forms. Meanwhile, the correspondence between climate scales and planning scales is not obvious and urban interventions may provide atmospheric effects crossing more climate scales. The modification

of land surfaces and features has impact of boundary layer and surface energy balance resulting in variable urban climates. Urban structure, building materials, density of urban developments can influence the UHI, producing alterations in net radiation, thermal storage and inertia, sensible and latent heat fluxes. According to Goward (1981), the urban canopy structure and composition, together with thermal properties of urban construction materials, are essential factors to explain the modification of urban climate.

These modifications could contrast with the targets of sustainability that contemporary cities attempt to achieve (COUTTS; BERINGER; TAPPER, 2007). At the local scale, the design of urban forms and open spaces also is related to the climatic variability; little local differences occur in temperature, wind flow and air pollution concentration (DUARTE, 2010). Aniello et al. (1995) calls these variations as *micro-urban heat islands* (MUHIs), "isolated urban locations that produce 'hot spots' within a city", related to canyon geometry, material thermal properties and waste heat from buildings. Effat and Hassan (2014) show that asphalt and roof metal strongly contribute creating micro-urban heat islands in Cairo, especially when green and shadows are missing. Although high-density developments take advantages from efficient land use, pedestrian walkability, public transport and infrastructure, a good planning is needed to avoid "the sunk cost" of an unsuccessful compatibility between urban design and environmental benefits (NG, 2009).

Among the multiple driving forces of urban modification, shading due to the built elements is responsible for creating climatic micro-differences within densified and verticalized urban fabrics. Urban areas under intense real estate activities, such as TOD, suffer the insertion of new real estate developments which promote new thermal contrasts between the sunny and the shaded areas. The construction of new real estate developments casts deep shadows over the recreational areas and gardens affecting the neighborhood livability, reduces the dwellings solar availability weakening the solar access right, lastly compromises the energy conversion potential (KNOWLES, 1980). Costa (2003) and Ribeiro, De Carvalho, Dos Santos (2010) state that the acceleration of the verticalization process increases the built area exposed to the solar radiation, prevents the release of stored thermal energy to atmosphere, as well as increases dependency from artificial lighting if the mutual shadowing between buildings is excessive. According to Monteiro and Oliveira (2013), the verticalization process affects roughness, re-shapes the skyline and waterproofs the land, leading to the degradation of the wind conditions, increasing the heat gain, compromising health and thermal comfort of inhabitants. Rossi, Krüger and Nikolopoulou (2011), in an outdoor space analysis carried out in Curitiba (Brazil), recommends the use of architectural elements such as pergolas and

galleries, as well as the use of deciduous trees to encourages sunshine in the winter period and guarantee shading in the summer. Similarly to Erell, Pearlmutter and Williamson (2011), shading is an inherent feature of any urban landscape, function of the canyon geometry (H and W), geographic location, daytime and season. Excessive compactness in east-west-oriented canyons may cause overshading on the sidewalks, north-south canyons mitigate this phenomena when the sun reaches the zenith. In addition, shading due to large real estate developments favors the humidity in the internal parts of the surrounding shaded dwellings, causing the proliferation of mold, fungi and termites, favorable to bronchopulmonary diseases (NUNES, 2011, p.59). Meanwhile, Emmanuel, Rosenlund and Johansson (2007) considers shading a potential mean for the improvement of human comfort that interferes with solar energy flows transmitted by radiation (input) and radiated back by urban mass (output). The input – output gap results in an accumulated energy, responsible for the increase of urban temperature, which will be returned to the atmosphere over the time, according to the first thermodynamic law. The built environment affects absorption and reflection of solar radiation, as well as absorption and emission of long-wave radiation from surfaces. The ratio between reflected and incident radiation represents albedo (OKE, 1987, p.6).

2.6   Urban Thermal Comfort

The existence of humans and all other organisms depends on energy. This energy, exchanged between places and converted from one form to another, is responsible for creating a wide range of environments on the Earth. Within this extremely various landscape, the challenge for everyone consists to successfully interact with own local environment (PARSONS, 1993). Weather and environment influence people daily life, allowing their open air activities, requiring certain clothes, favoring some transport means, as well as conditioning the state of mind (NICOL; HUMPHREYS; ROAF, 2012). Nevertheless, under the same atmospheric motions, city is able to provide different microclimate environments due to its urban fabric typology, buildings arrangement, outdoor spaces size, materials and surfaces diversity, vegetation and tree coverage. This kind of urban climate variability induces different conditions of thermal comfort within the urban open spaces generally out of the control of air-conditioning systems, influencing the thermal balance of people walking through these places (PINHEIRO *et al.,* 2016). Thus, bad thermal comfort conditions discourage the use of public spaces instead of enhancing pedestrian open air activity. According to Brown and Gillespie (1986), in order to create more thermally comfortable

outdoor places and minimize energy cost, planners should take advantage from the inherent physical characteristics of the different microclimates existing on the site. In the tropics, thermal comfort should manipulate buildings and streets geometry to enhance environmental diversity and avoid physical boundaries between people homes and surroundings (EMMANUEL, 2018). Such approach could be usefully applied in TOD areas, where walkability and livability of open spaces are promoted. In this regard, microclimate parameters affecting people thermal comfort should be considered and mitigating solutions implemented. Notwithstanding, most of the TOD literature and masterplan encourage urban practices that promote attractive facades, sense of safety, good accessibility and land use diversity, while thermal comfort principles are neglected (SALAT; OLLIVIER, 2017; SÃO PAULO MUNICIPALITY, 2014; 2016; 2017).

Thermal Comfort is defined as: "that condition of mind which expresses satisfaction with the thermal environment" (ASHRAE 55, 2017). Additionally, Ng (2008) states that the balance among air temperature, wind speed, humidity, solar radiation, activity and clothing could be crucial to achieve the outdoor thermal comfort. To express a thermal comfort condition in measurable terms, many efforts were addressed by research to universally estimate heat and physiological stress induced by climate (EPSTEIN; MORAN, 2006). Hence, the creation of a universal heat stress index is prevented due to the complexity of cultural and geographical involved factors. As consequence, a myriad of different indices continue to be applied by users and researchers. *Physiological Equivalent Temperature* (PET) is a thermal index to estimate the people state of comfort in outdoor urban spaces. Mathematically, its computation occurs by transferring the real outdoor bio-climate to an artificial indoor environment in which the same thermal stress is expected (MAYER; HÖPPE 1987). In this typical indoor environment, PET represents the physiological equivalent air temperature in which the human body thermal balance is maintained (HÖPPE, 1999). High PET values mean a very hot thermal sensation. The computation of PET can be obtained by means of different computational codes, requiring air temperature, wind speed, air humidity, mean radiant temperature, as well as other thermal-physiological data regarding people clothes and activity. *RayMan* is free open access software, suitable to evaluate thermal comfort in complex urban structures, since the estimation of short-wave radiation at the pedestrian level takes into account the presence of clouds, the incidence of sun, as well as the urban obstacles around the assessed point (MATZARAKIS; RUTZ, 2010). Johansson (2006) implemented PET to investigate the influence of urban geometry on the outdoor thermal

comfort in a hot dry climate (Morocco) showing how deep and shallow urban canyons supported comfortable or uncomfortable conditions depending on the season.

Recently, the European COST Action 730 (Cooperation in Science and Technical Development) project developed a Universal Thermal Comfort Index (UTCI), involving scientists from 19 European countries and experts from Australia, Canada, Israel and New Zealand (MCGREGOR, 2012). Blazejczyk et al. (2012) compared UTCI with more common thermal indices (dataset from different countries), demonstrating its sensitivity to environmental changes and a better capability to describe the temporal variability of thermal conditions than other indices (among which PET). In a thermal comfort survey in Curitiba (Brazil), Bröde et al. (2011) monitored climate and clothing parameters of people to test the predictive ability of UTCI in a sub-tropical region. They showed a good correspondence between the behavioral adaptive clothing model adopted by UTCI and the clothing insulation observed on site.

2.7   Techniques of measurement

All climate research activities and applications are essentially based on observations of the state of the atmosphere. The World Meteorological Organization (WMO) Global Observing System is a coordinated network of observing services providing high-quality and standardized meteorological observations from all parts of the earth. WMO climate stations are generally sited away from urbanization growth, in order to guarantee the widest sky view and the correct exposure of instruments (WMO, 2011). As consequence, records from WMO stations are representative of regional climates and rural-type sites, providing accurate and large-scale information which improve the global understanding of specific climates around world. Conversely, WMO is not representative enough to understand the city climate and a lack of urban climate observations can be easily detected. However, to enhance the design of our cities, meteorological observations are a crucial matter. Atmospheric observations in cities support the understanding of urban climates (GRIMMOND, 2006), the monitoring of urbanization effects, the estimation of air quality and health, the prediction for suitable future urban plans. Field observations are also very useful to observe the influence of urban geometry on climate and urban heat island phenomena. In agreement with Oke (2006), despite the great request for atmospheric data, urban meteorological stations have difficulty to provide data in accordance with the WMO guidelines, due to interferences from human activities and building obstructions. To surpass these circumstances, strict rules make little

sense; instead, an agreement between flexibility and intelligence should be needed to obtain careful and meaningful observations of the specific environment under study. Overall, urban field observation carried out into the city requires a special attention to avoid records unrelated with the location under observation.

According to WMO (2011), the climate system is a combination of meteorological elements. Among such meteorological elements, air temperature, precipitation, humidity, wind speed and direction, atmospheric pressure, evaporation and sunshine are highlighted. Similarly to Oke (2006) the measurement of these variables on an urban site requires specific procedures. The correct installation of the meteorological station is the first step. The station location should reflect the purpose of the investigation and "catch" the effects of the urban phenomena monitored (ex. building shading, urban density impact, urban canyon microclimate, district local climate). Extraneous climate influences and zones of climate transition should be avoided. The number of weather stations and their accuracy depend on the climate scale in which the atmospheric phenomenon is observed. Thus, the definition of the climate scale has great importance to design the field experiment.

Accessibility, as well as safety for operators and equipments has to be carefully considered. According to Grimmond (2006), stations have not to be placed on short grass, whilst on ground surfaces representative of the urban environment, sufficiently distant from obstacles and centered in the open space of the observing site. The best weather to collect data occurs under calm airflow and cloudless skies. The source area, that means the whole of urban features influencing the meteorological station, depends upon the variable observed, the sensor height, the underlying surface, the meteorological conditions (Grimmond, 2006). In accordance with Oke (2006), for radiation the source area is restricted by urban geometry and ground surface. For air temperature, humidity, wind speed and directions the source area includes the atmospheric properties transported to the sensor troughs turbulence motions. Air temperature sensors should be shielded from radiation and direct ventilation; heat from close engines, vehicles and glassed surfaces are not recommended. Whereas for rural sites the sensor height is required to be between 1.25 and 2 m above ground, for urban sites, this caution can be reconsidered to allow higher installations. Especially in compact built-up urban areas, this shift does not imply significant errors since in urban canyon slight air temperature gradient were empirically observed. As consequence, 3-5m high measurements little differ from the standard-ones; in addition, they ensure a greater source area and are more sheltered from vehicles transit and wastes. For humidity measurements, the same air temperature guidelines can be applied. Observations of wind speed and direction suffer the high risk of

distortion due to the numerous urban obstacles filling the urban space. For incoming solar radiation, it is recommended to avoid excessive reflection from mirrored and light-colored surrounding walls. Ideal sites of measurement are accessible and stable roofs. Observations from pyranometers can also signal the cloud coverage along with the day, as well as the undesired interference of building shading (Oke, 2006).

2.8   *Techniques of data analysis*

Climate data gained from meteorological stations represent an unrepeatable product, recorded with much effort and significant costs. However, the uniqueness of this product does not provide great utility if raw data are not converted in comprehensive information, accessible to urban planners, municipalities, and decision-makers (WMO, 2011). In addition, when measurements are needed to estimate input parameters into models, representative data have to be extracted from the whole dataset without loss of information. Hence, a data management process is needed to store, organize, consolidate, explore and analyze records in order to discover effective patterns and produce knowledge. In accordance with Trauth (2015, p.2), in Earth science data collection sample size is relatively small when compared with the large natural phenomena; data population may be heterogeneous and containing uncertainties related to the measurement equipments or to the environment variability. And even if a suitable sampling strategy is defined, the confidence of data could be undermined by numerous unpredictable factors. Within this complexity, statistical methods provide a framework to describe, manage and understand data variability (MONTGOMERY; RUNGER, 2011, p.3). When data are inserted in a graph, the overall pattern is displayed and unusual observations stand out (MOORE; MCCABE; CRAIG, 2009).

Methods of data analysis depend on the collected data typology. Climate collections as temperature records are *interval data,* sampled continuously or in discrete intervals, ordered in successive intervals of equal length (TRAUTH, 2015, p.6). Morphological collections as building heights are instead examples of *spatial data*, collected in a 3D study area to describe the spatial distribution of a certain urban feature. While *interval data* present a temporal variation and cyclicity*, spatial data* in urban environment are constant over a quite long-term period. *Spatial* and *temporal* data variation can be investigated by specific data analysis methods, including univariate methods, bivariate methods, time-series analysis, signal processing, and spatial analysis. Some of mining procedures can require the combination of more techniques. Similarly to Trauth (2015, p.7), *univariate methods* explore variables

individually on a series of points, allowing to obtain a collection of parameters including average, dispersion, minimum and maximum values. An example is the observation of temperature over a period of time. *Bivariate methods* explore two variables together in order to discover relationships between them through the computation of the correlation coefficient. An example is the bivariate plot intersecting the illuminance rates with the air temperature variation in a neighbourhood. When more than one variable is explored at a time, the analysis turns to be called *multivariate*. *Time-series analysis* explores sequences of data along time, separating the systematic component (cyclic, rhythmic trend) from the irregular component (random). Such type of analysis is usually coupled with *signal processing* techniques that apply filters to minimize noise and unwanted distortions from time-series. Mining of time-series and operations to enhance the "signal-to-noise ratio" are frequently used to explore climate dataset. Finally, *spatial analysis* explores geographically distributed data in order to highlight spatial patterns on a 2D or 3D space. Usually, GIS (Geographical information systems) codes as *Arch-Gis* and *QGis* allow developing such type of analysis through specific operations. Studies of urban surfaces distribution on a GIS ambient are examples of this technique.

2.9   Techniques of modeling

Besides allowing the understanding of reality and natural phenomena, data collection from urban environment provides essential information for modeling codes. Indeed, numerical models require setting large amounts of parameters that describe the environment in which the model is virtually built-up. A model is a simplified representation of the complex real world (ANDERSON; WOESSNER; HUNT, 2015, p.5). The understanding of complex urban systems involving multiple and interdependent factors can be considerably enhanced through the use of models (ORGANIZATION FOR ECONOMIC CO-OPERATION AND DEVELOPMENT, 2011). Models can be divided into *physical* and *mathematical*; while the first-ones are realized in laboratory, the second-ones use sets of equations to define the interaction between variables. Mathematical models using physic-based equations to describe the natural processes within the modelled space are further called *process-based* or *physically based* models. Mathematical *process-based* models consist of a *domain* in which the environmental problem is built-up, a set of *"governing" equations* describes the physical interactions between variables, *boundary conditions* define values or flows along the border of domain, *initial conditions* assign values and fluxes on the beginning of the simulation. The

solution of mathematical models can be fixed numerically or analytically. *Analytical* models achieve a "closed-form" (or exact) solution by mathematically solve high-simplified equations that subtract complexity to the real world interactions. Such assumptions limit the application of analytical models to only simple systems of variables (ANDERSON; WOESSNER; HUNT, 2015, p.6-9). Conversely, *numerical* models are able of handling much contemporary processes, different degrees of nonlinearities, large systems of equations often impossible to be solved analytically; their solutions are not exact but well enough approximated by numerical operations. Their application, both for finite-difference and finite-elements methods, is greater and well fit to complex real world problems. Before starting a modeling process, the model purpose should be defined. Models can function as *forecasting* tools to investigate the effects of certain actions on a selected domain; otherwise, they can be needed to virtually re-create past or present conditions (ANDERSON; WOESSNER; HUNT, 2015, p.9).

In the context of urban studies, models are emerging as key-tools due to their capability to simulate the complex interactions among urban elements, identify problems and provide effective predictions in support of decision-making and sustainable policy (ORGANIZATION FOR ECONOMIC CO-OPERATION AND DEVELOPMENT, 2011). Forecasting urban models behave as vehicle to enable predictions on unbuilt conditions and test hypotheses of future urban interventions (BATTY, 2009). The model purpose influences the choice for the most suitable computation code (the most suitable software), as well as allows defining assumptions and simplifications. Similarly to Anderson, Woessner and Hunt (2015, p.17), once the purposes are established, the modeling process may start following a rigorous workflow including *model purpose*, *conceptual model*, *model design*, *calibration*, *forecasting simulations*, *results and uncertainty*. Model purpose deal with what the modeler wants to achieve trough the modeling exercise. In the *conceptual model*, the modeler has to develop a system of interactions involving the variables characterizing the phenomena that should be described, including boundary conditions and field data. At the *model design* stage, conceptual model is converted in a true numerical model by setting boundaries, designing the grid, assigning initial parameters in accordance with the previous step. With this model, first simulations can be run. *Calibration* stage takes more time than other steps; it is the process core, since conferring validity to the conceptual and numerical model hypothesis. Calibration occurs by comparing modeling output with the field observations. During this phase, the modeler has to identify the parameters apt to be calibrated, generally looking for those with the highest uncertainty. *Forecasting simulations* allow exploring alternative or future model

configurations by using the calibrated values and stressing one or more features that are assumed to change in the future. Finally, model results can be extracted from the previous stage. Such results should not lead to incontrovertible conclusions, since carry an amount of possible uncertainties including computational limitations, errors in model design, measurement errors in field observation and incorrect future assumption. To deal with such uncertainties, *sensitivity analyses* may allow defining the effects of parameters on model results and performance, by identifying the sensitive variables. Meanwhile, sensitivity tests can be used in the parameterization modeling phase to support the estimation of unknown parameters and the identification of key-variables (SONG *et al*., 2015). Such phase is able to greatly improve the numerical code comprehension by the development of focused numerical experiments.

In the city, modeling approaches can be applied to different urban problems, such as land use policy, transportation network, population and employment distribution, slums growth, climate change and urban comfort (WEGENER, 1994). Among the current urban-scale models capable to simulate urban morphology-climate interactions, ENVI-met (BRUSE; FLEER, 1998), Grasshopper (RUTTEN, 2007), CitySim Pro (LESO-PB), Rayman (MATZARAKIS; RUTZ; BRAUNSCHWEIG, 2005), Autodesk CFD (AUTODESK, 2009), IMM (DABC, 2010) and Urban Weather Generator (BUENO et al. 2013) are the most used by scientific community (NABONI et al., 2017).

2.10 Envi-met code

ENVI-met is a three-dimensional non-hydrostatic numerical code capable to simulate urban surfaces-vegetation-atmosphere microscale interactions, largely used in the field of urban planning, urban climatology and urban design. The software is proprietary and can run on standard personal computers. Michael Bruse started to develop ENVI-met in 1995 at the Ruhr-Universit¨, Bochum (Germany). Between the urban microscale softwares, ENVI-met is one of most complete engines nowadays available. ENVI-met is coded in *Object Pascal* programming language by using DELPHI. Unlike large-scale atmospheric models, ENVI-met boasts a better temporal and spatial resolution, allowing meshing grids between 0.5 and 10 m and time steps $\leq 10s$. In addition, in order to guarantee an accurate simulation of atmospheric dynamics involving urban areas and the overhead boundary layer, software abilities include the computation of energy balance of all surfaces and the physiological contribution of plants, beside considering the atmospheric processes as transient and prognostic. ENVI-met is

developed on two parallel models; the main model (3D) and an additional mesoscale model (1D). The differential equations in the model are solved using the finite difference method. The spatial and temporal evolution of the three-dimensional turbulent flow is based on the computation of the Reynolds-averaged Navier–Stokes (RANS) equations (Eq. (1)-(3)) and the Continuity equation (Eq. 4), simplifying the air density to a constant value applying the Boussinesq approximation. In order to keep the flow field mass conserving, Equation (4) has to be satisfied for each time step (BRUSE; FLEER, 1998; BRUSE, 2004; HUTTNER, 2012; SIMON, 2016). Mathematically:

$$\frac{\partial u}{\partial t} + u_i \frac{\partial u}{\partial x_i} = -\frac{\partial p'}{\partial x} + K_m \left(\frac{\partial^2 u}{\partial x_i^2}\right) + f\left(v - v_g\right) - S_u \tag{1}$$

$$\frac{\partial v}{\partial t} + u_i \frac{\partial v}{\partial x_i} = -\frac{\partial p'}{\partial y} + K_m \left(\frac{\partial^2 v}{\partial x_i^2}\right) - f\left(u - u_g\right) - S_v \tag{2}$$

$$\frac{\partial w}{\partial t} + u_i \frac{\partial w}{\partial x_i} = -\frac{\partial p'}{\partial z} + K_m \left(\frac{\partial^2 w}{\partial x_i^2}\right) + g\,\frac{\theta(z)}{\theta_{ref}(z)} - S_w \tag{3}$$

$$u_i = (u, v, w) \ and \ x_i = (x, y, z) \ for \ i = 1, 2, 3$$

$$\frac{\partial u}{\partial x} + \frac{\partial v}{\partial y} + \frac{\partial w}{\partial z} = 0 \tag{4}$$

where *Km* is the turbulent exchange coefficient, *f* is the Coriolis force, *p'* is the local pressure perturbation, θ is the potential temperature at level z, *θref* is the reference temperature representing the average mesoscale conditions, computed by the one-dimensional model (1D) running parallel to the main model (3D). *Su*, *Sv* and *Sw* terms indicate wind speed losses due to drag forces close to vegetation elements. *Ui* and *xi* represent the three-dimensional advection and diffusion terms (BRUSE, 1999; 2004).

ENVI-met is largely used by the scientific community and a great amount of urban studies using such numerical code are available. Unfortunately, in the literature, only few models built with ENVI-met code developed a proper sensitivity analysis that helps to delve into the confusing relationship between input parameters and simulation results. Vos et al. (2013) investigated the impact of vegetation on the air quality by modifying building geometry, wind direction, pollutant, and vegetation features in the model, especially focusing on the two latter more sensitive parameters. Despite the range of tested parameters, this study essentially focused on the behavior of vegetation and pollutants into the model (less relevant for this thesis). Tan, Lau and Ng (2016) conducted a sensitivity test to explore the relationship between sky view factor (SVF), mean radiant temperature (MRT), surface temperature (Ts) and vegetation, showing a more significant cooling of trees in high SVF areas. Salata *et al.*

(2016) investigated the model mesh sensitivity by comparing Tar, MRT, relative humidity (RH) and global radiation trends between models with different grids sizes, between 1 and 3 m. As expected, the study showed more accurate numerical results with finer mesh, while the coarser mesh exhibited a higher error between numerical values and field measurements. Notwithstanding, the finer mesh was not viable due to the higher computational effort.

2.11 Grasshopper algorithm integrated with Rhino

Grasshopper is a generative algorithm editor integrated with Rhino's 3-D (CAD) modeling tools (https://www.grasshopper3d.com/). Grasshopper and Rhinoceros (or Rhino) are coupled by connecting the geometric forms designed within Rhinoceros to the Grasshopper programming environment. Even if the algorithm code was developed by David Rutten in 2007, the evolution of the tool is made up by a vast community of users that freely create and share plugins. Generally, these plugins are developed to overcome specific problems found by users dealing with architectural-everyday-practice. This motivation confers great utility to the software advancements, in contrast with other "monolithic" CAD environments and proprietary tools. One of more attractive characteristic of Grasshopper is the application programming interface (API) that structures data exchange and parameterization using collections of basic objects called "geometric primitives", favoring the interconnection between plugins (LAGIOS; NIEMASZ; REINHART, 2010; DAVIS; PETERS, 2013). Models can be built-up by dragging objects-components on the model space and linking them in a sequence of input-output connections. Applications concern the field of parametric modeling for structural engineering and architecture design, energy consumption for buildings, radiation and climate analysis.

2.12 Urban form and climate local studies

To complete the background section, a collection of interesting urban studies dealing with urban morphology and environmental problems are discussed. All the works address the understanding of urban forms and their impact on urban climate, attempting to provide consistent findings and tools in favor of a more sustainable urban growth. Meantime, studies differ in scale of application, method, modeling process and data analysis. Thus, a vast overview is proposed, showing the real application of most of the concepts described so far.

Different research methods, in various geographical latitudes, have been developed to monitor the climate changes connected with the development of urban territories by way of expansion and land use transformation. Indeed, the speed of changes in urban field requires high attention and monitoring activities to understand mutations and forecast their consequences. Heisler et al. (1994) examined the influence of trees in a Chicago neighborhood, using field measurements sampled at 39 different locations. The gist of their work can be extrapolated to neighbourhood with a similar urban structure and climate. More recently, Duarte et al. (2015) presented a modeling assessment on the vegetation cooling effects in a subtropical urban environment. In order to assess the effectiveness of greening in preventing warming, ENVI-met parametric scenarios were realized combining high-density urban blocks with tree coverage. Between scenarios, small air temperature differences were obtained, while noticeable variation in MRT and thermal comfort were observed. In a similar climate context, Assis and Frota (1999) use available urban climate data together with physical simulations to assess how climate change is affected by urban forms. Simulations were carried out by using scaled physical models realized with great thermal resistance materials. Findings indicated that very dense settlements of very low-rise or high-rise buildings are not suitable for the city of Belo Horizonte (Brazil). At high levels of density, low-rise areas lacking of vegetation showed greater temperatures during the day while high-rise zones were hotter during the night. Furthermore, larger thermal amplitude was observed in compact and low-rise urban areas than high-rise ones. In a tropical warm-humid context (Bangladesh), Sharmin, Steemers and Matzarakis (2017), modeled in ENVI-met two residential urban areas in which climate differences (Ta ~ 3.3 to 6.2°C, MRT ~ 10°C) were measured on site. From findings, relative differences between the two sites were highly overestimated in terms of modeled MRT, while no variations were predicted in terms of air temperature. According to the authors, ENVI-met was unable to produce different microclimatic environments resulting from the variation of urban geometry; therefore, more assessments of microclimatic variables will need to deal with the limitations of modeling techniques.

An interesting speculation on urban morphology and urban microclimate came also from Switzerland, where Allegrini, Dorer, Carmeliet (2015) realized computational fluid dynamics (CFD) *3D steady RANS* simulations and building energy simulations (BES) on *CitySim* to investigate the climate impact of four swiss building morphologies. Main findings of this work show that façade temperatures are mainly affected by the presence of non-uniform height buildings and by the distance between them. Meantime, the modeling process

was only based on numerical experiments, not calibrated or validated on field data. The urban morphologies were limited to parametric representations, even if similar to reality. With a different approach, Tadi et al. (2015) implemented the IMM (Integrated Modification Methodology) strategy to enhance urban metabolism of a Rio de Janeiro existing area (Porto Maravilha) under transformation, showing how urban morphology could be re-modeled in a lower energy consumption form. IMM is suitable to analyze great urban areas, considering cities as systems of key-categories; however its predictions have little utility if urban morphology-climate interactions are rigorously investigated. For São Paulo city (Brazil), Marins and Romero (2012; 2013) presented a method for urban energy planning at district scale, integrating the morphological urban structure with urban mobility, environmental aspects, energy demand and supply. Results suggested that building and urban density should be further balanced with open spaces to optimize energy performances, enhance urban climate and improve mobility services.

Overall, even if urban researchers address many efforts to develop intersectional studies, aiming to face city as a complex system of exchanges, relationships and interactions, multi-scale approaches are still rare in the field of urban climate studies (CHATZIDIMITRIOU; YANNAS, 2016), while mono-scale works prevail. According to Sassen (2009), cities embed a range of scales through which the environment dynamics occur; hierarchically, the large urban scales are divisible into a certain number of small-scale spaces (JIANG; CLARAMUNT, 2002). Mirzaei (2015) points out a gap between building-scale, micro-scale and meso-scale models studying UHI; weaknesses of such mono-scale models are highlighted and the need for more multi-scale studies is claimed. Ratti, Raydan and Steemers (2003) state that the environmental context in which cities grow constitutes a multi-dimensional issue; their study takes into account the influence of climate zones, the built forms proportion and building parameters a□ecting the shadows and daylight distribution. As stated by Emmanuel (2018), to enhance the indoor thermal comfort, more e□orts should be made at the neighborhood scale, designing linkages between building geometry and outdoor environments.

3   Case study

Goal: This chapter introduces the case study and the urban region in which it is inserted. In order to face the research challenges, up-close understanding the complex relationships linking urban transformations and climate change, a case study was selected as a place of investigation. The case study is a neighbourhood under urban development, located in the City of São Paulo, an effervescent and very populated metropolis of the South America. In this area, several fieldworks, inquires and measurement collections were carried out along four years. All this collected material contributed to understand the urban context under analysis, bringing out its inherent complexity and reveling issues. In a way, the process of land discovery has also guided the research process, suggesting which investigations should be conducted and which problems deserved further assessments.

3.1   *São Paulo context*

To be located near the Tropic of Capricorn, the metropolitan area of São Paulo (latitude -23°21', longitude -46°44') is part of a transition climatic region lying among the humid tropical climate of altitude and the subtropical climate. The topography of the Atlantic *plateau*, on which São Paulo is located, is characterized by the most varied geographic forms, with peaks between 720 m and 850 m, about 45 km (on average) away from the Atlantic Ocean (TARIFA; ARMANI, 2000). Despite its altitude and distance from oceanic side, at the early hours of the afternoon the city is skimmed by a sea breeze that put on interaction the city mass with the sea environment. This event takes on a certain importance, influencing the local climates within the entire urban region. The inertial property of the sea water contributes to release the heat slowly relative to air, favoring a milder climate. As consequence, the propagation of heat from the Atlantic to São Paulo, carried by wind, softens hot or cold temperature drops, beyond facilitating the dispersion of pollutants.

According to the Köppen-Geiger classification, São Paulo is identified as a wet subtropical climate (Cfb). The region is mainly characterized by a dry winter (from June to August), and a very rainy wet summer (from December to February). The daily temperature range is significant and higher than the annual temperature range (WEATHER STATION IAG-USP, 2019). The urban conglomeration of São Paulo constitutes the 4th metropolitan area in the world for population (21 million). In the center of this huge area, the municipality of São Paulo takes place, accommodating around 11 million inhabitants, distributed on

1,521,110 km² and 31 districts. The municipality boundaries include a watershed area at the South (*Represas Billings e Guarapiranga*) and an environmental reserve on the North side (*Serra da Cantareira*), providing water and greenwoods. The water system is characterized by the basin of Alto Tietê, in which Pinheiros and Tamanduateí rivers are tributaries (BARBOSA; FERNANDES, 2015). Over the time, the urban area has sprawled on the North and South directions, swallowing the land of the reserves. Highest population growth rates occurred in the first half of the 20th century, with peak in the 1950s (5.9% per year); then, among 1991 and 2000 the growth rate slowed, sharply decreasing in the central regions while remaining high in the suburb (MARQUES; REQUENA, 2013; LAMOUR, 2018). This grow pattern can be explained through the incessant limitations imposed by masterplan to density and floor area ratio, as well as to an increasing dwelling demand (MACEDO; IMBRONITO, 2016).

From the last demographic census (IBGE CENSUS, 2010), a more heterogeneous tendency was observed in the central regions of the city, where some districts decreased and others increased their rate; meantime, the sprawl persisted on the edges of the metropolitan region where low-income inhabitants live. This recent pattern could be due to the heterogeneity of contemporary real estate production that identifies niches of interest to explore, focusing on some districts and forgetting others (MARQUES; REQUENA, 2013, LAMOUR, 2018). Currently, the average population density is 74 inhabitants/ha. The average built density has FAR equal to 1. Since São Paulo urban morphology is extremely heterogeneous and grew-up rapidly, population density varies from district to district. In addition, in the same district, built and population density can diverge one from other. As an example, whereas the districts of República, Bela Vista and Santa Cecilia achieve the highest values of built and population density, other districts as Sé and Brasilândia show high values in only one of categories. In comparison with other metropolises, São Paulo counts a reasonably high average population density; however, if the densest districts of every city are compared, São Paulo shows values well below other urban areas (280 inhabitants/ha). As an example, the city of Los Angeles has an average population density equal to 30 inhabitants (in) for hectare (less than the half of São Paulo) while its denser district gathers 445 in/ha; the island of Hong Kong counts 63 in/ha as average people density, rising to 259 in/ha when non-buildable areas are excluded and achieving 520 in/ha in the denser districts of the city (GUSSON, 2014; GUSSON; DUARTE, 2016).

To introduce São Paulo urban morphology, a Local Climate Zone map is presented (Figure 1a), obtained adjusting the original LCZ map of the whole metropolitan area realized

by Ferreira et al., 2017 (WUDAPT methodology) to the boundaries of the municipality. The adjusting was made by GIS tools. Map shows a variegated mix of local climate zones, conventionally associated with certain urban features. All categories are included, except for LCZ 2 (compact mid-rise built class) and LCZ E (bare rock or paved land class) that had not been detected by Ferreira et al., 2017 due to a low number of samples and too small size areas. Furthermore, LCZ7 (lightweight low-rise built class) was integrated to LCZ3.

Figure 1 - São Paulo LCZ map with legend (a); percentage area of LCZ in São Paulo (b); Low-rise and High-rise LCZ map with TOD axes demarcated and legend (c); percentage area of high-rise and low-rise LCZs (d); example of low-rise and high-rise fabrics in São Paulo (e).
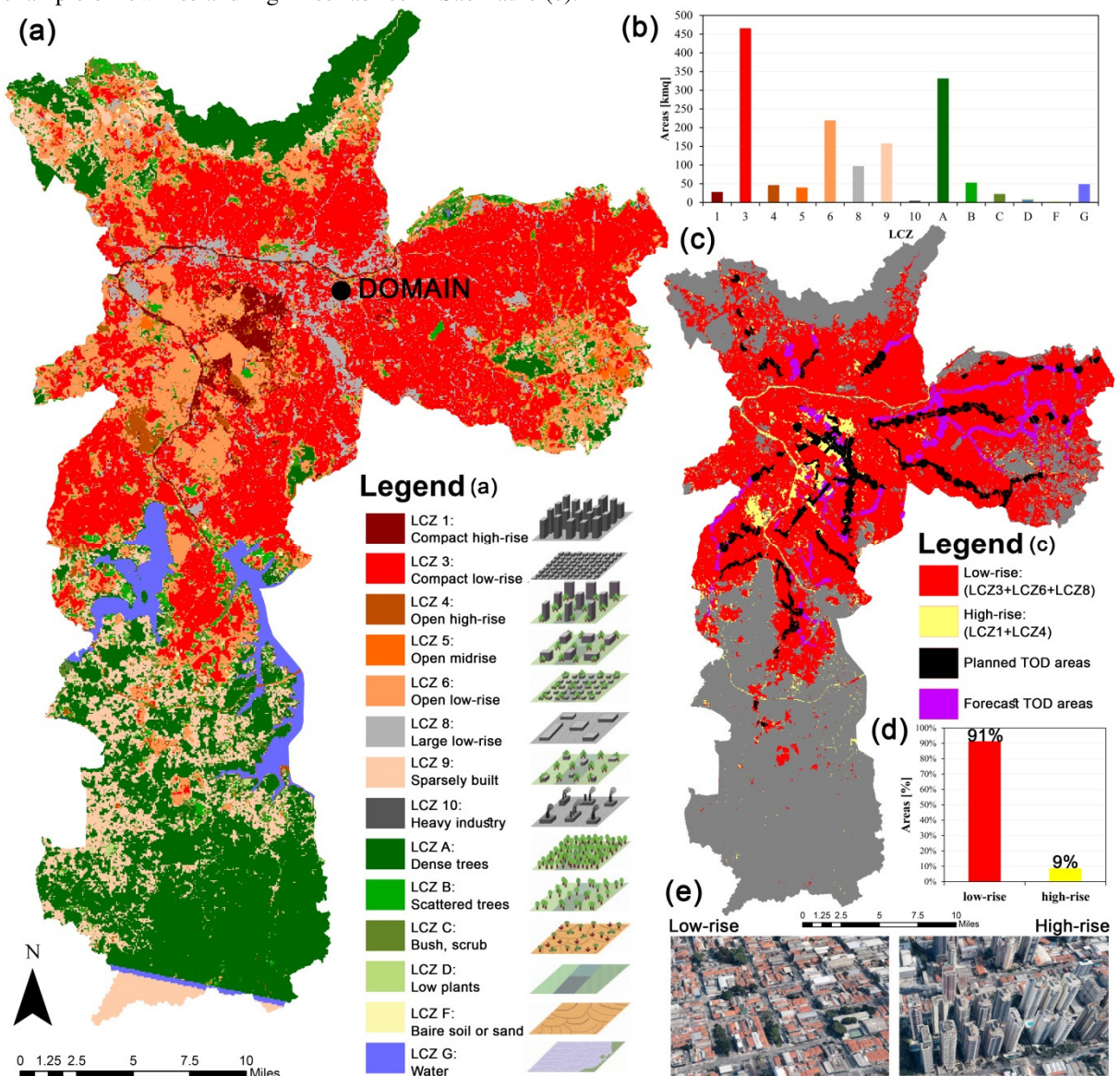
Source: Martina Pacifici, 2019, extracting LCZ map from (Ferreira et al., 2017) and adapting LCZ legend from Stewart and Oke (2014).

Within the boundaries of municipality, the highest frequency category (Figure 1 b) is LCZ 3 (30%) indicating compact low-rise zones with 1-3 floors buildings, stone and brick surfaces, few or no trees, mostly paved soils (Stewart and Oke, 2014). This built class surrounds the city downtown, sprawling toward the east-region and expanding to the south-water lands. On the north-direction its growth is stopped by forests. In these areas, a built coverage area (BCA) and a high SVF are expected. Historical workers' housing (Mooca), irregular dwellings (Brasilandia), favelas (Casa Verde, Cachoeirinha) and suburb residences (Penha, Itaquera, Itaim Paulista) are included (Figure 1e, left). The other low-rise categories contribute to the LCZ map by covering the 14% (LCZ 6) and the 6% (LCZ 8) of the total municipal area. LCZ 6, involving open arrangements of low-rise buildings (1–3 floors), built-up with various construction materials and surrounded by greenery and trees (STEWART; OKE; KRAYENHOFF, 2014), occupies the west region of the Municipality (Jardins, Morumbi, Alto da Lapa) in which high-income people sectors live, and the northern edge close to *Cantareira*. LCZs 8, with open clusters of large low-rise buildings, arranged on paved lands, built up with concrete and metal construction materials, few or no trees around (STEWART; OKE; KRAYENHOFF, 2014), are distributed along the *Marginal Tiete* avenue and the industrial axis that from *Mooca* continues toward south-east direction along *Avenida do Estado*.

All the low-rise categories (LCZ 3, LCZ6, LCZ8) cover together the 91% of Sao Paulo Municipality. The remaining 9% is interested by taller built classes or no built-up land (Figure 1d). Mid-rise built classes occurs in the map only arranged in open layouts (LCZ 5), while compact arrangements are insignificant. LCZs 5 (3%) are classified as 3-9 floors mid-rise buildings organized in open arrangements covered by green pervious lands (BCA = 50%), scattered trees, constructed using concrete, steel, stone, and glass (STEWART; OKE; KRAYENHOFF, 2014). LCZs 5 are generally organized in little arrangements scattered on the edges of the municipal territory; a higher frequency of this class can be observed on the far east of the city. The union of compact high-rise built classes (LCZ 1) and open high-rise (LCZ 4) is 5% of the Municipal area, showing the low percentage of verticalized urban areas in São Paulo (Figure 1e, right). LCZs 1 (2%) are limited to city center, including blocks around *Sé*, *Bela Vista* and *Higienópolis*, arranged in a dense mix of tall buildings made up of concrete and glass, poor vegetation and paved soils. LCZs 4 (3%) are isolated zones through the south-west region (Morumbi, Vila Mariana, Congonhas) in which tall buildings and open spaces are more balanced, opening to greater SVF and lower BCA. In terms of land classes, the most frequent category is LCZ A (22%) populated by dense trees, followed by LCZ B and

LCZ G (3%) including respectively scattered trees and water, ending with LCZ C and LCZ D (1%) providing bushes and low plants. On the south tail of the Municipality, where LCZs A and LCZs G abound, the urban pattern leaves space to a natural landscape of forests and water bodies. Nevertheless, the rural-urban border is an ever moving transition line, thus small and medium-sized buildings sparsely arranged (LCZ 10) expand all around, decreasing the natural-urban land ratio.

The LCZ study constituted a general premise, able to characterize the urban region as a whole. The amount of local climate zones described above, together with their diversity, reveals an extremely varied morphological landscape. Climatically, such diversity leads to a set of different homogeneous environments, associated with certain regimes of temperature (STEWART; OKE, 2012).

The morphological heterogeneity implies different lifestyles, income, forms of mobility and accessibility to city opportunities. In this perspective, urban morphology is related to a certain quality of life. In suburbs, urban supply of educational, health and entertainment equipments is little and poorly qualified in comparison with the city center. To take advantage of good services, inhabitants spend a lot of time and money in mobility. According to Maricato (2013), in São Paulo the average time for traveling is estimated to 2 hours and 42 minutes; however, for 1/3 of inhabitants this time is greater than 3 hours, while for 1/5 of people the average time grow up to 4 hours (Pequisa Origem Destino 2007). In accordance with Santos (1990), when the travel time increases, physical and mental exhaustions grows too; the worker free-time is degraded to an extension of the working day. Among 1977 and 1988, the construction of low-income residences in the east zone, together with the industrial impetus in the south zone, induced a great amount of commuters traveling between the suburb and the center (VILLAÇA, 2001; MEYER; GROSTEIN; BIDERMAN, 2004; ARBEX et al., 2016). This mobility pattern continues until today, exacerbating the city fragmentation and consolidating suburban ghettos.

In order to further explore the consequences of such dysfunctional system, a preliminary assessment was developed on the spatial distribution of accessibility in São Paulo municipality (ARBEX et al., 2016). In this work, an accessibility index representing the amount of urban equipment accessible in 30 minutes was computed. Combing this index with other variables (*Pesquisa Origem Destino* 2007), such as average traveller income and first user boarding, the pattern of spatial segregation in the city was visualized.

Figure 2 - First users boarding density at 4h, 6h and 8h (a); intensity of equipment on the Sao Paulo Municipality for Leisure, Health, Education and All equipment.
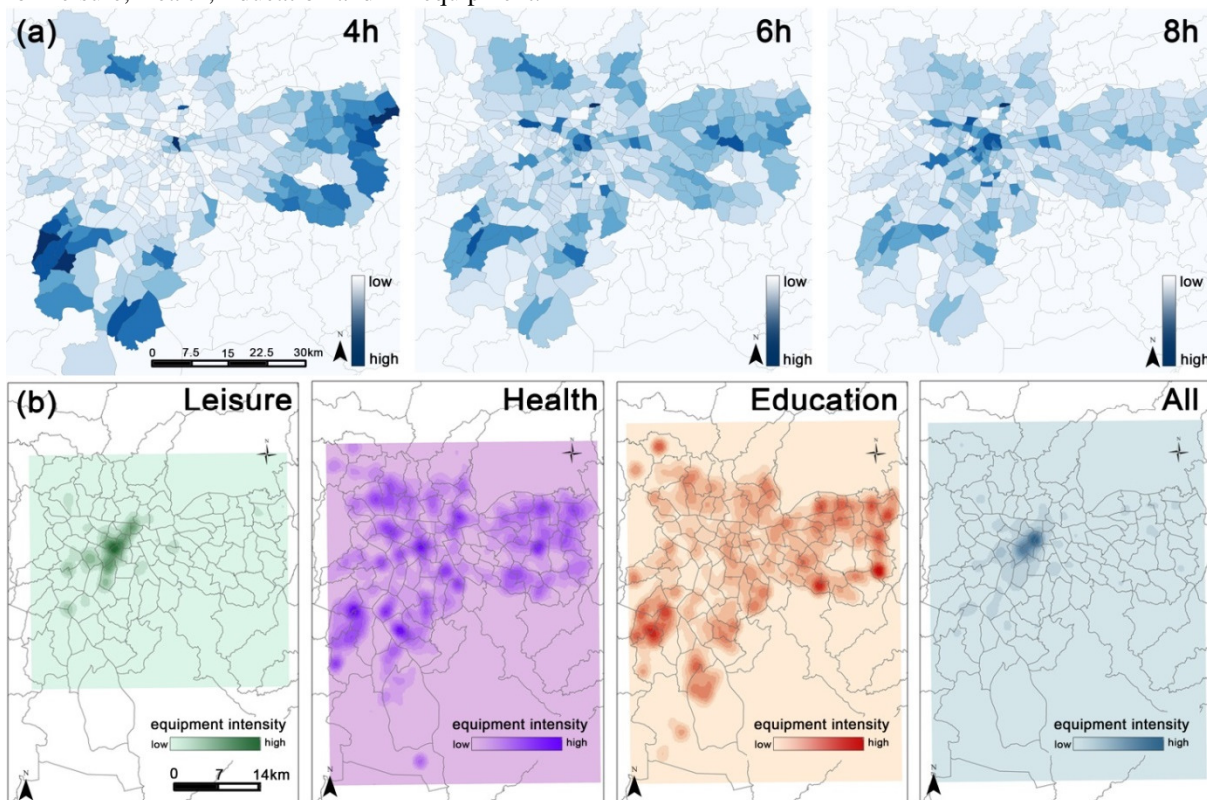
Source: Martina Pacifici, 2019, developed with colleagues along the course Exploratory Analysis of Spatial Data applied to Planning, Operation and Transport Infrastructure research and published in Arbex et al. (2016)

On the whole municipality, Figure 2a shows that the first boarding occurs in the suburb where residents are undergone to travel times greater than 30 minutes to access their final destinations. Basically, suburban people have to start their journeys at very early morning hours, such as 4 a.m. and 5 a.m., to work or simply "use" the city. Further analyses associated this low accessibility with a low income. Additional investigations highlighted the concentration of urban equipment in the central areas of the city; such pattern was well evident in the categories of shopping and entertainment, while much more widespread in the case of health and education equipment (Figure 2b).

3.2   São Paulo planning

The urban growth rates at the city edges, the emptying of city center and poor accessibility conditions for low-income inhabitants, highlighted the need to redistribute people density and re-orientate real estate production in São Paulo. According to Lamour (2018), in 2006 the *Integrated Urban Transport Plan for the Metropolitan Region of São Paulo 2025- PITU 2025* (STMSP, 2006) claims the need to combine the development of

transport axes with a suitable land use policy, densifying the urban areas around train stations, urban equipments and services. In agreement to this call, in 2014, the reviewed Masterplan of São Paulo Municipality sealed a new proposal in favor of an integrated urban development, involving transports, urban density and land use policy. The main targets of this Plan concern: the preservation of green boundaries, containing sprawl (Art.7, I), the allocation of urban growth along the medium-high capacity transport network (Art. 7, II), the closeness among dwelling and workplaces, decreasing daily transfers (Art. 7, III), the expansion of collective urban transport, decreasing cars (Art., IV), the reduction of anthropogenic factors, promoting renewal energies and enhancing the sustainable built construction (Art 7., XI). To attend these aims, the Masterplan theorizes a network of urban areas along the main transport lines, called *Structuring Axes of the Urban Transformation* (EETU), in which people and built density have to be promoted (Figure 1c). The guidelines orienting EETUs are based on TOD principles, in accordance with other megacities around world (Figure 3a). The EETU influence area is defined along the transport lines (150 m from the road axis for both sides) and around train stations (circumscribed in a ray of 400m) (Figure 3b). Two years later, the EETU strategy was detailed through the reviewed zoning plan, called *Law of Land Parceling, Use and Occupation* (LPUOS) (SAO PAULO MUNICIPALITY, 2016), that introduced the urban zones structuring the urban transformation, including on-active (ZEU) and forecasted (ZEUP) areas. In ZEU and ZEUP, high density, accessibility, mix uses and high-quality urban spaces are enhanced. The minimum FAR index is 1 while the maximum is 4, granted through a financial contribution. No limits are applied to building height. In terms of BCA, the maximum land coverage is 0.85 for lots smaller than 500 m^2 and 0.70 for lots greater than 500 m^2. The setbacks are at least 5 m for front sides and 3 m for back and lateral ones. Parking spaces per housing unit are limited. For lots among 10,000 and 20,000 m^2, perimetral walls are limited to 25% of the lot border, 25% of the building façades have to be designed as streetfront interfaces and 20% of the lot has to be allocated to public use to improve pedestrian circulation and vivacity. Areas not addressed to residential activities are not computed within the FAR index, until 20% of building total built area, in order to incentive mixed uses. Lastly, the apartment size is limited since a minimal quantity of housing units is imposed per lot, obliging to 20 m^2 (for ZEU) and 40 m^2 (for ZEUP) the maximum land portion per unit.

Despite the valorous intents, the definition of ZEU and ZEUP is supposed to be insufficient to produce a good implementation of TOD principles. Lamour (2018) criticized the application of certain precepts concerning social diversity, mixed land use and active

facades. Marins et al. (2017) state that the actual urban regulation does not provide precepts to improve the pedestrian experience into open spaces and lacks of appropriate assessment tools to monitor the microclimate effects related to the increase of density. Environmentally, a quite shallow approach was observed through the law guidelines, letting fall some important considerations into oblivion. The allocation of new built elements into the city transforms the morphology of districts and consequently leads to climate changes of little and larger scale. Why environmental risks were not included within the urban discussion dealing with EETU? Which climate implications can be related with the insertion of higher and denser fabrics into the city?

Figure 3 - Design Concept for ZEU and ZEUP (a); support information (b); excerpt of a ZEU influence area (c)
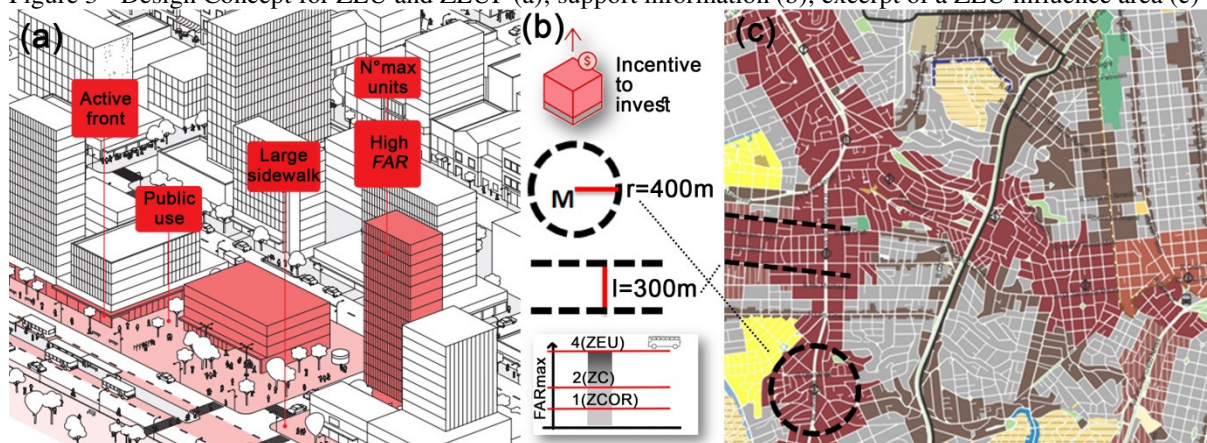
Source: Martina Pacifici, 2019, adapted from illustrated PDE text (a), adapted from illustrated LPUOS text (B)

3.3 Domain

To understand the implications of TOD strategies and recent land use policies on the context of São Paulo city, a case study was selected within EETU zones (Figure 4a-b) and an in-depth urban morphology and climate investigation was carried out. The case study-domain (~10 ha) is sited in the East zone of the city (Figure 4c), in the neighborhood of Belenzinho. Domain belongs to ZEU influence area of Belem metro station (Figure 4d-e). Topography consists of flat terraces and wide hills, marked by the presence of old factories and warehouses, with roofs and surfaces of high solar absorption, in which a strong heating was proved by daytime satellite imagery (TARIFA; ARMANI, 2000). The domain consists of eight blocks and is crossed by two important transport axes. Blocks' morphology is hybrid since two different building typologies coexist: newer fabric (a) and the oldest fabric (b) (Figure 4f).

Figure 4 - Belenzinho in the city of São Paulo (a), transport axis crossing Belenzinho and EETU zones (b), case study domain (c), influence areas of ZEU and ZEUP (d) Metro lines and Belem station (e), two fabrics *a* and *b* (f).
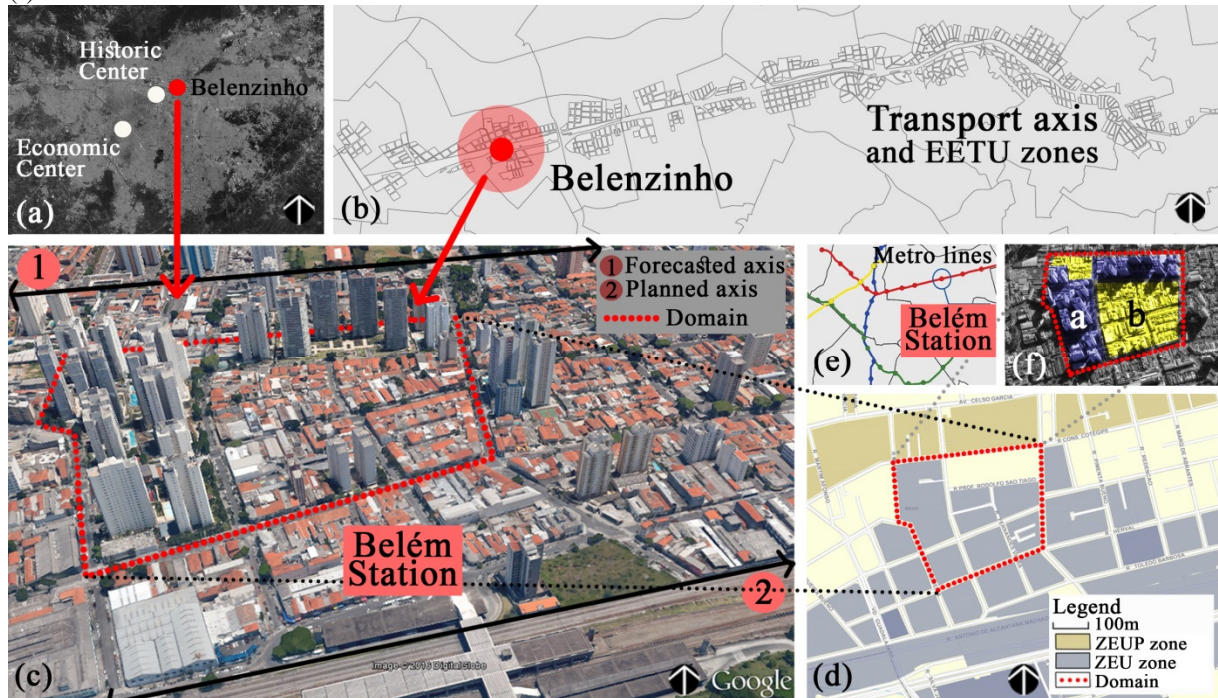
Source: Martina Pacifici, 2019 (a-f), adapted from Google Earth (a-c-f), based on the Geosampa-Digital Map of São Paulo City 2016 (b-d), adapted from Lamour, 2018 (e).

Fabric *a* was classified as high-rise fabric while fabric *b* as compact low-rise fabric (Figure 4f). Blocks belonging to fabric *a* are private condominiums organized in clusters of towers, from one to four buildings. Around the towers, open spaces occupy the rest of the lot. Towers' height goes from 40 to 89 m, thus relevant shadings are projected on the ground and on other buildings' surfaces. The most common materials are concrete, white plaster and wide glass surfaces. Moderate tree coverage is found along streets, while ornamental plants populate the inner-blocks-open spaces. Large road sections receive different forms of mobility, even if in same cases narrow streets were maintained.

Blocks belonging to fabric *b*, instead, are constituted by 2-3 floors houses, without lateral and front setbacks, with dentate backyards of different dimensions, no visible and accessible from the street. Buildings' structure is made of bricks or concrete; wall and roof surfaces are of various types (ceramic, plaster of different colors, bare brick, terracotta and metallic tiles). Tree coverage is poor, both inside the backyard and along the streets. Restricted road sections slowdown cars and invite to walk. The high-rise fabric is of more recent construction than the traditional low-rise zone: generally, in last decades towers have replaced factories, warehouses and workers' housings of the industrial past. Evidences of such

ancient equipments are still present in the district and a land use re-conversion is currently a process underway (Figure 5).

Such modifications induced by the real estate market leaded to lots' exploitation processes and morphological modification of the preexisting low-rise fabric, until then populated by small residences and industrial factories. This intensification in construction activities increased the pedestrian traffic, the parked or in motion vehicles, as well as the need for services and commercial activities. The proliferation of high buildings, close to each other, implicates the arrival of urban canyons and deep shaded areas.

More recently, with the acceptance of the reviewed land use (SÃO PAULO MUNICIPALITY, 2016) following *TOD* strategies, new real estate market initiatives are expected due to the incentives granted by municipality. As in the past, these circumstances could seriously affect the current pedestrian comfort conditions, as well as the indoor well-being at surrounding housings, if the study of the existing climatic environment is not taken into account to orient urban future developments and densification in ZEU and ZEUP. Understanding the environment of these urban territories under change is of critical importance to predict the insertion of new buildings in the existing landscape, as well as to mitigate adverse climate effects.

Figure 5 – Views from the neighborhood of Belenzinho, showing contrasts between fabrics *a* and *b*.

Source: Martina Pacifici, 2019; map adapted from Google Earth

4 Material and methods

Goal: This chapter introduces the whole procedure of investigation, detailing the set of methods, equipment, specifications and software that were implemented along the research process. The initial two sections (4.1, 4.2) explain the procedures of data collection and analysis, split in two phases, according to the real research chronology. The rest of sections (4.3, 4.4) concern the modeling activities performed in ENVI-met, Grasshopper and Matlab codes. In addition, the chapter intends clarify the sequence of the different research phases, showing the combination and interdependence among all stages.

In order to approach the issue of urban transformation and measure its climate impact, an integrated procedure of modeling assessment was developed, focusing on the interactions among urban morphology and climate. The creation of an urban model supports the interpretation of reality, the understanding of the present, but also should be able to forecast the effects of future planning actions. Since the whole complexity of real world involves uncountable processes, a simplification of the urban system is needed to develop a manageable representative tool. To base such simplification on solid hypothesis, a conceptual model of the urban system has to be developed. A conceptual model summarizes the main processes characterizing the real world and is sustained by field information from the site in analysis, together with knowledge produced in similar contexts (ANDERSON; WOESSNER; HUNT, 2015, p.29). In a nutshell, a good modeling process is based in an accurate conceptual model which in turn depends on a thorough understanding of the urban problem under analysis. Therefore, to assess urban fabrics affected by densification, verticalization and urban transformations, a specific case study had to be chosen in the context of the recognized problem. The case study was selected from the city of São Paulo, in which these urban phenomena are currently underway. In this site, to nourish the conceptual model design, an in-depth fieldwork was realized, identifying the essential features, processes and events produced by the morpho-climatic interactions and induced by the anthropogenic actions. The whole fieldwork was accomplished in two phases. The first phase (4.1) was purely explorative (PACIFICI et al., 2017), while the second-one (4.2) produced long-term data series to calibrate and verify the model (PACIFICI; RAMA; MARINS, 2019). Both phases were functional to the design of a conceptual processes-based model, as well as to produce a robust data collection gathering many kind of information. From data analysis, the most accurate explanation of the field processes was attempted and findings were transferred to the modeling phase. This new stage was realized in an ENVI-met modeling environment, and

subsequently integrated in a Grasshopper system. In ENVI-met, after the calibration, forecasting simulations were developed and design considerations raised. The whole workflow (Figure 6) was applied to a specific context of São Paulo, but is suitable and rather general to be replicated to different urban situations and climate conditions, providing an effective method for the morphological and climatic investigation of cities at multiple scales.

Figure 6 - Workflow of the integrated procedure proposed
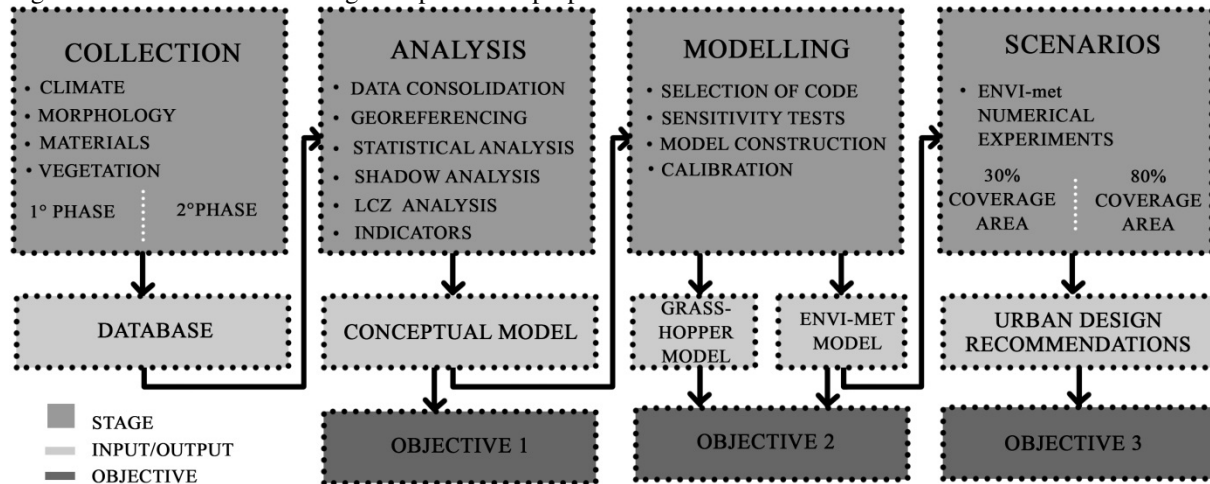
Source: Martina Pacifici, 2019

4.1 Climate and morphological analysis (phase I)

To get start, a preliminary delimitation of the study domain at the neighbourhood scale was required. More than one urban site was considered in the city of São Paulo (not showed). The chosen domain was selected to be enough representative for the research purposes. Its size was limited to the local scale, considering the feasibility of field surveys, the equipment and operator security. Once the domain was defined, the study of its spatial structure was undertaken and its shapes were characterized as a whole. Available geometric and spatial data of urban features – heights, land coverage, land use, built volumes, backsides, vegetation - were collected from the available databases and integrated by field measurements. Subsequently, they were explored by data analysis tools to understand the spatial distribution of urban elements and features. After the morphological survey, a climatic collection was conducted in the study area; representative study points were selected in the domain (Figure 7).

Figure 7 – Domain and climate points (left), meteorological station on transect (right, up), low-rise and high-rise fabrics in Belenzinho (right, down).
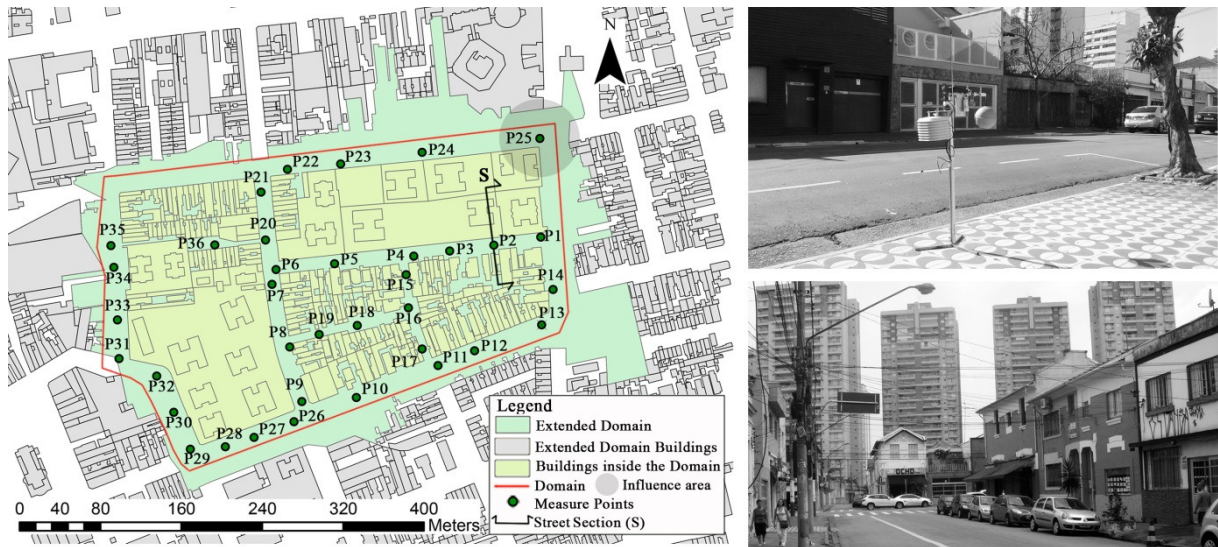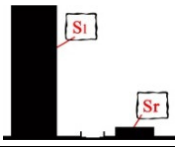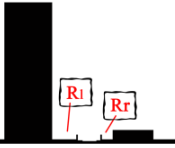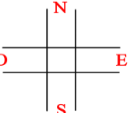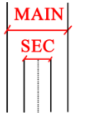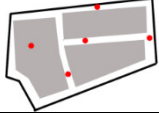
Source: Pacifici et al. (2017)

Each climate point was associated with a section of urban canyon to be explored. Thus, thirty-six representative road-sections were investigated inside the domain (Figure 7) as instances of different spatial situations to be analyzed. All street sections are made up by the street space flanked by built elements on both sides. Each section differs from the others by one or more of morphological properties. Such morphological properties (also called *categories*) include the height of buildings (from 0 to 100m), the length of building setback from street (from 0m to > 10m), the street orientation (north-south, east-west), the street typology (main or secondary), and the placement of road section in relation to the fabric (inside or outside the block). Categories allowed distinguishing one urban section from the others and are summarized in Table 1. The building height category affects the buildings shading, while the setback category influences the fabric compacity. The street typology affects the traffic volume, as the transport of pollutants. The street geographical orientation is taken into account owing to its influence on natural ventilation and surface temperatures. Finally, the last category informs about the influence of the surrounding domain on each point. The thirty-six samples represent a wide range of climate conditions pedestrians may experience by standing and walking across the neighborhood open spaces, testing different comfort environments. In fact, for Oke (1987), on the canopy layer, the air performance is related to the type of canyons and the distance between buildings. Points occupied public spaces, because the entrance to most of the blocks was closed with gratings. In accordance

with Oke (2006), points close to crossroads were just a little retreated from the intersection to avoid interferences with the orthogonal street.

Table 1 - Characterization of Domain in Categories and Classes

Categories		Sketch	Description	Classes (m; -)	Measured Points
Built Space	Buildings Height		Street sections are bordered by a pair of buildings, on both sides. Building heights belong to one of the 4 classes.	$0.0 < H1 \leq 0.5$	6,14,25,27,34,35
				$0.5 < H2 \leq 10.0$	2-22,24,26,28,29,31,33,35,36
				$10.0 < H3 \leq 30.0$	10,13,21-23,27,32
				$30.0 < H4 \leq 100.0$	1-5,7-9,23,25,26,28-32,34
Open Space	Buildings Setback		Street sections are bordered by a pair of buildings, on both sides. Building setbacks belong to one of the 4 classes.	$R = 0.0$	6-15,17,20-22,24,26-29,31-33,35,36
				$0.0 < R \leq 5.0$	1,3-5,15,16,18,19,23-25,28
				$5.0 < R \leq 10.0$	1,2,5,9,26,30,32,34
				$R > 10.0$	2-4,6-8,14,23,25,27,29-31,34,35
	Street orientation		The street in which the urban sections are traced can have one of two orientations.	North-South	4, 6-9,12,14-17,20,21,29-35
				East-West	1-7,10-13,18,19,22-28
	Street Typology		Streets can be main or secondary; first one receives a greater traffic volume than other	Main street: St > 12.5	6-14,20-35
				Secondary street: St ≤ 12.5	1-7,12,15-19,36
	Position within the fabric		Urban sections take place inside or on the domain boundaries, inside or outside blocks	Along boundaries	10-14, 22-35
				Inside boundaries	1-9,15-21,36
				Inside block	36
				Outside block	1-35

Climate measurements were strived as much as possible simultaneous, analyzing the climatic variability between points under similar weather conditions. A transect path was traced through the thirty-six points to explore the microclimate environments that make up the urban domain by a mobile weather station, under autumnal and winter meteorological conditions. Simplification was necessary to create an applicable protocol, taking into account the few resources availables (two operators and one meteorological station). The collection points were placed in the same relief conditions, on the sidewalk, a space of morphologic binding and meeting between urban forms. The equipment was thus protected from the cars movement and accessible by operators. The equipment used and variables measured are included in table 2:

Table 2 - List of used equipments

Equipment	Model	Measured variable	Accuracy
Datalogger	Hobo, U23-001	Air temperature and	± 0.21 °C (from 0°C to
Solar shield	Hobo, RS-1	Air temperature and	50°C)
Hot wire anemometer	Testo, 425	Wind	± 0. 10 m/s
Digital lux meter	Homis, 630	Illuminance	
Thermographic	Fluke, Ti105	Surface temperature	±2°C
Photographic camera	Nikon, Coolpix 4500	Sky view	
Fisheye lens	Nikon, FC-E8 0.21x	Sky view	
Electronic tape	Leica, DISTO D810 touch	Geometric lengths and heights	

In order to assess the climate variations under approximately simultaneous atmospheric conditions, the measure time between the sample points was minimized to 15 minutes; this is the time required for the HOBO equipment to stabilize (5-10 minutes), for the hand measurements, plus the time required to move the equipment from one point to the next (3-5 minutes). It was thus possible to measure 12 points a day twice, in the morning (6 a.m. to 9 a.m.) and along the afternoon (13 a.m. to 16 a.m.). These temporal ranges were chosen by detaching the colder and the warmer periods that mark the daily temperature trend during the cold season. The weather bulletins of the nearest fixed meteorological stations – IAG USP (WMO: 83004, LAT: -23.65, LONG: -46.62) and CETESB Marg. Tietê Ponte dos Remédios (LAT: -23.52, LONG: -46.73) - were taken as a reference. In the case of the morning period, the band 5-6 a.m., albeit suitable to intercept the minimums, was discarded to protect the equipment and operators from nocturnal criminality; hence, no measurement was made before 6:00 a.m.

To achieve the real moisture content in the air, specific humidity was found more useful to be observed in comparison with relative one. Specific humidity (water vapor mass *per* mass of the air parcel) was obtained from relative humidity by means of a free humidity calculator *Rotronic* (www.rotronic.com). To perform the transformation, values of atmospheric pressure were mined from CETESB database - Marg.Tietê-Pte Remédios meteorological station - in the measurement period.

To measure the surface temperature, a thermographic camera (Operator 1) was used. The measurements were taken at three points of each cross-section: the street pavement, the sidewalk pavement and the building façade wall adjacent to the sidewalk. A specific emissivity was set before measuring each material. These emissivity values were obtained from Oke (1987); in the case of asphalt, an experimental measurement of the emissivity was performed on a sample of the material, made available by the Paving Technology Laboratory

of the Transport Engineering Department (LTP) of USP. The resulting value, 0.96, was adopted in the field. Eighteen hours distributed on three days of fieldwork were necessary to complete the measurement of the study area by two operators. The entire measurement cycle was repeated twice, once in the autumn and the other in the winter. In the first test, because of bad weather conditions, the three days were not consecutive (4, 25 and 26 of May 2016). In the second case, the progression was respected (12, 13, 14 and 15 of July 2016). Table 3 summarizes the organization of tasks which guided the field measurements.

Table 3 - Organization of field work - Execution Sequence for simultaneous measurements in field

Intervals	15 minutes		
	5 minutes	3 minutes	7 minutes
Hobo Equipment	transport	stabilization and one automatic measurement of Ta and RH	
Other Equipments	transport	manual measurement by operators of T_s, w_s, w_d, Illuminance	
Operator 1	- go from one point to the next	- measures* T_s of pavements and wall - takes sky view photos	- measures the street length, sidewalk length, retreat length, building height, by electric tape placed on the tripod *one measurement for each pavement*
Operator 2		- notes sky condition, shading, tree coverage, equipment location	- measures intensity and direction of wind^ - measures the illuminance^ ^ *one measurement per minute (7 times)*

Source: Pacifici et al. (2017)

After the fieldwork, data were organized and processed to observe micro-climatic variations between collected points. The average correlation between surface temperatures and illuminance was computed at all the points by Spearman's Rank-Order Correlation. Subsequently, the Sky View Factor (SVF) was chosen as split parameter to cluster the data population in two groups (high SVF, low SVF). SVF was obtained from the photos taken with fisheye lens, using the software Rayman 1.2. 25% was considered as the SVF cut-off value to improve the correlation between surface temperature and illuminance. Finally, the presence of tree coverage was also observed and correlated with temperature.

In order to understand the implication of the urban form on the collected climatic data, the influence area around the measured points was also explored in greater detail, evaluating its morphological attributes. To design a proper and well-sized influence area, several references were consulted. According to Oke (2006), for the temperature and humidity sensors, the influence circle varies with the building density around a radius of 0.5 km. However, when the sensors acquire the signals via turbulent transport, the source area is an elliptical shape, aligned in the upwind direction. For Grimmond (2006), additional factors

should be considered in the choice of the influence area, such as the measurement method, the equipment location, the surface on which it is positioned, the weather conditions, the research objective and the type of climatic variables measured.

In the case of this work, because of the great amount and diversity of the variables considered, distinct influences areas should have been defined. Therefore, in order to evaluate the influence of urban morphology around the climate station, a compromise was achieved and a round 40m-large influence area was adopted for all measuring points. The influence area includes the urban sections along the climate points and all the surrounding built elements within the 40 m radius (i.e. Figure 7 at point 25). To assess the contents of influence areas, six types of morphological indicators were computed (see section 5.1).

Moreover, the thermal comfort within the 36 climate points was estimated by computing PET index. PET values are computed for a 35 years man, according to the average Brazilian age; its representative height is 1,70m and its weight is 70kg (IBGE, 2003). The pedestrian is supposed walking at a velocity of 1.6 km/h on a horizontal plan, since no slopes are included in the study area, consuming 116 W/m^2 for body surface (FANGER, 1972). Wind velocity is set to 1 m/s, according to field measurements, while the vapor pressure is 12.5 hPa. The global radiation trend (W/m^2) is obtained from a close urban weather station (CETESB, Marg.Tietê-Pte Remédios). The isolation of clothes (0.9 clo) is computed by considering the sum of each clothing component. The rest of variables (Air temperature, Humidity and Mean Radiant Temperature) are obtained by climate points. Results were compared with the thermal classes defined by Monteiro (2008) for the City of São Paulo.

Additionally, to conclude this first stage of data assessment, a solar analysis was also implemented to observe the shading potential within the study area. The investigation was carried out within Rhinoceros and Grasshopper modeling tools, applying the Sunlight Hour Analysis (Figure 8). In the model developed, only direct radiation and shading from buildings were considered. Firstly, four symbolic dates, including spring and autumn equinox, as well as summer and winter solstices (March, 21th; September, 23th; June, 21th; December, 21th) were analyzed to observer the direct sunlight under extreme (solstices) and intermediate (equinox) astronomical conditions, at the domain geographical position and in four different seasons (plug-in DIVA). Secondly, a representative date (May, 26th) among the days of climate collection, was selected to parametrically simulate the sun path along the whole day (24 h) and to assess the number of hours of direct sunlight received by the input domain geometry, using sun vectors from the generated Sun Path (plug-in Ladybug). Correlations were performed between direct sunlight hours at the ground surface, SVF, measured air and

ground surface temperature in the climate points, in order to verify the shading role in generating intra-point temperature differences. Later, two alternative densification scenarios (A and B) were created to show the variation of sunlight hours related to these possible configurations, due to the alteration of shading landscape. Scenarios represent a different density pattern, susceptible to bring distinct thermal changes. In scenario A, the current lots occupied by low-rise buildings were replaced by towers, using the same architecture of neighboring lots; in scenario B, instead, only 21 lots were densified, increasing existing buildings height of ten stories combining the existing low-rise urban fabric with taller buildings. In both scenarios a similar build-up of volumes was implemented, resulting in a comparable densification.

Figure 8 - Algorithm model linking Sun Path and Sunlight Hours Analysis (Grasshopper) on the base of the geometric model (Rhinoceros) with descriptive sentences.
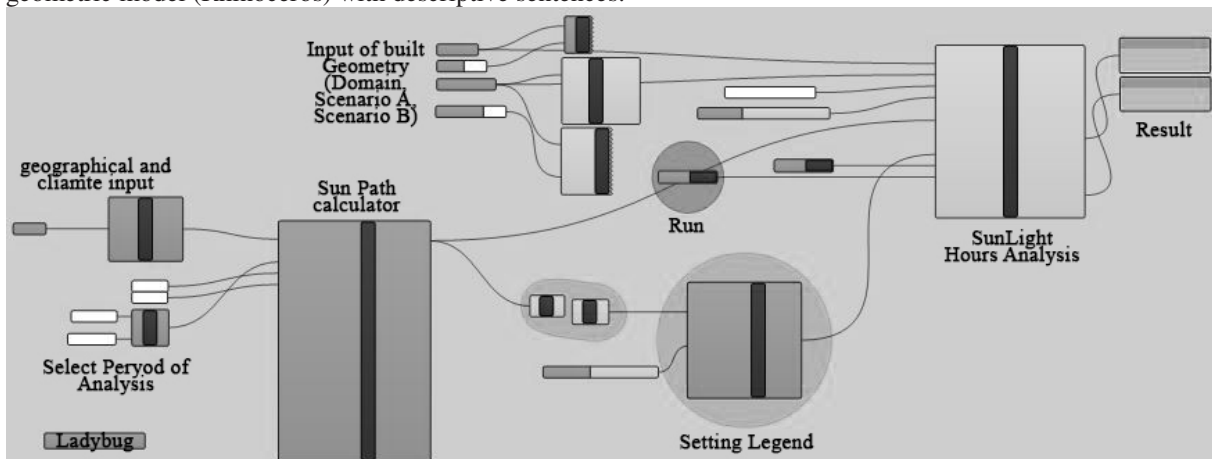
Source: Martina Pacifici, 2019

4.2   *Limitations and purposes for 2nd phase*

First phase analysis correlated the spatial arrangement of urban cross-sections and the related micro-climate conditions to assess urban fabrics affected by densification and verticalization. A simplified and easily applicable approach was proposed with regard to the combined study of urban form and climate, focusing on the microscale in which the pedestrian comfort varies significantly.

Notwithstanding, some limitations had been found in the analysis implementation. Indeed, the method was limited to a small daily window data (3h at morning and 3h at the afternoon), losing climatic occurrences in the remaining hours. Secondly, the availability of only one meteorological station was found insufficient to accomplish all purposes and take

care of such a large number of climatic points. Also, the transect path for each cycle of measures had to be closed on the same starting point as reference. Thirdly, since only one scale of analysis was approached, the boundaries of domain remained unexplored and influences from greater climatic scales had not been considered. Lastly, to guarantee simultaneity between measures, the collection time in each climatic point was extremely reduced, providing only two samples per point for temperatures and humidity (at morning and at the afternoon). Furthermore, although clear and cloudless sky conditions had been maintained, the entire measurement cycle of the points was split on 3 consecutive days, which could have involved small daily variations.

In a nutshell, the transect path was suitable to include a rich set of morphological arrangements, while little reliable to achieve solid relations on the interactions between morphological features and thermal variations. Despite its preliminary usefulness, the assessment stage was no able to return a clear comprehension of the complex urban dynamics involving climate and forms.

To bridge these gaps, a second climate and morphological assessment was implemented in the same case study. In this new phase, a more robust methodological approach was desired in order to enhance the spectrum of findings. The second assessment stage is complementary to the first field experience that anyhow had produced significant information on the on-site climate dynamics and the existing built morphology, contributing to the development of the conceptual model of the area.

4.3   Climate and morphological analysis (phase 2)

To fill the previous gaps, a more integrated and in-depth assessment procedure was drafted to exploring processes that affect the domain temperature behavior. The main advantages of the new collection procedure includes the operation of long-term measurements, the installation of more instruments on the field (fixed and in movement), a different conceptualization of the domain extruded in three scale of analysis (Figure 9a). The development of a three analysis scales analysis is based on the Oke concepts mentioned in section 2.5. According to him, three scales of interest may be pursued to climatically analyze an urban area: the meso-scale, the local scale and the micro-scale (OKE, 2006). Thus, a multidimensional perspective was introduced, going beyond the domain boundaries at the local scale. Mesoscale phenomena influencing the whole city were included, and microclimate analyses were conducted on specific urban features inducing to the immediate

vicinity thermal differences even of numerous degrees. Scales were robustly characterized from a climate and morphological point of view. Great emphasis was given to solar access and reverse shading between buildings. A larger data collection was made continuously in 1-month time, and statistical techniques were widely implemented, allowing building linkages between urban forms arrangement and thermal variations. A simple analytical model was also built to correlate daylight and geometrical parameters in a selected urban canyon. Findings from this phase aimed to enhance the understanding about urban morphology and its potential for climate variability on outdoor urban spaces, highlighting relevant interactions between buildings and atmosphere, occurring at each scale. Thus, for each step of analysis, these questions were raised: *i)* Is the city morphology responsible for climate variability at meso-scale? *ii)* How does the local differentiated heating depend on the fabrics shape? *iii)* In which way is the existence of microclimate environments related to buildings geometric parameters? The discussion on these questions rather contributed to integrate the conceptual model deriving from the first phase, making possible the beginning of the modeling process. To explain clearly the procedure applied, the morphological and climate assessment (phase 2) will be divided in 3 steps, following the sequence of assessed scales.

4.3.1 Mesoscale

According to Pacifici, Rama and Marins (2019), at the *mesoscale,* the urban mass was approached as a single leaving body, relating its size and density to a certain climate environment, and thermal variations were investigated. Mesoscale is affected by latitude and the effects of heat island are also notable at this stage. A meso-scale region (~31,400 ha) was defined by drawing a circle area of radius equal to 10 km around the local scale domain considered in the first phase. Within this region, the arrangement of the urban fabrics was studied and a large scale climatic analysis was conducted from fixed weather stations data to explore the relationship between air temperature variations and urban fabrics.

For the morphological analysis (Figure 9b), the most recent LCZ classification for São Paulo (FERREIRA et al., 2017), based on the WUDAPT methodology, was adopted (overall map accuracy 68%). Percentages of LCZ built types were calculated by GIS tools inside the meso-climate region to represent the urban fabric of the study domain, by calculating the percentages of LCZ built types inside the meso-climate region (Figure 9c). The map from Ferreira et al. (2017) was imported into a GIS environment as a *shapefile* and analyzed with embedded tools. A *buffer* of 10 km was traced to crop the LCZ areas included in the study

region. Thus, each LCZ percentage was computed as the ratio of the area covered by each urban type and the total *buffer*.

Data from six meteorological stations all around the domain were used in the climate analysis (Figure 9b). In fact, at the meso-scale*,* when city influences climate for dozens of kilometers, a single station is not enough to represent the whole urban region under analysis (OKE, 2006*)*. In order to consider a representative climate dataset, meteorological stations were selected by different urban morphologies. Some of the selected stations are installed in open locations, others are embedded in the city context. The urban morphologies were defined again in a GIS environment, accounting the LCZ built types found in a radius of 500 m around each station (zoom on the Figure 9b). Thus, selected stations were obtained from CETESB (State of Sao Paulo Environmental Sanitation Technology Company), INMET (National Institute of Meteorology) and CGE (Emergency Management Center) databases. Elevation, geographical coordinates, codes and acronyms of all stations are displayed on Table 4.

Table 4 - Mesoscale meteorological stations characteristics

Meteorological Station	Acronym	Database	Code	Elevation (a.s.l.)	Coordinates
Mirante Santana	(MS_INM)	INMET	A701	786 m	23°29′S, 46°37′W
Vila Prudente	(VP_CGE)	CGE	PMSP/VP-01	757 m	23°35′S, 46°33′W
Penha	(Pe_CGE)	CGE	PMSP/ PE-01	740 m	23°31′S, 46°31′W
Vila Mariana	(VM_CGE)	CGE	PMSP/VM-01	819 m	23°35′S, 46°38′W
Sé	(Se_CGE)	CGE	PMSP/SE- 01	820 m	23°33′S, 46°39′W
Dom Pedro	(DP_CET)	CETESB	---	731 m	23°32′S, 46°37′W

Source: Martina Pacifici, 2019

The stations MS_INM and DP_CET are installed in the middle of a great open space, greener in the first case, more urbanized in the second-one. VP_CGE and VM_CGE are placed in a mixed urban fabric. Pe_CGE is representative of a road infrastructure-marked urban site. Finally, Se_CGE is installed on a higher position than other stations, probably due to the high-rise density of the fabric around, for which it can be considered representative. It is worth stressing that, regardless the variety of urban fabrics around stations, all meteorological sites were well comparable due to their similar installation. The difference between stations' elevation was less than 100m; conversely, above this value, a thermal gradient related to the different altitudes would be found (adiabatic gradient: 1°C/100m, normal gradient: 0.65°C/100m). Aerial images and pictures of all the stations show the exposure conditions of the pieces of equipment (Figure 9d).

Figure 9 - Outline of the microscale, local scale and mesocale (a), mesoscale area and LCZs distribution (b), percentage areas of LCZs inside the 10km circumference around the case study (c), installation site of weather stations: aerial photos and pictures of the pieces of equipment (d).
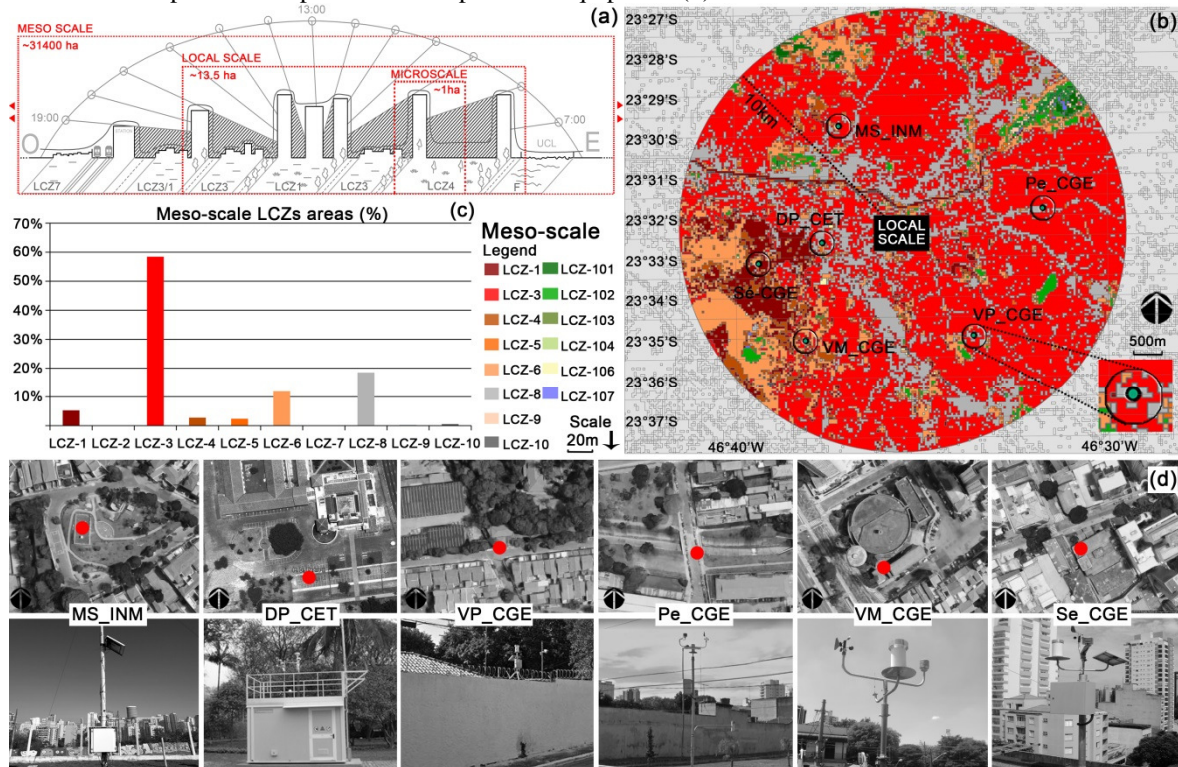
Source: LCZ map selected from Ferreira et al. (2017) (b), INMET, CETESB,CGE photograph archive and Google map (d)

Summertime dry bulb temperature data, from November 13th, 2017 to December 14th, 2017, were mainly analyzed, according to the time window of the local scale collection that will be described further on. All the data series were synchronized to the local time; that is in practice, displacing values of -2 hours (CGE stations) and -2 hours (INMET stations). Accuracy and precision of measurements implicate a maximum total error of ± 0.3°C. Afterwards, a temporal analysis of these variables was made, in order to visually assess the trends and the differences between stations (not show). In a congruence analysis, the series were consolidated, removing errors and noise. In addition, the series were filtered by a moving average filter (MAF) and resampled to 1-h rate to be fully comparable. Further on, a distribution analysis for air temperature was performed, to describe the climate behavior of every station point with few values. For this reason, the central position, distribution and shape of the air temperature data for every station were computed. Moreover, the two-tailed Mann-Whitney and Ansari-Bradley tests were applied to different pair of stations to verify the hypothesis of the same central position and dispersion for air temperature record distributions, assessing if different stations trends were statistically "equal". These two methods are non-parametric hypothesis tests and represent alternatives to the t-test and F-test for comparing the

medians and dispersions of two data sets without having to assume a Gaussian distribution for the whole population (TRAUTH, 2015, p. 103).

4.3.2   Local scale

The *local scale* area (~13.5 ha) was selected inside the previous mesoscale region (Fig. 2c) and its perimeter coincides with the boundaries of the first phase domain (4.1), in the Belenzinho district (Figure 10a). The fabric assortment was defined overlapping the building plan with the LCZs map in the area of interest. Although four climate urban zones were detected (Figure 10c), only the most common climate zones were included in the climate analysis: the compact high-rise and the compact low-rise zones.

Figure 10 - Domain at local scale analysis (a), Measurement sites, Sky View Factor with solar arc for stations 1, 2, 3 (b), LCZs distribution (c), Station 1 and 4 during a comparative test (d).
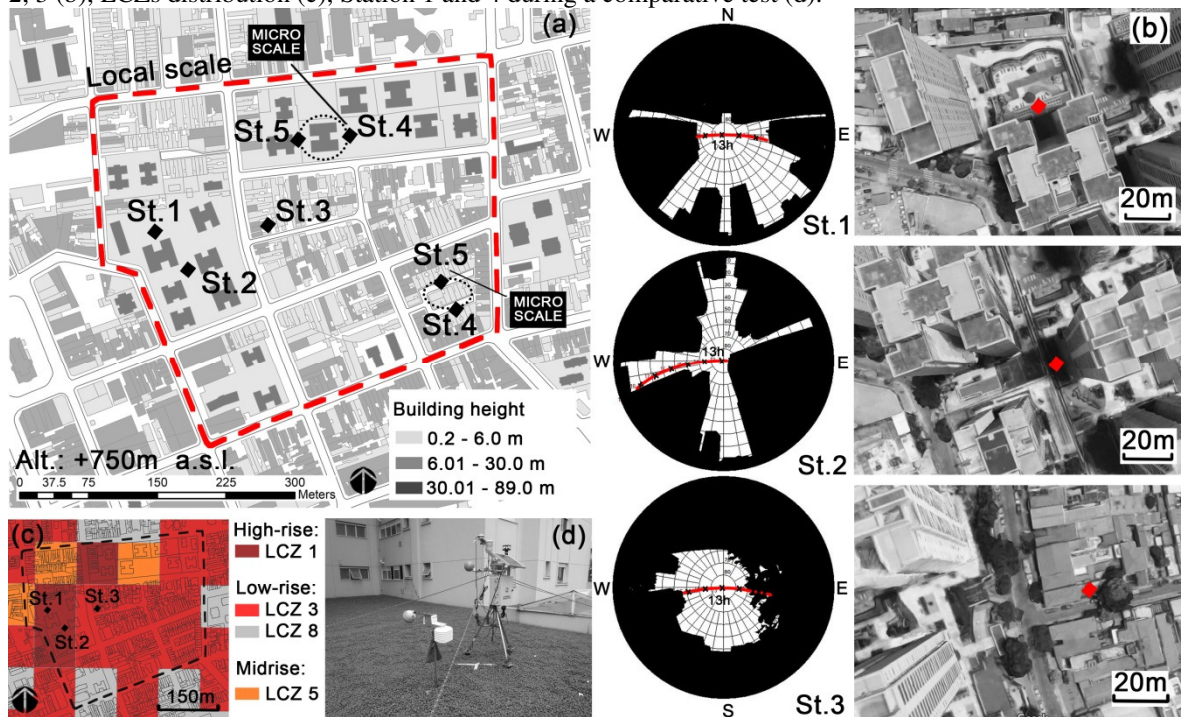
Source: Pacifici et al. (2019), LCZs obtained from Ferreira et al. (2017) (c)

In order to assess the impact of these two different urban morphology on the air temperature variations in outdoor space, three meteorological stations were installed in the area: station 1 and station 2 - equipped with a Campbell Scientific Inc. CR800 datalogger, a Campbell Scientific Inc. HMP45C sensor with a solar shield Vaisala 41003-5 (measuring air temperature Ta), a Campbell Scientific Inc. 108 (measuring ground surface temperature Tgs and globe temperature Tg), an ultrasonic anemometer Gill Instruments LTD WindSonic1

(measuring wind speed w_s) - and station 3 - equipped with a Hobo Pro v2 U23-001 datalogger with a solar shield Hobo RS-1 (Ta), a Hobo U12-013 datalogger with sensor cable TMCx–HD (Tgs), a Hobo U23-004 datalogger with grey globe whose emissivity is $\varepsilon = 0.41$ and diameter $D = 0.17$ m (Tg). Since the pieces of equipment differ slightly in technical specifications, a multi-day comparative calibration were carried out indoor and outdoor, showing negligible differences between the field stations (less than 0.5 degrees). Table 5 summarizes stations details; total accuracy is obtained by adding the errors of the individual components.

All the three stations were installed outdoor, within the open spaces of the built blocks. Stations 1 and 2 were placed in the newly-verticalized high-rise compact zone while station 3 in the low-rise traditional compact zone (Figure 10a). The first ones were close to the towers and were representative of a densely built urban site, in which the several-floor buildings determine the irradiation or the shadowing of the surrounding open spaces. Conversely, station 3 was installed in a courtyard and is representative of an urban site composed of 2-3-floor houses, whose exposure was not affected by higher buildings. Two stations were placed in the verticalized compact fabric in order to characterise two different sub-cases in the same zone: a) East-West-oriented towers with an open space in the middle (station 1, Figure 10d), and b) East-West-oriented towers belonging to a North-South urban canyon (station 2). The local scale station positions along with the Sky View Factor and the solar path on the representative day of December 3rd are shown in Figure 10b. The number of solar exposition hours is easily recognizable for Station 1 (4.5h), Station 2 (6.0h), Station 3 (4.5h). The chosen position, as many times in the field works and campaigns, is a compromise between technical choices (e.g. representative area, enough distance from obstacles) and practical details (e.g. security, inhabitant distrust, condominium regulations). However, all the data were collected between 1.0 m (station 3) and 2.0 m (station 1 and 2) from the building pedestal, which are considered the zero reference for the altitudes. The stations, synchronized at the local time, monitored climate variables in a 31-day-time window, from November 13th, 2017 to December 14th, 2017, with a 30-minute sampling rate, resulting in 1,483 total records per variable, per station. In the measurement period, 10 rainy days with over 5mm of daily cumulative rain were concentrated between the 17th and 27th of November, while the average wind speed measured by field stations had been found in the range between 0.5 and 1.4 m/s.

The Tg was converted into mean radiant temperature (MRT) before being analyzed, according to ISO 7726:1998 formulation (Equation 5), where globe emissivity (ε_g) is 0.41, globe diameter (D) is 0.17m, air velocity (v_a,) is the average wind speed. In order to avoid unwanted noise due to turbulence, the v_a was obtained from the lognormal wind series

measured in field (station 1 and 2), firstly log-transforming the values and then averaging them. The mean values, in this case, represent the central position of distribution; therefore, it is easy to reconstruct wind values by the Eulerian exponential of mean.

In addition, a distribution analysis was carried out by computing the probability density function (pdf) of variables. For all the stations, bin widths were equally-spaced to allow the comparison between stations: bins are at intervals of 0.5°C for Ta and Tgs, at 1.5°C for MRT. Subsequently, to observe the data set over the day time, a distribution analysis along 24 hours was implemented at the three stations (PACIFICI et al., 2019).

$$MRT = \left[\left(t_g + 273\right)^4 + \frac{1.1 \times 10^8 \times v_a^{0.6}}{\varepsilon_g \times D^{0.4}}\left(t_g - t_a\right)\right]^{1/4} - 273 \qquad (5)$$

Table 5 - Stations at local scale and microscale

Station	Scale	Type	Morphology	Accuracy (Ta)	Accuracy (Tgs)	Accuracy (Tg)
1	local		compact high-rise fabric	± 0.28 °C (from 0°C to 40°C)	±0.21°C (from 0° to 70°C)	
2	local	stationary	compact high-rise fabric			
3	local		compact low-rise fabric			
4	micro		high-rise block	± 0.21 °C (from 0°C to 50°C)	± 0.6°C (from 0° to 50°C);	± 0.21 °C (from 0°C to 50°C)
5	micro	moving	low-rise block			

4.3.3 Microscale

Finally, at the micro-scale (~1 ha), the effects of geometry and building proportions within the local climate zone were faced. Field measurements were conducted in transect, to assess the influence of "isolated" urban elements on the fluctuations of climate variables (Figure 11). Assuming the sun obstruction as the driving force for microclimate fluctuations, a couple of mobile stations (called stations 4 and 5), with the same specification of station 3, were located around individual buildings in high-rise and low-rise zone, investigating the effect of shading caused by the built morphology. Two representative morphological features were chosen to be investigated: the tower within the high-rise zone (Figure 11a) and the housing block within the low-rise fabric (Figure 11b). Transect was executed turning the stations around these two features, from morning to evening, with 30' sampling rate, in the four exposures (N-S-E-W). Stations 4 and 5 were placed simultaneously in the field, placed

on similar pavements, in diametrically opposite positions (N-S or W-E). The exposure was changed every one hour and a half. At every displacement, an interval of 20 minutes was considered for the equipment stabilization. For each point, also thermographic collections were taken from the ground floor and from the façade in front of the climate station. Stations were synchronized at the same local time. Measurements occurred on November 14th and 24th, 2017, and December 4th and 12th, 2017. Only air temperature T_a values were analyzed, together with the thermographic photos. The trend of different urban microclimates at four exposures, basically caused by the sun transit and shadow projection, was assessed by scatter plot diagrams (PACIFICI; RAMA; MARINS, 2019).

Figure 11 - High-rise microscale field collection (a), low-rise microscale field collection (b)
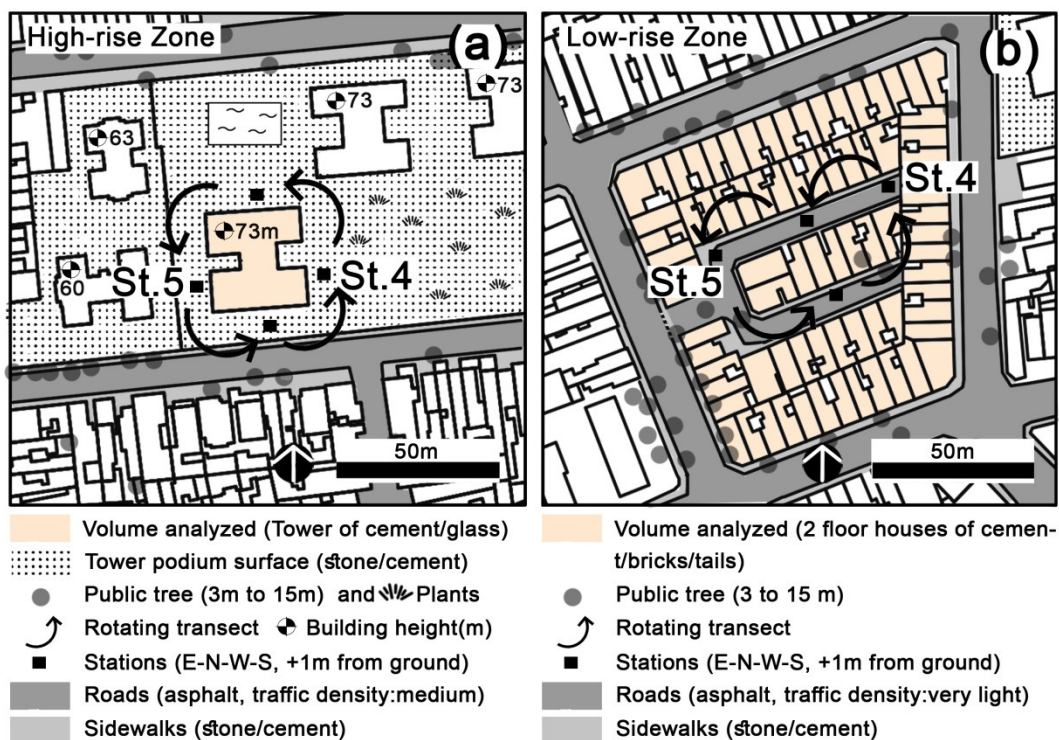
Source: Pacifici et al. (2019)

At this step, together with the field data analysis, an analytical 2D model was built in Matlab code, estimating the solar access variation provided by a typical urban canyon. This effort aimed to explain, in a simple way, the effect of shading caused by canyon geometry. The model was based on trigonometric formulas, assuming a 2D infinite plane at which a hypothetical canyon (H_1, H_2, W) is cut. The canyon under analysis has infinite length and is E-W-oriented, since on this exposure the shadow projection is more variable. Solar access (γ) was derived by computing the intercepted sun hours for the middle point O on ground line W (Figure 12a). As shown in Equation 6, solar access cone γ, delimited by building 1 (right-side)

and 2 (left-side), was obtained by subtracting the building obstruction angles ($\alpha1$, $\alpha2$) from the daily east-west solar arc (180°). Building height H and canyon width W were supposed varying from 0 to 100m. Angles $\alpha1$ and $\alpha2$ were computable by the inverse of the tangent trigonometric function *tan^{-1} (2H/W)* for buildings of height H_1 and H_2. Mathematically:

$$\gamma = 180° - \alpha_2 - \alpha_1 = 180° - \tan^{-1}\left(\frac{2H_1}{W}\right) - \tan^{-1}\left(\frac{2H_2}{W}\right) \tag{6}$$

To convert the sun access angle γ in effective solar hours in the canyon, the daily sun path was derived by solar chart; thus, elevation (β) and azimuth (θ) angles were defined at each hour of the day. For the present analysis, the São Paulo solar chart (https://www.sunearthtools.com/), on November 29th 2017, was considered. Since this date is the middle of the temporal window of local scale analysis, it was considered representative of the whole period under analysis. Subtracting sunset (19:38) from sunrise time (6:11), the number of solar daily hours (13.27 hours), distributed over the whole sun arc (180°), was obtained.

Afterwards, the solar elevation angles were compared with $\alpha1$ *and* $\alpha2$ to obtain the minimum and maximum light access angles for every buildings configuration. Note that only when the 2D plan cutting canyon and sun azimuth are parallel (θ =90° and SP=S'P'), $\alpha1$ and $\alpha2$ are directly comparable with the sun elevation angle, by overlapping the canyon geometry with the solar chart. In all the other cases, the real sun elevation angle (β) has to be subtracted from the component ($\eth$) to obtain its projection (αs) on the 2D plan (Figure 12b). Thus, αs was mathematically defined as:

$$\tan(\alpha_s) = \frac{\tan(\beta)}{\cos(\eth)} \tag{7}$$

Since the 2D projected vertical plane is E-W-oriented, horizontal angle $\eth$ is the displacement in the horizontal plane between the 2D vertical plane and a hypothetical plane going through the sun. Thus, $\eth$ could be hourly derived from sun azimuths (θ) in the Belenzinho solar chart. It is worth stressing that azimuths are conventionally referred to the north-south axis (N), making it necessary to subtract 90° for east-angles (until 12 p.m.) and 270° for west-angles (after 13 p.m.) from θ to obtain $\eth$ angles. Once αs was computed by Equation 7 for each hour of the day (gray degrees in Figure 12a), the comparison with $\alpha1$ and $\alpha2$ provided the number of light hours intercepted by the canyon. Hour fractions were derived

by linear interpolation of angles at the two following hours (PACIFICI; RAMA; MARINS, 2019).

Figure 12 - 2D representation of a hypothetical canyon E-W oriented and sun access (a), 3D representation of the true solar angle (β), the projected solar angle (αs) and the obstruction angles ($\alpha 1$, $\alpha 2$) (b)
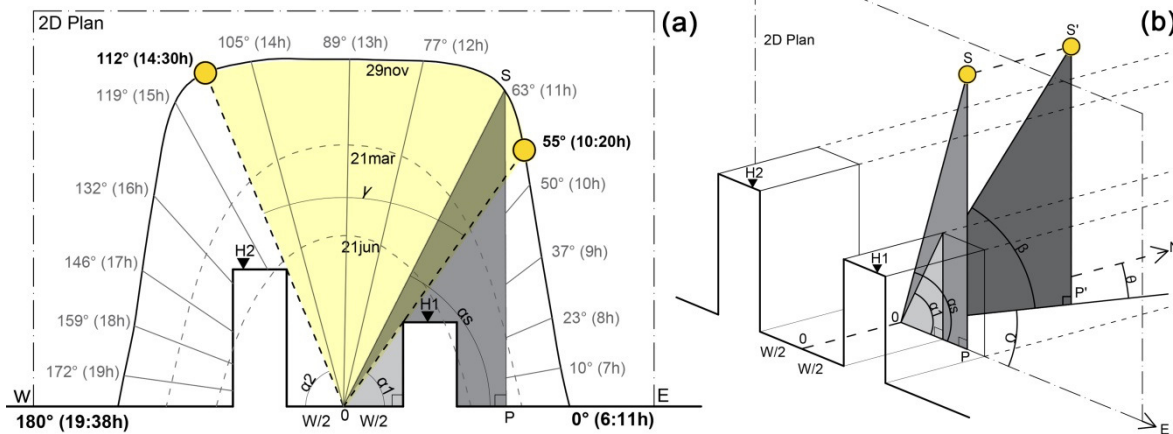
Source: Pacifici et al. (2019)

4.3.4 Complementary investigations: vegetation and materials

Complementary investigations were realized at the local scale to collect surface materials and vegetation. This research phase was developed in strict collaboration with two young researchers, Guilherme Kalleder and Antonio Fulco, in the framework of two initiation scientific projects (FULCO, 2018; KALLENDER, 2018). The amount of information collected in this last phase accomplished the set of field information addressed to the construction of the conceptual model. Indeed, material and vegetation parameterization within ENVI-met model was based on these surveys. Both the investigations of materials and vegetation were developed on the whole domain, at the local scale. A brief summary of the realized works is presented.

With regard to urban surfaces, a work of materials characterization, climate collection, data spatialization and analysis was developed in collaboration with Guilherme Kallender, to understand the role of materials, as well as the impact of urban form arrangements on their performance. Firstly, the survey of materials covering all buildings and horizontal surfaces was realized, recording typology and color of materials, their areal extension, their constructive patterns. Secondly, such information was processed and only predominant materials were selected. The filtered data were mapped and georeferenced, in order to associate the collected materials with the relative building forms. Thermal and optical materials properties were estimated by the student based on bibliography, once the buildings

age and constructive patterns had been classified for each urban form. Lastly, the amount of area per material was computed in order to achieve the real superficial extension of selected materials. Together with the morphological analysis, a thermographic collection was realized within the temporal window of local scale analysis, on December 14th, 2017, from 6 a.m. to 7 p.m. On this date, almost simultaneous thermographic photos were taken from 8 sample facades, every 2 hours, to follow the materials thermal behavior through the daily heating and cooling phases of the day. Sample façade were selected from North, South, East, West exposures for both high-rise and low-rise fabrics (Figure 13). The used thermographic camera, model FLIR i40, has resolution 120 x 120 pixels, accuracy ±2°C, object temperature range from -20° to 350°, thermal sensitivity < 0.1 (25°C), minimum focus distance 0.1 m.

Figure 13 – Thermographic climate points
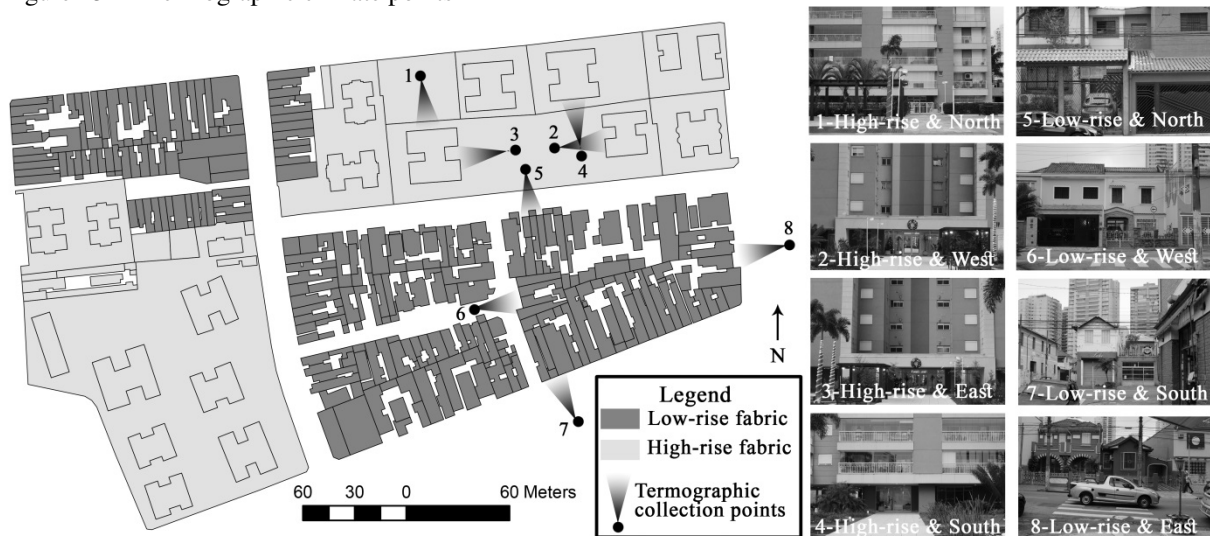
Source: Martina Pacifici, 2019

Thermographic photos processing was conducted in FLIR Tools software, setting specific parameters as emissivity, distance between camera and object, atmospheric humidity and temperature, graphic scale. In the subsequent analysis, the material thermal behavior was observed under the daily solar exposure. Comparative analyses were realized: a) between similar materials, at the same hour and exposure, into distinct urban fabrics; b) between similar materials, at the same hour and fabric, in different exposure; c) between similar materials, at the same exposure and fabric, along the day time. On November 25th 2017, additional climate data (temperature, humidity, globe temperature) and thermographic photos were concurrently taken in two different point of domain to compare the microclimate difference occurring in field between a cement paved surface and a cement paved surface covered with grass. The aim of this experiment regarded the effective benefit of the layer of

overlapping vegetation, covering large portions of open spaces inside the condominium. Later, the results of this measurement allowed equating these two types of surfaces in the construction of the ENVI-met and Grasshopper models.

With regard to vegetation, a work of trees characterization, climate collection, data spatialization and analysis was developed in collaboration with Antonio Fulco, to understand the intensity of trees coverage within the case study, as well as the combined effect due to buildings and trees shading at the local and micro scale. Firstly, climate measurements were performed on November 15th, 2017 using 2 meteorological stations (Datalogger: Hobo, U23-001; Solar shield: Hobo, RS-1). A transect strategy was adopted, in order to collect data from more than one point of domain. The fieldwork aimed to isolate the shading tree effect, by realizing one hour measurements on each location, placing one station under the tree shadow and the other station under the sun, at a really close distance (Figure 14). From a morphological perspective, the mapping of all trees present in the domain area was made, merging the available (but incomplete) *shapefile* provided by municipal database (Geosampa) with field observations plotted in a *GIS* map (Figure 14).

Secondly, the characterization of trees was carried out by field surveys, collecting the main attributes including tree height, trees' species, crown height and width, leaf density, crown shape. The tree species were visually identified with the help of Natalia Carvalho, forest engineer, during a field visit (1.12.2018), in order to obtain by bibliography the attributes not measurable in the fieldwork (ex. leaf albedo). The leaf density was measured by collecting hemispheric photos, from ground to sky, using fish eye lens, Nikon, FC-E8 0.21x, on a digital camera, Nikon, Coolpix 4500. Geometrical dimensions were measured by electronic meter Leica, DISTO D810 touch.

Thirdly, due to the heterogeneity of the collected material, built morphologies and trees were gathered in four classes of analysis. For each class, a representative average *leaf area index* (LAI) was computed trough the *Can-Eye* software (Weiss, 2017), and *leaf area density* (LAD) values were obtained to be inserted in the ENVI-met parameterization further on. In order to obtain accurate values of LAI, sensitivity tests were realized on *Can-Eye* concerning the *Clumping Parameter* (selecting 8 as the most appropriated value) (FULCO, 2018). Subsequently, the Leaf Area Density (LAD) was obtained from LAI values.

Indeed, LAD and LAI are strictly connected and linked by an integral function. According to Weiss (2017), $LAI = \int_0^H l(h)dh$, where l(h) should be intended as the LAD component. To solve the computation of this value, an approximate solution was obtained by

a three dimensional geometrical method, developed by the author. In this procedure, the tree shape was approximated to a parallelepiped shape, made up of 10x10x10 units. In this way, the tree vertical dimension was gathered in 10 layers. Subsequently, a certain percentage of leaf coverage was assigned to each layer, based on a visual analysis of tree crown. The LAD value was estimated firstly for one unit and secondly was multiplied until to fulfill all the green units contained in each layer. 10 values of LAD were obtained, suitable to be implemented into the ENVI-met tree database.

Figure 14 – Map of tree coverage including available tree from *Geosampa* database, integrated trees from fieldwork collection and climate measurement points. A diagram displaying the station positions for each climate point is also provided.
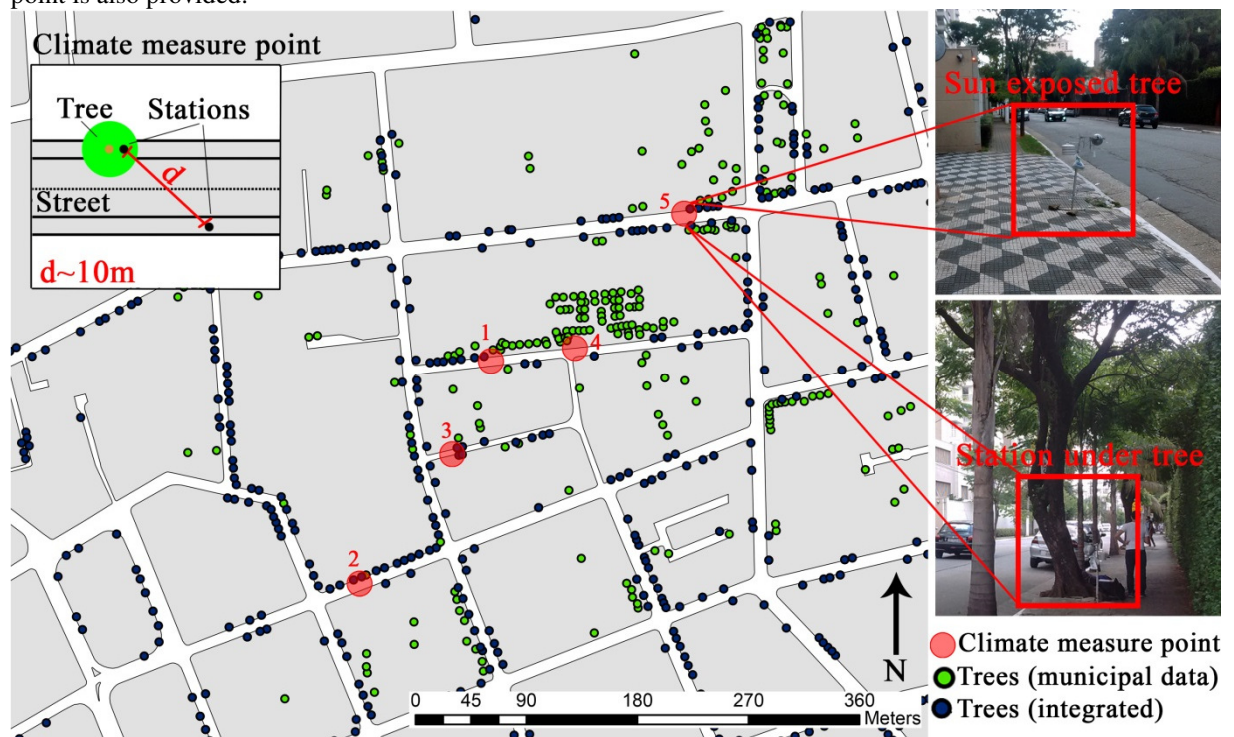
Source: Martina Pacifici, 2019

4.4 ENVI-met modeling

Once the data collection and analysis had widely characterized the site under study, the modeling process was enabled to get start including the following stages: definition of modeling purpose (1), development of the conceptual model (2), the selection of a suitable modeling code (3), the implementation of sensitivity analysis (3), the construction of model (4), the calibration (5) and experimental scenarios (6). The definition of the model purpose is needed to formulate the questions that motivate the modeling activity (1). The conceptual

model dealt with the system of knowledge collected and analyzed in site (2). These two steps were essential to choose the appropriate computational package (3). Once ENVI-met was selected as the best code to the defined purposes, a sensitivity study was implemented to understand the impact of certain parameters, not measured during the fieldwork and no available from online database (3). Afterword, the model could be designed and calibrated with real field data (5). On the base of the calibrated model, forecasting simulations were realized to investigate alternative buildings arrangements in which built density was increased (6). Together with the discussion of results, model limitations were also highlighted and purposes were verified (7). The methodology of the most important steps (2, 3, 4-5, 6) follows in the next sections.

4.4.1   Conceptual model

The whole knowledge acquired along the two field assessing phases was synthetized in the conceptual model. In practice, from the complexity observed on the analyzed site, the most important processes affecting the interaction between built morphology and climate were selected, while secondary phenomena were excluded. The selection of the main processes implies a simplification of the real world. Nevertheless, this simplification is critical to overcome software limitations and reduce the complexity of model architecture, although it must not undermine the achievement of the model purposes.

Table 6 - Data used in the construction of the site conceptual model

Climate framework	
field data	Daily microscale measurements Ta, RH, Tg (2)
	Daily urban canyon measurements Ta, RH, Tg (1)
	1 month local scale measurements Ta, RH, Tg, w_s and $w_{dir,}$ RADG (2)
	Daily local scale sun hours (1)
	E-O urban canyon sun access (2)
	Daily surface temperatures for exposure (2)
	Daily microclimate tree measurements (2)
available database	1 month-mesoscale-data from meteorological stations, Ta, RH (2)
	2500 m humidity from Depart. Atmospheric Science - University Wyoming
	Soil temperature and humidity from INPE
Morphological framework	
field data	land use map (1)
	materials, constructive typologies, state of buildings (2)
	tree vegetation map, LAI, LAD, species, hemispherical photos (2)
	SVF for climate points (1 and 2)
available database	Built morphology from municipal database (1)
	Building ages, land use information, soil characteristics (1 and 2)
	Shapefile of sidewalks, blocks, zones, trees, topography, etc. (1)

The amount of data and processes used to develop the conceptual model are summarized in Table 6. The building of the conceptual model leaded to the selection of ENVI-met as computational code, suitable to the defined purpose and available field data.

4.4.2   Sensitivity analysis

A sensitivity analysis (SA) was carried out to evaluate the sensitivity of the modeling outputs to the variation of the input parameters, in a model built with ENVI-met code. Such study was considered necessary to overcome the lack of a well-documented user manual. Thus, numerical experiments were realized changing the fundamental parameters of the code input and analyzing the results in terms of climatic variables. These tests were carried out on a reduced domain, obtained from the original domain. This choice was due to the very long simulation times and is considered the best compromise between code comprehension and computational efficiency. The values attributed to the input parameters were left to vary within the range provided by the software. The parameters analyzed were: roughness length, empty cells on the border, nested grids, specific humidity at 2500 m, lateral boundary conditions, material (density coefficient, thickness coefficient, albedo). The sensitivity to these parameters was observed on the following output variables: air temperature, relative humidity, surface temperature, wind speed, wind direction, mean radiant temperature, façade temperature (outside), façade temperature (inside) and building temperature (inside). Output variables were extracted from all domain and specific receptors. Output variables in the receptors were statistically analysed over a 24h time period; conversely, output variables from the rest of domain were together analysed at 8 a.m., 12 a.m., 4 p.m., 8 p.m. (due to a code limitation in the data download). The reduced model had size equal to 53 x 53 x 24 grid cells and included towers and low-rise housings, as well as a 1m-high podium under the towers. Grid cells sized 3m x 3m on the *xy* space; on the *z* axis, the first 5 cells were more detailed (2 m), while an increasing telescopic factor was applied from 10m, enlarging progressively the grid cells height. Thus, 31 simulations were run developing a univariate analysis of main input parameters. Model setup information are described in Figure 15.

Figure 15 – Reduced model domain parameters

Name	Reduced Model
Model Version	Basic
Grid size	53x53x24 grid cells
Cell spacing (dx x dy x dz)	3 x 3 x 2 m
Telescoping factor	15% starting from 10m
Model rotation	-13.5°
Nested grids	1
Wall and roof material	concrete
Roof material	concrete
Soil material	concrete + asphalt
Distance from border	0 m
Tree	no
Receptors	9
Starting	13/11/2017 at 9 p.m.
Forcing	yes
Curve of forcing	aver. 6 weather stations
Lateral Boundary Conditions	forced, forced
Turbulence Model	Default
Solar adjusted factor	1
Clouds	0-0-0
Wind direction	135°
Wind speed	1 m/s
Roughness length	0.01
Humidity at 2500 m	10
Soil Temperature Layer 1- 2 - 3	292.15 K
Soil Wetness Layer 1 - 2- 3	50 – 60 – 60 %

Source: Martina Pacifici, 2019

Nine receptors were set, five on the ground surface and four on the building facades. Façade receptors were located on the four cardinal exposures (North, South, East and West) of a central building (R6, R7, R8, R9). On the ground surface, four receptors (R1, R2, R4, R5) were located on the podium layer (at z = 1m), closes to the four cardinal exposures of different buildings, and 1 receptor (R3) was at street level (at z = 0m). Two of the ground surface receptors also coincided with the field measurement points (R1, R2). All receptors were 3 m high from the ground. No receptors were selected within the first 21 m (7 grids) from domain borders, in order to avoid specific boundary effects.

4.4.3   Model Construction

The definition of model was achieved through a complex iterative process that collected contributions from conceptual models, sensitivity testes, data field and observations, in order to bridge the gap between the characterization of the real environment and a reliable model. The model domain was built as a three dimensional system of abstractions representing the most significant urban features characterizing the urban site. The

configuration of the model involved the definition of 3 ENVI-met virtual environments: the 3D model space, the 1D model and the soil model (Figure 16).

Figure 16 –ENVI-met structure
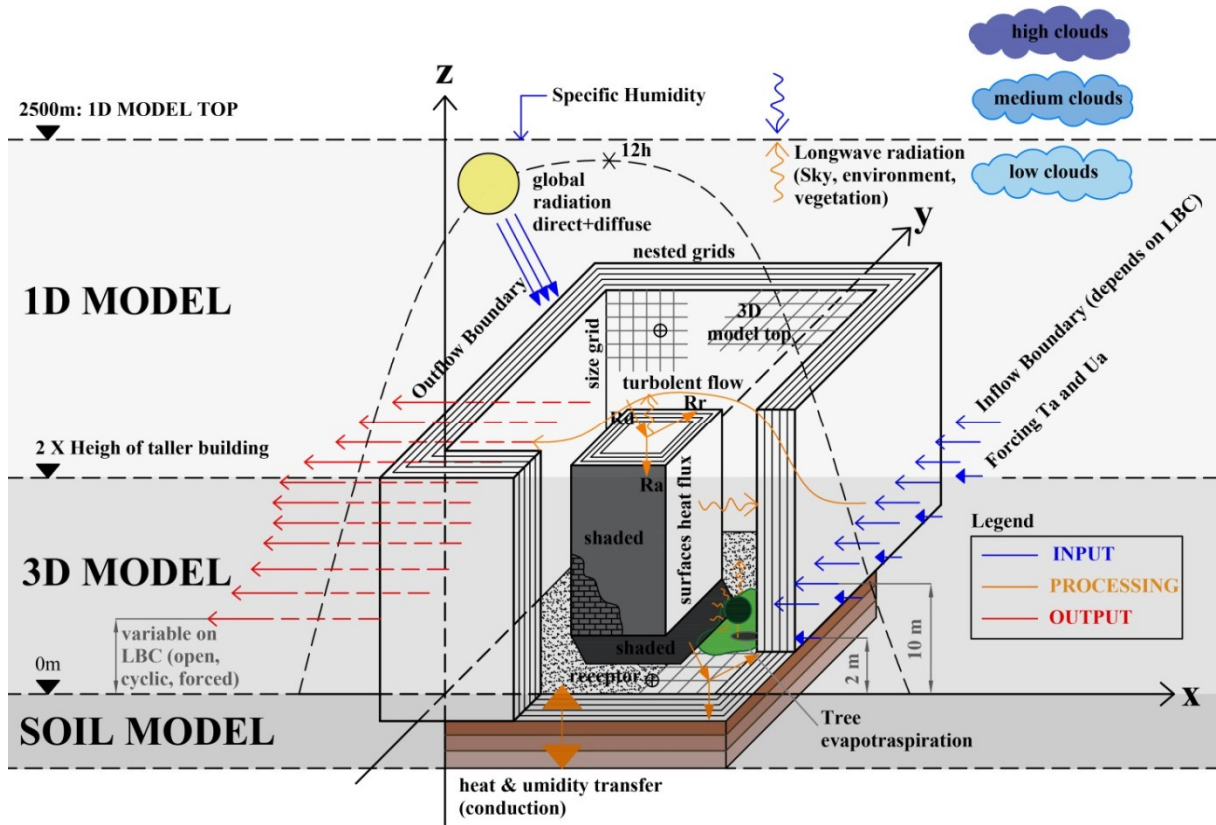
Source: Martina Pacifici, 2019

The *3D model* or *core model* allowed designing in 3 spatial dimensions (x, y, z) all the features representing the urban area under study, including buildings, open spaces, vegetation and surfaces. Features had to be integrated into a discretized space, made up of grids, in which the spacing between nodes (dx, dy, dz) determines a finer (high accuracy, high CPU time) or a courser (low accuracy, low CPU time) mesh. Thus, the 3D model size depended on grids resolution and domain size, horizontally and vertically constrained from buildings layout and heights. Since on the borders of the 3D space, the model calculation was less accurate, a larger domain was adopted to guarantee real values for the interest zone in combination with a band of *nested grids* cells.

On the surroundings of the 3D model, the definition of the *1D model* allowed controlling the boundary layer processes and providing the inflow boundary data to the 3D model. The 1D model entailed the extension of the 3D model top up to 2500m (2500m is the atmospheric boundary layer average height). The 1D model provide the boundary conditions

to be applied on the 3D model, by computing one-dimensional vertical profiles of air temperature, specific humidity, wind vectors, kinetic energy and turbulent exchanges. The vertical structure of the 1D model was subdivided in 14 layers made up of grids whose size increases with the height. Lastly, the soil model guaranteed the computation of the heat transfer through the ground, setting soil temperature and humidity that affected tree evapotranspiration (BRUSE, 1999; SIMON, 2016).

In the 3D model, the urban morphology was little simplified, to avoid a too long simulation time and errors. For the low-rise buildings, the myriad of different buildings heights were homologated to constant-height-zones, as well as the small courtyards and recesses were suppressed; thus, only the largest ones remained (Figure 17). Under high-rise buildings, the podium was not designed as built element, since observed to be climatically irrelevant in the sensitivity analysis (not showed). Also the use of the DEM strategy (elevation of the ground surface) was seen unimportant.

Figure 17 – Example of model design simplification: real building heights (a), simplified model heights (b).

Source: Martina Pacifici, 2019

About vegetation, a selection of the most significant trees was made on the base of field studies and a reference size was set for all of them. Moreover, to fit the real buildings sizes into the model grids, the original lengths and heights were stretched or shorten to occupy the full area of the cells (Figure 17). This approximation is rather insignificant for grids close to the ground surface, while becomes more visible for the higher cells close to the model top, enlarged by the telescoping factor. As an example, towers 80m-high, falling between the grids at 73 m and 84 m, were approximated to 84 m. In addition, since a lot of buildings were obliquely arranged with respect to the north orientation, the original urban layout was clockwise rotated to avoid as much as possible too irregular building shapes.

Within the 3D model, the conditions of air temperature and humidity were forced by using the *Simple Forcing* tool. The application of *Forcing* defines the diurnal variation of the atmospheric boundary conditions. In order to implement a representative simple forcing, input values were obtained by the field measurements realized from November 13th, 2017 to December 14th, 2017 in the urban site. From this dataset, two average 24h-curves were extracted for both air temperature and humidity, considering the most stable measurement window extended from December 4th, 2017 to December 6th, 2017 collected in the model heart (Station 3). Since ENVI-met does not take into account the Daylight Saving Time (Summer Time), data series were synchronized to Brasilia Time, displacing values of -1 h from Local Time. In addition, the series were resampled to 1-h rate to be entered in the forcing window. Once air temperature and humidity were defined and applied as forcing components, their transfer inside the 3D model atmosphere was mathematically described by the combined advection-diffusion equations:

$$\frac{\partial \theta}{\partial t} + u_i \frac{\partial \theta}{\partial x_i} = K_h \left(\frac{\partial^2 \theta}{\partial x_i^2} \right) + Q_h \tag{8}$$

$$\frac{\partial q}{\partial t} + u_i \frac{\partial q}{\partial x_i} = K_q \left(\frac{\partial^2 q}{\partial x_i^2} \right) + Q_q \tag{9}$$

Here, θ is the air potential temperature, q is specific humidity, K_h and K_q are the turbulent exchange coefficients, Qh and Qq are internal sources/sinks provided by the vegetation model, linking the heat and vapor exchange close to plants with the atmospheric model (BRUSE AND FLEER, 1998). The heat transport equations were obtained from conservation law of energy in which the first term represents the variation (derivative) of temperature and humidity on time, the second one is the advection term, followed by the

diffusion terms, and finally the internal sources/sinks. The diffuse term is a second-order derivative; thus, its weight was smaller than the advection term.

To set a representative value of wind speed and direction at 10 m height (constant during the simulation), annual average from December 8th 2017 to December 7th 2018 collected by INMET Mirante Santana (MSA) were considered, since field measurement were not collected at 10 m from ground surface.

Together with the wind speed and direction, ENVI-met required setting roughness length at measurement site. The choice of this parameter was obtained by observing sensitivity testes results and urban site features, characterized by tall buildings and compact houses in opposition to the wind flow. Thus, the highest available roughness parameter was set. About solar radiation, a little adjustment was applied to the shortwave solar energy flux automatically calculated by ENVI-met. The adjustment factor was estimated comparing the real sun parable crossing the Belenzinho sky with the sun parable ENVI-met-computed, obtained from geographical input data, as Latitude and Longitude. In order to estimate the real sun parable, global radiation data (W/m2) from the closest meteorological station CETESB Parque Dom Pedro (DP_CET) were used. On this dataset, the comparison between the real global radiation peak (1126 W/m^2) and the ENVI-met peak (1098 W/m^2) was realized. By multiplying 1098 W/m^2 for the solar adjustment 1.03, the new peak 1131 W/m^2 resulted to be closer to the true value (1126 W/m^2).

As the wind, the specific humidity at the top of 1D model (2500m, g/kg) is kept constant during the simulation. Such start parameter depends on the atmospheric and physical conditions characterizing the air mass and its horizontal motes at the location in analysis, taking into account its altitude on the sea. To define the initial value of humidity at such great heights, no collected data were available at meteorological stations of São Paulo. As an alternative, the value of humidity was estimated from the dataset of the Department of Atmospheric Science - University of Wyoming (http://weather.uwyo.edu/upperair/sounding.html) which displays data from *Campo de Marte* Station (Station identifier: SBMT, number: 83779, latitude: -23.52, longitude: -46.63, elevation: 722 m, 5 km distant from urban site). This dataset provided values of humidity at specific heights (m) above sea level, at two daytimes, 00h and 12h, expressed in UTC (21h and 9h Brasília local time). However, gaps between known heights were large and intermediate values difficult to be estimated without losing meaningfulness (for example, an interpolation would not be suitable). In addition, it would be considered that, even if ENVI-met requires data at 2500 m, *Campo de Marte* Station is located at 722 m above the see level

and the real reference height becomes 1778 m (2500 m – 722 m). Hence, to discover the most representative ENVI-met humidity parameter, a dataset including the months of November and December 2017 was considered, in order to exclude values linked to seasonal effects unrelated with the season under analysis. Within this dataset, only 00h UTC values (that mean 21h for São Paulo local time, without summer time) were analyzed and the simulation start (21h) was set accordingly. Practically, for each day, the 00h specific humidity values, whose reference height was as close as possible to 1778m, were selected. Then, the heights of selected data were analyzed to verify that not too distant heights had been included. A Gaussian distribution of heights data was observed, with coincident mean and median (at 1714 m and 1702 m) really close to the reference value (1778 m) and a degree of asymmetry or distortion (-0.109) between -2 and 2. Later, the humidity values were analyzed too and, also in this case, a Gaussian distribution was found with coincident mean and median (10.31, 10.87) and a degree of symmetry and distortion (-1.47) between -2 and 2. As consequence, the specific humidity parameter at 2500m was defined as an intermediate value between mean and median, equal to 10.6 g/kg.

Other initialization parameters regarded the soil Model. ENVI-met model required temperature (K) and wetness (%) at 3 levels: upper layer (0 – 20 cm), middle layer (20 – 50 cm), deep layer (50 – 200 cm). When not measured, such soil initialization parameters are extremely variable to be estimated, since they vary not linearly with the land composition, the atmospheric conditions, the season and daytime, beyond that with the distance from ground surface. However, their value was obtained from the *São Jose dos Campos/SP station* (PCD 30893, Latitude: -23.205, Longitude: -45.868, Height: 621) within the datasets of the Brazilian National Institute of Spatial Researches INPE, (http://sinda.crn2.inpe.br/PCD/SITE/novo/site/historico/index.php). The station was selected to be closer to domain area than other meteorological structures; it provided soil humidity at 10, 20 and 50 cm from ground surface. A dataset window from October 1st, 2008 to January 1st, 2009 including wetness values at 21h and 00h was used, since only hot season and night conditions were considered to estimate such ENVI-met initialization parameter. In terms of soil temperature, in the first layer (0-20cm), the soil temperature was estimated to be similar to the surface temperature measured on Belenzinho site; therefore, the collected values from field stations, between 21h and 23h (initialization phase), were mediated and the value 24°C was found. Soil temperature in the second layer (20-50cm) was extracted from INPE dataset at 20 cm, obtaining 25°C. Finally, the soil temperature at the third layer had been set to 26°C, in order to keep constant the temperature increasing factor between the first and the second

layer. Nevertheless, the little influence of this latter layer was noticed in sensitivity tests (not showed).

Besides morphology and atmospheric parameters, ENVI-met allowed detailing the physical characteristics of façade materials, roof materials, plants and soils in the model. All these information were set in a *Manage Database* and stored in a personal project database ASCII-file (.edb). To define representative parameters for materials, plants and soils, findings from field analyses were used. However, to avoid an overload of information in the model, the myriad of urban components resulting from the field analysis were summarized.

Once a model was built up, its calibration was verified by comparing modeled values with observed field data. Key variables including air temperature, relative humidity, surface temperature and mean radiant temperature were considered. In terms of air temperature and relative humidity, the modeled-observed comparison was performed on average values since the slow variability of these variables. Such average was computed from the three field stations (station 1 and 2 representing the high-rise fabric and station 3 representing the low-rise fabric) installed on the domain in the months of November and December, 2017. Conversely, for mean radiant temperature and surface temperature, a calibration on specific receptors (coinciding with stations 1, 2 and 3) was implemented, due to the high variability of such variables depending on site characteristics. The comparison between modeled and observed trends was summarized on 24 h. To take into account reliable field data series, the most stable period of field observations was considered. Thus, data daily and consecutive intervals were selected within the time window between December 5th and December 10th. A moving average filter over 1.5-3.0 h interval without resampling was used to process raw series and obtaining a less noisy signal. Data were synchronized on Brasilia time (UTC-3).

4.4.4 Numerical experiments on the calibrated domain

The outgoings of the calibrated model were used to develop numerical experiments on the urban region under analysis. Six ENVI-met scenarios were simulated, testing different patterns of land occupation and exploitation for a selected small area in the core of the model. Scenarios aimed to explore the climate impact related to the use of such patterns on the site, investigating the implications of a possible densification process. To implement credible urban interventions, a preliminary study of the existing "state of density" was carried out, comparing BCA and FAR of all block by GIS tools. Then, three blocks among the less dense and verticalized areas were selected to modify the urban morphology and test future urban

developments. To recreate new urban arrangements, in each block the unification of single lots was supposed. The resulting areas have a size comparable to the real estate developments, usually built up in the urban region of São Paulo. The three blocks are located on the center of the model, surrounded by a frame of other peripheral blocks. Given their central position (in the core of model), extracted results were considered strongly reliable.

To discuss real urban design solutions, suitable to be applied to the reality of São Paulo City, the six scenarios of urban transformation were elaborated on ENVI-met observing the masterplan guidelines [Strategic Director Plan (PDE) + Parceling, Use and Coverage Land Law (LPUOS) + Buildings Code/Ordinance/Annex (COE)]. The set of law constraints for the area under analysis included: *a)* maximum land coverage *BCA* equal to 85% (lots < 500 m^2) and 70% (lots > 500 m^2); *b)* maximum land exploitation *FAR* equal to 4; *c)* no limit to buildings heights; *d)* minimum front distance from borders equal to 5 m. In addition, two equations from COE were considered to obtain the minimum distance from back and lateral borders (Equation 10), and the minimum relative distance between buildings (Equation 11).

$$D_{bor} = (H \text{ building} - 6) \div 10] \text{ or } 3 \text{ m} \tag{10}$$

$$D_{bld} = \sum_{Hb=1}^{n} [(H \text{ building} - 6) \div 10] \text{ or } 3 \text{ m} \tag{11}$$

To understand the microclimate effects caused by each scenario, an assessment area was defined within the ENVI-met domain. Such area was designed around the three blocks under transformation. Results were extracted from this region, at the pedestrian level (z=1 and 3m), analyzed and compared. This strategy allowed restricting the range of analysis, focusing on the region in which the built morphology had been modified. The assessment area (91x45 grids) extends from line 87 to 177 (along x axis) and from line 40 to 84 (along y axis). From the assessment area, the grid nodes occupied by buildings were excluded from the data analysis; thus, only open air exposed cells were considered.

Scenarios were explored on ENVI-met visualization tool (called LEONARDO) and MATLAB by developing *difference maps* in which scenarios were compared by subtracting point-to-point values for selected variables. For each scenario, selected variables included air temperature, relative humidity, mean radiant temperature, sky view factor, direct shortwave radiation, surface temperature. Given the great amount of data, difference maps were visualized and compared on four significant hours: 8h, 12h, 16h, 20h. A three-dimensional representation of difference maps was plotted to make easer the spatial understanding of this tool. To complement the visual analysis, correlation between scenarios was measured using a

non- parametric *Kendall's tau rank correlation coefficient*, comparing pairs of scenarios' observations (level of significance: α=0.05). Relative to other types of correlations (i.e. *Pearson*), such test does not rely on any assumptions on data distribution (not Gaussian population). Furthmore, sky view factor data were displayed on a probability density function (PDF). The hypothesis of Gaussian distributions was verified by a box-cox transformation. Bin widths were equidistant and set on 0.014%. For wind speed a cumulative distribution function (CDF) was used to display the probability that the variable will have a value less than or equal to *x*. A CDF can be understood as the sum of the frequencies of a PDF. With regard the wind direction, a polar histogram of occurrences was plot. Data of wind speed and direction modeled at the pedestrian level and 30 m above ground were considered. Probability density function were also realized to investigate air temperature, relative humidity and mean radiant temperature.

4.5   *Grasshopper modeling*

The ENVI-met model had been developed as the best compromise between time simulation, computational effort and accurateness of results. To investigate other modeling possibilities on the case study area, an additional model was built up using Grasshopper & Rhino tools. Grasshopper (G/R) and ENVI-met (E) models were developed for the same study area, but were based on different conceptual hypotheses and distinct mathematic formulations. Practically, the parallel use of the two tools allowed the investigation of domain thermal behavior starting from different driving processes, further contributing to the understanding of morphological and climate interactions.

The G/R modeling process involved the definition of a 3D geometric model in Rhino and the development of an algorithmic model on a graphical programming environment (Grasshopper). The algorithmic model set the parameterization and processes that have to be applied on the geometric model including solid objects and surfaces. The algorithm model relied on the interoperability of different plugins, including *Honeybee*, *Ladybug*, and *Dragonfly* (Figure 18). The last-one plugin was used to develop the model core that calculated urban air temperatures at the studied area using climate data measured at an operational meteorological station. This procedure was essentially opposite to that followed in ENVI-met. In ENVI-met, air temperature and relative humidity measured in site had been applied as boundary conditions to force the model. This choice had been necessary to calibrate the model, since T_{ar} and RH variables were strongly dependent on forcing. This fact compels

modelers and users to conduct an accurate data collection in the domain area. Moreover, the simulation period will be bound to the fieldwork time-series and other periods of the year will remain unknown. In Grasshopper, instead, the use of *Dragonfly* allowed scaling meteorological station data until to the urban area under analysis, relying on long-term time series. To make it feasible, Dragonfly uses *Urban Weather Generator* (UWG) integrated engine (Bueno et al., 2013). UWG is a powerful numerical algorithm becoming standard in the field of urban modeling; it enables to account for Urban Heat Island effect to simulate the urban temperatures and humidity in the study area. To estimate such values, UWG interrelates four coupled models called Rural Station Model (RSM), Vertical Diffusion Model (VDM), Urban Boundary Layer (UBL), Urban Canopy and Building Energy Model (UC-BEM), whose physical meaning is well explained in Bueno et. al (2013).

Figure 18 – Grasshopper modeling workflow
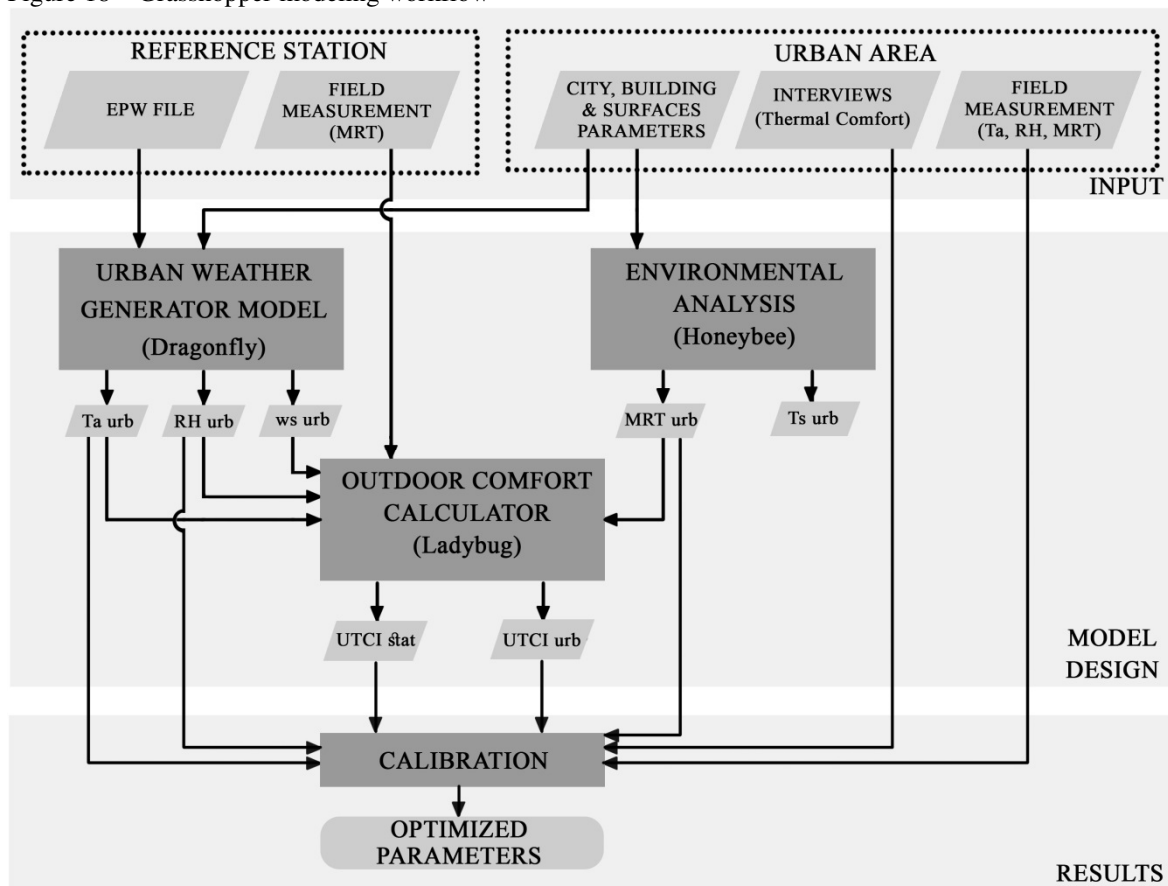
Source: Martina Pacifici, 2019

To enable UWG, Dragonfly provides a set of components to parameterize. Parameters characterizing the domain urban area included buildings shapes, use and age, materials, vegetation coverage, waste heat from air conditioning, sensible anthropogenic heat generated

by cars and boundary layer conditions. Climate data from meteorological station had to be provided in *EnergyPlus weather* format (epw). *Epw* files for cities around the world may be downloaded on: https://energyplus.net/weather. However, for the case of São Paulo, only 2008 *epw* data from *Mirante Santana* and *Congonhas* Airport were available (probably representing the average time-series of the last years). *Mirante de Santana* (MSA) was selected to be more representative of a rural weather station, according to UWG developers. To overcome the inconvenience of the date, a novel input epw file was formatted using an EnergyPlus wheater converter (*Wheater Statistic and Conversion*) in combination with the program *Elements* developed by *Big Ladder Software*. Such new epw was updated with more recent data (2018) from Mirante Santana station.

In addition, to verify the calibration between modeled and real data, field measurements were carried out on December 10th 2018. Such climate data collection occurred simultaneously in two places (the urban area and *Mirante Santana*) by means of two field stations. Specificities of equipment are equal to stations 3, 4, 5 at Table 5. In both of places air temperature, relative humidity and globe temperature were recorder at 1.2 m above ground surface, from 10 a.m. to 19 p.m. (local hour). It worth stressing that in the case of *Mirante Santana,* the data collection had been necessary to measure globe temperature (not measured from official station); the rest of the variables (T_{ar} and UR) were used to verify the congruence between field stations and official station. The field station was installed close to the WMO station. In the case of Belenzinho, the field station was placed outdoor, in the middle of domain, on a sidewalk between the low-rise and the high-rise zone. Furthermore, the comfort sensation of people was also collected on the same day, at the two places, by means of interviews.

The domain model coincided with the interest area of ENVI-met model space. However, to extract findings, a reduced area was considered, including parts of low-rise and high-rise zone. Dragonfly allowed reproducing Tar and RH on the urban area, as well as the *Universal Thermal Comfort Index* (UTCI) at both sites (urban area and *Mirante de Santana*). UTCI was selected as the most reliable outdoor comfort index made available by Ladybug tool. UTCI findings (°C) were converted in comfort classes according to the São Paulo calibration (MONTEIRO, 2018, p.174). Mean radiant temperature and surface temperature in the domain were instead computed by Honebee plugin. The output MRT was introduced into the UTCI calculator to achieve the comfort index in the urban area (domain). For the comfort index of Mirante, MRT was obtained by recorder field data, converting T_g in TMR. To obtain UTCI index in representative points of domain, a pedestrian path was defined and four

significant points fixated on its length (A-D). Point A, B and D were placed in correspondence of Station 1, 2 and 3 of the previous data collection. Point D is an intermediate point in which the most recent field measurement were collected (December, 2018). From point A to D, the comfort sensation of a symbolic pedestrian walking from the high-rise zone to the low-rise zone was assessed.

5   Results and discussion

Goal: This chapter summarizes results obtained along with the application of the investigation procedure developed, including the climate-morphological assessments, as well as finding from ENVI-met and Grasshopper models. Overall, findings are embedded and those from assessment stages were utilized to develop the modeling activities. At each step, the complex knowledge learnt on urban forms and climates interactions gets richer. The chapter's content regarding climate and morphology data analysis was published on two international journals, *Urban Climate* (PACIFICI; RAMA; MARINS, 2019) and *Sustainable Cities and Society* (PACIFICI et al., 2017). The most part of the rest of material was presented on Conferences (PACIFICI; MARINS, 2015; PACIFICI; MARINS, 2017; MARINS et al., 2017; MARINS et al., 2018; PINHEIRO et al., 2016) or journals (ARBEX et al., 2016).

5.1   Results from 1st climate and morphological analysis

These results concern the first phase of analysis assembled and put in practice on the domain. A selected urban area under transformation and densification was spatially analyzed, detecting all the possible configurations in which urban forms and open spaces are combined. Then, the climate and morphological state of these spatial configurations was assessed, showing thermal contrasts inside the domain. Three climate zones were found distributed according to distinct morphological patterns. Materials and methods concerning these results are available on 4.1.

From a morphological perspective, the assessment of domain urban fabric started with the study of buildings vertical extension. Therefore, the buildings heights - available in the São Paulo Municipality database (Geosampa, http://geosampa.prefeitura.sp.gov.br/PaginasPublicas/_SBC.aspx) - were classified in four vertical scales: *scale S1 = 0 floor*, (0 m< S1 ≤ 0.5 m), *scale S2 = 1-3 floors*, (0 m < S2 ≤ 10 m), *scale S3 = 4-9 floors*, (10 m < S3 ≤ 30 m); *scale S4 = >10 floors*, (S4 > 30 m).   The first scale gathers the unbuilt spaces, impervious or permeable, while the others segregated buildings. Heights generally allow evaluating a certain degree of verticalization in the area. Figure 19 displays such built forms heights, ranging inside the red perimeter of domain and surroundings. Very verticalized forms (burgundy) and other lower built blocks (orange shades) were found juxtaposed at very close distances, contributing to the scattering of the urban fabric.

Once the buildings scales were defined, the urban forms distribution was valued through four categories: number of buildings (1), heights (2), areas (3) and volumes (4). Reciprocal influences between categories and scales were investigated in four graphs (Figure 20). The four graphs constitute a simple tool of morphological assessment, obtained from easily available data.

Figure 19 - Ranging of scales inside the study area
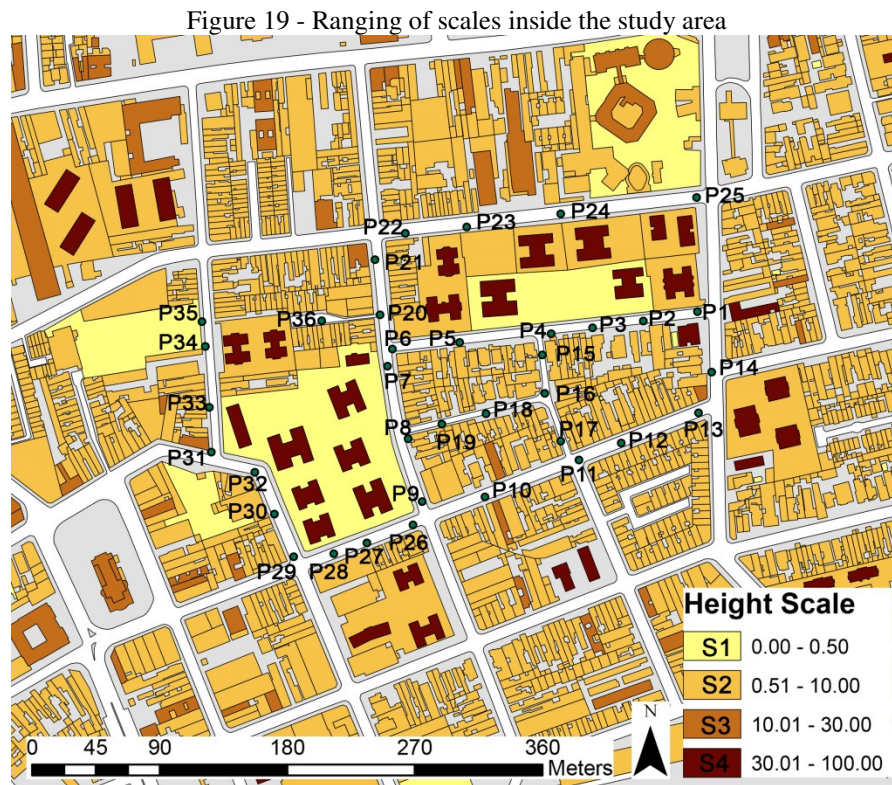
Source: Martina Pacifici, 2019, based on the Geosampa-Digital Map of São Paulo City

Figure 20a shows Scale S2 is the most widespread, gathering the great majority of buildings present in the study area, followed by S4; just few urban elements of S3 and S1 were found, since lots do not have many open spaces (S1) or intermediate-scale buildings (S3). Despite this scale disparity, in Figure 20b, Scale S4 reaches S2, or rather the amount of meters measured in height is roughly the same between the two scales (1,400 m versus 1,200 m in length). This means that the two scales approximately provide the same number of inhabited floors, despite their different footprint, once scale S4 benefits from the verticalization potential. Scale S1 shows a rising behavior only in Figure 20c, where the large tower podiums (around 0.1 m to 0.5 m of paved built thickness emerging from the ground level) significantly influence the amount of constructed area. The final overcoming of Scale

(4) with respect to Scale (2) occurs in Figure 20d, wherein the built volume amount is calculated for each scale.

In general, it may be clearly observed that the scales are not equally and gradually distributed in the domain. A gap between the largest (S4) and smallest (S1 and S2) scales was found; meantime, the near absence of intermediate scales (S3) was noticed. This result is in agreement with Salingaros and West (1999) findings, for whom the largest amount of estate activities are currently addressed to develop giant projects, to the detriment of small and intermediate size projects that, instead, could favor an organic growth of the urban fabric.

Figure 20 – Analysis of Buildings (a), Buildings Heights (b), Built Areas (c), Built Volumes (d).
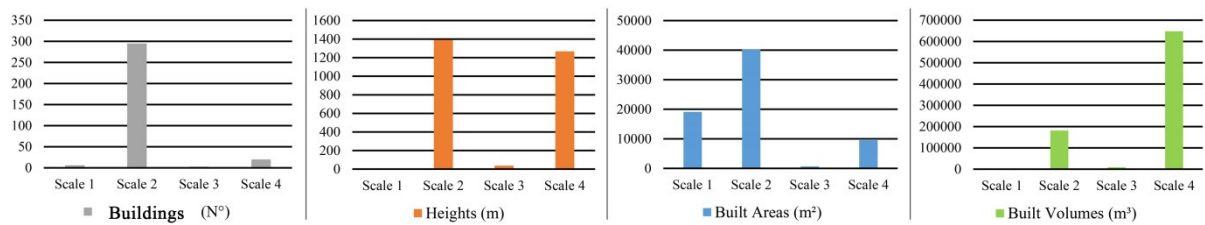
Source: Pacifici et al. (2017)

Meanwhile, the land use study clearly revealed the coexistence of residential and commercial land uses as shown in Figure 21a. The residential use is organized in vertical housing lots and in low-rise housings mixed with commercial lots.

Figure 21 - Map of land use analysis (a). 1954 cadastral map of the study area (b)

Source: Pacifici et al. (2017), based on the Geosampa-Digital Map of São Paulo City 2016 (a), based on Vasp Cruzeiro, PMSP, 1954 (b)

Figure 21b presents a 1954 cadastral map of the study area, in which the lots formerly occupied by industries or warehouses are red highlighted. As showed, vertical housing has occupied vast properties of recent receding industrial activity in the neighborhood, while low-

rise blocks of small lots still retain their original structure. Real estate developers, in fact, face difficulty in pooling several small lots and focus their action on areas with fewer larger lots.

Figure 22 (*a* and *b*) shows the course of the specific humidity (g/kg) and air temperature (°C) collected from 36 points (or road sections) along canyons.

Figure 22 - Average morning and afternoon temperatures, average morning and afternoon moistures (up). Three climatic zones (down)

(a)

(b)
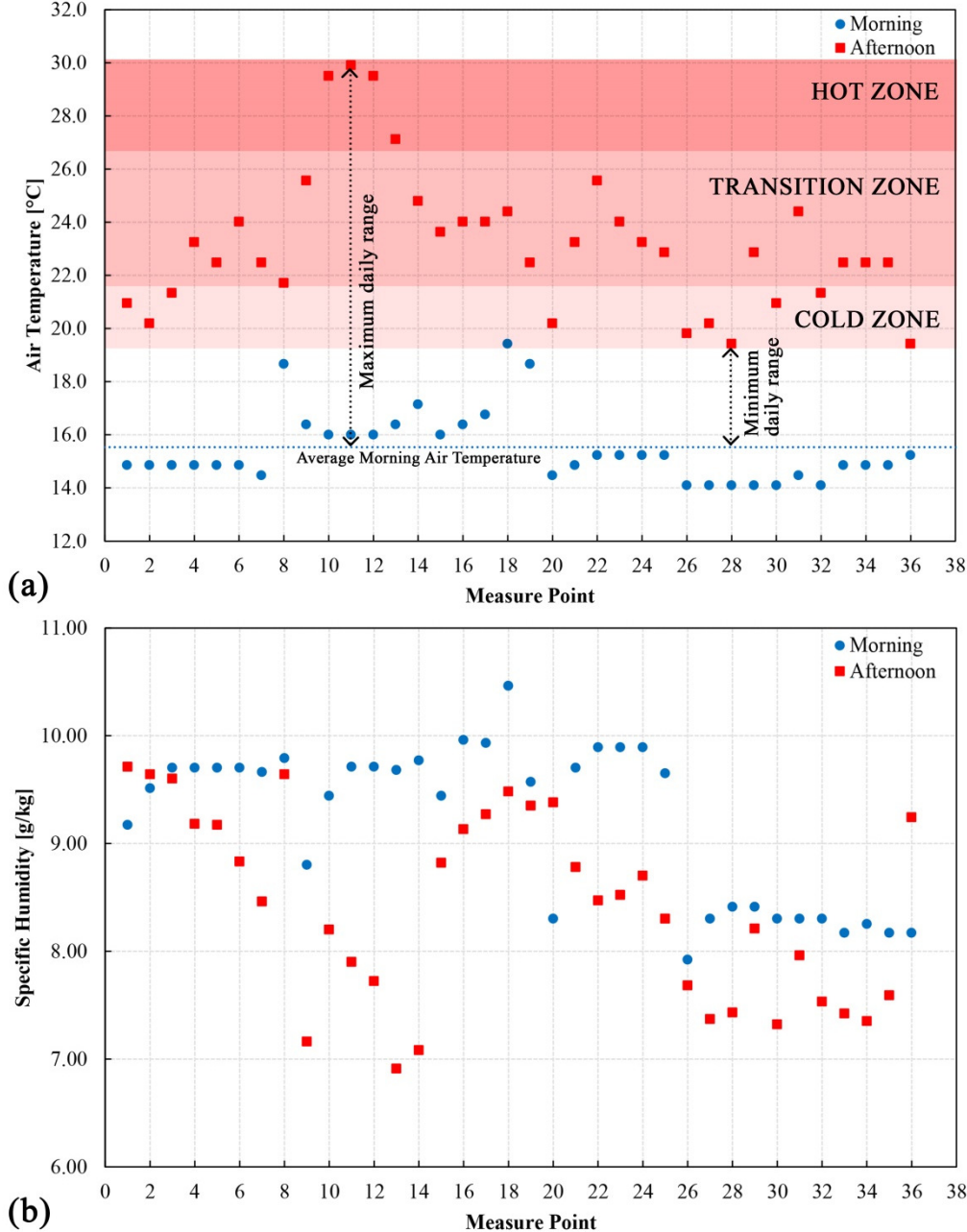
Source: Pacifici et al. (2017)

Morning temperatures are approximately constant, ranging around the average value of Ta = 15.5 °C, with only points P8, P18, P19 emerging above the general tendency,

confirming the average minimum value (15.8°C in July) found for São Paulo by Tarifa and Armani (2000). This constant trend represents a common initial condition for all points, given by the night cooling, from which the city will begin gaining daily heat. Conversely, in the afternoon, a larger variation may be observed, to the extent that each of the morphological groups overheats with different intensities. Therefore, the afternoon temperature trend was split into three bands – hot (1), transition (2) and cold (3) zones – in which the measured points can be segregated (Figure 22a). Conversely to air temperature, specific humidity values (22b) displayed an opposite trend, with the lowest values concentrated in the period of afternoon.In terms of surface temperature, taken at three points of each road section (street pavement, sidewalk pavement and building façade adjacent to the sidewalk), thermal variations between 15°C and 50°C were observed between different climate points. In Figure 23, surface and air temperature were overlapped with values relating to the illuminance level encountered on site, in the morning and afternoon periods. The average correlation between surface temperatures and illuminance was computed at all the points by Spearman's Rank-Order Correlation.

Figure 23 - Illuminance and Temperature in the morning and afternoon (up). Spearman Rank Order Correlation (down)
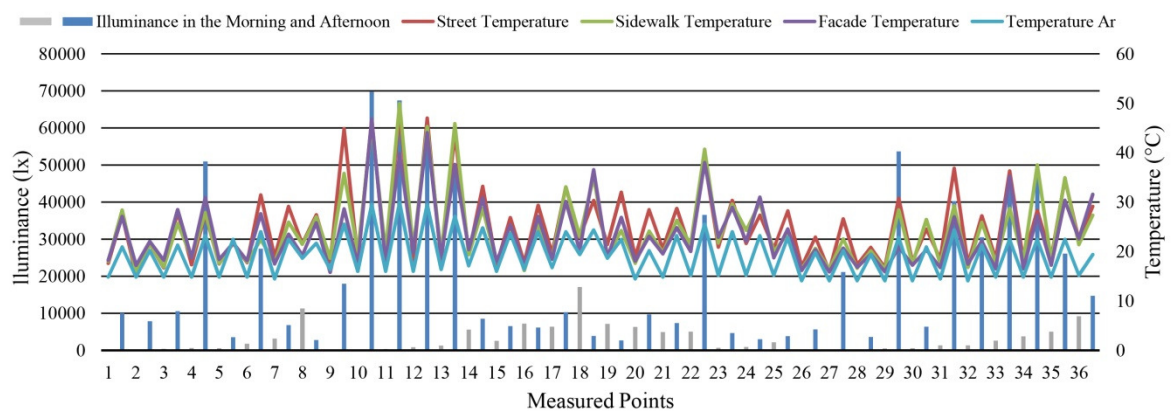
Surface Temperature	Illuminance		
	All points	High SVF	Low SVF
Street	0.771	0.822	0.581
Sidewalk	0.705	0.755	0.509
Façade	0.661	0.739	0.377
*Significant correlation at p < 0.05			
**Cut-off value between High and Low SVF = 25%			

Source: Pacifici et al. (2017)

From the scatter plot (Figure 24a), it may be seen that the three surface temperatures have almost parallel regression lines and are therefore related to the illuminance on a similar way. A threshold in the correlation distribution could be verified, denoting a data bilinear behavior. Subsequently, the Sky View Factor (SVF) was chosen as split parameter to cluster the data population in two groups (high SVF, low SVF). SVF was obtained by using the software *Rayman 1.2* for all climate points. 25% was considered as the SVF cut-off value. By repeating the correlation in these two groups, the correlation of high SVF group was observed to increase when compared to the average results, whereas the low SVF group decreased strongly. As expected, among other factors, a wide sky view enhances the correlation between illuminance and temperature, while the presence of obstructing objects disturbs it (Figure 24b).

Figure 24- Surface Temperatures and Illuminance Scatter Plot (a). 3D representation of an urban section S at points P1, P2, P3, at 7:30 a.m. (b). Air Temperature and Tree Coverage (c)
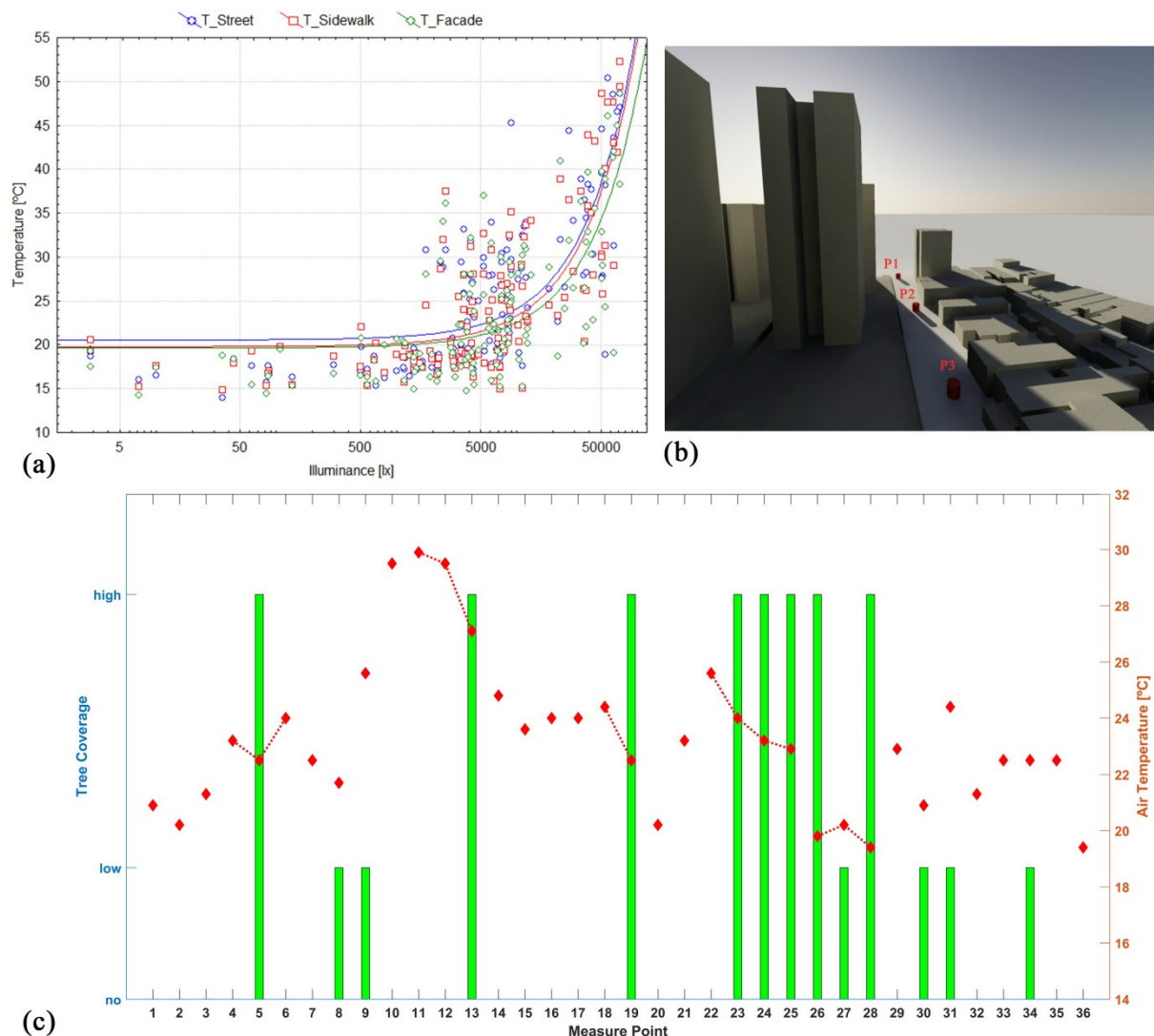
Source: Pacifici et al. (2017)

Moreover, the effect of tree coverage was also observed. Three classes of urban tree coverage were qualitatively detected in the study area at the 36 points: (i) no tree coverage, (ii) low tree coverage, (iii) high tree coverage (later, a more accurate tree classification will be showed). At tree-covered points (ii, iii), the climate variables were measured below the canopy shade. Figure 24c visualizes how street tree coverage contributed to mitigate the local micro-climate by decreasing hot temperatures; points with green bins have lower temperatures than points without green bins. Among the air temperature points measured in transect, five sets of points were highlighted (dotted line). Each set is formed by points in similar local conditions - same street, same street orientation, similar built surrounding, at really close distance. It can be observed that, in these sets, high tree coverage is largely responsible for the temperature drop (descending trend between one point and another).

Furthmore, to enhance the linkage between the study of climate and morphology, six indicators dealing with the urban form were estimated in the influence area of climate points. Computation of indicators is explained in Table 7.

Table 7 - Indicators

(1) Indicators of Coverage:
Open Coverage (%) = $100 * [(\sum_1^n Open\ area)/Sample\ area]$ with n = number of open areas
Built Coverage (%)= $100 * [(\sum_1^n Built\ area)/Sample\ area]$ with n = number of built elements
(2) Indicators of Intensity:
Open Volume (%) = 100% - Built Volume
Built Volume (%) = $100 * [(\sum_1^n Built\ volume)/Ideal\ volume]$ with n = number of built elements   with *Ideal Volume (m³) = Sample Area * Built Element Average Height* = 100%
(3) Indicators of Quantity:
Building quantity (n°) = $\sum_1^n Building$ with n = number of buildings
Open space quantity (n°) = $\sum_1^V Open\ space$ with n = number of open spaces
(4) Indicator of Compacity:
Built Elements Proximity (n°) = $\sum_1^n Wall\ shared\ by\ more\ Built\ Elements$ with n = number of built elements
(5) Indicators of Permeability:
Lot wall permeability (%) = $100 * [(\sum_1^n Openings\ Length)/Lot\ Perimeter]$ with n = number of lots
(6) Indicator of Diversity:
Height Scale (n°) = $\sum_1^n Scale$ with n = number of built elements
Setback Scale (n°) = $\sum_1^n Setback$ with n = number of built elements

Source: Pacifici et al. (2017)

The indicators of *intensity*, *diversity* and *compacity* taken up the proposal for indicators of Bourdic, Salat, Nowacki (2012), while the indicator of *quantity* was based on the ideas of *multiplicity* well expressed by Salingaros and West (1999) within their studies on urban morphology. The purpose of indicators was related to the need of understanding in how many possible ways the built morphology was influencing the points' microclimate. Indicators were displayed on Figure 25.

Coverage indicators, including built and open areas, show how the influence area around the measurement point is occupied by buildings or is free of them. The highest value was found at point P36 (80%), the only road section located inside the block; the lowest (27%), instead, occurs close to a group of towers (P25). Overall, the amount of built area surpasses open areas in almost all points, although the contribution of streets areas. The indicators of intensity, including open and built volumes (cakes), display how the land occupation is heavily or slightly built, by computing the amount of built volume contained in the influence area and its opposite. The highest built volume value (70%) was found at point P24, which included two towers in its influence area; the lowest one (10%) occurred close to a large condominium open space (P4).

The indicators of quantity (No. of buildings and open spaces contained within the influence area) and compacity indicator (n° of facades shared by two building) performed similar trends; indeed, by increasing the number of built elements, the compacity of urban fabric rose, since the proximity of built elements increased, too. A reciprocal relationship was also found between the indicators of diversity that measure the degree of morphological diversification on the vertical (height scales) and horizontal (setback scales) plan. As the number of height scales grew (vertical diversity), the number of setback scales also rose (horizontal diversity). Finally, the inverse relationship between lot wall permeability (percentage of permeable wall along the lot perimeter) and quantity of open areas (number of open spaces) could be observed. As the first indicator increased, revealing the continuity between the street level and the open spaces inside the lots, the degree of space fragmentation of urban fabric (high number of open areas) followed the reverse path. This means that, the more a lot presents permeability of its boundaries, the more the lot exhibits a low quantity of open areas within it.

Figure 25 – Building quantity, Open space Quantity, Height Scale and Setback Scales (1° chart, up); built coverage, open coverage and Lot Permeability (2° chart, down); Built Volume and Open Volume displayed on the cakes; map of influence areas around climate points (center).
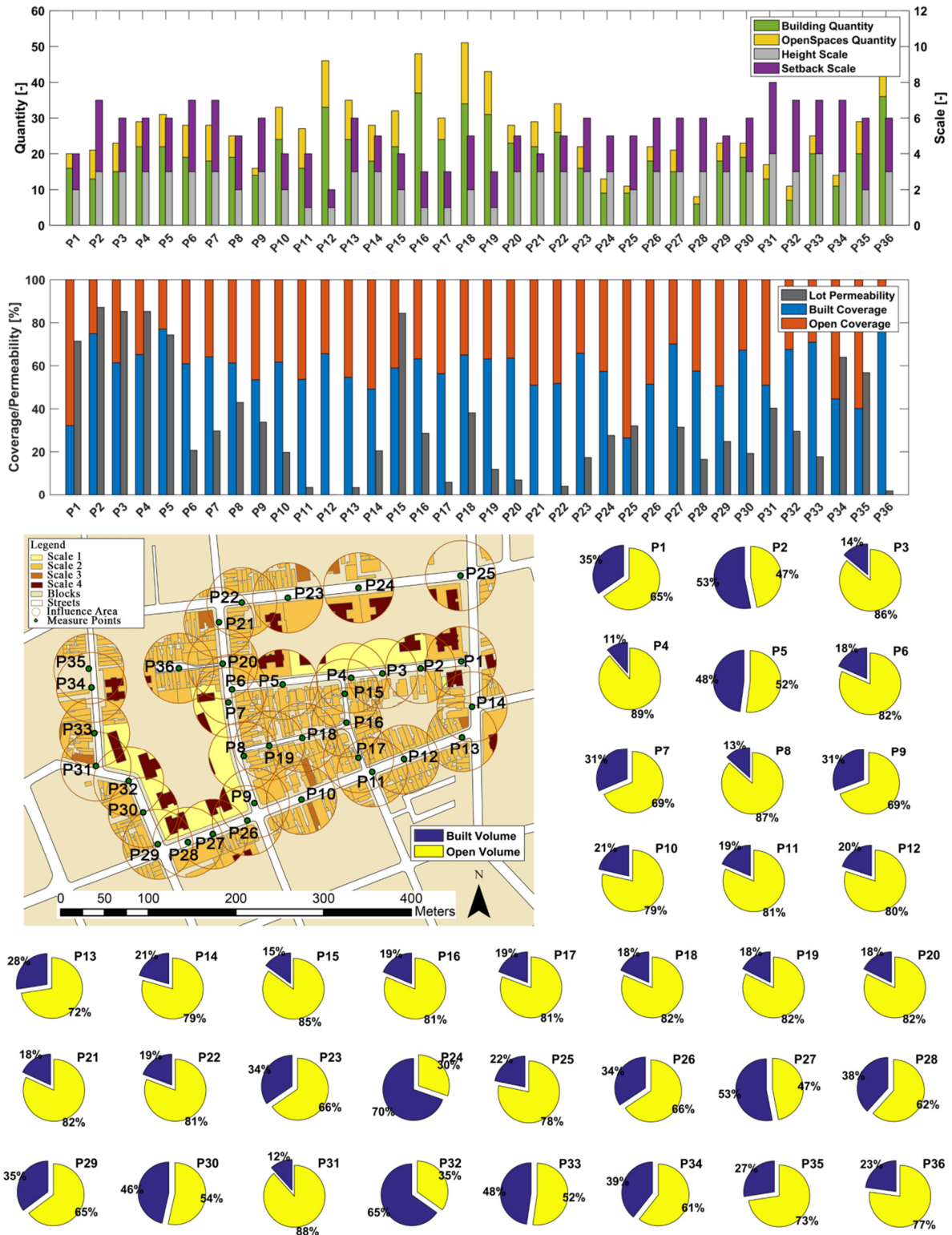
Source: Martina Pacifici, 2019

Once the attributes of urban form and climate were characterized in 36 selected points of the domain, a comparative analysis was developed. The first important observation

suggests that, despite the small size of the domain, climate variability was measured on the points; a strong correlation between climate patterns and morphological structures of the studied area was observed. These results agree with Stewart, Oke and Krayenhoff (2014), for whom building height and spacing between buildings contribute to creating thermal contrasts among different localities, together with tree density, soil wetness and permeability.

In the afternoon, the occurrence of such thermal contrasts resulted in various climate zones. Thus, three climatic zones were identified: hot zones (1), transition zones (2) and cold zones (3). While transition zones presented intermediate temperatures, cold and hot zones showed temperature peaks. Therefore, it could be inferred that, in the cold season, the domain favored a certain diversity of microclimate environments, differently affecting people activities and pedestrian circulation. Each point of domain falls on one of three zones. Figure 26 shows how these climatic zones are distributed inside the domain, grouped into sets of points. It is also strongly stressed that the terminology (hot and cold zones) is used to describe the reciprocal temperature differences between points; indeed, in a hot climate such as Brazilian one, a winter afternoon could be uncomfortable but improbable freezing.

- *HOT ZONE: Uncovered Spaces in low-rise fabric (P10, P11, P12, P13)*

The "hot zone" is the region in which the domain presents the highest heating. Here, starting from a pretty constant morning trend, points P10, P11, P12, and P13 together reached the highest afternoon temperature, exhibiting the larger thermal daily excursion (13.50 °C, 13.90 °C, 13.30 °C and 10.70°C) and the lowest values of relative humidity. In addition, the highest values of surface temperature were found in correspondence with the street, sidewalk and façade of the same points.

This exceptional trend is performed by four street cross-sections, placed in sequence along the same canyon (Figure 26). These source points are characterized by unshaded open spaces, free from architectural obstructions. The main block of towers is quite far. In addition, as the building heights in these points are modest, the proximity of houses to the sidewalks does not prevent solar access, as the sky views show (Figure 26). Therefore, the sun path – following the arc East-North-West, permitted a full radiation of the road sections, their exposed materials, as well as of the building roofs, causing high levels of outdoor temperatures.

From the morphological analysis of the "hot" road sections, a small amount of built volumes (21%, 19% and 20%) was measured at points 10, 11, 12, implying high percentages of open air spaces above roofs. Also, low Diversity (20%, 3% and 0%) and low Permeability of lot perimeter were found. At points 11 and 12, in fact, just scale S2 is present (0.50 m < S2

< 10 m), precluding the presence of buildings with different heights, which would favor ventilation. Few or no openings cross the lot boundary, also preventing any cooling action exercised by secondary air streams. In addition, at point 12, just one type of setback was observed (0m), and the perimeter of the lot directly faced the street.

Figure 26 - Map of climatic zones (left, a), representative pictures of the three zones (center, b), sky view photos (right, c)
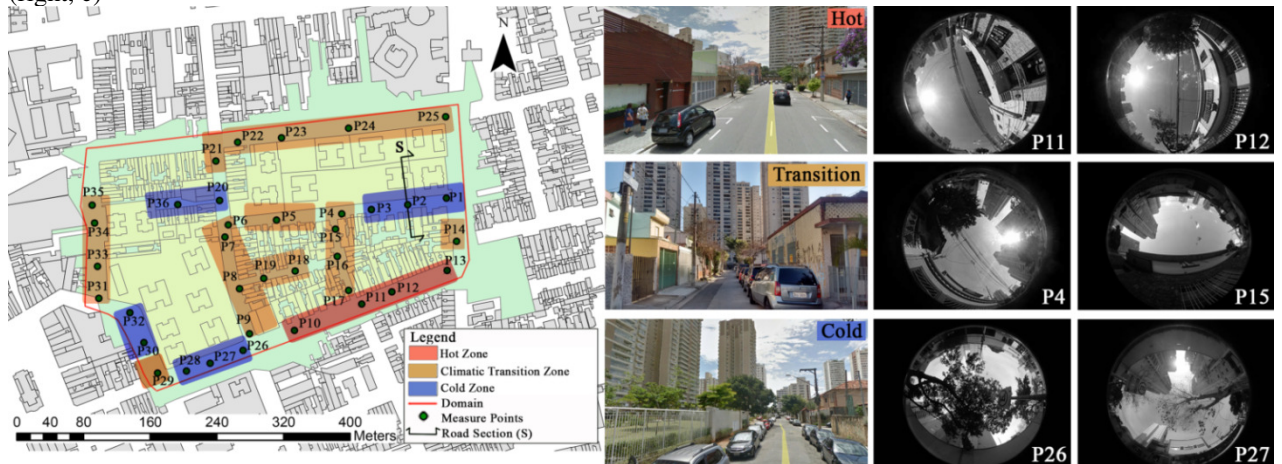
Source: Pacifici et al. (2016); based on Geosampa-Digital Map of São Paulo City 2016 (c)

- COLD ZONE: Shaded Spaces (P1, P2, P3 and P26, P27, P28)

The "cold zone" includes the coolest regions of the domain. In this range, two groups of contiguous urban sections – P1, P2, P3 (set 1) and P26, P27, P28 (set 2) – performed the "lows" in the afternoon temperature line (between 19°C and 21 °C) with small thermal excursions from the morning constant temperature. Both of these sets are characterized by open spaces widely shaded by towers on the north side; this prevented a direct irradiation on the south side and slowed down the daily heating process.

Points P1, P2 and P3 are located between a group of towers on the north side and a fabric of low-rise housing on the south one. The shading towers are arranged in two distinct lines of the lot; one facing the street, and the other at the back of the plot. This shifting creates a dense urban arrangement that permanently or temporarily casted shadows on the points below (Figure 27). According to Knowles and Berry (1980), the larger the built volumes, more the buildings conflict with each other by shadowing. Thus, when the measured points were intercepted by more towers (P2), the temperature tended to fall, since the points were longer shaded.

Figure 27 - 3-dimensional domain representation at 7:30 a.m. (a) and at 2:30 p.m. (b) showing the points P11, P12, P13, P14 constantly lighted
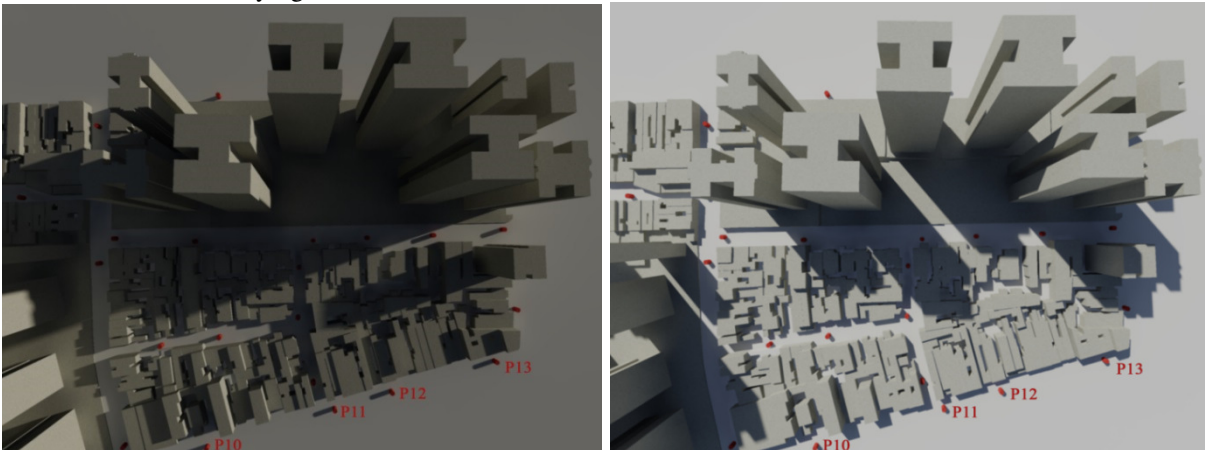
Source: Pacifici et al. (2016)

On the same street, along with hot spots - Rua Júlio de Castilhos –, the second set of cold points were pinpointed (P26, P27, P28). Between the hottest and coldest regions on this street, an excursion of 9.7°C was measured. Here, besides the shading caused by the high-rise buildings, an additional solar shield was caused by trees. The tree coverage contributed to additional cooling effects. While a fall of afternoon solar incidence was observed from P27 (tree low coverage) to P26 and P28 (tree high coverage), a surface temperature decrease was verified, especially in terms of road asphalt (20.8°C (P26), 25.0°C (P27) and 19.1°C (P28)). Consequently, despite the small distance between the points, an air temperature excursion occurred between P26 (19.8°C), P27 (20.2°C) and P28 (19.4°C).

In terms of morphology, cold points are composed of a variety of different height classes and setbacks, since different building typologies are found within a walking distance. All of them include towers, ensuring an abundance of setback types and the presence of the major height scale (S4). When influence areas were analyzed, different values of lot Permeability were computed between the two sets of points. While the first set (P1 to P3) had high values on the Permeability indicator (71%, 87%, 85%) due to the absence of walls along the block perimeter, the second one (P26 to P28) had quite closed boundaries and, consequently, low values of openings (0%, 31%, 16%); hence, air dynamics could differently affected pedestrians' walk in these two zones. According to Emmanuel et. al (2007), shading strategies should be coupled with a street level ventilation study at building and neighborhood scale.

- *TRANSITION ZONE: Internal and Protected Spaces (P4, P15, P16, P17)*

Between the "hot" and "cold" zones, transition regions took place. In the case of the study domain, the zones of climatic transition were rather scattered. However, similarities could be identified between points P4, P15, P16 and P17. This group of four points is aligned along the North-South direction, between the "hot" and the "cold" zone, benefitting of partial shading and slight ventilation. To the North of point P4 (see Figure 26), a large square provides an open space that favors more radiation and avoids the direct shading of the towers. Because of this opening, P4 received a good afternoon level of illuminance and multidirectional ventilation, both parallel to the street. Conforming to the air temperature trends, the surface temperatures achieved intermediate values in this zone (Figure 23).

In a morphological prospective other considerations could be extracted. The influence area of transition zone points showed a quite balanced coverage proportion between the built and open areas (65-35%, 59-41%, 63-37% and 56-44%). Concurrently, the small built volume percentages (11%, 15%, 19% and 19%) turned out a modest compactness and verticalization in these influence areas. The built volume percentage around point P4 is the smallest. In addition, since the transition zone corresponds to a historical fabric, a high quantity of built elements occurred, especially in the influence area of point P16, in which the major value was found (n°37 buildings).

In the same line of P1, P2, P3, sample P6, located on the corner, stood out from the previous cold spots, exhibiting warmer transitional temperature (24.0°C). In fact, despite being skirted by towers, it left the morning shadowing area before the other points, benefiting from the afternoon sun. This circumstance came from the arrangement of built forms around the point; in fact, from P1 to P6, the towers fade from a height of 73 to 59 meters, before disappearing near the lot corner, in which a playground is located.

- *THERMAL COMFORT*

The climate variability found at the three climate zones was also observed in terms of thermal comfort. The PET trend, computed by *Rayman* computational package and calibrated for São Paulo in accordance with Monteiro (2008), crossed most of the thermal sensations and varied from "little cold" to "very hot". Few points fell into the neutral range of comfort (Figure 28). Overall, hot zones (sun-exposed spaces in low-rise fabric) could be associated with a warmer street microclimate, worsen by the trees lack, while cold zones (shaded spaces close to high-rise fabric) showed cooler open areas. Such differences stood out in the afternoon period.

In the morning (6 a.m. to 9 a.m.), most points remained between the sensation of "little cold" and "neutral". In this period, PET trended uniformly and no points provided hot sensation. The sets P1 (13.4°C), P2 (13.5°C), P3 (15.3°C) and P26 (13.6°C), P27 (13.8°C), P28 (13.5°C) recorded the lowest PET values in agreement with the demarcation of the cold zone. Both these sets of points are distributed on the south side of high-rise buildings, as well as close to tree crowns. Conversely, out of the continuous shading of towers and trees, morning "neutral" comfort points were found, in agreement with the demarcation of the transition zone. In general, before 9 a.m., the most of the cases showed a slight thermal discomfort tending to coldness.

In the afternoon, (1p.m. to 4 p.m.), PET values varied from "neutral" to "very hot". In comparison with morning, a greater PET variability was observed. A majority of hot points was found and no cold sensations were noted. A gap of 15°C isolated the "very hot" comfort points P9 (56.6°C), P10 (56.4°C), P11 (57.1°C) and P12 (48.8°C) from the rest of sources, in agreement with the demarcation of "hot zone". The demarcated "cold" and "transition" zones in the afternoon were occupied by "hot" and "slight hot" points, ranging between 26°C and 43°C. Along all the day, even if in winter, no points at "very cold" sensation were found.

Figure 28 - PET Comfort index
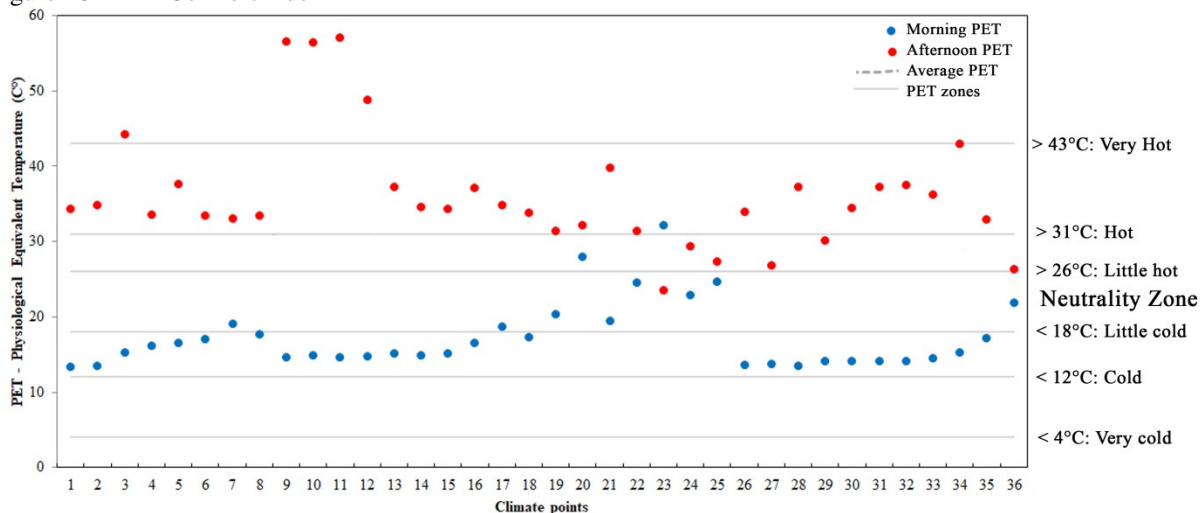
Source: Martina Pacifici (2019)

- *SOLAR ACCESS*

In the solar access analysis, the influence of shadows projected by urban elements on the microclimate zones of domain was investigated. A sun path was simulated above domain, parametrically obtained by DIVA plugin within Grasshopper on Rhinoceros software. Such

sun path enabled the assessments of interactions between sun and buildings geometry, given a time during the year and a location. The seasons of autumn and winter caused a greater incidence of shadows in the domain, due to the presence of towers and lower inclination of the sun's rays on the horizon. Close to the condominiums, high buildings led to permanently shadowing large parts of street spaces, while little buildings projected smaller shadows, guaranteeing a higher amount of sun hours *per* day. In addition, while in the hot summer and spring more shadows are desirable, in the colder season an excess of shading could compromise the open spaces experience at some times of the day, while exposure to direct radiation can be beneficial to their use (Figure 29).

Figure 29 - Summer (a) and winter (b) shading
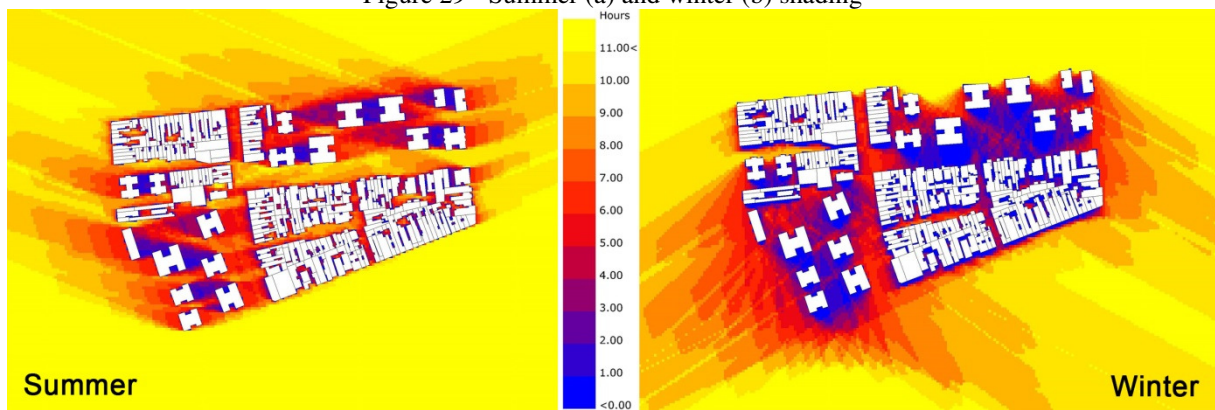
Source: Pacifici and Marins (2017)

In a representative day of the climate collection within the domain, a high coincidence was found between sun access and climate zones (Figure 30, bottom line). Analyzed climate points were free from the interference of tree shadows and only the impact of building geometry was considered. In a 12h sun path, all points in the cold zone were affected by large periods of shaded hours, exhibiting 7 (P1, P30), 8 (P27, P36, P20) and 10 (P2 and P3) hours of shading *per* point. The lowest values of shaded hours were found in the hot zone climate points, with 4 hours (P10) and 3 hours (P11 and P12) of shading. In the transition zone, contrasting values were observed ranging from to 5 to 10 hours of sun access *per* day. The analysis of *Spearman* correlation coefficient (rs), suitable for no-linear relationships among variables, revealed correlation between the number of sun hours and temperatures collected at the climate points. The best correlation was obtained for street surface temperature (rs = 0.700949), due to the great heating that characterizes asphalt.

Figure 30 – Sunlight hours analysis

Points	1	2	3	4	5	7	8	9	10	11	12	14	15	16	17	18	20	21	27	29	30	31	32	33	34	35	36
Sun hours	5	2	2	2	6	4	5	5	8	9	9	7	2	3	4	8	4	5	2	5	5	6	5	7	7	7	4
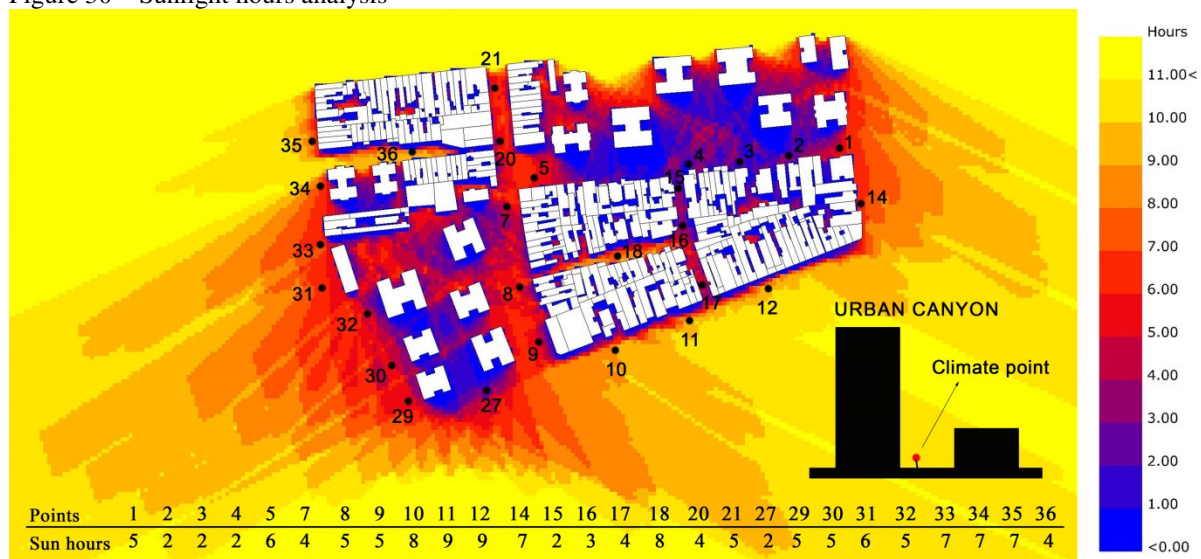
Source: Pacifici and Mains (2017)

Nevertheless, the significance of shadows impact should not be equally considered through the day, since shading tends to become more important during the central daytime hours (ERELL; PEARLMUTTER; WILLIAMSON, 2011). By applying a multiplicative factor to the solar hours, an adjusted correlation improved the correspondence between sun hours and temperatures to rs = 0.741302 (Figure 31).

Figure 31 - Correlation between Air Temperature, Street Temperature and sun hours (using multiplicative factor)
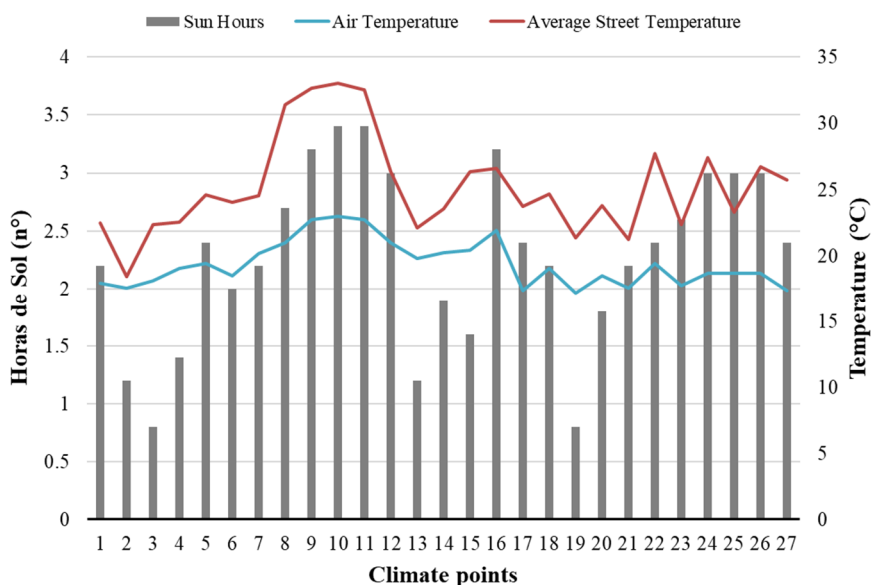
Source: Pacifici and Marins (2017)

The multiplicative factor was achieved by taking into account the potential of solar energy provided along the day. In the simulated day (May, 26), the sun arose at 6:19 p.m., set at 7:47 p.m., while the zenith occurred at 1:07 p.m. Within this solar interval, three slots were segregated: a morning slot (7 - 11 a.m.), a central slot (11 a.m. - 3 p.m.) and an afternoon slot (3 - 7 p.m.). The central slot, around the noon, was energetically characterized by high values of global radiation in comparison with two lateral slots (Table 8). In Belenzinho domain, 19% of solar hours were in the first slot, 60% in the second slot and 21% in the third slot, showing that the greater sun availability occurs close to noon, when sun is high and buildings prevent less direct rays. According to the closest weather station (CETESB station Marg.Tietê - Ponte dos Remédios), the amount of global solar radiation was estimated to be 967 W/m^2 in the first slot, 2860 W/m^2 in the second one, and 954 W/m^2 in the third group. The central slot provided a triple solar energy when compared with the lateral ones. As a consequence, a low multiplicative factor was applied to morning and afternoon periods (0.2), since in these slots the solar global radiation is less significant, while a higher factor was assigned to the central period (0.6), given its triple contribution.

The implementation of multiplicative factors allowed transforming simple solar hours in more accurate information, according to the sun energetic potential causing differentiate heating in the climate points along with the day. Overall, the correlations obtained corroborated that the sun access is a suitable variable to explain the phenomenon of the infra-urban differentiated warming, although not the only one, given the large number of variables involved in the urban energy balance.

Table 8 – Global solar radiation grouped into three slots

Weather station Marg.Tietê-Pte Remédios (code 270)				
Date	h	RADG (W/m2)	Slots	RADG/slot (W/m2)
	7	2		
	8	39	1	967
	9	99		
	10	256		
	11	571		
26/05/2016	12	613		
	13	678	2	2860
	14	492		
	15	506		
	16	314		
	17	125	3	954
	18	9		
	19	0		

Source: Pacifici and Marins (2017), based on data from CETESB station Marg.Tietê - Ponte dos Remédios

An alternative multiplicative factor was also tested considering the SVF measured in the climate points. Indeed, beyond the amount of solar hours intercepted, a high SVF implies high visible sky portions. When surrounding buildings are distant from the climate point guaranteeing a great amount of diffuse radiation is scattered in the sky and a high percentage of reflective radiation coming from ground surface and walls is expected. According to ERELL; PEARLMUTTER; WILLIAMSON (2011), SVF is a crucial variable to quantify the diffuse radiation related to the canyon. As consequence, higher multiplicative factor was assigned to climate points with higher SVF and a new adjusted correlation coefficient was computed ($rs = 0.716227$). Notwithstanding, such strategy was found less efficient than the previous multiplicative factor.

Lastly, the application of sun path to two alternative scenarios resulted in two distinct shadowing landscapes (A and B). Scenario A and B (Figure 32) were quite comparable since they provided a similar built density increase (around 300.000m² of built-up area).

Figure 32 – Scenario A and B (a) and solar hours (b)

		Sun hours	
Points	Current	Scenario A	Scenario B
1	5	5	5
2	2	2	2
3	2	2	2
4	2	2	2
5	6	6	6
6	4	4	4
7	5	3	5
8	5	3	4
9	8	2	3
10	9	3	4
11	9	4	6
12	7	7	7
13	2	4	2
14	3	2	1
15	4	1	2
16	8	0	1
17	4	4	4
18	5	5	5
19	2	0	2
20	5	5	5
21	5	5	5
22	6	6	6
23	5	5	5
24	7	7	7
25	7	7	7
26	7	7	7
27	4	4	4
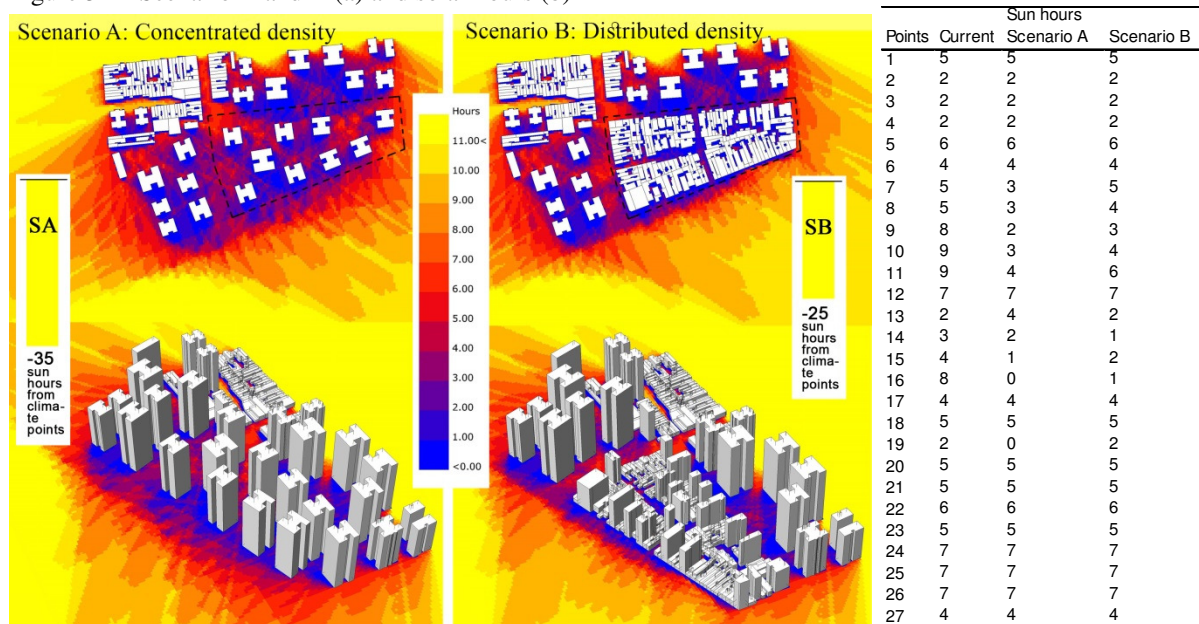
Fonte: Pacifici and Marins (2017)

Scenario A, implementing a densification strategy of high FAR (4) and low BCA (18%), caused a great impact in the domain and obstructed 35 sun hours more than the current domain. This amount gathered all the sun hours shielded by new buildings, within the simulated period (24h) and from all points. In scenario A, the increase of density was condensed in 9 towers. New inserted buildings were purely vertical and projected deep shadows on large parts of ground surface and walls. The great part of shadows affected the

central climate points of domain (P8 to P20) close to which new high-rise buildings had been introduced. Scenario B, implementing a 10-story increasing to 21 low-rise existent buildings (FAR, 8), displayed a minor impact in terms of number of sun hours, shielding 10 hours less than Scenario A. In scenario B a "distributed" densification was tested and the BCA of the new dense block was no modified (70%). Scenario A reduced the 25% of sun hours than the existing domain, while Scenario B decreased this percentage to 18%. Scenario B, promoting a built densification made up of modest buildings, resulted in a higher solar access for open spaces.

5.2   *Limitations and purposes for 2nd phase*

The analysis results of the first phase provided important information to base the conceptual model of the area, revealing the spatial distribution of built forms, the overall climate behavior of the domain and the existence of microclimate zones. Furthermore, the impact of high-rise areas, the centrality of shading phenomena, the role of urban canyon on the definition of urban space, were also observed. Moreover, besides giving a faithful depiction of the area, the general structure of field procedures is suitable to be adapted to other urban areas under built modification, due to the easiness and economy of its application. The results could support municipal planners involved in the conception of neighborhood plans, as well as in larger scale TOD strategies.

In continuity with these findings, the 2nd phase results aimed to fix the 1st phase methodological weaknesses highlighted in section 4.2. In this way, a more consistent field database was developed for a better understanding of domain phenomena and a well-informed modeling process.

5.3   *Results from 2nd climate and morphological analysis*

Within the framework of the same 1st phase case study, outdoor urban climate was evaluated considering three scales of assessments. At different scales, findings showed different degrees of outdoor temperature variability. The predominance of the geographical position and whole-city heat island on the urban morphology was detected in the mesoscale domain, while climate contrasts between compact high-rise and low-rise local zones were highlighted. The climate analysis around isolated urban elements showed that high-rise

building exposure induced various surrounding microclimates, having the shadow projection as driving force. An urban canyon model was finally proposed as a practical and replicable urban tool to correlate daylight and geometrical parameters. Materials and methods concerning these results are available on 4.2.

5.3.1 Mesoscale data assessment

The mesoscale urban analysis showed large prevalence of compact (LCZ-3) and open (LCZ-6) low-rise fabrics (together, 70%), low presence of compact (LCZ-1) and open (LCZ-4) high-rise zones (together, 8%), and a total absence of compact mid-rise (LCZ-2) fabric (0%) (Figure 33). A similar LCZ distribution was observed in the entire São Paulo municipality (Figure 1). In fact, the city is characterized by the prevalence of horizontal areas (LCZ-3, LCZ-6) and only at the boundary of the metropolis, where sprawl pushes forward, LCZ-9 (sparsely built) surpasses the other LCZs. At this step, the total of 20,736 records from meteorological stations was used in the climate assessment. The LCZ estimation showed that MS_INM, VP_CGE and Pe_CGE are largely composed for 69%, 81%, 83% by LCZ-3 (compact low-rise fabric) while VM_CGE has the majority of LCZ-6 (open low-rise fabric) and LCZ-3 (44% and 41%), Se_CGE has a prevalence of 58% of LCZ-1 (compact high-rise fabric) and DP_CET a larger percentage of LCZ-8 (large low-rise fabric) followed by LCZ-3 (42% and 37%).

Figure 33 – Percentage of LCZ areas at the meso scale
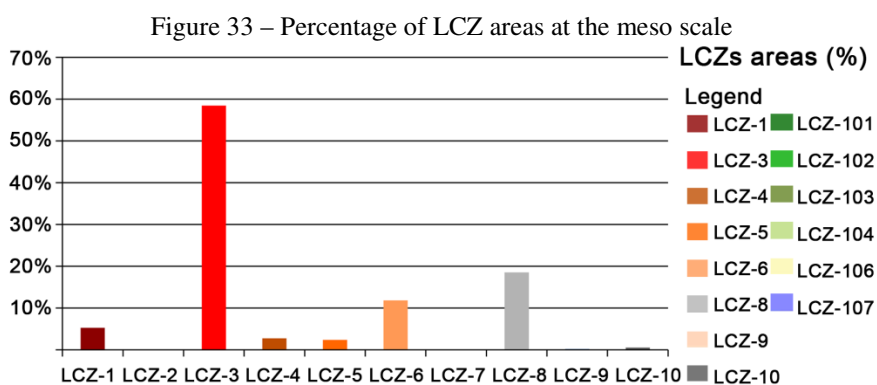
Source: Martina Pacifici, 2019

Notwithstanding the different urban fabrics around the stations and the geographical distance between them, the analysis of air temperature trends and daily ranges showed agreement between the different locations. When analyzed in time (Figure 33), air

temperatures were well stackable and the histograms displayed a close probability density function (PDF) between the series, with a statistical coincidence in the behaviors. It follows that, at the meso-scale or macro-geographically speaking, under the "same" latitude and heat island effects, the São Paulo climate behaved homogeneously, as a unique climate unit, regardless of the zones. These findings integrated the discussion on climate zones, showing that attention had to be paid to the analyzed variable. In the case of air temperature, in fact, we find that local differences between LCZs were overcome by geographical effects and heat island influence.

As shown in Figure 34a, air temperature histograms were unimodal and displayed exponential distributions with variances proportional to the square function of mean values. This behavior was confirmed by a Box-Cox transformation that showed lambdas in the range of -0.78 to -1.04 for every station. All the stations presented similar central position with a trend around the median of 20.6 (± 1) °C. The median was used to represent the central "equally likely" position in the distribution, instead of the mean, not suitable to no-pure Gaussian distribution. Distributions displayed an asymmetric shape, with large tails and positive skewness, probably due to the solar heat concentration in the central hours of the days (typical in hot season in São Paulo). An overall similar behavior for all the stations was corroborated. Table 9 summarized statistics and showed similar central position, dispersion and shape for air temperature distributions. More specifically, MS_INM, Se_CGE, Pe_CGE and DP_CET showed a great proximity with a maximum distance between stations falling within the instrumental error (0.35°C in average). Conversely, VM_CGE and VP_CGE extended the divergence: median and range departed from MS_INM of 1 °C and 3°C, respectively.

Table 9 - Statistical summary for the meteorological stations at mesoscale analysis

Parameters	MS_INM	Se_CGE	Pe_CGE	DP_CET	VM_CGE	VP_CGE
Median	20.65	20.67	20.92	21.00	20.02	19.66
Range	18.30	18.73	19.48	18.60	20.83	21.60
Standard deviation	3.54	3.47	3.59	3.77	3.94	4.04
Skewness	0.66	0.79	0.80	0.74	0.81	0.79
Kurtosis	2.97	3.26	3.33	2.98	3.09	3.10

This behavior was statistically confirmed by non-parametric tests (Mann-Whitney and Ansari-Bradley test). Mann-Whitney, or two-sided rank sum test, verifies that two independent samples come from distributions with equal medians. For MS_INM, Se_CGE,

Pe_CGE and DP_CET distributions, the null hypothesis (equal central position) could not be rejected without another cause at a 5% significance level and p-value from 0.51 to 0.99. The p-value represented the chances of observing either the same result or a more extreme result from similar experiments than the null hypothesis. Only for VM_CGE and VP_CGE was it impossible to consolidate the test: median for air temperature in these two stations were not statistically equal to the others. The Ansari-Bradley test agrees with the Mann-Whitney test showing similar dispersions for all the air temperature distributions, except for VM_CGE and VP_CGE, only equal to each other. Therefore, air temperature series at MS_INM, Se_CGE, Pe_CGE and DP_CET resulted statistically equal, slightly different from VM_CGE and VP_CGE, only equal to each other. These small differences seemed to be unrelated to the urban fabric around stations, since morphological differences were noted between all fabrics and not only among VP_CGE and VM_CGE. Nonetheless, as Figure 1 displayed, VM_CGE and VP_CGE were the southern stations, far from the downtown and the arid East zone. For this reason, the urban heat island effects could have less influence on these stations.

Figure 34 - Probability density function of temperature values (a), daily temporal analysis of the 1-h rate air temperature (b) for meteorological stations at mesoscale analysis.
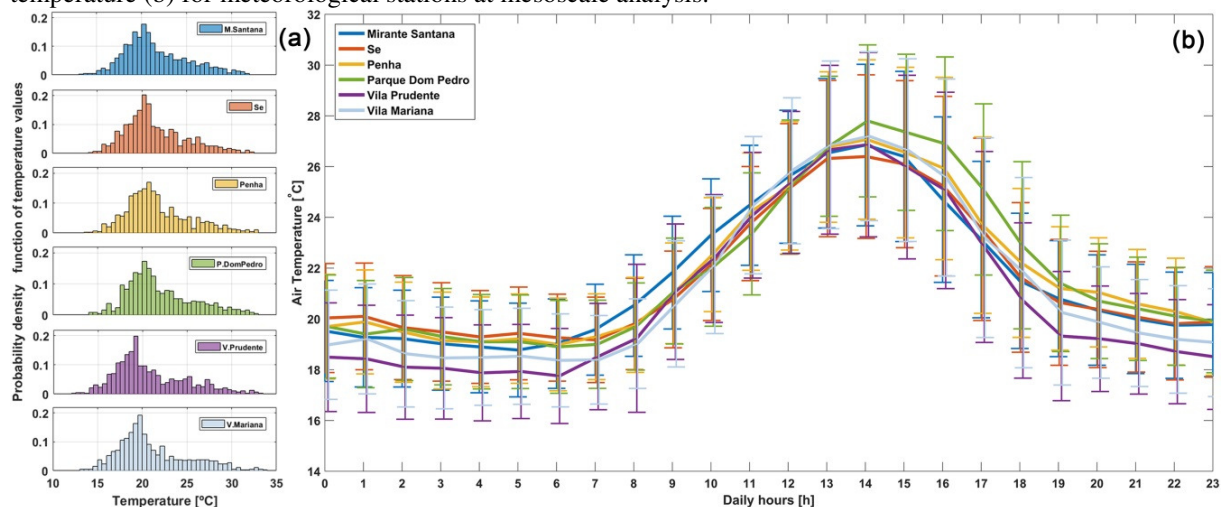
Source: Pacifici et al. (2019)

Subsequently, the daily temporal analysis of the 1-h rate air temperature, averaged in the entire time window, was performed (Figure 34b). In order to represent the typical day in the monitored time, averaged line plots with deviation bars were used. The curves obtained were in agreement with the *PDF* considerations and showed a good correlation between the stations. The length of whisker in the bars represented the standard deviation at each hour, indicating the dispersion of hour records in the whole dataset, while the line plot showed the

median for each hour. The maximum distance in hour curves was always less than 2 ℃ and about 0.5℃ on average.

5.3.2   Local data assessment

Unlike the fairly homogeneous mesoscale results, prominent data sets diversity was observed at the local scale. Climate contrasts emerged more explicitly and differences between morphological clusters were confirmed by field data analysis. Within high and low-rise fabrics, two different climate environments arouse, despite the closeness of measurements. Analyzing the histograms (Figure 35a), a much more relevant distance was highlighted between the local scale series as compared to the meso-scale histograms. The air temperature series presented an exponential behavior, but markedly larger values in kurtosis (crushing) and skewness (asymmetry) were found in comparison with the meso-scale stations (Figure 34). In station 3 (low-rise fabric), the distribution of the data collected showed a major crushing and tail; a greater probability of high temperatures to occur was verified. This is probably due to the type of fabric morphology under analysis, compact, free of tall buildings and shadows, sheltered from winds, prone to retaining the absorbed heat. In addition, there is a smaller distance between the ground floor, where the station is installed, and roofs or building walls that, hit by solar waves, thermalize more easily than the high-rise zones. In fact, stations 2 and 3 (high-rise fabric) displayed a lower temperature concentration; their small tails confirmed the smaller probability of high temperatures to occur, obtaining lower daily ranges on average. In these zones, towers increased the total shaded area, cutting the amount of sunlight striking horizontal and vertical surfaces. Reducing light hours and daily absorbed heat, 'great heights' prevented the temperature from rising, yet they aided the heat release higher up, far from the street, where the wind dissipated its effects. Within the same high-rise fabric, no relevant differences were noted between the two stations (station 1 and 2), despite their different placement (Figure 10). Therefore, it was possible to reject the initial hypothesis, which predicted different air temperatures resulting from the fabric openness.

In order to investigate the average daily temperature trends at each recorded hour, line plots with deviation bars were applied again. Figure 35b showed the comparison of averaged air temperature curves, along 24 hours. Despite the similar trend from 6 a.m. to 11 a.m., the air temperature in station 3 showed a complete different behavior from 12 p.m., displaying a maximum at 3 p.m., 1-2 hours later than high-rise zone stations. This temperature

augmentation at the central hours of the day should be due to a greater solar access, as well as to the compactness of the low-rise zone. In fact, buildings mutually interact transferring heat to the nearest built forms; after noon, the thermal equilibrium is achieved and temperatures stabilize around a mean value until 4p.m. In the same time interval, a larger dispersion around the average denoted air temperature variability; in fact, thermalisation strongly depends on the effective direct irradiance, basically given by cloud cover.

Figure 35 - Probability density function of air and ground surface temperature (a-c), daily temporal analysis of the 1-h rate air and ground surface temperature values (b-d) for stations at local scale.
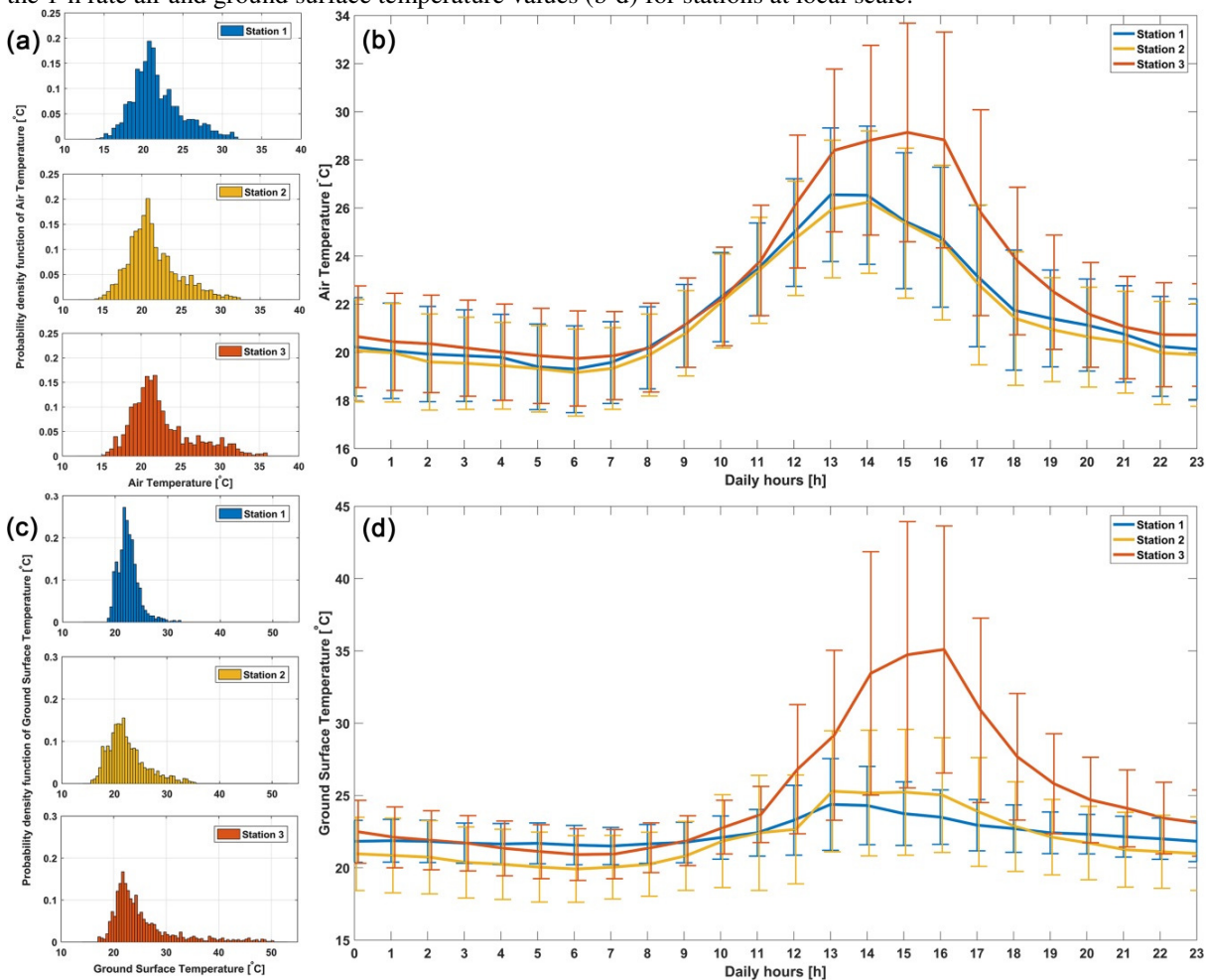
Source: Pacifici et al. (2019)

In the high-rise fabric, after the warming up in the early morning hours, temperatures tended to cool. The probability of shadows affecting ground surface and facades is high; concurrently, the podium layer permeability promotes air circulation and cooling around the towers. At high-rise fabric, dispersion around the average remained almost constant throughout the day; since building shadows always prevent sun access, clouds lose importance, therefore just small T_a variations were observed. In general, direct shadowing

concurred to climate differences between low-rise and high-rise zones; these differences were invisible in the mesoscale analysis. Findings are in accordance with Assis and Frota (1999) who denoted smaller thermal amplitude in high-rise zones in comparison to the compact low-rise zones in which hot stress conditions could be fall during summer afternoons.

To further explore the shadow effect on temperature within the local scale, T_{gs} and MRT were also assessed. From findings (Figure 35c-d), both variables had exponential form and followed the air temperature trend in all the stations. Besides, divergences between high-rise and low-rise fabrics appeared clearer. In agreement with Figure 35a, histograms of T_{gs} displayed a very long tail for station 3, confirming the great ability of low-rise ground surfaces to absorb heat and reach very high temperatures when the fabric is largely exposed to solar irradiance (Figure 35c). This is emphasized by the low latitude of São Paulo, which implies a more vertical incidence of solar rays on the ground surface. Between station 1 and 2, slight differences could be noted in histogram crushing. This can be due to a lower number of direct solar hours intercepted by station 1 (4.5 h) as compared to station 2 (6.0 h), which is exposed to irradiance from 12:30 p.m. to 6:30 p.m.

Figure 35d allowed verifying that station 3 T_{gs} growth was steeper than that of T_a and extended until 4p.m. This behavior could depend on the great heat storage capacity of man-made ground materials, generally of dark shades, rough and characterized by a low albedo. Furthermore, a greater variability in daily T_{gs} compared to T_a was observed. Station 3 error bars showed strongly stretched standard deviation values from 2 p.m. to 4 p.m.; however, station 2 whiskers[1] range was also noticeable along all the day. At nigh hours, the absorbed heat took a long time to be released and station 3 only reached station 1 at 2 a.m. The low-rise fabric compactness actually slowed the surfaces cooling, reducing the absorbed heat transferred by convection to the atmosphere after sunset. This phenomenon occurred with less evidence in stations 1 and 2; in fact, as in high-rise zones the temperature increase was not too high because of the daily shadows, the nocturnal long-wave fluxes were low anyway.

The T_{gs} findings agreed with the daily temporal analysis of *MRT*, which also confirmed a strong dependence between its values and short-wave fluxes. In particular, when T_g is converted to *MRT*, its value is raised to the fourth power; it follows that *MRT* is strongly dependent on short-wave radiant fluxes, much then T_a, exhibiting a positive correlation with them. Including the total amount of radiant energy to which the human body is exposed, the

---

[1] lines extending vertically from the average, indicating the data variability along with the measured period

mean radiant temperature is of great importance in order to assess the pedestrian comfort at stations 1, 2 and 3. In Figure 36a, histograms displayed the probability density function (pdf) for Station 1, Station 2 and Station 3; in agreement with T_a and T_{gs}, the low-rise Station 3 tail stood out, to be longer than high-rise tails.

Subsequently, in order to investigate the average daily temperature trends at each recorded hour, line plots with deviation bars were applied (Figure 36b). In this chart, small length error bars were found along most of the day, while an explosion in length was observed at central hours when the stations are directly irradiated. Once again Station 3 stayed at the top during the central hours; however, its fall was abrupt from 3:00 p.m., when direct radiation quitted irradiating the station. Between station 1 and 2 slight differences could be noted. From 12 a.m. to 2:30 p.m., when both stations are free of shadows, station 1 displayed higher values of *MRT* then station 2. In fact, while the former was progressively heating from 10 a.m., the other came out of shadows just at 12:30 p.m. However, out of the interval 12 a.m.-2:30 p.m., the relation was inverted, with station 2 just above station 1 and 3, even at night. Indeed, while station 1 and 3 leaved the sun exposure after 2:30 p.m., station 2 continued to receive solar rays until 6:30 p.m., delaying its cooling.

Figure 36 - Probability density function of mean radiant temperature (a) Daily temporal analysis of the 1-h rate mean radiant temperature values (b) for stations at local scale
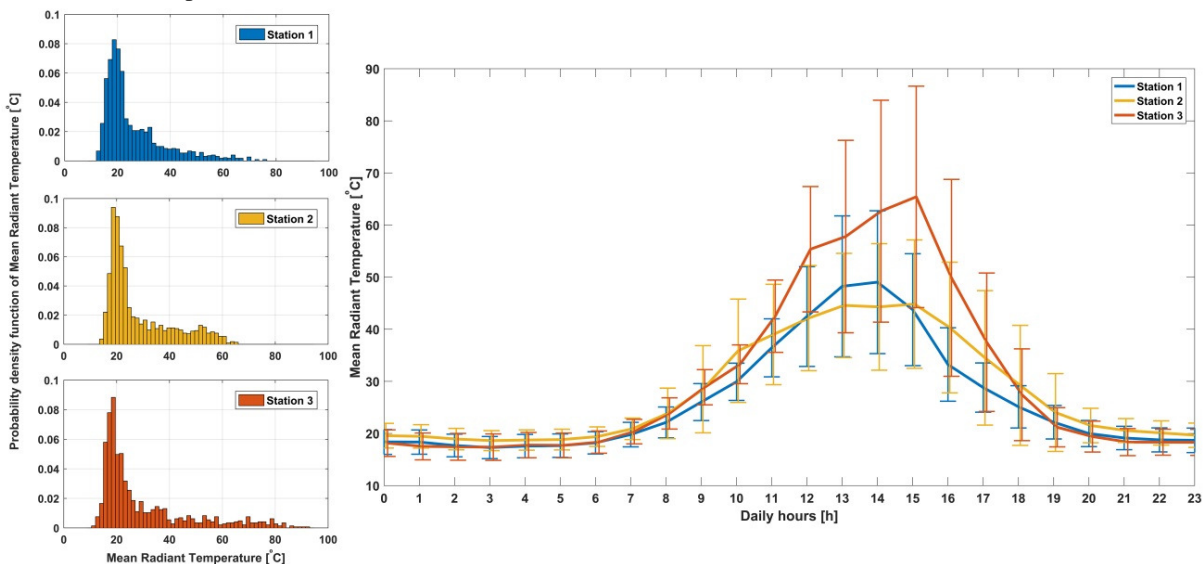
Source: Pacifici et al. (2019)

Finally, a comparative plot of T_a and *MRT* over the whole measurement period was shown (Figure 37*a* and *b*) to confirm similar trends for the two stations installed in the high–rise fabric (Station 1 and Station 2). In accordance with the daily analysis (Figure 35b),

stations 1 and 2 air temperatures trended together, except for some peaks, when station 1 exceeded station 2 in the order of one degree. Coincident curves were also observed for the *MRT* variable, even if station 2 showed lower maximums than station 1 (Figure 36b), amplifying by Equation 5 the small differences highlighted in air temperatures. By estimating the averaged wind speed, which was applied to the 3 stations, the local wind differences were not included in the *MRT* calculation. Indeed, the wind speed differences highlighted in Figure 37c were mainly due to the building arrangement among which the stations were inserted; therefore, while station 1 seemed to be more sheltered from air fluxes, station 2 was exposed to the winds coming from the south, running along the canyon. Furthermore, Figure 37c showed the correspondences between the temperature drops and the precipitation events, behavior generally anticipated by hotter daily curves.

Figure 37 **-** Comparative plot of air temperature, *MRT*, local and average wind, and precipitation for Station 1 and 2 over the whole period of field measurements
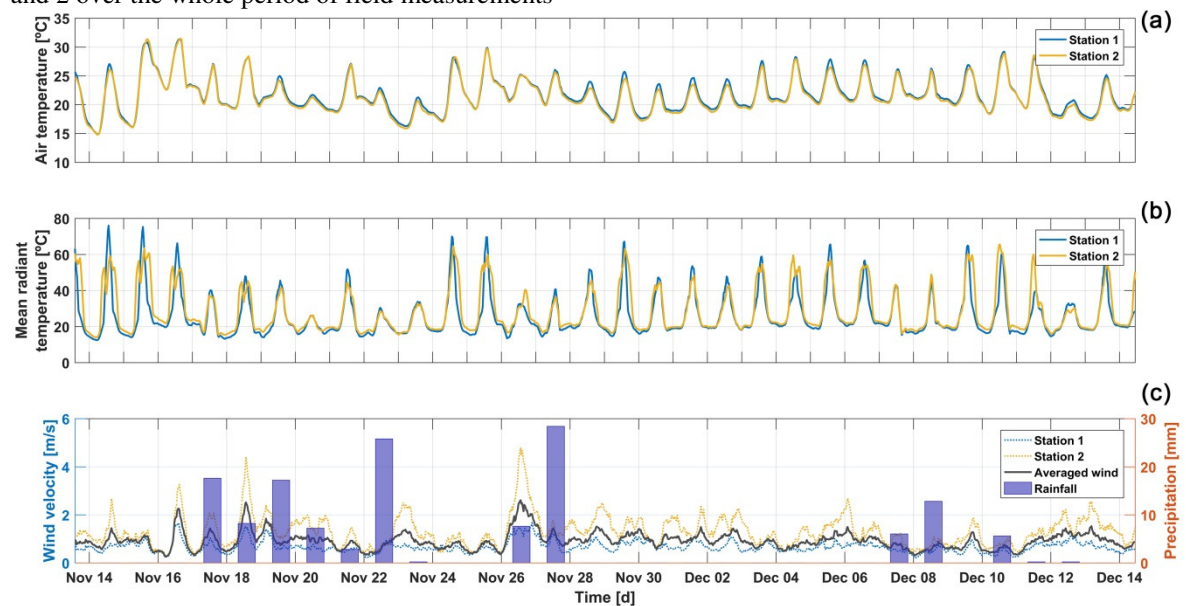
Source: Pacifici et al. (2019); accumulated daily rainfall are obtained from MS_INM station.

5.3.3 Microclimate data assessment

Again reducing the scale analysis, microscale differences within the same local climate zone were investigated. More heterogeneous findings resulted from the high-rise measurements with sharper air temperature variations in the opposite stations. Indeed, to the extent that shadows rotated around the tower along the day, the surroundings warmed differently and various microclimates emerged. Conversely, around the low-rise block,

exposures influenced much less and did not cause air temperature gradients; close and low-rise buildings behaved as a single element, shadows were meaningless, and no distinct microscale environments could be recognized. To explore these relations, a scatter plot diagram was used (Figure 38). It showed air temperature records along two couples of opposite exposures (N-S, E-W), around high-rise and low-rise volumes. On the *x- axis*, North (N) and East (E) records were found, while the *y- axis* hosted South (S) and West (W) ones. Mathematically speaking, the building-obstacle could be considered the function linking the independent (N-E exposures on the *x-axis*) and the dependent variables (S-W exposures on the *y-axis*) at opposite sides. The mutual variations between opposite air temperatures around an urban element helped to deduce the direct influence of this element on the variable.

As verified in the linear regression in Figure 38, a similar relationship between opposite air temperatures was found around the low-rise element, since N-S and E-W inclinations did not present relevant differences (almost coincident regression lines). Conversely, in the high-rise zone, buildings showed a much more consistent influence on T_a, as quite different slopes characterised N-S and E-W regression lines. It could also be noted that the high-rise N-S regression line slope markedly differed from all the other inclinations and its angular coefficient *a* was notably lower. It followed that the high-rise N-S exposures performed a flatter trend, with closer minimum and maximum temperatures, resulting in a smaller thermal gradient between the north and the south high-rise façades. However, in comparison with the low-rise fabric, the high-rise air temperatures values had a larger extension along the north facade (x-axis) than the south-facade (y-axis). Indeed, when exposures are antithetical to the solar arc and the building is tall, the North side is more irradiated during the central hottest hours of the day compared to the South side, implying air temperature differences between the two sides until 2:30 p.m. At low-rise volume, due to a lower shading height and to the sun vertical position at this time of the year, the same N-S gap did not occur.

Conversely to N-S, high-rise and low-rise E-W regression lines were parallel, as their similar angular coefficients proved (see Figure 38 table). The shift between the regression lines could be easily understood if the scatter plot points were observed in the chart. While at hot temperatures (above 26°C) high-rise E-W and N-S points were similarly distributed, at lower temperatures (below 26°C) a substantial difference was noted between the two couples of high-rise exposures (the same difference did not occur in the low-rise case). This means that during the hottest hours, when the sun is close to the zenith, the influence of the exposure is minimal in the high-rise fabric. Conversely, at the start and at the end of the day, when the

sun is farther and shadows are longer, E-W exposures describe a very different trend. In particular, W-exposure tended to stand above the E-exposure in the afternoon, while E-exposure was greater in the morning, displaying a shift of 2°C on average as compared with the E-W low-rise exposure. Thus, it could be inferred that E-W was the axis in which shadows took on more weight, due to their capacity to change air temperatures as a consequence of their projection. Conversely, along the N-S axis, the daily shadow rotation was less significant.

Findings were valid for the subtropical latitudes. According to Arnfield (1990), in December, in N-S and E-W oriented canyons, the wall and floor irradiance decreases with the increase of the latitude; for H/W ratios greater than 1.5, the street level solar access depends more strongly on the latitude. In comparison with the climate differences found at the meso-scale, the presence of high buildings inside an urban fabric favored greater microclimate variability. High-rise LCZs resulted in blended thermal environments, strongly influenced by building orientation and solar access.

Figure 38 - Scatter plot diagram correlating air temperatures between opposite exposures (N-S, E-W) into high-rise and low-rise zones

Source: Pacifici et al. (2019)
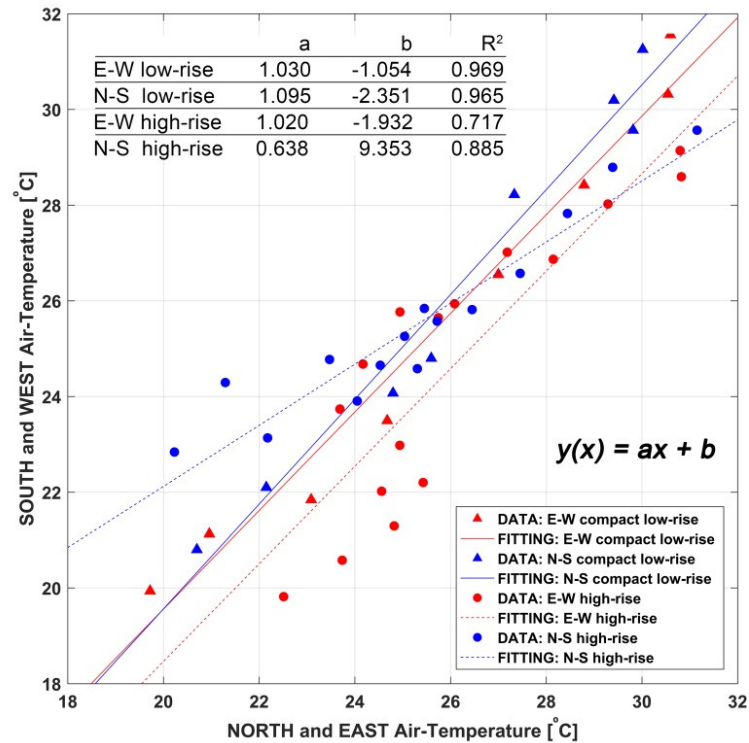
Finally, it was possible to build a 3D light-hours matrix, based on the analytical formulation of Equation 6 (section 4.2.3). Since direct shadows resulted in the driving force

for temperature variations in microscale analysis, a correlation between direct solar access, air temperature and geometrical features in a canyon was implemented. This assumption is strengthened by Yang et al. (2012), for which solar radiation is the most powerful conditioning affecting the thermal comfort in outdoor spaces. Despite starting from a simplification of the urban reality with a 2D canyon, the following matrix and the related findings can be relevant for practical applications, making Equation 6 implications visually accessible.

As we showed in Materials and Methods (section 4.2.3), the matrix summarized how building heights (*H1*, *H2*) and the middle space (*W*) affected the number of solar hours received by the canyon. As shown in Figure 39a, solar access is expressed in light angles (degrees) and converted into hours when the 3D matrix is split into 2D views (Figure 39b); greater light angles mean a larger amount of light hours received. On the *W*-axis, the matrix was stretched twice its size to be better displayed. Mathematically speaking, the matrix described *H/W* ratios in the range from 1 to ∞ for the whole domain. To assess lower *H/W* ratios for *H* near 100, we should extend the domain along the *W* direction, although this range extension is out of interest when real urban environments are analyzed.

According to the findings, the more the building height increased, the more its light exposure was reduced for the same canyon width. For small canyon widths, the building height lost importance; shadow was always present and only very small buildings (less than 10 m high) were able to let the light enter. Particularly, when *W* tended to zero, the arctangent argument of Equation 6 (2*H/W*) went to infinity; this condition represented a discontinuity slice in the 3D matrix. Similarly, for large distances *W*, small variations in building heights were unimportant.

In order to enhance the visualization, a split 2D matrix was extracted from the same data. Figure 39b presented a width-axis slicing of the 3D matrix showing the solar access (hours per day) at four different canyon widths (*W*=10m, *W*=40m, *W*=70m, *W*=100m) for all the possible combinations of *H1* and *H2*. These 2D matrixes are symmetrical along the diagonal and invariant by the order of *H1* and *H2*. It should also be noted that, for both *H* ranging from 0 to 100m, the curve underlying the solar obstruction moved progressively, with clearer colour bands expanding along the NW-SE direction. In addition, all the slices showed an almost asymptotic behavior of colors when *H1* and *H2* had markedly different values (areas near the top and the left side axis). In this condition, the amount of solar access, expressed by angle *γ*, only depended on the taller building. Mathematically, this means that just the greater *H/W* ratio was significant for computing *γ* in Eq.(6); the contribution of the

lower building was trivial and small variations (5-10m) of its height were negligible. As a consequence, the shadow projection of a small building was lost in the shadow cone of a taller one.

Figure 39 - 3D light-hours matrix (a), 2D width-axis slicing of the 3D matrix at W=10m, W=40m, W=60m, W=90m (b), canyon geometrical representation at each 2D slicing (c).
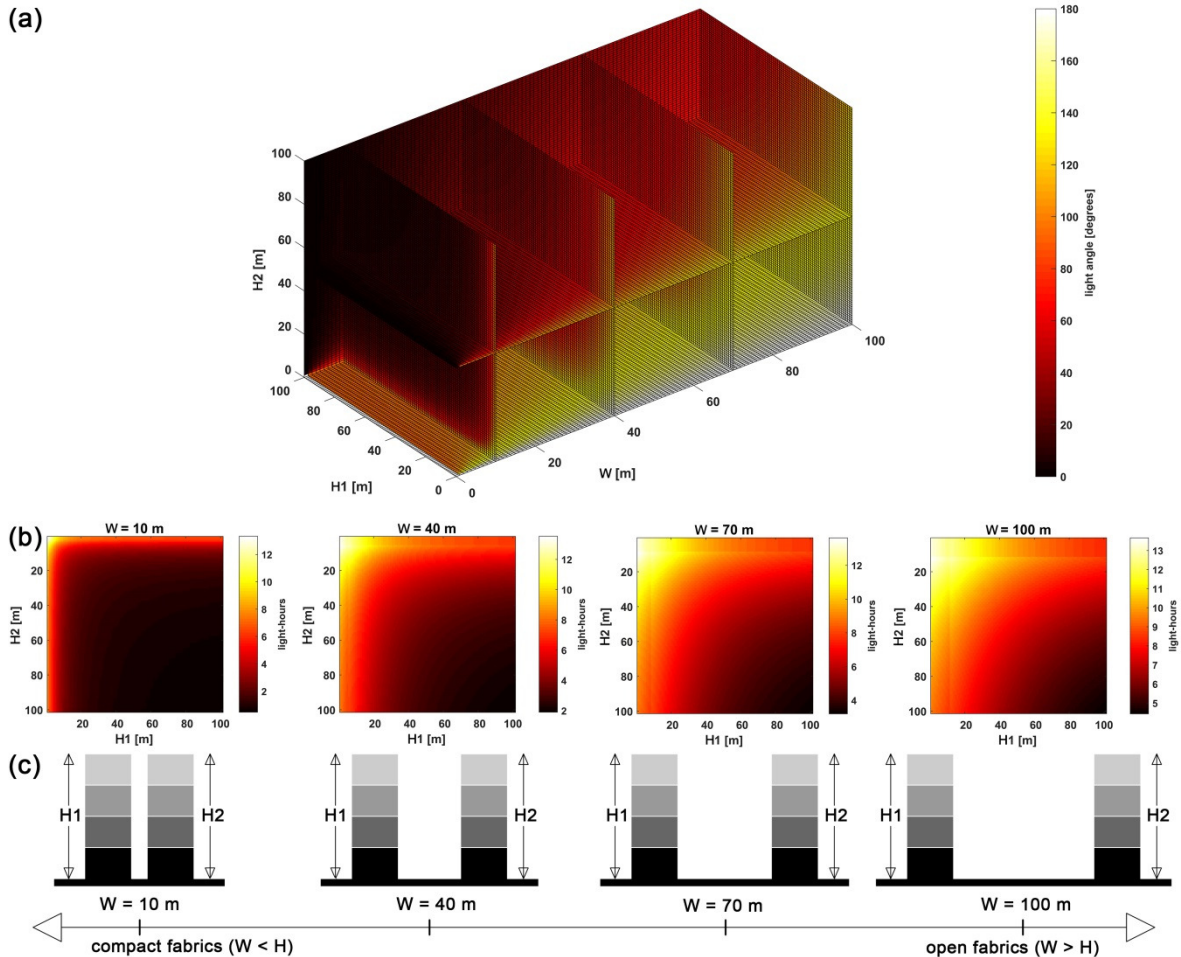
Source: Pacifici et al. (2019)

As shown in Figure 39c, great *H* may be associated with high-rise fabrics, while small *H* with low-rise fabric; meanwhile, large *W* is associable with open fabrics, while small *W* with compact urban fabric. Matrix of *W*=10m represents a narrow canyon performing an almost total sun obstruction. Since the light cone is quite small in the space between buildings, direct irradiation is prevented; however, in such *W* conditions, housings from 1 to 3 floors can guarantee a notable number of solar hours per day (Figure 39b). The matrix of *W*=100m is the brighter slice; its light cone intercepts a good portion of the daily solar arc. It represents a wide canyon whose buildings interfere much less with the shading of the open space between them. However, for *H/W* ratios close to 1, light hours are drastically reduced.

Other studies for urban hot climates relate large differences in daytime temperature and thermal comfort between deep and shallow canyons (JOHANSSON, 2006; SHASHUA-BAR; TZAMIR; HOFFMAN, 2004). Matrixes of *W*=40m and *W*=70m represent intermediary cases; narrowness or wideness of such canyons basically depend on the urban fabric in which they are inserted, or else on their *H1/W* and *H2/W* ratios. From W=40m to *W*=70m matrixes, an increase of light hours can be observed when the same heights are considered in both cases.

In sum, this geometrical model explored the amount of solar access provided by a typical canyon in the space between its border buildings. Since the built morphology, and its potential of projecting shadows, was considered the main driving force of temperatures variations, the model could be used as a practical tool to estimate the temperature behaviour when the canyon proportion changed. Although the results dealt with the influence of just two buildings, it should be observed that an urban canyon constitutes a basic element from which urban fabrics are composed and from which the new urban developments take shape.

5.3.4   Results from supplementary analyses

Supplementary analyses on vegetation and materials improved the morphological and climatic characterization of the area, as well as provided knowledge to complete the parameterization of the modeling processes.

Overall, the material field survey revealed a glaring homogeneity of the constructive patterns in the buildings located in the high-rise fabric, while in the low-rise zone a greater heterogeneity was observed. In term of vertical surfaces, glass (21%), light colored plaster (62%) and ceramic (15%) were predominant in the high-rise fabric, while in the low-rise zone a more variegated mix of materials found, including dark-colored plaster (12%) and ceramics (4%) , light-colored plaster (37%) and ceramics (25%), metallic doors (4%), rock (5%) and glass (13%). With regard to roofs, in the entire domain an equilibrated distribution of ceramic tiles (39%), fiberglass tiles (32%) and concrete slab (29%) was found. However, tiles were abundant on the low-rise zone, while concrete slabs were mainly observed in the high-rise fabric. Lastly, the characterization of ground surfaces showed 30% of concrete floor, 28% of street asphalt, 21% and 17% of grass and marble. These two last categories were mainly concentrated within the private condominiums. The percentage of grass could seem high; actually, it is an artificial lawn, covering a concrete slab under which underground parking levels take placed. In order to associate materials with reliable properties (required by

modeling), a supplementary study on the historical periods characterizing the domain buildings was realized. Indeed, the typology of material can vary significantly with the constructive technique implemented and, thus, with the building age. Online available *IPTU* data (http://geosampa.prefeitura.sp.gov.br/PaginasPublicas/_SBC.aspx) revealed buildings ages ranging from 1920 to 2015. The great part of the low-rise fabric was built between 1940s and 1960s; the verticalization process occurred from 1980 and strengthened from 2000s to 2015s. Figure 40 displays the assortment of findings above described. Material properties of façades, roofs and ground surface materials were summarized in the IC report (KALLENDER, 2018) and subsequently applied in the ENVI-met parameterization.

Figure 40 – Façade materials (a), roof materials (b), age materials (c)
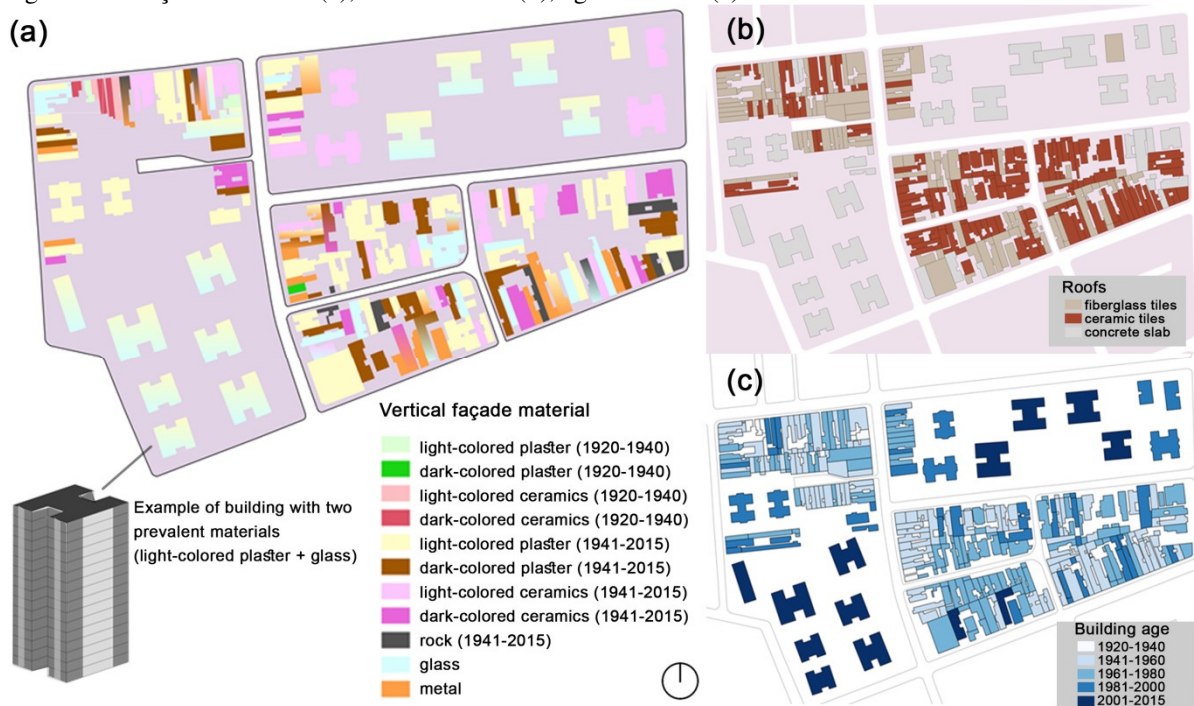
Source: Adapted from Kallender (2018)

Overall, thermographic investigations provided additional knowledge on the thermal behavior differentiating the low-rise and the high-rise fabric.

On November, 14th and 24th, 2017, the micro-climate analysis around towers (high-rise) and a horizontal block (low-rise) were combined with two thermographic campaigns. Results displayed the evolution of surface temperatures on the facades and ground surfaces. Thermal contrasts occurred between opposite exposures in the high-rise fabric, especially when West and East exposures were compared. Less evident gaps emerged between North and South facades. Between 10 and 11:30 a.m., the highest average (~19°C) difference was

observed between East (~38°C) and West (~19°C) exposed facades. The same comparison, in the afternoon (2 – 3 p.m.), decreased to ~2°C. Conversely, among North and South exposed facades little average differences (~4°) were observed from 12 a.m. to 1:30 p.m., quite insignificant (1°C) between 4 p.m. and 5:30 p.m. Similar but more emphasized trends were observed on ground surfaces. On this regards, East exposed floor at the morning was above the West curve of 28°C on average, while in the afternoon the same decreasing rate (~2°C) was observed. Less contrasting findings were obtained on November, 24th, 2017, in the low-rise micro-climate study. Thermographic collections revealed smaller gaps between East and West exposures, in the morning and in the afternoon, for ground surfaces (~8°C a.m. and ~1°C p.m.) and façade surfaces (~4°C a.m. and 1°C p.m.). As in the high-rise zone, East-exposed surfaces carried on higher surface temperatures until 2 p.m., even if minor intensities were found. At the opposite north-south exposures, average differences did not exceed 4°C. Figure 41 was selected to show the different heating and cooling process occurring simultaneously on the west and east exposures around towers.

Figure 41 - Thermographic samples on the west and east exposure, for ground surfaces (concrete) and facades (light-colored plaster), displayed ranging from 15°C to 55°C.
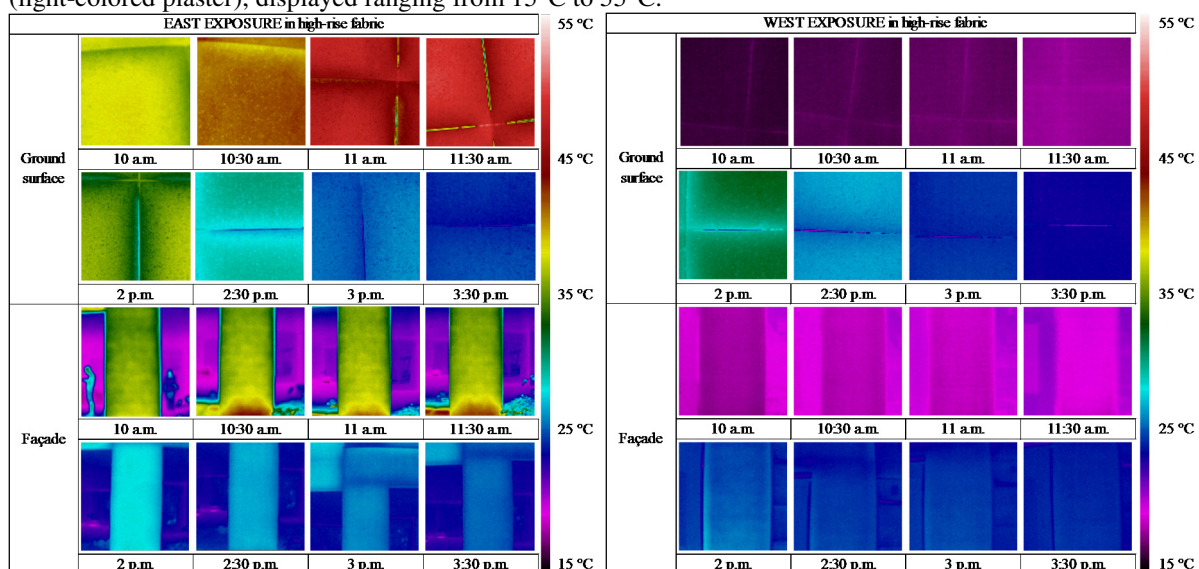
Source: Kallender (2018)

From a second and complementary thermographic analysis, conducted on December, 14th, 2017 the thermal behavior of the materials was observed along the all the day (from 6 a.m. to 7 p.m) on 8 representative sample of domain collected in transect. Each thermographic sample was realized on a selected portion of façade, allowing the collection of one or more materials. Overall, dark-colored plasters displayed the heights peaks of surface temperature,

while the lower temperature where observed on light-colored plasters and ceramics (average gradient between 10 a.m. and 6 p.m.: 3.4°C; maximum difference: 8.8°C). As the dark-colored surfaces are mainly localized in low-rise fabric, their presence could exacerbate the daily heating process already analyzed in terms of urban morphology. Light-colored plaster and ceramics showed coincident thermal trends. Also fiberglass and ceramic tiles showed very similar trends. The exposure of facades, on which thermographic samples were collected, affected the occurrence of temperature peaks throughout the day. When the same material was observed in different exposures and fabrics, distinct thermal curves were observed. On the most of exposures, low-rise light plaster showed higher surface temperatures than high-rise light plaster. The only exception occurred from 10 a.m. to 2 p.m., on the east exposure, probably due to the quick heating of the tower façade compared to the little house. In comparison with other Brazilian studies, trends of light-colored plaster and ceramics were found in accordance with Guimarães *et al.* (2002), while the similarity between fiberglass and ceramic tiles was confirmed by Sampaio *et al.* (2011).

Furthermore, on November, 25th, 2017, two climate data collections were simultaneously carried out comparing two climate points (with and without grass) on the same concrete ground floor. From findings, the influence of grass was observed quite insignificant in terms of outdoor air temperature that showed similar trends on both pavements. Meantime, a departure of 10°C was observed on surface temperature, with the climate station located above the concrete pavement recording higher values when compared with the grass covered concrete floor. Figure 42 displayed surface temperature for facades of light-colored plaster, in the low-rise and high-rise zone, at all exposures (above); surface and air temperature for only concrete ground surface and grass & concrete ground surface (below).

Overall, it worth stressed that the results relative to materials are based on daily investigations; the analysis of larger database would allow recognize more solid trends.

Figure 42- Façade surface temperature at 4 exposures on the high-rise fabric (above), ground surface and air temperature on grass & concrete or only concrete pavement (below).
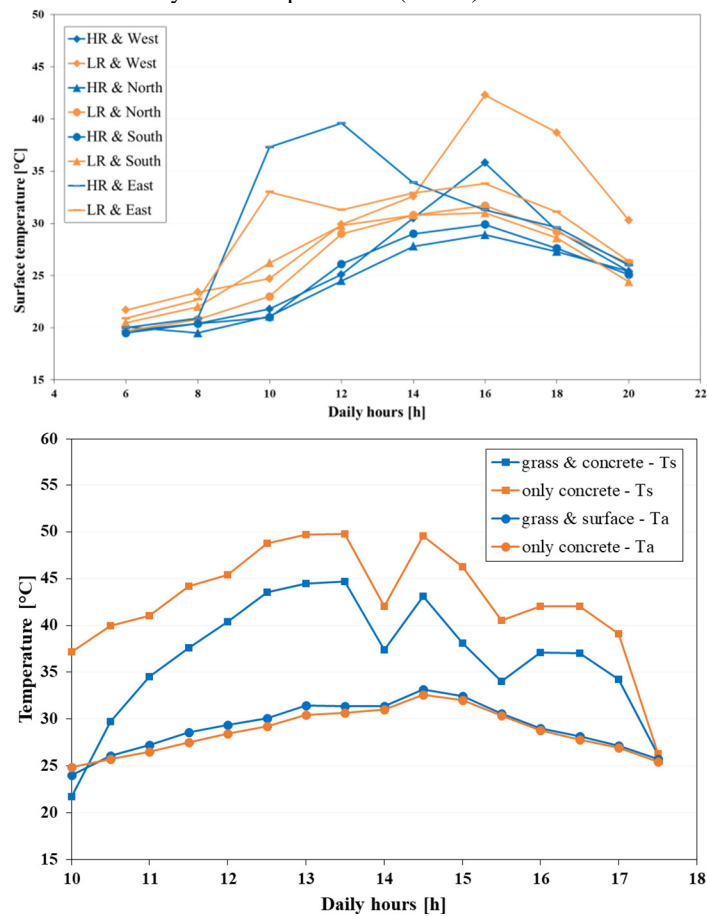
Source: Pacifici (2019)

The study of the domain green infrastructure allowed characterizing the tree coverage more accurately than the first assessment phase and realizing dedicated measurements. In terms of climate performances, the analysis of air temperature, relative humidity, globe and ground surface temperature showed distinct thermal behavior between sunny and tree-shaded points. Even if at very close distance (~10 meters), climate points under the tree canopy resulted in lower values of temperatures (~1°C on average T_a, ~9°C on average T_g) than hotter sun-exposed points, (Figure 43). As consequence, the little extension of the tree microclimate was observed, since the cooling effect measured under the canopy was not found few meters ago. Conversely, the projection of shadows provided by the tree canopy was able to create little fresh islands along with sidewalks, very appreciable in hot summer days. In synthesis, trees under assessment were able to interfere in the microscale of the place, but unable to affects the local scale dimension, since their benefit was lost in the close surrounding. Probably, denser tree groups could be more effective to really impact the thermal balance of

the neighbourhood. As consequence, isolated or too spaced rows of trees should be seen as an opportunity to reinforce the city's green infrastructure.

Figure 43 – Air temperature (T_a) and globe temperature (T_g) at climate points; green line indicate measures collected under tree canopy, while orange line indicate measures collected out of the tree canopy (sun exposed)
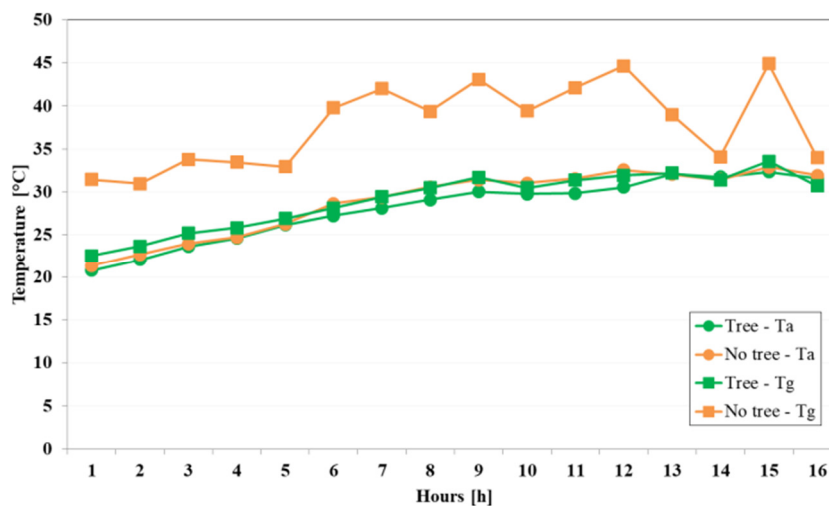
Source: Martina Pacifici (2019)

Regarding tree morphology, the field survey of the existent domain trees revealed a great complexity of tree species, a considerable amount of scattered and isolated plants, mutilated and sick trees, as wells as interferences among the aerial electricity lines and crowns. To summarize this complexity in few determinant information ready to be used in the modeling of domain, the most significant tree concentrations were identified and gathered in four studied groups. The rest of the plants were considered unimportant given their little microclimate influence. The first group included trees of great height, placed on the sidewalks of the high-rise fabric; the second cluster was composed by large and high trees, placed on the sidewalks of the low-rise zone; the third group gathered a group of medium but numerous trees planted in the private outdoor spaces of the high-rise zone; lastly, the four cluster joint very high and large trees grouped in a square surrounded by low-rise housings. The average height (h) and crown diameter (c) were respectively estimated for each group as: 9.5 m and 6.0 m (group 1), 11.7 m and 10.5 m (group 2), 5.7 m and 3.1 m (group 3), 10.3 m and 9.1 m (group 4) (Figure 44).

The application of *Can Eye* software to calculate LAI values for isolated trees from hemispheric pictures was found very hard. The computation of LAI was realized with the best accurateness (Sample Factor = 1) for representative tree in each group. Average values are

displayed in Figure 44. The masking tool was selected to be the best strategy to discriminate vegetation from background. Conversely, LAI computation without masking led to outlier values in comparison with bibliography. Notwithstanding, great difficulty was found to force *Can-Eye* to distinguish leafs from other urban elements. Thus, other methods for the estimation of LAI should be considered in the future studies. The initial calibration of the optical center was provided by LABAUT (University of Sao Paulo) database. A clumping parameter equal to 8 was used, according to sensitivity tests. For each studied tree, sets of 9-12 hemispheric images were employed. LAI and albedo from Caesalpinia Echinata tree (Group 3) were selected to be implemented in the ENVI-met model. This choice was based on the abundance of this tree species in the domain, as well as its characteristics really close to the average. To be used in ENVI-met, LAI values were transformed in LAD values distributed in 10 layers (Table 11).

Figure 44 – Four tree groups with the average Leaf Area Index (LAI) and leaf albedo values
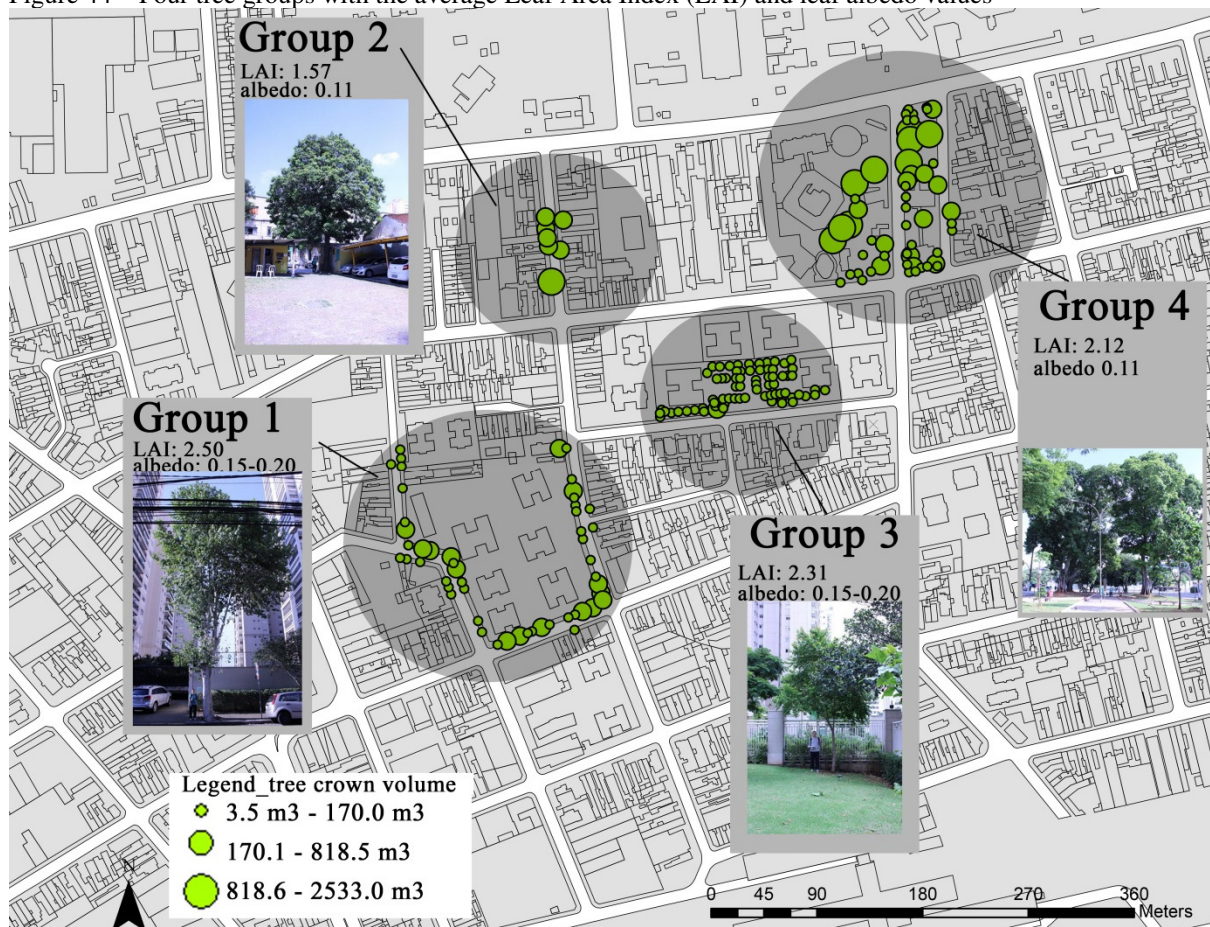
Source: Martina Pacifici, 2019

5.4   Results from ENVI-met model

5.4.1   Definition of model purpose

The model aims to a) reproduce the most important interactions observed on site, among which the local climate difference between high-rise and low-rise fabric was highlighted; b) estimate the climatic effects of alternative scenarios related to the insertion of a verticalized and dense urban fabric in the tradition low-rise zone.

5.4.2   Building of conceptual model

The conceptual model for the selected urban area under analysis has the objective to describe the main physical processes affecting a low latitude urban area, in which recent real estate processes led to the transformation of the traditional urban fabric through the insertion of new multi-story urban elements (ongoing densification). Conceptual model was built through collected and available data, including morphological and climatic features (Figure 45).

The model of the studied area is characterized by hybrid morphology, including both high-scale buildings (S4) and low-scale buildings (S2), while intermediated-scale typologies are almost absent. Vegetation coverage is modest but diversified; four noticeable trees groups were identified, mainly concentrated around condominiums. Due to the low latitude, solar radiation is the most significant driver of urban heating, while buildings shading is the main cause producing climatic differences in the area. The seasons of autumn and winter caused a greater incidence of shadows in the domain, due to the presence of towers and lower inclination of the sun's rays on the horizon. Conversely, the seasons of spring and summer brought about smaller shadows and the propensity for a greater energy gain.

Overall, at the morning, domain showed a homogenous thermal behavior given by the night cooling. Along with the day, urban morphology filtered the sun access, creating exposed or shaded urban spaces that granted or prevented the heat gain of streets and walls. As a result, in the afternoon, a larger climate variation occurred. In the afternoon, 3 distinct thermal zones were segregated: a hot zone, a colder zone, and a transition zone between the other two.

The hotter zone took place on the surroundings of low-rise fabric, far from towers. Here, buildings heights are all pretty similar discouraging ventilation; lots boundaries are

continuous and closed to air streams, sheltering backyards from winds. Streets had wide sky view and very few trees, guaranteeing sun access for about 8-9 solar hours *per* day. The sun path, following the arc East-North-West, permitted a full radiation of the roads, their exposed materials, as well as of the building roofs, causing high levels of outdoor air and surface temperatures. High thermal daily excursions amounted to 13°C. Due to the close distance between ground floor, walls and roofs, the low-rise built mass hit by solar waves, thermalized and retained heat, conserving its temperature until 4 p.m. Such behavior was even more evident on ground surfaces temperatures, due to a great heat storage capacity and a low albedo of their materials. After sunset, the compactness and wide exposure of built mass implied slower cooling of surfaces, occurring transferring heat toward atmosphere by convection. Materials characterizing facades and roofs are pretty heterogeneous, including a noticeable amount of dark-colored surfaces (16% plaster, 4% metal, 5% rock) and fiberglass/ceramic tiles, more inclined to absorb and retain heat.

Colder zones occurred on the south side of high-rise buildings. In such zones, shadowing caused by built volumes overlap reaching 8-10 shading hours *per* day, preventing direct irradiation and absorbed heat, decreasing the daily heating and the nocturnal long-wave fluxes at the pedestrian level. Even on the upper floors, façade and roofs hit by solar waves are distant from streets; their heat release was far away from pedestrians and more easily dissipated from wind. Smaller daily thermal excursions characterized this area and minimal afternoon temperatures were recorded around 20 °C.

Additional cooling effects were caused by high trees, decreasing surface temperatures up to 6°C (road asphalt), and air temperatures by up to 1 °C. Open spaces among towers enhanced air circulation and increased the H to W ratio, guaranteeing more direct sunshine and less interference with other buildings. The great part of surfaces is made-up of high reflective and emissive materials, including light-colored facades (77%), concrete slabs as roofs and white concrete ground floors. A large amount of windows (21%) is also observed, while no dark-colored surfaces are found. Among hottest and coldest fabrics, considerable daily excursions occurred. At the night, low-rise and high-rise zones come back to the same temperatures around 2 a.m.

Zones of climate transition were scattered, highlighting the landscape change, benefitting of slight ventilation, shading ranging from 5 to 10 hours *per* day and variable tree coverage. Such areas reveal a well-balanced ratio among built and open space, modest compactness and verticalization. Due to the presence of these 3 zones, thermal comfort sensations were observed in the domain, ranging from "little cold" to "very hot". A high

correlated linkage was observed between sun hours, SVF and temperatures. The heating trend of ground surface well followed the variation of sun hours collected, due to a more vertical incidence of solar rays, exhibiting thermal variations between 15°C and 50°C.

Furthermore, within the same local climate zones, micro-climate environments were found, above all around tall buildings, with temperature contrasts at opposite exposures. E-W exposures displayed great air temperature differences on the early hours of morning and the last hours of afternoon. N-S exposure performed a smaller gradient with differences until 2 p.m. The multi-faceted urban surfaces follow the air temperature trends, with more prominent differences between E-W exposures within the high-rise zone. On morning, east exposed ground floors and facades performed high infrared radiation exchanges with atmosphere, resulting in higher surface temperatures relative to west shaded exposures.

On a larger prospective, the local scale domain is surrounded by a wider meso-scale region geographically influenced by latitude and homogeneously carrying on heat island effects. The mesoscale region is mainly made up of compact and open low-rise fabrics (LCZ-1, LCZ-4), while a low presence of compact and open high-rise fabrics was observed. A graphical representation of the conceptual model of the area was displayed on Figure 45.

Figure 45 – Representation of the conceptual model of the area
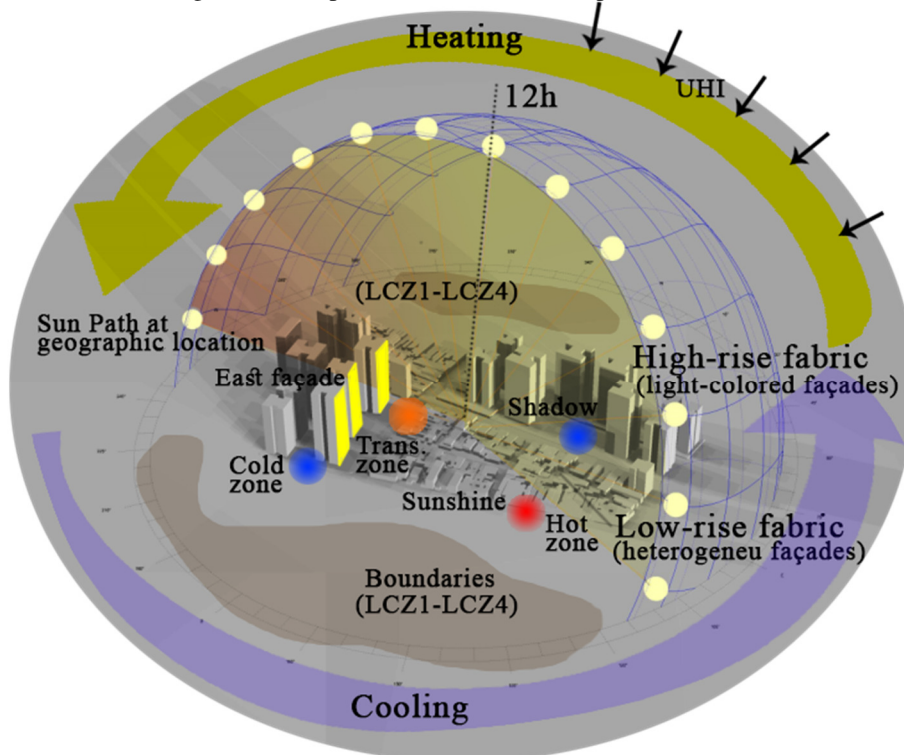
Source: Martina Pacifici (2019)

5.4.3 Selection of modeling code

The conceptual model highlighted the complexity of processes involved in the daily exchange interrelating urban forms and climate variables. It was stressed the importance of shadowing and buildings heights, the role of fabric compactness, the interference of vegetation, the strong influence of materials and façade exposures. Given the abundance of phenomena and their mutual relationship, the choice for a suitable modeling tool was addressed to a holistic and three-dimensional code. The selected code had to be able to reproduce complex geometries at local-scale as well as microclimate effects, including the simulation of interactions between buildings surfaces, air fluxes and vegetation. ENVI-met was selected as the most appropriate tool today available on the urban model scene. It is a three-dimensional numerical code implementing a finite-difference method (FDM) to solve partial differential equations that represent the conceptual model physical processes. On the basis of this choice, a simplification of urban geometries was needed to allow FDM use. Conversely, finite element software packages would permit to model complex urban forms; however, the availability of such type of softwares was found only limited to building scale (*FreeCAD* and *Autodesk simulation*).

5.4.4 Model sensitivity tests

Sensitivity analysis was developed in ENVI-met 4.3 (basic version), by implementing numerical tests on a reduced model (4.3.2), extracted from the original domain. Table 10 summarizes main findings. Then, a detailed explanation of results.

Table 10 – Sensitivity tests

Field	Parameter	Case	Value	SI	Understanding	Tendency
Roughness length	z_0	a	0.01	m	* Sensitive to w_s and w_{dir}	↑↑ z0 ws
		b	0.001	m		
		c	0.1	m		
Nested grids	NG	a	1	-	* Sensitive to RH, w_s and w_{dir} * Flatten trends of RH and departure from forcing to the increase of NG.	↑↑ NG ws
		b	2	-		
		c	3	-		
		d	4	-		
		e	5	-		
		f	6	-		
		g	10	-		
Empty grids on border	Domain size	a	53x53	-	* High computational cost * Sensitive to RH, Ta, w_s and w_{dir} * Flatten trends of T_a and RH and departure from forcing to the increase of domain size.	↑↑↑ grids ws cost
		b	63x63	-		
		c	73x73	-		
		d	83x83	-		
		e	93x93	-		
		f	99x99	-		
Specific humidity at 2500m	q	a	1	g/kg	* Sensitive to RH	↑↑ q RH
		b	10	g/kg		
Lateral boundary condition	LBC	a	Forced	-	*b & c trend similarly, different from a *a sensitive to T_a, RH, wind; more reactive and close to forcing	↓↑ Ta RH
		b	Cyclic	-		
		c	Open	-		
Emissivity (wall /roof material)	ε	a	0.1	-	* Sensitive to MRT, T_{gs}, and T_f	↑↑↓ ε Tgs Tf
		b	0.9	-		
Density (wall/roof material)	ρ	a	4000	kg/m³	* Sensitive to RH, MRT, T_f	↑↓↕ ρ RH Tf
		b	620	kg/m³		
		c	7900	kg/m³		
Thickness (wall/roof material)	t_{ck}	a	0.26	m	* Sensitive to T_f, MRT (little), during the night	↑↑↑ tck MRT Tf
		b	0.56	m		
		c	1.00	m		
Albedo (wall /roof material)	α	a	0.8	-	* Sensitive to T_{gs}, MRT (little)	↑↑↓ α Tgs MRT
		b	0.05	-		

- Roughness length

Roughness length (z_0) represents the theoretical height at which wind speed is zero. Canopy height, density, vegetation, land cover and land use affect surface roughness (Bonan, 2016, p.213). In ENVI-met, such parameter indicates the surface roughness at the wind measurement site and can only be set on three values: 0.001m, 0.01m, 0.1 m. Together with the wind speed, ENVI-met uses roughness length at the initialization phase (not after), to compute the geostrophic wind (a theoretical balance between Coriolis force and pression gradient force, occurring when isobars are parallel and no ground friction affects the wind field) (ENVI-met 3.1 User Manual). According to Oke (1987, pp.57) a roughness length ranging from 0.001 to 0.1 m describes natural soils. Due to the uncertainty on the use of a suitable value, as well as the difficulty of its real estimation on the site, three simulation were compared (Case a, b, c). Roughness length varied with a factor 10 between each simulation.

Overall, the variation of the roughness length affected distinctly the wind speed field. Increasing the roughness length parameter, the wind speed raised at all receptors analyzed along 24 hours. Two representative receptors at street and podium level were showed in Figure 46.

Figure 46 - Wind speed at receptor R2 and R3 for Cases a, b, c, where R2 is located on a basement while R3 on the street, at z=3m
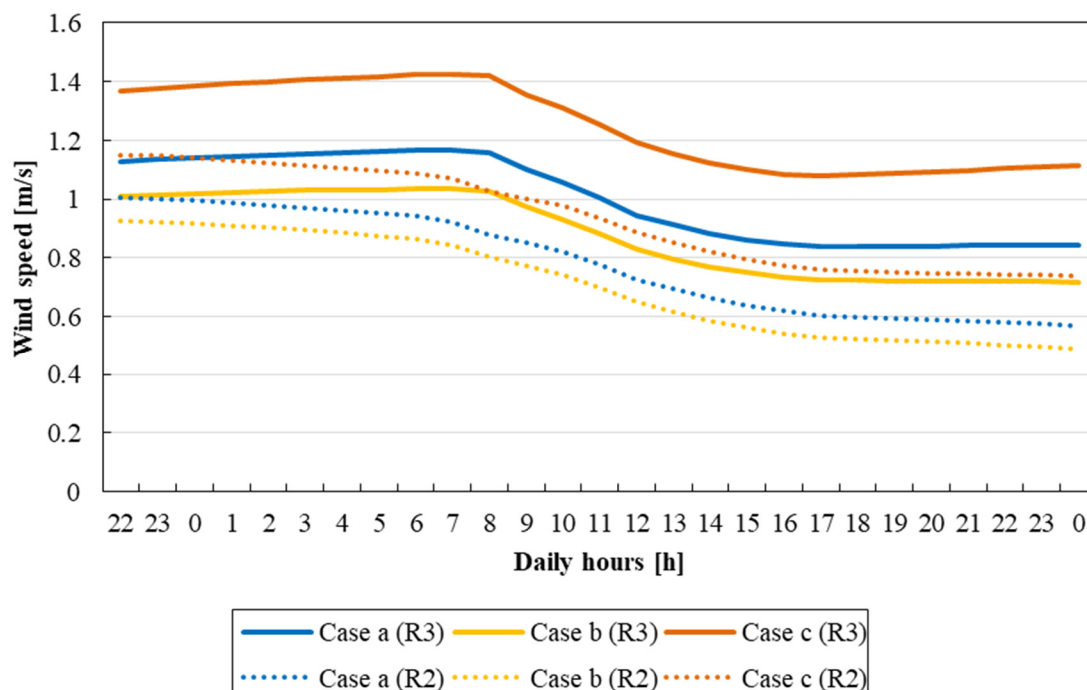
A double increasing was observed for higher values of roughness, between *a* (0.01m) and *c* (0.1 m), while a smaller gap occurred between *b* (0.001) and *a* (0.01). Other effects were found on the vectors of wind direction, displaying smaller differences between the three cases. On cases a, b, c, wind directions ranging around 150°, showing a prevalent deviation of 15 ° from the input direction (135°) (Figure 48). Meanwhile, air temperature, relative humidity, mean radiant temperature, surface temperature and façade temperatures were not affected by roughness adjustments.

Moreover, a spatial analysis comparing the two extreme cases (*b* and *c*) was plotted on all domain nodes at specific hours to assess the distribution of differences. Overall, the frequency distribution "*case c – case b*" showed a lognormal tendency. At 12 a.m., two peaks could be observed close to 0.0 m/s and 0.3 m/s (Figure 47). The first peak highlighted small or null differences between *case c* and *b*, therefore showing the wind speed insignificant sensitivity to the roughness change. The second peak showed the highest frequency of data close to 0.3m/s. The physical occurrence of peak 1 and 2 could be observed in the map of wind speed absolute differences displayed at k=1.

Figure 47 - Wind speed comparison between Case b and Case c at 12a.m. and k=1 (3m), by means of histogram representation and ENVI-met map
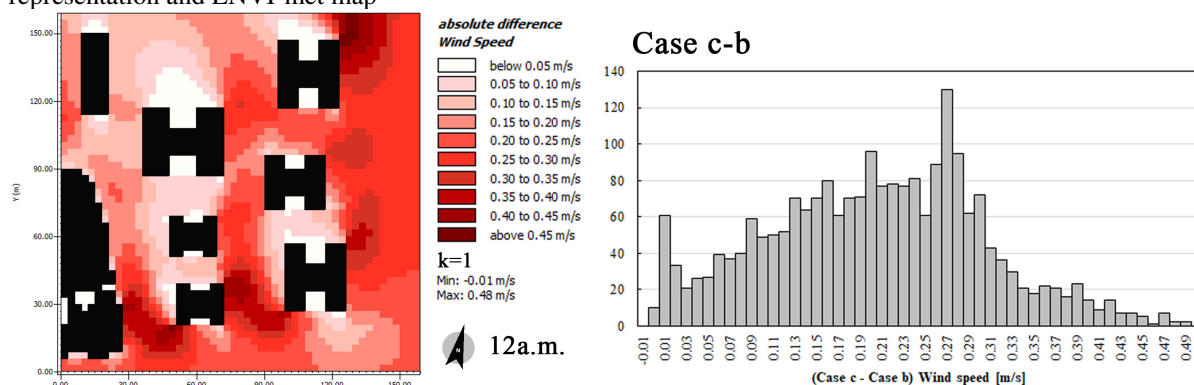
According this map, greater roughness variations (~ 0.3 m/s) were found along canyons, in which no obstacle was opposed to the propagation of the wind and a higher roughness length favored air accelerations. Conversely, smaller or null variations (~ 0.0 m/s) were distributed on the downwind zones, behind towers, where wind speed was lower and the effect of the roughness adjustment lost importance. In terms of wind direction, differences between *b* and *c* showed smaller ranges relative to wind speed. In addition, these variations

were scattered on domain, mainly concentrated between the towers, where turbulence affected w_{dir}; in the rest of model, differences were limited to 1-2 deg (Figure 48). Accordingly, by visualizing wind speed and direction together in the polar histogram (Figure 49), similar distributions were noticed. The most probable wind direction (bin width = 3°) had an occurrence of 11%. Far from this direction, less probability was found in the N-W quadrant. For all detected wind directions, a prevalence of air speeds was observed between 0.8 m/s and 1.2 m/s (case b), 1.0 m/s and 1.5 m/s (case c). A great amount of low air speeds was highlighted too (blue color).

Figure 48 - Wind direction of case b and c (left), deviation from input direction for case c (right) at 8 a.m. and k=1 (3m)
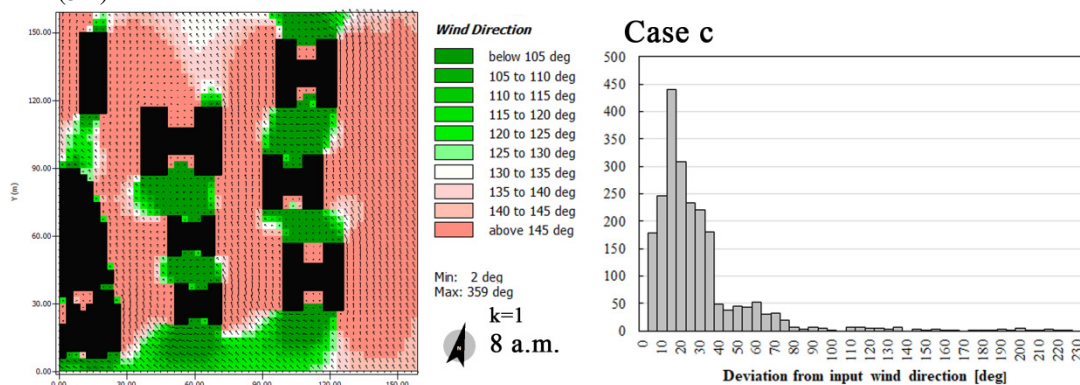
Source: Martina Pacifici (2019)

In summary, findings from roughness length analysis showed little impacts on overall model and a sensitivity response from wind. Indeed, during the initialization phase, the roughness length input is introduced in the calculation of geostrophic wind. Such calculation follows a logarithmic law that could be the cause of the double increasing between *a* and *c*. Starting from the wind speed at 10m, the logarithm law was applied to compute wind at 2500m. Afterword, along with the rest of simulation, the turbulent flow computation at all layers below 2500m was given by the one-dimensional *Navier–Stokes* equations (1D model), in which z_0 is not included. This fact explains why along the 24 hours bias between cases remains constant. Meanwhile, even if turbulent flow and thermal stratification are mathematically dependent, different initial wind speeds were not enough to produce relevant effects on the rest of variables analyzed. Above all, air temperature and humidity were insensitive to the adjustments of z_0. Such information should be considered during the calibration phase, given the low interaction between roughness and the main key-variables. Consequently, more accurate estimations of roughness length on site make little sense given its poor influence on the model.

Figure 49 – Wind direction and speed for case b (left) and case c (right) at 8 a.m., at street level (z=3m)
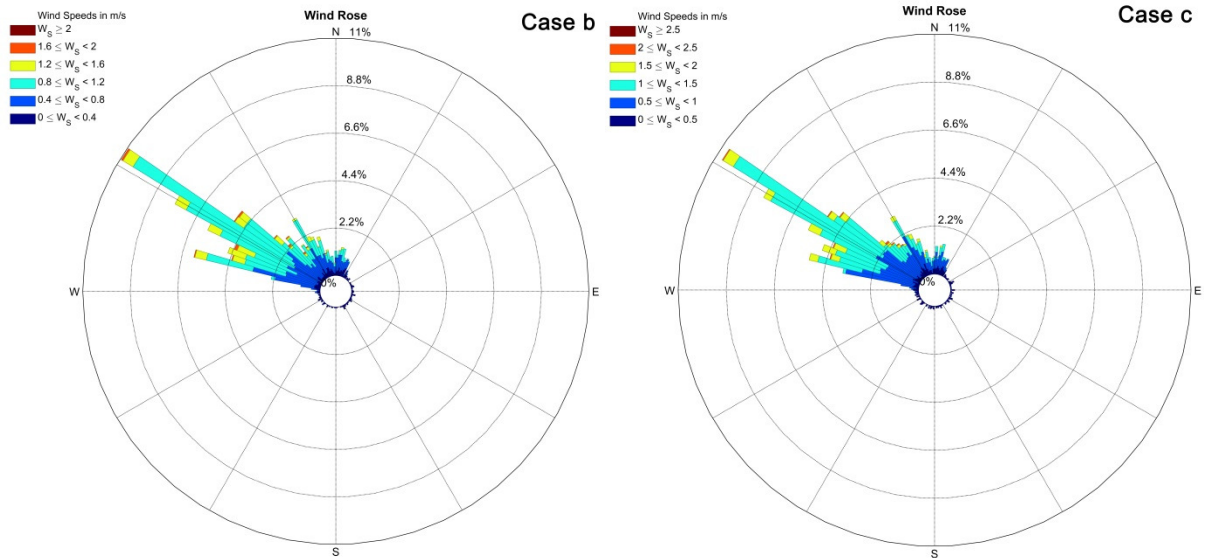
Source: Martina Pacifici (2019), developed in Matlab 2016a

- Nested Grids

Nested grids (NG) are additional grids around the 3D model. Their aim is minimizing undesired boundary effects by moving the model boundary away from the core area (ENVI-met 3.1 User Manual). NG may be used to increase the minimal distance between border buildings and boundaries required by the software; their number does not influence or increases the size domain and is not restricted by the model license. However, it worth underlying that warnings messages about small distance between building and boundaries are not correlated with run successful for simple models. To observe the impact of boundary nested grids on the 3D model seven simulations were realized, increasing 1 nested grid at each case. For case g a greater value (10 NG) was set. From case *a* to *g*, a growing simulation time was observed (~2h30); in larger and more complex domains, a greater increase is expected. As in the study of roughness, the change of nested grids led to a notable variation in wind speed and direction in all receptors analyzed. The wind was found a very sensible variable (Figure 50a), while a little reactivity was observed on the other variables. From case *a* to *g*, smooth fluctuations could be seen around the relative humidity curves (Figure 50b), and only very small variations on the air temperature; no reactions from mean radiant temperature and surface temperature. In general, the model showed to be wind-driven and, in spite of the abundance of the physical processes and variables involved, wind seemed to be the only truth reactive variable. Differences between curves of relative humidity or air temperature are probably secondary effects, depending on wind field alterations, in turn due to

the change of the nested grids number. Findings from R5 were displayed in terms of wind speed and relative humidity. A decreasing trend was found on wind speed to the increasing of NGs around model. For relative humidity, instead, the increase of NG caused a nocturnal decrease and a diurnal growth, resulting in a flatter trend and departing from forcing values (Figure 50).

Figure 50 - Wind speed and Relative humidity at receptor R5 from Case *a* to *g* along 24h, (z=3m)
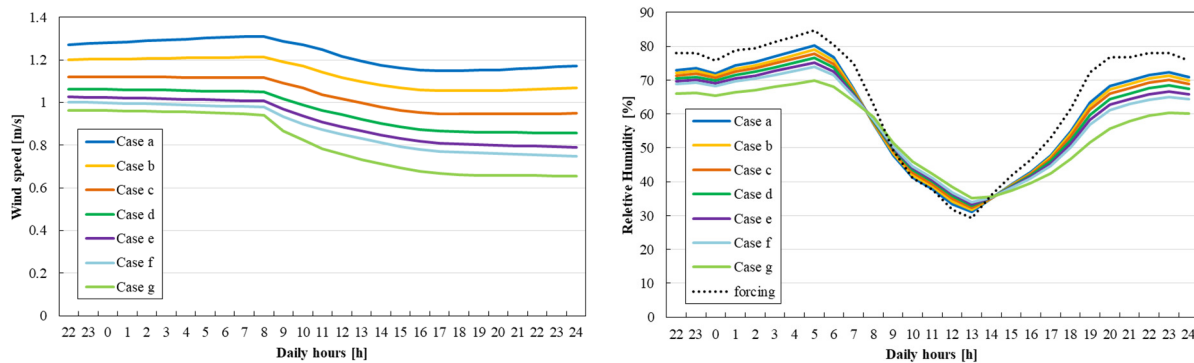
Source: Martina Pacifici (2019)

At 8 p.m. (Figure 51), on the entire domain, differences in terms of relative humidity "case *a – g*" were distributed around the value of 15%. Zones of domain with this probability were located on the inflow boundary and along large open spaces; in the vicinity of buildings, instead, mutual differences decreased. A long tail was given by greater values (> 20%) caused by computational errors in the holes of built morphology. Overall, the increasing of nested grids affected the RH inflow values on the boundary of domain, while less contrast zones were observed along with the air flow propagation.

It should be noted that relevant differences were obtained mainly comparing cases *a* (1 NG) and *g* (10 NG), while little differences were found between close cases. Meantime, great numbers of nested grids, as in case *g*, are useless in large domains due to the high computational cost. In terms of relative humidity, the introduction of additional nested grids let the model less reactive, decreasing the range between maximums and minimums. This flatten behavior implied a departure between forcing conditions and modeled curves. A similar pattern was observed on air temperature, to a lesser extent. Indeed, since temperature and humidity forcing are applied on the boundaries, more nested grids relax these input values on the border of the model; however, such effect faded far from borders, since in the interest model zone smaller differences were found.

Figure 51 - Relative Humidity comparison between Case *a* and Case *g* at 20h, z=3m, by means of histogram representation and ENVI-met map
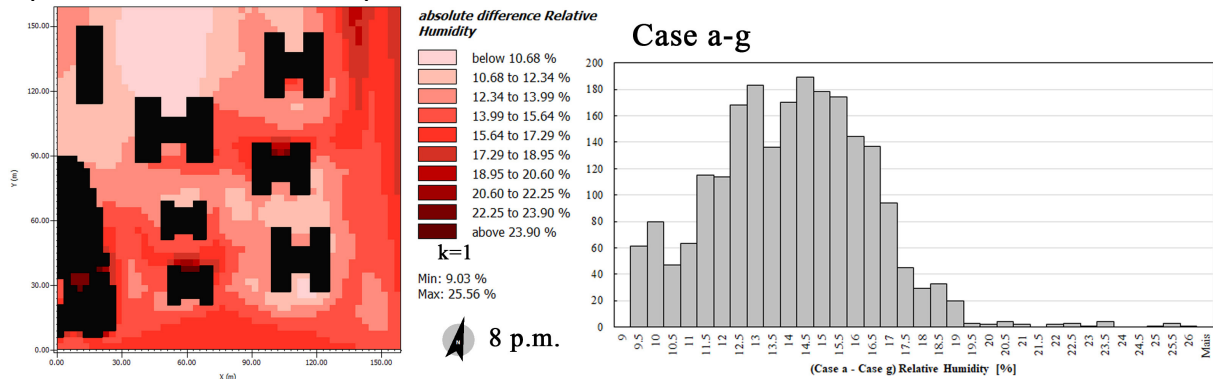
Source: Martina Pacifici (2019)

- Empty grids on the border

According to ENVI-met team advices, empty grids (EG) on the model domain borders can facilitate the turbulence calculation and avoid errors. In addition, by adding empty grids on the borders (instead of the nested grids) the distance between lateral boundary conditions and core morphology increases. To understand the feasibility of this strategy, six simulations were realized to observe the model sensitivity when rows of empty grids were added from *Case a* to *f*. All simulations ran successfully, in spite of a little space between model borders and peripheral buildings in the first cases. For *Case a,* some calculation errors were observed on the left side of domain, within the little cavities of morphology. Overall, to the increase of empty grids on borders, larger *xy* domains were created, even if the design of built mass was kept constant. In terms of running time, a significant increase was observed when new cells were added. Therefore, the strategy of empty grids required a greater simulation time in comparison with the introduction of nested grids. By comparing case *e* in NG and EG experiments, it would be noted that simulation took 11 hours by using nested grids, while 28 hours by using empty grids; at both cases, enough space between borders and buildings was guaranteed (according to ENVI-met recommendations). Case g (NG) is slightly out of time simulation tendency because it was realized with science license instead of basic one (Figure 52).

Figure 52 - Simulation Time from Nested Grids sensibility analysis (NG) and Empty Cells (EC) tests, averaged over 24 hours.

Source: Martina Pacifici (2019)

The addition of empty grids on the border of the model led to the variation of wind speed in all receptors analyzed and wind direction in some ones. Variation was more evident between *case a* (no empty cells on the border) and the rest of *cases* (*b - f*), that present similar behaviors. As a consequence, the variation of the number of empty cells did not have significant influence on variables; meanwhile, the lack or the presence of empty cells was more visible. In some receptors, air temperature and relative humidity were slightly found more sensitive in comparison with nested grids and roughness analyses. Also in this case, differences occurred between case *a* and the rest of cases. Similarly to nested grids, with the increase of distance between core morphology and boundaries (from *a* to *f*), flatter trends could be observed on air temperature and relative humidity; conversely, smaller domains favor the proximity between the modeled air temperature and forcing. Air temperature exhibited greater differences from 8h to 16h (Figure 53).

The different domain size characterizing this set of simulations prevented a direct comparison between cases, since the model changed each time with the addition of new empty grids. However, when *a* and *f* were simultaneously observed (Figure 54), a similar distribution of variables was recognized around buildings, while unchanged values were kept on the borders of Case *f*, practically recreating a boundary condition. The distribution of Case *f* air temperature at 8 a.m. well described the cooling effect of a warm boundary air flow blowing from south-east and impacting a cooler built morphology. Thus, in this case, domain temperature was cooler than *forcing*. The joint observation of cases *a* and *f* emphasized how

boundary conditions were propagated along the wind direction, strongly conditioning the distribution of the temperature field.

Figure 53 - Air Temperature at receptor R3 (z=0m) and Wind speed at receptor R5 (z=3m) from Case *a* to *f* along 24h
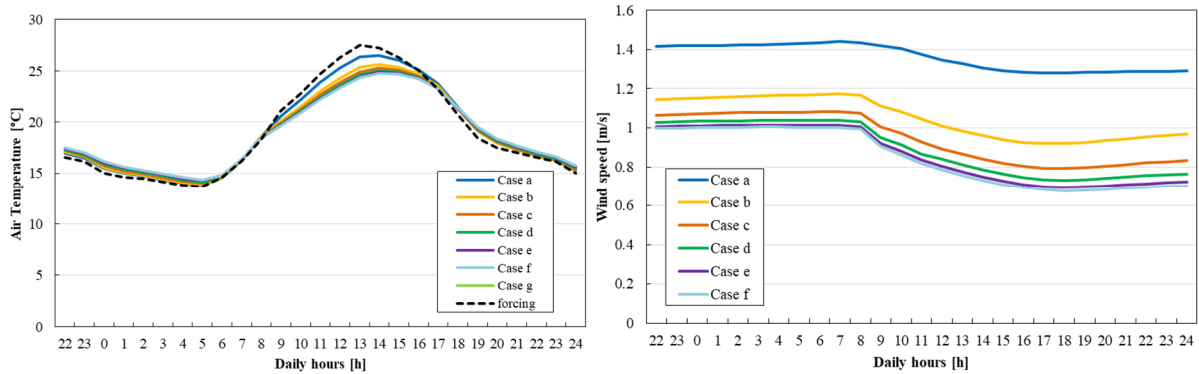
Source: Martina Pacifici (2019)

To summarize, the observed model had been found sensitive to adjustments on nested grids and empty grids at the border. When NG and EG were increased, losses could be observed on wind speeds. Furthmore, reduced model reactivity was found in terms of air temperature and relative humidity, as well as a departure from forcing curve. As consequence of this last result, the use of nested grids and empty grids/larger grids around the interest zone should be minimized to achieve more accurate results. Meanwhile, it worth stressing that such considerations were based on the observation of slight differences between cases; overall, the trend of air temperature and relative humidity always remained much tied to the forcing trend.

Figure 54 - Air Temperature at 8h from *Case a - grid: 53x53x24* (left) and *Case f - grid: 99x99x24* (right)
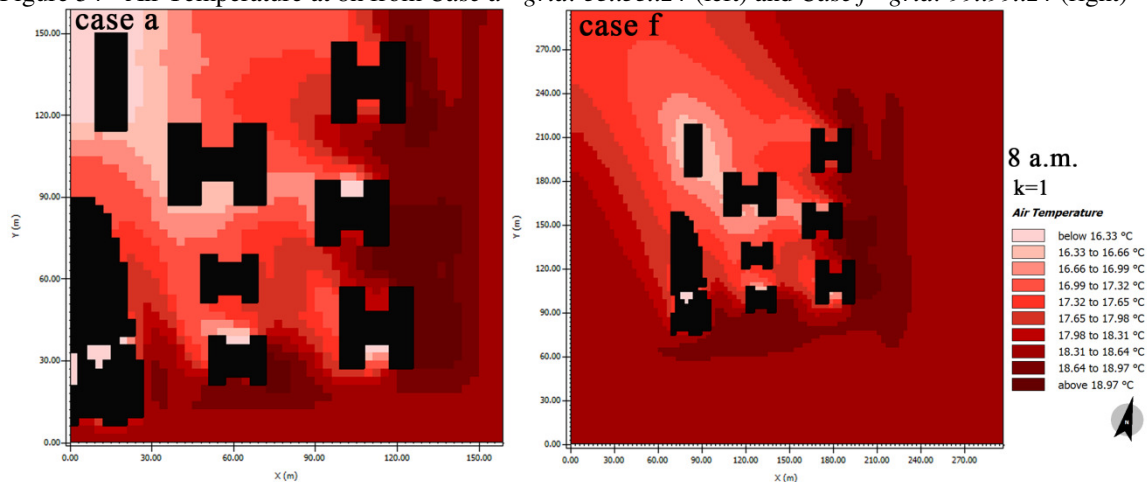
Source: Martina Pacifici (2019)

- Specific Humidity at 2500 m

Specific humidity at 2500 m is a mesoscale value forcing the advected air mass in the domain. It is a basic setting parameter applied to the top of the model and kept constant during the simulation. Such value can be estimated from meteorological data by interpolation; however, its high variability represents an important source of uncertainty in the climate model. For this reason, results sensitivity was tested on two values with factor 10 (1 and 10 10g/kg). On all the receptors, with the increasing of specific humidity from 1 to 10 g/kg, a growth of relative humidity from *a* to *b* was observed along the day (Figure 55, left). Other parameters were observed insensitive. Meantime, a greater mutual variability was displayed between the receptors of case *a* relative to receptors of case *b*. Other observation regards the size of differences (Figure 55, right); thus, little gaps appear during the day (~ 3%) while greater gaps can be observed in the night (5%~12%).

Figure 55- Relative Humidity at all receptors, from Case *a* and *b* along 24h at k=1(left), only differences (right)
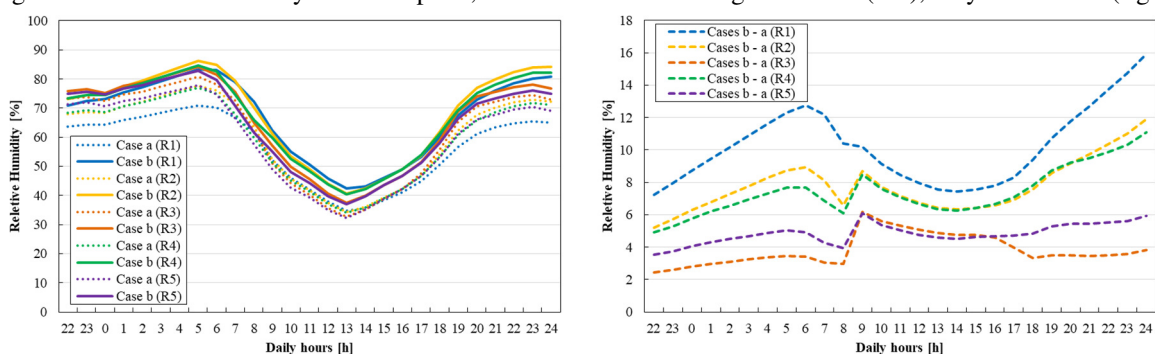
Source: Martina Pacifici (2019)

When the absolute differences between *a* and *b* were displayed on 2D map, zones with low values of difference were recognized on the inflow boundary conditions, while zones with higher values of difference were found on the outflow border of the model. Therefore, the increasing of specific humidity at 2500m had slightly interfered with the humidity inflow boundary conditions. Afterwards, such influence progressively increased from the inflow side to the outflow opposite one, affected by the combined advection-diffusion equations computing the relative humidity field. The histograms probability distribution "case b – case a" confirmed this trend, showing a bimodal trend (Figure 56).

Figure 56 - Relative Humidity difference between Case *a* and Case *b* at 20h and k=1 (z=3m), by means of histogram representation and ENVI-met map
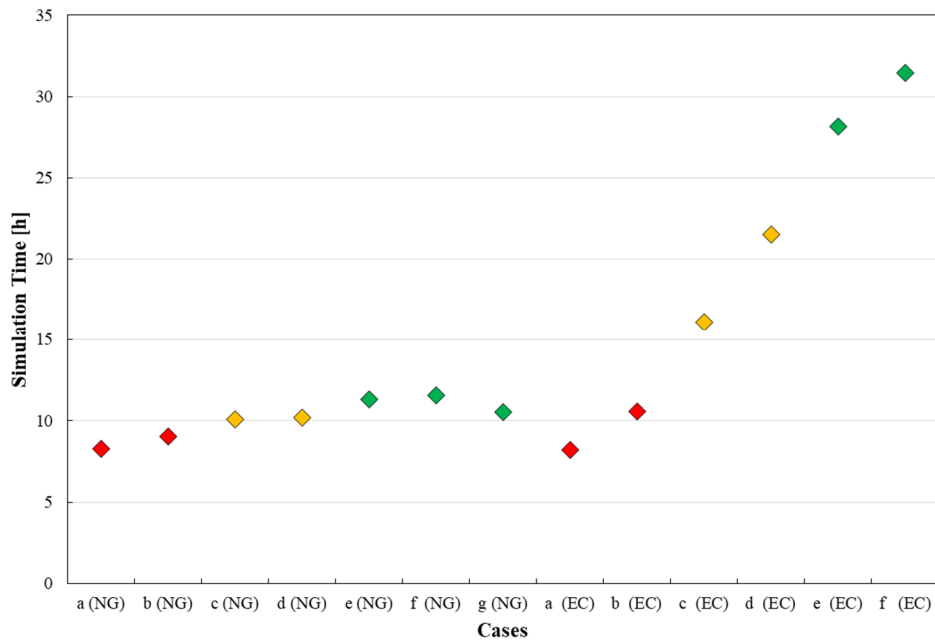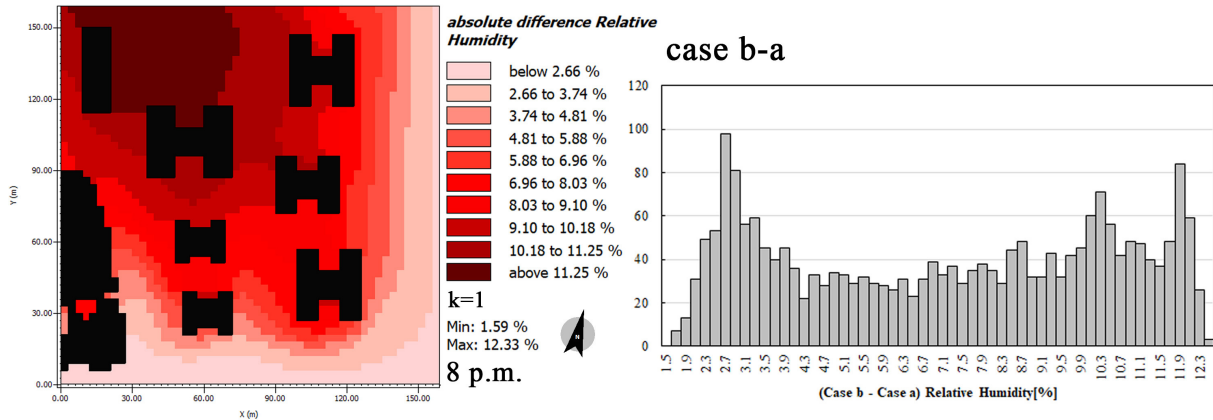
Source: Martina Pacifici (2019)

It follows that the adjustment of specific humidity at 2500m on the initial conditions of model slightly affected the inflow humidity on the boundaries; later, this departure increased towards the outflow border, following the flux spreading. Radiation behaved as a prevalent driving condition, since fewer differences between the two cases were observed between 9 a.m. and 6 p.m., while nightly clearer gaps were observed.

- Lateral boundary conditions (LBC)

ENVI-met provides three types of lateral boundary conditions (forced, open, cyclic) to define the flux exchange on the border of the model (Figure 57). Lateral boundary conditions can be set for air temperature and humidity, as well as for turbulence. However, when *forcing* is used, LBC for air temperature and humidity can not to be set arbitrarily, since the software will set them on "forced" in any case. Given this limitation, only the arbitrary LBC for Turbulence were explored by means of three simulations. Cases *a*, *b*, *c* explored respectively the forced, cyclic and open turbulence condition. *Forced or closed* LBCs for turbulence determine every hour the initial condition of inflow boundary, controlling the two turbulence variables, E (kinetic energy) and ε (dissipation rate), previously computed in the 1D model. Thus, under forced LBC conditions, the vertical profile of the kinetic energy and its dissipation rate calculated in the 1D model are copied on the right model inflow boundary each hour (Figure 57a). In the other cases, *cyclic* LBCs feed the inflow boundary profile by copying back the outflow boundary values to the right model boundary (Figure 57c), while under *open* LBCs the values of the inner points are copied back to the right model inflow boundary (Figure 57b). Furthermore, under forced LBC, the vertical Km profile at the inflow boundary looks clearly different from the average Km distribution in the 3D model. The flow

is forced upward and downward, modifying the *K*m profile, especially close to building. This effect was reduced with the use of open LBC as long as, under cyclic LBC, the inflow profile is even similar to the average *K*m distribution inside the 3D model (ENVI-met official webpage).

Figure 57 – Forced, Open and Cyclic Boundary Conditions (LBC) for a model example consisting of one 20m high building and a tree in front. A 3 m/s wind is set coming from the east, at 10 m above ground. The isoline distance is 0.3 m²/s; only *K*m values up to 10 m²/s are plotted.

(a) *K*m distribution for **Forced LBC** (b) *K*m distribution for **Open LBC** (c) *K*m distribution for **Cyclic LBC**
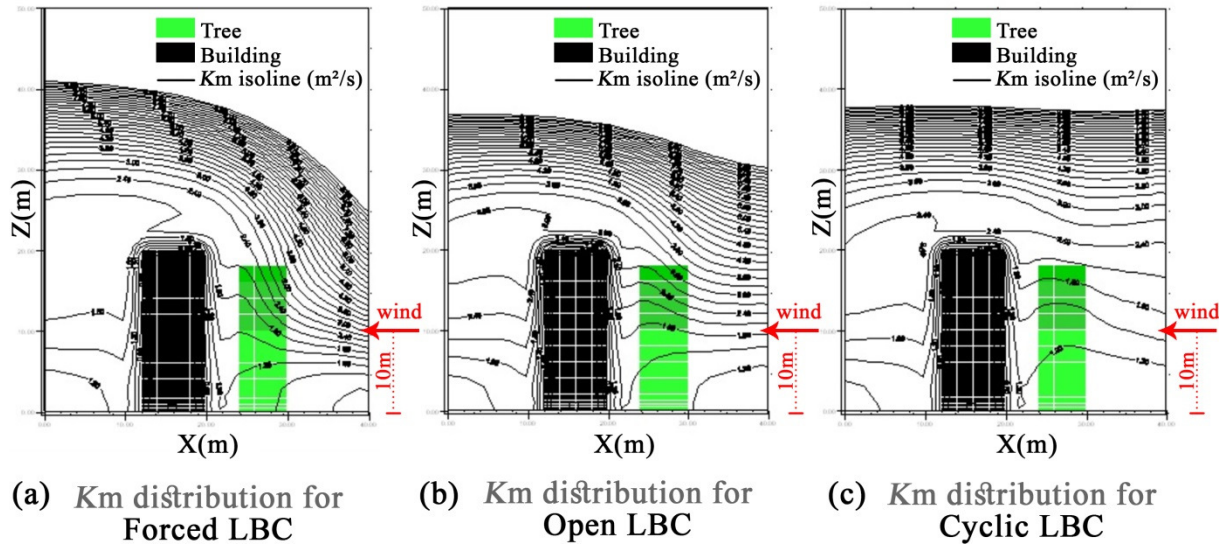
Source: Martina Pacifici (2019), adapted from ENVI-met official webpage (http://www.envi-met.info/doku.php?id=kb:lbc)

Subsequently, in the 3D model, the turbulent exchanges coefficients (*K*) were alimented from buildings and vegetation sheareding the main air flow. The relationships among turbulence (Equation 12) and dissipation (Equation 13) that allow predicting the turbulence in the air of the 3D model are mathematically described in the following k-ε equations:

$$\frac{\partial E}{\partial t} + u\frac{\partial E}{\partial x} + v\frac{\partial E}{\partial y} + w\frac{\partial E}{\partial z} = \frac{\partial}{\partial x}\left(K_E \frac{\partial E}{\partial x}\right) + \frac{\partial}{\partial y}\left(K_E \frac{\partial E}{\partial y}\right) + \frac{\partial}{\partial z}\left(K_E \frac{\partial E}{\partial z}\right) +$$

$$K_m \left[2\left(\frac{\partial u}{\partial x}\right)^2 + \left(\frac{\partial u}{\partial y}+\frac{\partial v}{\partial x}\right)^2 + \left(\frac{\partial u}{\partial z}+\frac{\partial w}{\partial x}\right)^2 + 2\left(\frac{\partial v}{\partial y}\right)^2 + \left(\frac{\partial v}{\partial z}+\frac{\partial w}{\partial y}\right)^2 + 2\left(\frac{\partial w}{\partial z}\right)^2\right] - T_h + Q_E(x,y,z) - \varepsilon \qquad (12)$$

$$\frac{\partial \varepsilon}{\partial t} + u\frac{\partial \varepsilon}{\partial x} + v\frac{\partial \varepsilon}{\partial y} + w\frac{\partial \varepsilon}{\partial z} = \frac{\partial}{\partial x}\left(K_\varepsilon \frac{\partial \varepsilon}{\partial x}\right) + \frac{\partial}{\partial y}\left(K_\varepsilon \frac{\partial \varepsilon}{\partial y}\right) + \frac{\partial}{\partial z}\left(K_\varepsilon \frac{\partial \varepsilon}{\partial z}\right) +$$

$$c1_\varepsilon \frac{\varepsilon}{E}K_m \left[2\left(\frac{\partial u}{\partial x}\right)^2 + \left(\frac{\partial u}{\partial y}+\frac{\partial v}{\partial x}\right)^2 + \left(\frac{\partial u}{\partial z}+\frac{\partial w}{\partial x}\right)^2 + 2\left(\frac{\partial v}{\partial y}\right)^2 + \left(\frac{\partial v}{\partial z}+\frac{\partial w}{\partial y}\right)^2 + 2\left(\frac{\partial w}{\partial z}\right)^2\right] - c3_\varepsilon \frac{\varepsilon}{E}T_h - c2_\varepsilon \frac{\varepsilon^2}{E} +$$

$$Q_\varepsilon(x,y,z) \qquad (13)$$

where E is the kinetic energy in the air affecting the local turbulence, ε is the dissipation rate, K_m and related terms between parentheses indicate the mechanical production of turbulent energy (Pr) due to the wind shear while T_h the dissipation of turbulent energy due to the thermal stratification. Additional turbulences produced and dissipated near to plants are represented by Q_E and Q_ε; c1=1.44 c2=1.92 and c3=1.44 are standard values given by Launder and Spalding (1974) used to calibrate the ε-equation. Computation of P_r, T_h, Q_E and Q_ε are detailed on Bruse (1999). From the calculated E-ε field, the computation of turbulent exchange coefficient K_m is obtained. K_E and K_ε are obtained by assuming the local turbulence isotropy and keeping constants c_μ=0.09, σ_E=1, σ_ε=1.3. Mathematically:

$$K_m = c_\mu \frac{E^2}{\varepsilon}; K_E = \frac{K_m}{\sigma_E}; \ K_\varepsilon = \frac{K_m}{\sigma_\varepsilon} \tag{14}$$

For all the variables analyzed, *Case b* and *c* showed coincident trends, therefore the cyclic and open conditions were found equivalent in terms of air temperature, relative humidity, mean radiant temperature, surface temperature, wind speed, wind direction and façade temperature (external, internal, inside). Conversely, case *a*, implementing forced turbulence conditions, moved away from cases *b* and *c* when the variables of Ta, RH and wind were considered. Especially, at all receptors analyzed, c*ase a* was more suitable to reproduce the forcing curve (as expected) and showed a better reactivity, with greater peaks and smaller minimums, in comparison with the flatter trend of *cases b* and *c* (Figure 58).

Figure 58 - Air Temperature and Relative Humidity at receptor 2 from Case *a, b, c* along 24h at k=1 (z=3m) with the comparison of Forcing trend.
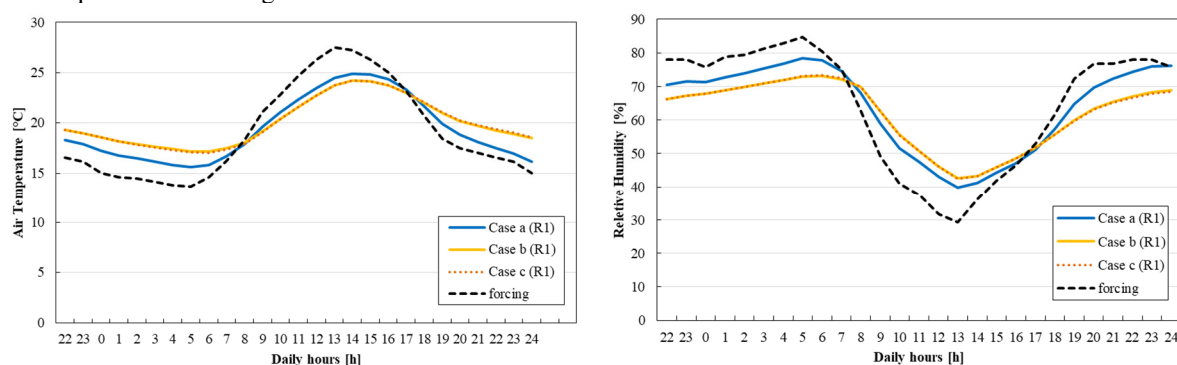
Source: Martina Pacifici (2019)

This result encourages selecting the "Forced" Turbulence option as the best lateral boundary condition to be used in couple with the air temperature and humidity "forced" condition to calibrate the model. When the three *cases* were spatially observed together on all

domain, a heat decreasing could be seen from the forced to the cyclic and open condition at 8 a.m. Furthmore, the interaction buildings-atmosphere seemed to be more prominent in the case of Forced LBC (Figure 59). It is also emphasized that in the future versions of the software, the Open and Cyclic boundaries conditions will be eliminated and only Forced conditions will be maintained and improved. The Full Forcing option, already available for paying users, allows the forcing of many climate variables, as well as the import of *epw Energyplus* files.

Figure 59 - Air Temperature at Case *a* (Forced LBC), *b* (Cyclic LBC) and *c* (Open LBC) at 8h and k=1
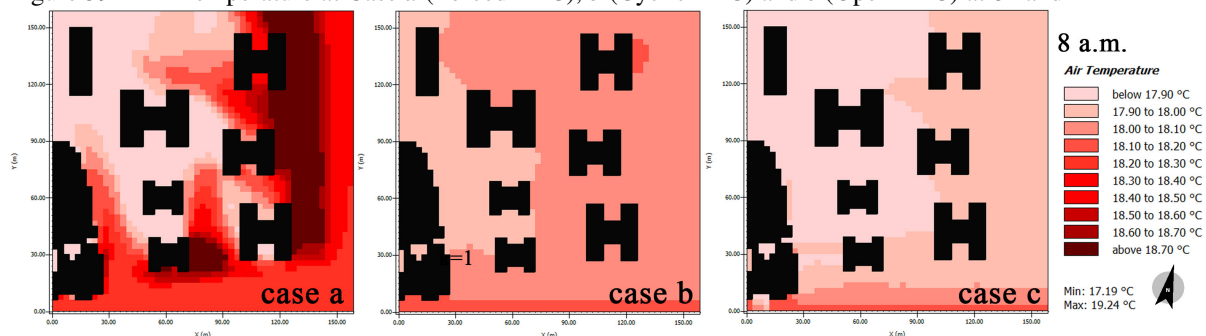
Source: Martina Pacifici (2019)

- Materials

In order to verify material properties effects, numerical experiments were developed on emissivity, density, thickness and albedo material properties. Surfaces with a single material were considered, setting the same values for the three layers (0.03-0.2-0.03 m thick) that composed walls and roofs in ENVI-met.

o *Emissivity Coefficient*

The "emissivity" coefficient (0 < ε < 1) refers to the ability of material bodies to emit thermal radiations in comparison with a black body at the same temperature. In ENVI-met, the coefficient was changed from 0.1 (*case a*) to 0.9 (*case b*) in order to test the modeling effects associated to the extreme values of this parameter. An emissivity as 0.1 is typical of aluminum or steal, while an emissivity of 0.9 characterizes brick, tiles, terracotta and concrete. Adjustments of ε interested building façades, roofs and podium.

As occurred on most of previous analyses, air temperature and humidity were insensitive to emissivity changes in all receptors. Even wind speed and direction were less or no affected. Conversely, mean radiant temperature, surface temperature and outside façade

temperature were more reactive. Overall, a growth of ground surface temperature and mean radiant temperature (from *a* to *b*) was noticed to the increase of emissivity coefficient (from 0.1 to 0.9), while a decreasing trend was observed on facades temperature. Greater differences between *Case a* and *b* occurred during the cooler hours, while small distances were displayed between 8 a.m. and 5 p.m., depending on the variable (Figure 60, Figure 61).

Figure 60 **–** Surface temperature at receptor 3 (left), façade temperature at receptors 7 and 9 (right), from Case *a* and *b,* along 24h at k=1 (z=3m).
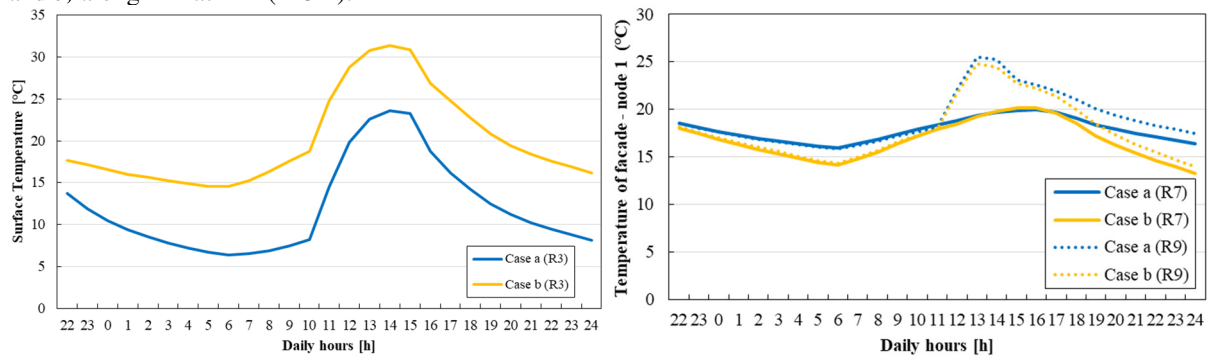
Source: Martina Pacifici (2019)

Figure 61 - Differences of mean radiant temperature between case *b* and *a*, at receptor 2, 3, 4, 5
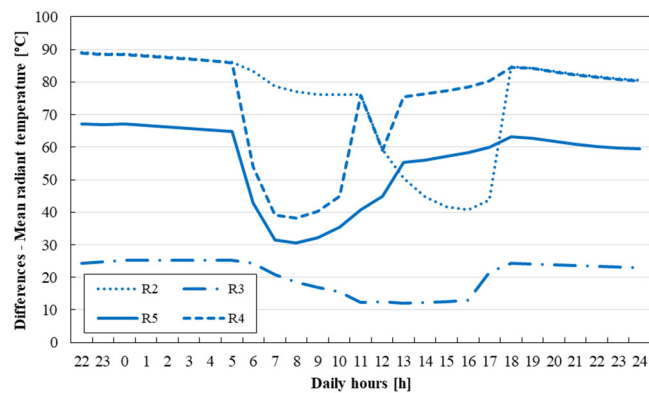
Source: Martina Pacifici (2019)

In terms of emissivity, mean radiant temperature was observed as an extremely sensitive variable; the use of a low emissivity as 0.1 (typical of polished metals), at *Case b,* led to deep gaps between the two cases, probably due to the use of a very low coefficient (Figure 60). A strict relationship was observed between access to solar radiation and drop of MRT differences. It could be noted that in R4 and R5, to be east-exposed, an early decreasing of MRT differences was observed; conversely, in R2, the drop occurred later, when the receptor started to be accessed by sun. In a receptor quite far from surfaces (R3), a littler bias was found between case *a* and *b* (Figure 61).

To investigate the entire domain, two representative hours were selected on noon (12 a.m.) and evening (8 p.m.). The comparison *case b – case a* caused positive differences on all domain (Figure 62). However, such gaps were more accentuated at night. The high emissivity of case *b* produced higher mean radiant temperatures concentrated in the model core, where the towers were located, and minor values along the street. This double behavior *street – podium* occurred at night and during the day. As consequence, a bimodal trend was recognized on histograms, in which two distinct peaks could be found (on 8K and 58K at 12 a.m., on 14K and 64K at 8 p.m.)

Figure 62 - Maps and Histograms showing the Absolute Difference of Mean Radiant Temperature between Case *a* and *b* at 12h (right) and 20h (left)
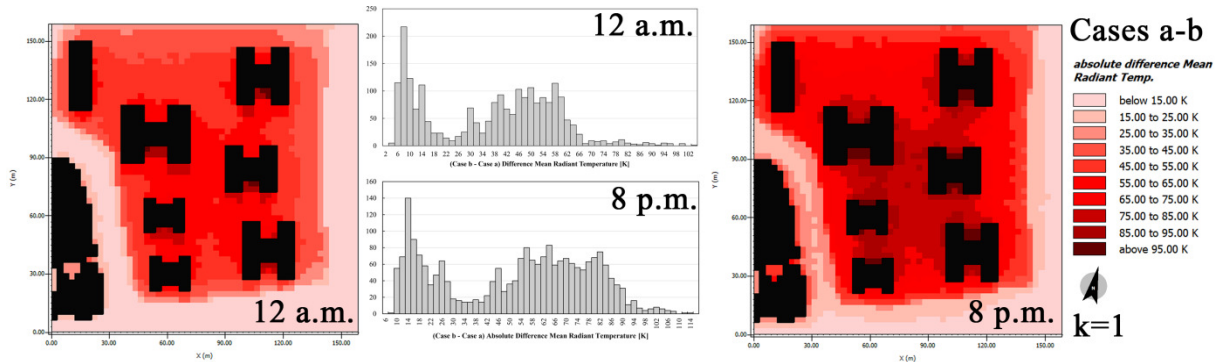
Source: Martina Pacifici (2019)

Findings reveal two important evidences. On one hand, a good response of *MRT*, ground surface and facades temperatures was observed to the adjustment of emissivity, confirming the centrality of this variable in the heat exchange between materials and atmosphere. On the other hand, the absolute insensitivity of air temperature and relative humidity were quite worrying, further considering that only extreme values had been tested. Once again, air temperature and humidity showed a low reactivity, only controlled by forcing. Between façade surfaces (on which the emissivity is set) and surrounding variables (ground surface and *MRT*) opposite trends were observed: more emissive materials decreased the temperature of walls and roofs, while increased outdoor variables, with sensitive effects on ground temperature and radiant fluxes. Such inverse relation between façade temperature and emissivity mainly occurred at night and was in accordance with the Stefan–Boltzmann law, for which emissivity is inversely related to the fourth power of body temperature ($E_r = \varepsilon \sigma T^4$, with E_r, total energy radiated and σ, Stefan–Boltzmann constant). Lastly, tests on emissivity led to greater effects during the night, when the heat is released after the daily warming (high emissivity materials retain more hot and releases it slower).

o   *Density Coefficient*

The density of materials defines the amount of material mass (kg) per unit volume (m^3). Three sensitivity simulations were performed testing default values representatives of lightweight concrete (case b, 620 kg/m^3), iron (case c, 7900 kg/m^3) and an intermediate value between them (case a, 4000 kg/m^3). It worth stressing that such values were functional to the implementation of sensitivity studies, even if they are uncommon for an urban environment.

Findings from density adjustments showed clearly effects on façade temperatures and mean radiant temperatures, while only minor (R1, R2, R4) or null (R3, R5) variations characterized air temperature and relative humidity (Figure 63).

Figure 63 **-** Temperature of façade – node 1 [°C] at receptors 8 and 9 from Case *a, b, c* along 24h at k=1, Relative Humidity [%] at receptors 2 and 3 from Case *a, b, c* along 24h at k=1
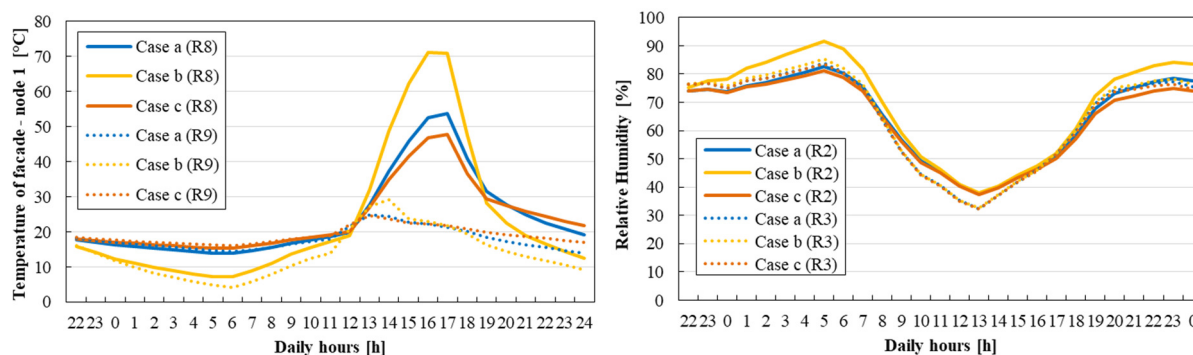
Source: Martina Pacifici (2019)

Between density increase and façade temperatures, on the west exposure (R8) and north exposure (R9), an inverse proportionality was found on the central hours of the day (12 a.m. to 7 p.m.), while a direct proportionality occurred during night, getting smaller in the morning hours. Furthermore, low densities favored deeper trends, with greater maximum and lower minimum of façade temperature at west (R8) and north exposure (R9). However, at south and east exposures, only lower minimum were observed and the reverse diurnal trend did not occurred (Figure 63, left). Similarly, relative humidity and mean radiant temperature showed sensitivity to density adjustment during the cooler periods, while a coincident trend was found at *a*, *b*, *c* cases on the central part of the day (Figure 63). No recognizable trends could be observed in terms of wind speed and direction.

The difference between night and day hours was also visible for Relative Humidity on all domain, by comparing absolute differences between cases *b* and *c* (the extreme-ones) during the cold (5 a.m.) and hot period (12 a.m.) at Figure 64.

Figure 64 **-** Maps showing the Absolute Difference of Relative Humidity between Case *b* and *c* at 5h (right) and 12h (left).
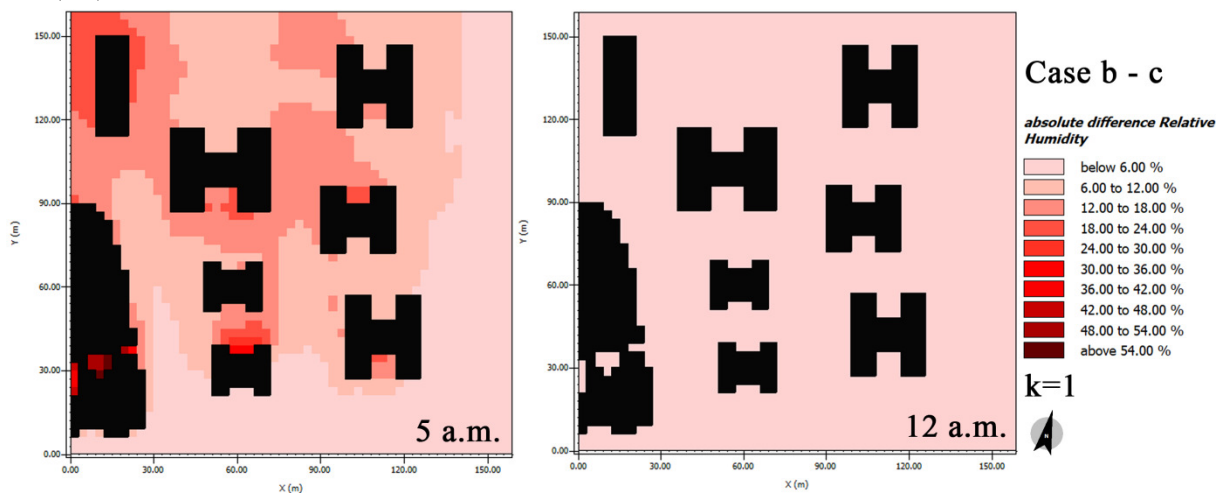
Source: Martina Pacifici (2019)

Overall, the model was found sensitive to density tests mainly on the cooler hours (evening-night-first part of the morning). During the day, only facades temperatures displayed significant differences among the three cases. Such differences had distinct trends relative to the exposure. On west and north exposure, direct (on the night) and indirect proportionality (on the day) was detected, between low and high density. On the east and south exposure, instead, only a nightly reactivity was observed, with low densities providing deeper minimum and a fast cooling of surfaces. In general, the use of high densities caused a more slowly release of hot retained at night.

o   *Thickness Coefficient*

Such coefficient defines the size of wall and roof elements, assigning the thickness to the three layers that make up walls and roofs. At urban scale-simulation, this is a very uncertain parameter, since the variety of building typologies, the mixture of construction periods, the quality and income-standards involve the use of different construction materials and techniques (as found on the fieldwork). Therefore, thickness of walls and roofs is usually estimated and made equal for all the buildings of the domain. Thus, three cases where simulated, changing the thickness of walls and roofs. Again, extreme values were tested. From *a* to *c*, the thickness of the wall and roof was increased from 0.26 m (new buildings) to 1 m (old houses).

In general, the model was found little reactive to the changes of this parameter. Atmosphere variables were insensitive, except for mean radiant temperature that was

observed changing on the nightly hours in the majority of receptors, while façade temperature at the external node was more reactive. Also for façade temperature, the great part of variations occurred on the night, while the sunny period was quite insensitive to the thickness adjustment. On all exposures, thicker layers led to the increase of façade temperature, as well as to flatten the thermal variability of the wall throughout the day. Thin walls, instead, reduced the thermal inertia of the element that most easily could gain and lose heat. It should be noted that when gaps between cases were compared, *b* and *c* displayed very similar behaviors relative to a more isolated case *a* (Figure 65, left). This evidence was not caused by a minor increment in thickness (c - b = 44cm, b - a = 30cm); rather, beyond a certain thickness, the wall lost the ability to affect heat exchanges. Furthermore, cases *b* and *c* kept constant the temperature of buildings (inside) along 24h at 19.85 °C, probably due to the great surfaces thickness adopted. Case *a*, instead, allowed the variation of buildings temperature. The same behavior (Figure 65, right) regarded façade temperatures on the internal side (7 node).

Figure 65 - Temperature of façade – node 1 or outside (left) and node 7 or inside (right) [°C] at receptors 7 (south exposure) and 9 (north exposure) from Case *a, b, c* along 24h at k=1
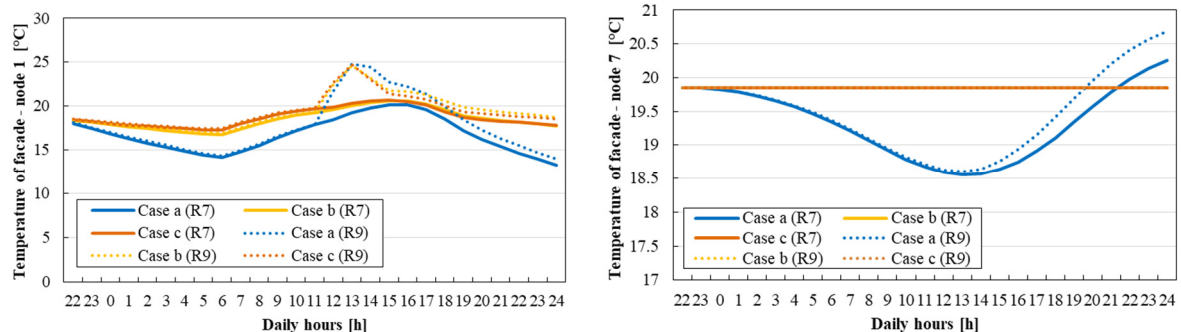
Source: Martina Pacifici (2019)

o   *Albedo of pavement*

Albedo is the fraction of the incident solar radiation reflected from surfaces. Dark-coloured surfaces (low albedo) absorb a large part of solar rays, while light-coloured surfaces (high albedo) return a great amount of sunrays back to the atmosphere. Values of albedo at the urban local scale depends on the reflection ability of roofs, trees, canyons and open spaces, combined with the diversity of materials, city structure and geographical location (OKE *et al.*, 2017, p.142). ENVI-met allowed assigning the albedo coefficient only to soil surfaces, while for vertical surfaces a rate of absorption, transmission and reflection could be set up.

Therefore, two cases with very different values of street pavement albedo were compared: *case a* (0.8) and *case b* (0.05).

From sensitivity analysis, the variation of albedo parameter from 0.8 to 0.05 led to a pronounced fluctuation of ground surface temperature at the street level (R3) from 10 a.m. up to night. As expected, when albedo was small, reflecting the 5% and absorbing the 95% of shortwave radiation, ground surface heated up and its temperature increase could be noted (Figure 66, left). At receptor 3, also the mean radiant temperature was found slightly affected (Figure 66, right). Overall, no relevant changes were observed in the trend of air temperature, relative humidity, wind speed and direction, façade temperatures (except slight variations for façade temperature at external node). The trend of ground surface temperature was further investigated, taking into account the totality of domain cells, and showed at two times, 1 p.m. (the instant in which *a* and *b cases* are more distant) and 11 p.m. (when the curves meet again) at k=0 (Figure 67). At 1 p.m., thermal differences were found between the street floor (for which the albedo was adjusted) and the sidewalks (for which albedo was kept constant in both cases, equal to 0.8). At 11 p.m., when the heating phase is completed, *a* and *b* cases return to be similar, both on the street floor and on the sidewalk.

Figure 66 - Surface Temperature at k = 0 (left) and Mean Radiant Temperature at k = 1 (right) [°C] at receptor 3 from Case *a* and *b,* along 24h
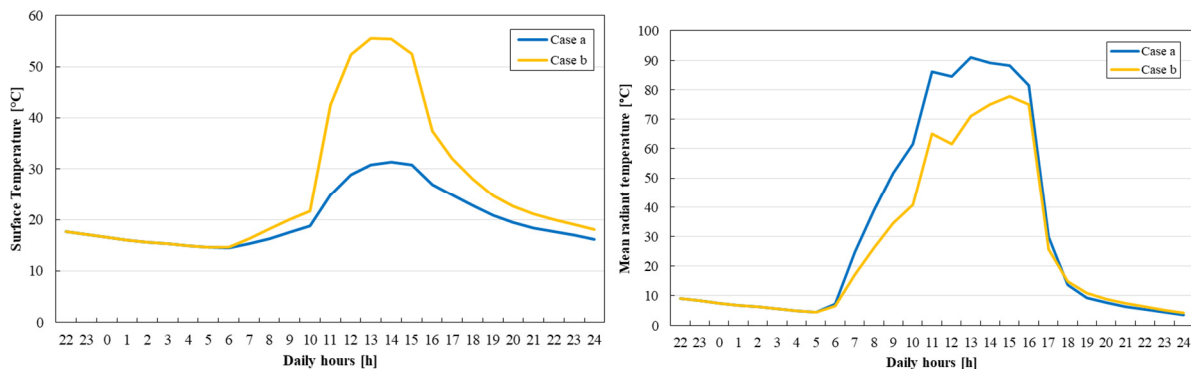
Figure 67 - Maps showing the Absolute Difference of Surface Temperature between Case *b* and *a* at 13h (left) and 23h (right) and a histogram showing the different behavior between sidewalk and street at 13h.
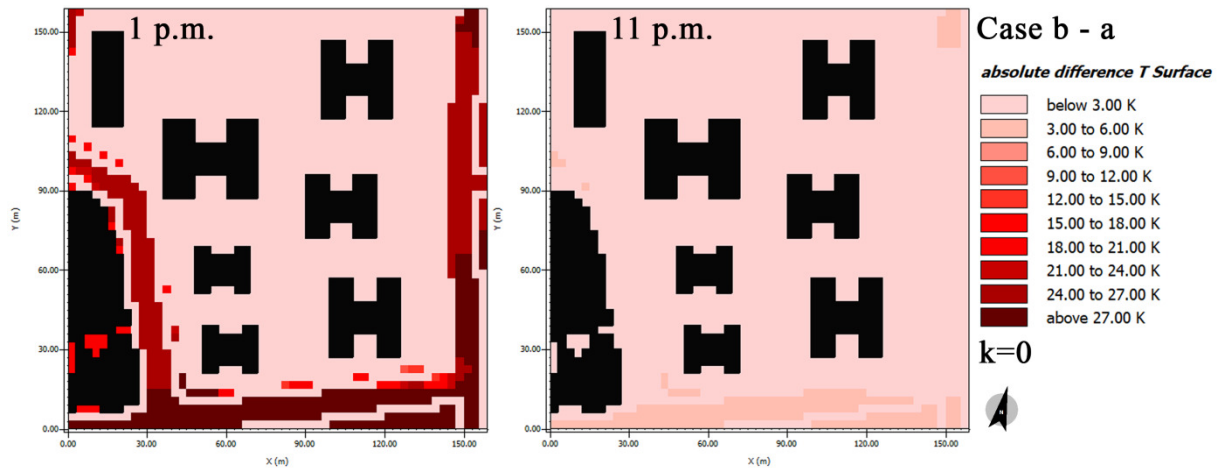
Source: Martina Pacifici (2019)

In brief, the model displayed a limited sensitivity to the fluctuations of ground floor albedo: surface temperature and mean radiant temperature were the main variables affected. Such result was intended as a considerable code limitation, since in the real world albedo plays an essential role in the urban thermal balance. Through convective and radiative processes, it absorbs and dissipates heat back to the atmosphere, affecting the outdoor temperature and contributing to HUI effects (MORINI *et al.*, 2016; AKBARI et al., 2016). In spite of this, within the ENVI-met virtual environment, air temperature showed to be irrelevant to albedo, even if drastic values were tested. Furthermore, neither ground surface temperature increase, nor MRT variations succeeded inducing secondary effects on air temperature.

5.4.5   Model Construction

At this stage, the conceptual model (5.4.2) was translated into the numerical model. The model under development incorporates both open spaces, trees, building forms and materials, intertwined in a realistic layout. Practically, to build the model, three ENVI-met frameworks were fulfilled: model space (1), simulation file (2), plant and material database (3). Table 11 summarizes all settings in these three fields.

The overall model space size is 480m x 669m x 174m that resulted in 223 grids x 160 grids on the horizontal plane (xy) and 24 grids on the vertical (z) axis. The vertical height of the model (174m) corresponds to the top of the 3D model and was defined as the double of the highest model building (87m). The model mesh is equidistant on the xy plane, while has a variable and progressive extension on the z axis. In fact, while the xy grid size is keep constant (3m x 3m), the z axis is made to vary according to a "telescoping factor" of 15%.

The telescoping factor starts after 10 m from ground surface and increases the mesh spacing as far as it moves upwards (Figure 17). Compared to the original layout, the model space is rotated of 13.5° and includes two main areas: the area of interest and the border. The area of interest is the model "heart" and contains the climate source points that will be used to calibrate the model; results coming from this central zone are the most reliable since free from border "effects". The border area contributes to characterize the surrounding urban morphology but it will not be considered reliable to analysis results; on each of the four sides, the edge area is larger than 100m (Figure 68).

Figure 68 - Model rotation (a); Model domain and definition of high-rise and low-rise zone (b); Area Input File – horizontal view (c); Area Input file – vertical view (c).
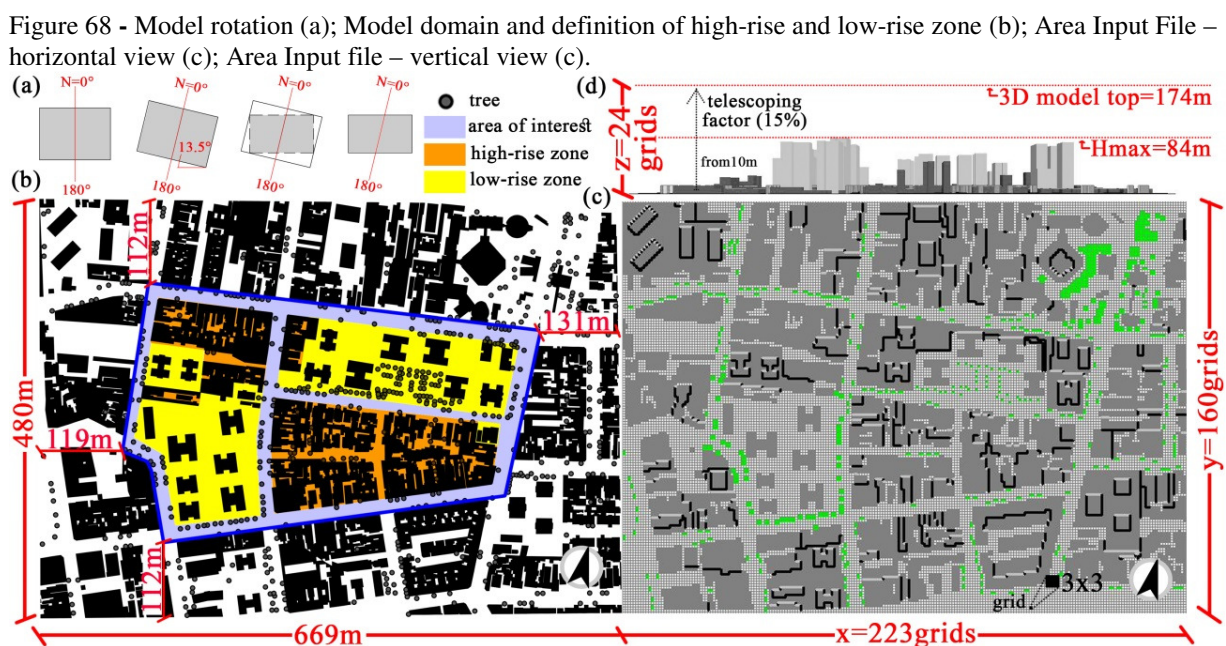
The Simulation File *.SIM* (2) contains all the meteorology parameters, soil characteristics, computing options and model timing that needed to run the model. The start date of simulations was set on December, 4th, 2017, at 9 p.m. In this way, the initialization phase was processed during the night, without the interference of radiation and other complex phenomena related to the sunrise. Wind speed at 10 m and direction were set on 2.5m/s and 163°, while roughness length on 0.1. Air temperature and humidity curves were forced in *Simple Forcing* tool according to the Figure 69.

Figure 69- Forcing of air temperature and relative humidity
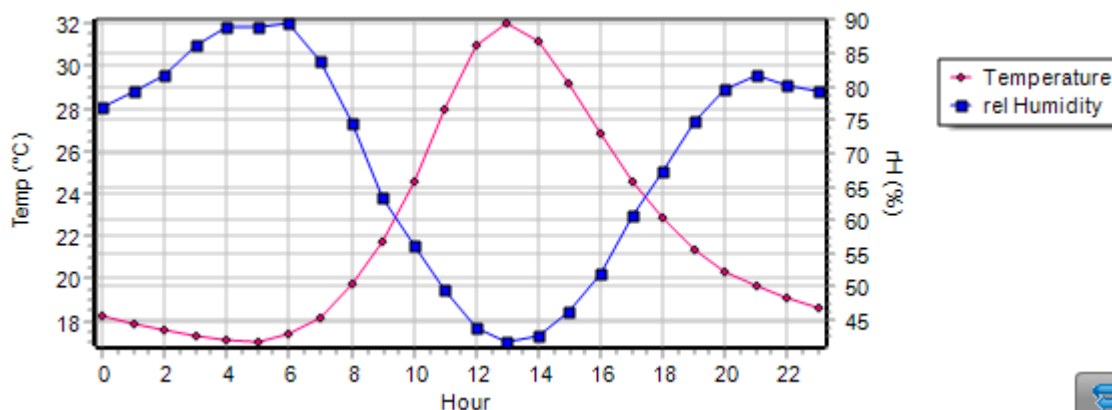
Table 11 – Setting of parameter and conditions

Configuration of Space Model	
Location	São Paulo
Latitude (+N, -S), Longitude (-W, +E)	- 23.53; - 46.59
Reference Time Zone	GMT-3
Grid	223 x 160 x 24 grid cells
Domain Size XY	480 x 669 m
dx = dy; dz	3 m; 2m
Telescoping factor	15% starting from 10m
Highest building in the Domain	84 m
Height of 3D model top	174 m
Model rotation out of grid north	-13.5°
Nested grids	5
Empty grids rows at border	1
Trees	Plant TA
Wall and roof material at high-rise zone	Wall A
Wall and roof material at low-rise zone	Wall B
Soil materials	Ground A, B, C, D
Configuration of Simulation File	
Start Date and Time	4.12.2017 at 21:00h
Initial temperature of atmosphere	22.14 °C
Relative humidity in 2m	81.57 %
Simple forcing curve	Average of six weather stations
LBC for temperature and humidity	Forced
LBC for turbulence	Forced
Turbulence Model	Standard TKE Model (1982)
Adjustment factor for solar radiation	1.03
Cover of low, medium, high clouds	0.0; 0.0; 0.0 octas
Wind direction and speed at 10 m	163 deg; 2.5 m/s
Roughness length at measurement site	0.1
Specific humidity at model top (2500 m)	10.6 g/kg
Initial soil temperature (0–20, 20-50, 50-200 cm)	297.65 K; 298.65 K; 299.65 K
Initial soil wetness (0–20; 20-50; 50-200 cm)	58 %; 64%; 69%
Configuration of Database	
Ground A	g1 (0-3cm) + g2 (3-10cm) + g3 (10cm-4.5m)
Ground B	g4 (0-3cm) + g2 (3-10cm) + g3 (10cm-4.5m)
Ground C	g5 (0-10cm) + g3 (10cm-4.5m)
Ground D	g6 (0-4.5m)
Wall A	w1 (10cm) + w1 (10cm) + w1 (10cm)
Wall B	w2 (10cm) + w2 (10cm) + w2 (10cm)
Plant A	Deciduous; albedo: 0.25; root depth: 2m; size: 9x3 m
	LAD (from 1 to 10): 0.00, 0.00, 0.00, 0.19, 1.84, 2.91, 1.84, 0.76, 0.60, 0.23

Source: Martina Pacifici (2019)

In the *Profiles Database* (3), four different profiles were set in order to characterize the high-rise ground surface [Ground A], the low-rise ground surface [Ground B], the street floor [Ground C] and the soil underlining plants [Ground D] (Table 12). The latter is a natural and irrigated soil type; it was set under the tree grids to guarantee the plant evapotranspiration. All other grounds are artificial; *Ground C* profile was employed to cover street connections and is composed of asphalt layers (called by ENVI-met *Soils*) on the underlying natural terrain. *Ground A* and *Ground B* profiles were implemented to characterize the ground surfaces covering the high-rise developments (A), as well as the older floors dressing the low-rise housings (B). Both of them are made up overlapping three *Soil* types (g1/g4, g2, g3) and only differ in the surface layer (Table 12 ‑ Ground Layers properties). On the *Wall Database*, *Wall A* was implemented in the high-rise fabric while *Wall B* was used in the low-rise fabric (Table 12). To simplify the model, *Wall A* and *B* characterize vertical facades as well as roofs; in both cases, they were made up of three identical layers, or *Materials*, called *w1* and *w2* (Table 13). Within the *Plant Database*, the diversity of trees collected on the urban site were summarized in a unique and representative tree type, called *Plant A,* corresponding to Caesalpinia Echinata species (Figure 70).

Figure 70 ‑ Materials (g1-w2) and Plant A properties (Caesalpinia Echinata tree)
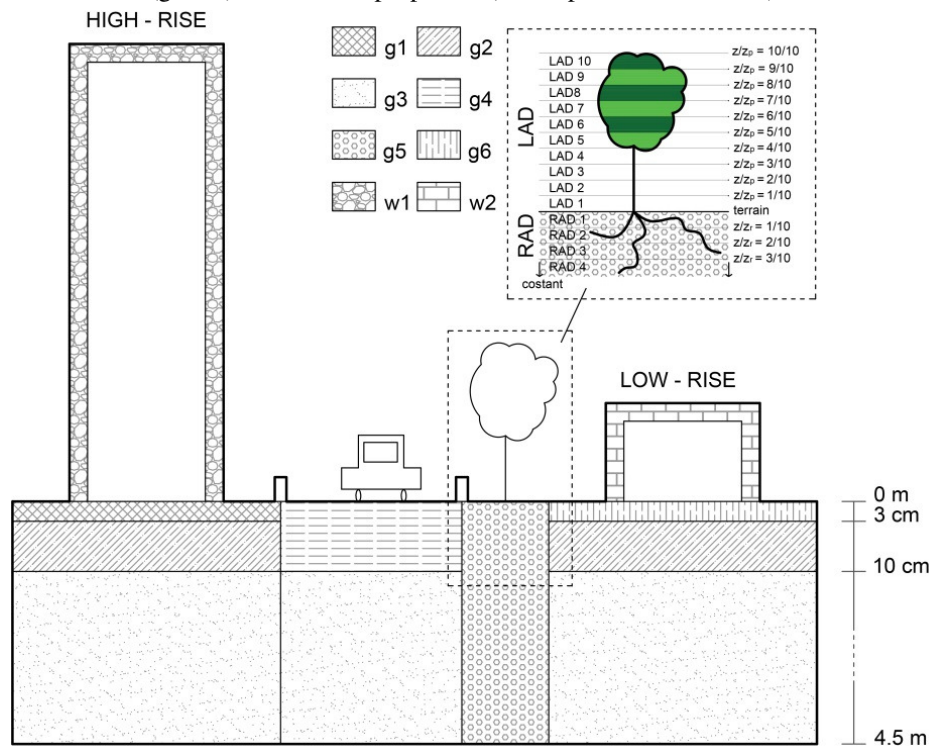
Source: Martina Pacifici, 2019

Table 12- Ground Layers properties

ID	type	η_s [m^{3}m^{-3}]	η_{fc} [m3m$^-$3]	H_{wilt} [m^{3}m^{-3}]	MatPot [m]	Kμs [ms^{-1}10^{-6}]	CP [Jm^{-3}K^{-1}10^6]	b [-]	HCN [Wm^{-1}K^{-1}]
g1	artificial	0.00	0.00	0.00	0.00	0.00	1.00	0.00	4.60
g2	artificial	0.00	0.00	0.00	0.00	0.00	2.00	0.00	1.50
g3	natural	0.42	0.25	0.17	-0.30	6.30	1.17	10.40	0.00
g4	artificial	0.00	0.00	0.00	0.00	0.00	2.40	0.00	0.90
g5	artificial	0.00	0.00	0.00	0.00	0.00	1.90	0.00	3.00
g6	natural	0.43	0.31	0.22	-0.15	2.20	1.17	10.40	0.00

Table 13 - Wall Layers properties

ID	d [m]	A [-]	T [-]	R [-]	E [-]	c [Jkg^{-1}K^{-1}]	HCN [Wm^{-1}K^{-1}]	ρ [kg m^{-3}]
w1	0.10	0.60	0.00	0.40	0.60	1000.00	0.80	1600.00
w2	0.10	0.90	0.00	0.10	0.90	700.00	0.90	2000.00

- *Calibration*

Overall, the model could reproduce the data field with regard the average air temperature and relative humidity (Figure 71). Hence, the modeled domain responded coherently to the boundary conditions on which the forcing was applied. The ENVI-met simulated curve was rather coincident with the average observed curve throughout most of the day, even if little differences were observed at the extremities (maximum and minimum). A similar coincident behavior was observed on relative humidity. To leave more information to the reader, the daily curves used to extract the average observed curve have been included in the calibration graph (see grey lines).

Results from the calibrated domain were also showed on the entire domain (Figure 72). Air temperature differences were gathered in classes of 0.5°C, while gaps under this value were unconsidered (according to field measurements). It worth stressing that more reliable results have to be observed in the core of model, while the border blocks could be influenced by boundary conditions. At morning, model buildings are surrounded by the same air temperature field. The sun had just risen (8h), illuminating facades and interstices exposed to East. Several areas to the North-West exposure of the main towers appeared darken colored, showing lower temperatures (~ 0.5 - 0.9°C) relative to the rest of domain. Such phenomenon was more evident in the proximity of groups of towers (see station 1 and 2), resulting in extended cooler zones; conversely, behind isolated tall buildings, only concentrated differences were noted. In the early afternoon, at 15h, domain warmed up and overall air temperatures raised about 8°C; greater excursions between the model points were

observed (2.7°C) then morning (1.2°C), resulting in a more complex stratification of thermal zones.

Figure 71 - Comparison between observed and modeled temperature and humidity
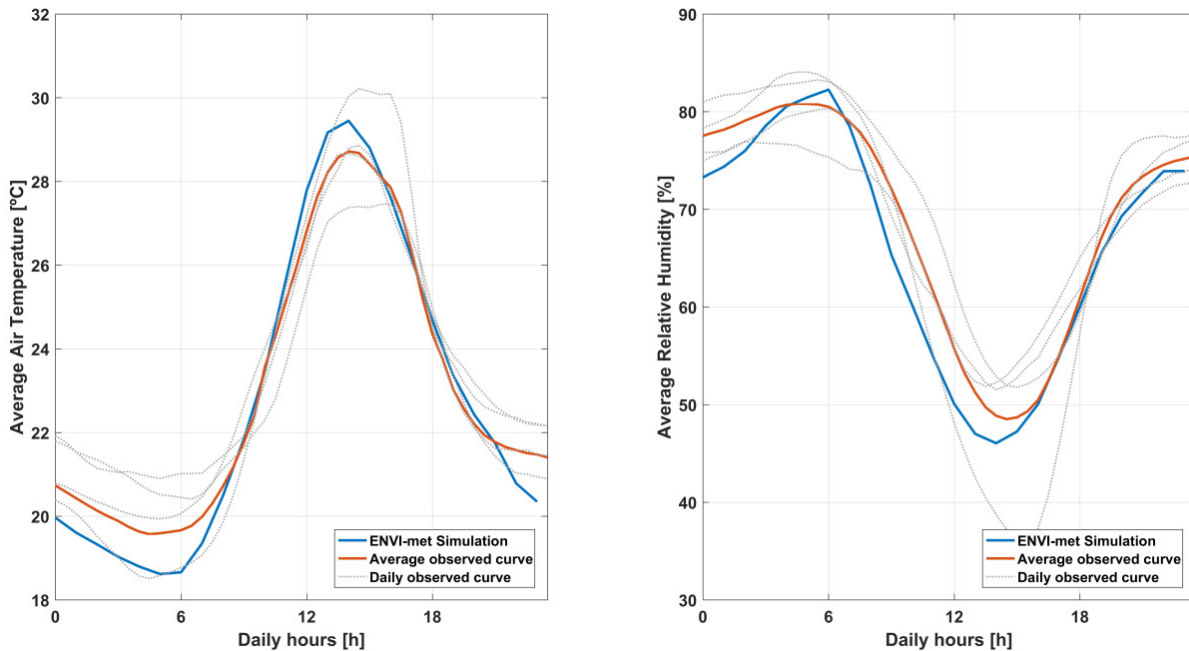
Source: Martina Pacifici (2019)

Due to the transport of boundary conditions along wind direction (blowing from southeast), the bottom edge of domain showed hotter temperature (imposed by forcing). Such hotter air flow cooled when crossing the domain (from South to North), due to interaction with colder bodies (buildings). Despite this model trend (not characterizing reality), the air cooling process occurred differently in the different domain zones. In general, the encounter with high-rise zones sharpened the cooling, while the passage through low-rise zones or unconstructed areas slowed down this process. Thus, thermal differences between fabrics empirically found on the site were reproduced by the model in the afternoon period. Notwithstanding, such differences were inferior (~1-1.5°C) to the gaps measured between station 3 and stations 1-2 on the field (~3-4°C). In the morning, a similar flatten air temperature distribution was also recorded in the fieldwork. Overall, ENVI-met was found strongly conditioned by forcing setting, ensuring the daily heating process on all studied area. The distribution of air temperature zones was overcome by the boundary conditions transport; consequently, the effect of urban morphology was weakened, underestimating the thermal contrasts found in the field.

Figure 72 – Modeled air temperature, k=1, at 8h and 15h
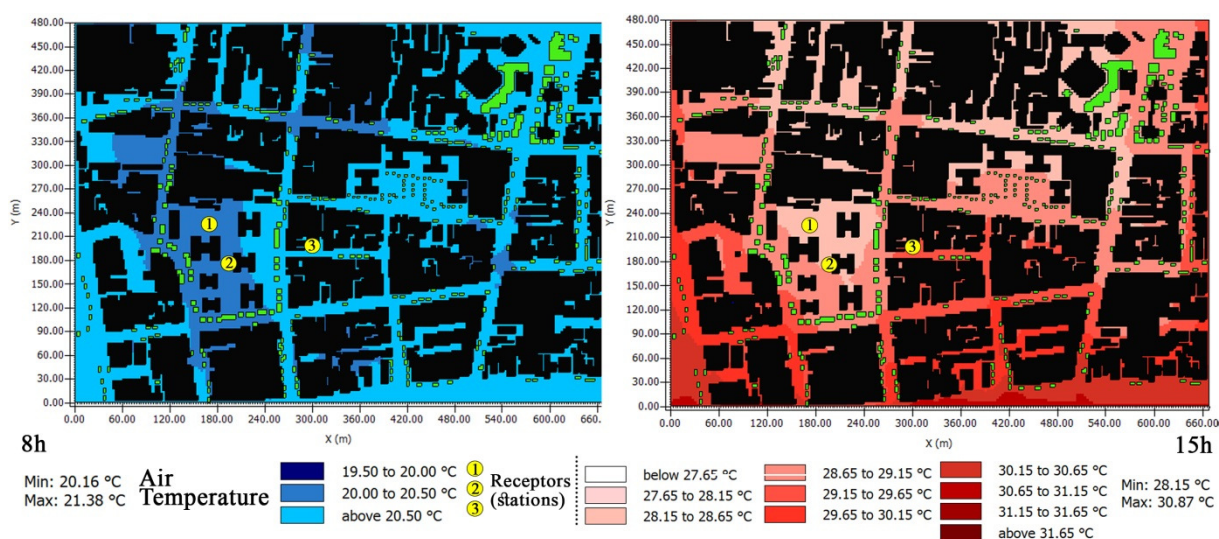
Source: Martina Pacifici (2019)

In addition, mean radiant and ground surface temperatures were calibrated within three significant points. Thus, similar trends were observed between the three field stations and the correspondent modeled receptors. According to the field measurements, contrasts between station 3 (low-rise fabric) and the other two ones (high-rise) were found in terms of local ground surface temperature (Figure 73).

Figure 73 - Comparison between observed and modeled ground surface temperature at station 1, 2 and 3
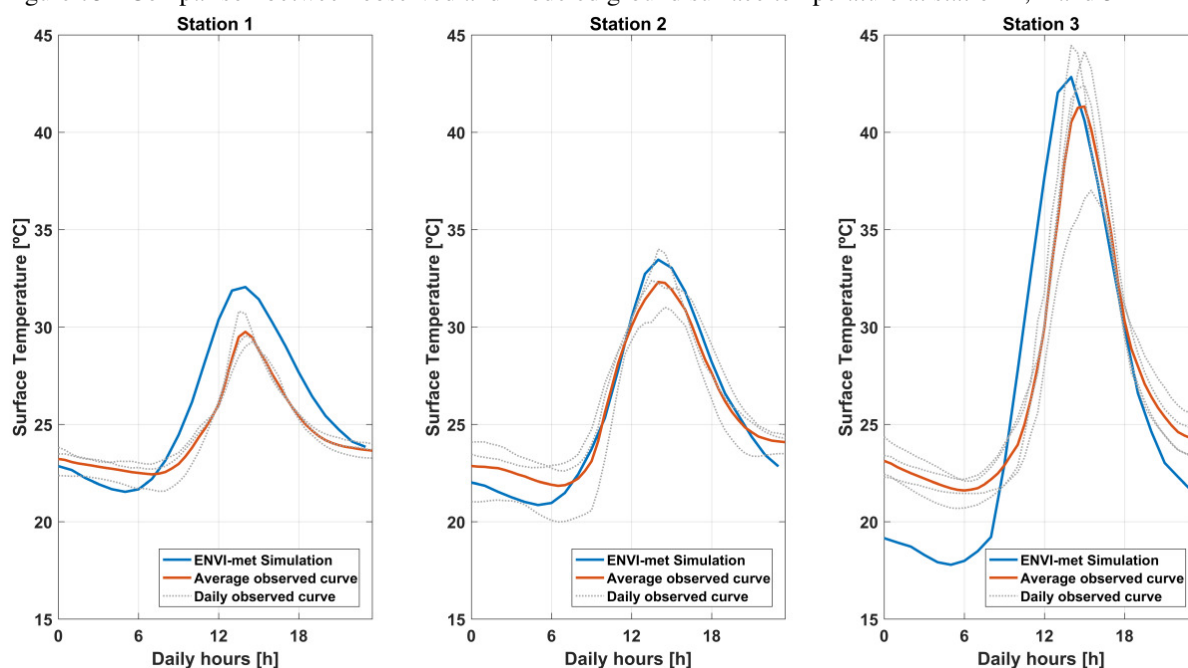
Source: Martina Pacifici (2019)

In all curves, lower minimum were observed on the modeled lines. Such behavior occurred with more evidence in the case of station 3, where nightly hours showed a bias around 4°C. Before 2 p.m., modeled station 3 presented a sharper trend, keeping lower its values until 10h and then raised quickly anticipating the observed curve. Close to the peak, the modeled and observed curve met, aligning their performance up to the 22h. However, station 3 exhibited the highest peak around 2 p.m., followed by station 2 and then station 1. Slight highest peaks (~1-2°C) were found on the modeled trends, little overestimating the growth of temperature.

As expected from sensitivity analysis, modeled surface temperatures displayed higher variability then air temperature maps (Figure 74), above all in the morning. Between 8h and 15h, a bias around 16°C was observed on average. In the afternoon a twice difference between maximum and minimum (29.25°C) was found in comparison with the morning period (13.28°C). Overall, cooler zones were concentered on the high-rise zones, in the proximity of towers and trees, especially in the afternoon. Along asphalt street high temperature above 48°C were achieved during the afternoon hours.

Figure 74 - Modeled ground surface temperature, k=1, at 8h and 15h
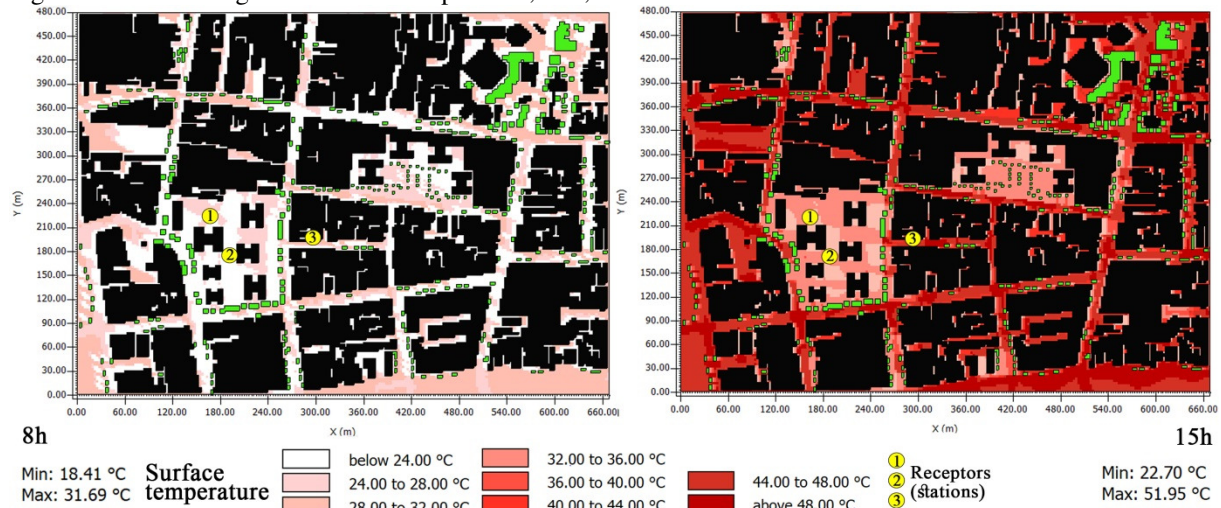
Source: Martina Pacifici (2019)

Modeled mean radiant temperatures showed a greater variability in comparison with T_{gs}; temperatures ranged between 10°C and 60°C (Figure 75). Station *3* remained the warmer receptor, while at night quite similar temperatures were simulated in all points analyzed. Overall, *MRT* peaks and minimum were slight underestimated than field observations. As consequence, temperatures around 10°C were found between 12 p.m. and 6 a.m., moving

away from field conditions. The best correspondences were noticed in the intermediate daily hours, between the maximum heating and the minimum cooling.

Figure 75 - Comparison between observed and modeled ground surface temperature at station 1, 2 and 3
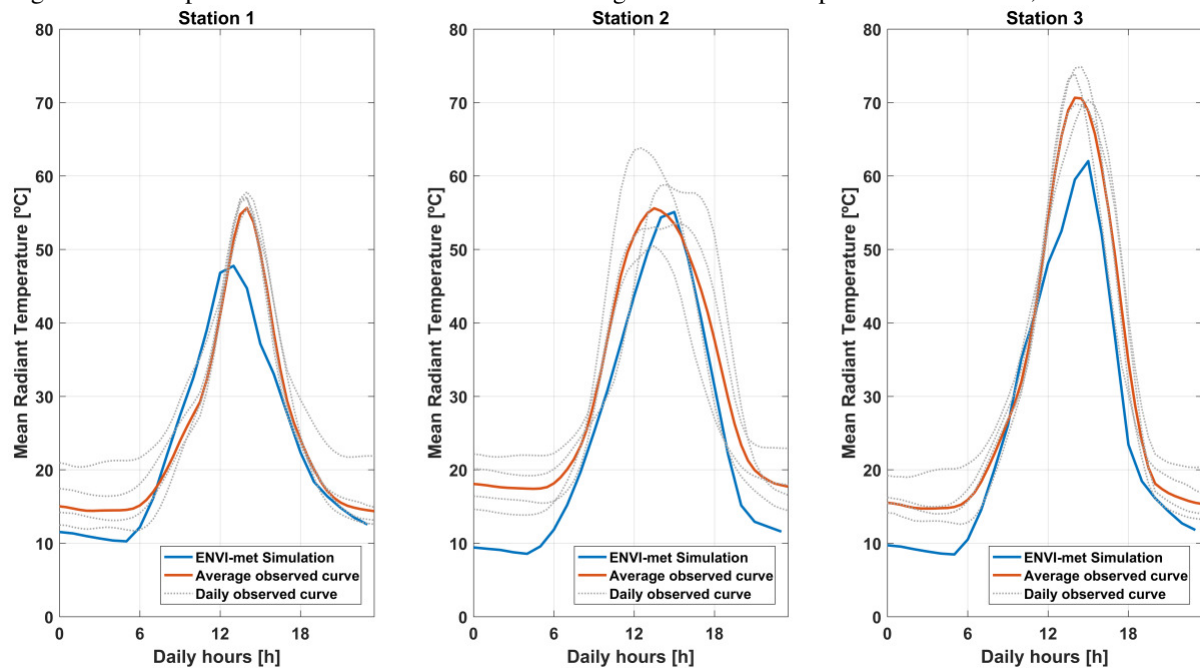
Source: Martina Pacifici (2019)

The spatial analysis on the entire domain highlighted the occurrence of contrast hot and cool zones, while a poor presence of middle *MRT* ranges (Figure 76). This polarized distribution was more evident in the afternoon, when temperature curves reached the thermal peaks. Both at 8 a.m. and 12 a.m., visible gaps could be observed among maximum and minimum values. A strong relationship between built morphology and temperatures patterns was observed, in even greater extent than the ground temperature. At each hour, the distribution of the mean radiant temperature changed, depending on to the displacement of the shadow cones in the domain. As a consequence, larger cooler zones emerged along the shadows projection of taller buildings; additional contributions were performed by trees canopies. In the high-rise zone, cooler zones appeared both at morning and afternoon. In the low-rise fabric, only morning cooler zones were observed since the low-inclination of sun rays allowed shadows projections; conversely, in the afternoon, such fabric was totally exposed to the solar irradiance and only high mean radiant temperatures were noticed.

In summary, the model could reproduce the main physical processes found in the field campaign. The calibration of the model was achieved by using four of the main climate variables: air temperature, relative humidity, mean radiant temperature and ground surface

temperature. With regard Tar and RH, some limitations were highlighted. The cause of such limitations had been attributed to the excessive importance given to the solving algorithm of boundary conditions (forcing).

Figure 76 - Modeled mean radiant temperature, k=1, at 8h and 15h
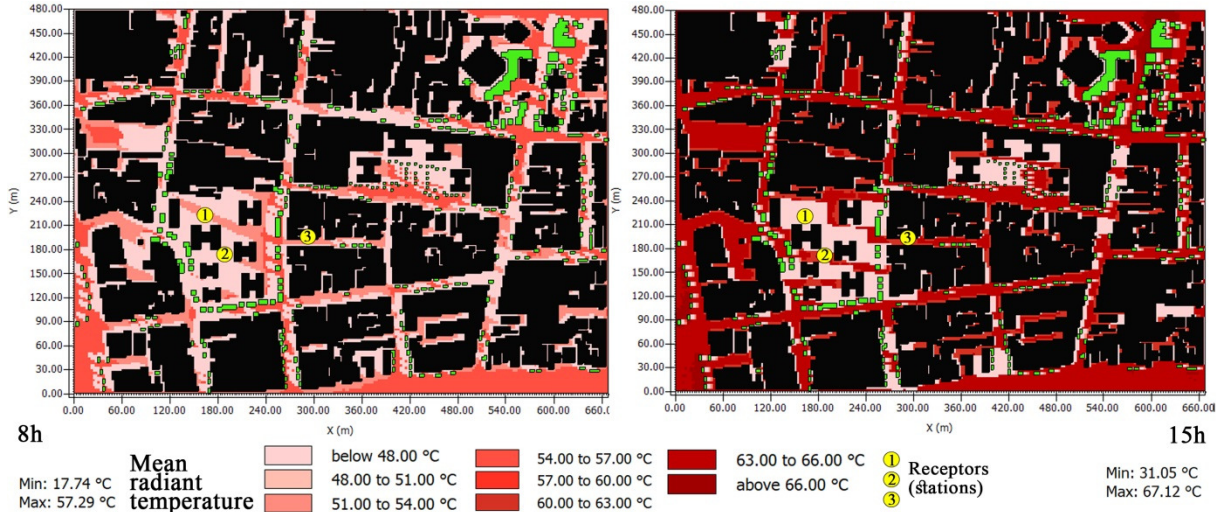
Source: Martina Pacifici (2019)

5.4.6 Numerical experiments (scenarios)

Figure 77 summarizes the Building Covered Ratio (BCR) and the Floor Area Ratio (FAR) computed in each lot by GIS tools and clustered in average values for high-rise zone, low-rise zone and the whole domain.

Figure 77 - Identification of clusters in the high-rise and low-rise zones (a); computation of Building Covered Ratio -BCR- and the Floor Area Ratio –FAR- on the clusters (b); average values of BCR and FAR for fabrics and all domain (c)
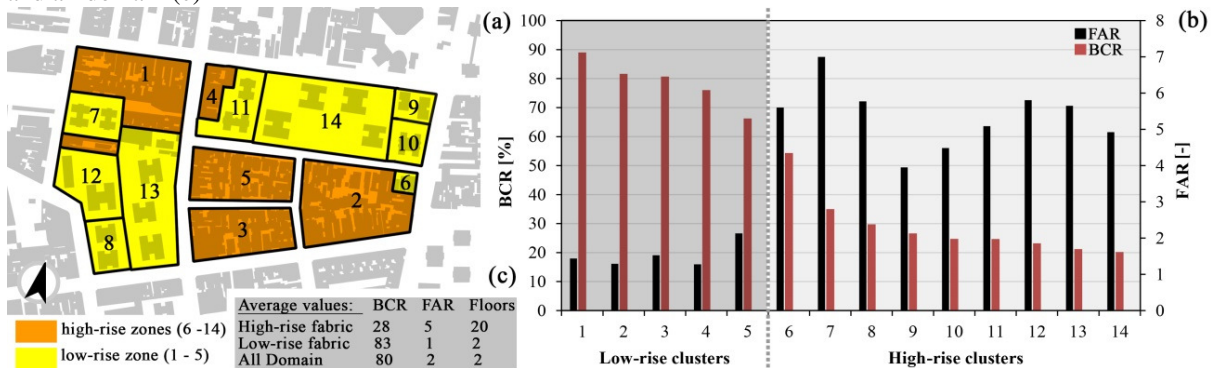
Source: Martina Pacifici (2019)

As expected, results show that the low-rise fabric is largely below the building concessions granted by the city masterplan, while the high-rise fabric exceeds them. In order

to explore the climate consequences caused by a densification process for this low-rise zone, six numerical experiments or *scenarios* were implemented by ENVI-met on the calibrated domain modifying blocks 2, 3 and 5.

A summary of the implemented scenarios is proposed in the following Table 14, together with information of modified blocks. All scenarios provide the same amount of built area (92,270m^2), obtained by applying a FAR 4 to the amount of the three block's areas.

Table 14 - Implemented scenarios and modified blocks

Case	FAR	BCA	Height	Floor	Buildings	Distance between buildings		Modified blocks in ENVI-met model
						Average	Range	
	[-]	[%]	[m]	[-]	[-]	[m]	[m]	
1	4	80	18	6	10	11.6	5 – 20.8	
2	4	80	18	6	20	6.9	3.5 – 17.7	
3	4	30	40	13	10	19.2	12.6 – 26.5	
4	4	30	40	13	10	20.9	15.4 – 42.7	
5	4	30	11 to 85	3 to 28	10	20.9	15.4 – 42.7	
6	4	30	11 to 85	3 to 28	10	20.9	15.4 – 42.7	

Source: Martina Pacifici (2019)

o Description of scenarios

Case 1: The first case adopts the maximum indexes allowed by the São Paulo Masterplan: (FAR=4, BCA=80%) distributed on 10 buildings. All buildings have the same height: 18m (6 floors). In general, the built blocks are large and short; they occupy the most of ground surface and are cut by narrow alleys along the *y* direction (Figure 78).

Figure 78 - Case 1: region for the analysis of results (left), detail of the new entered buildings with measures of heights and distances (right) on the horizontal (up) and vertical view (down).
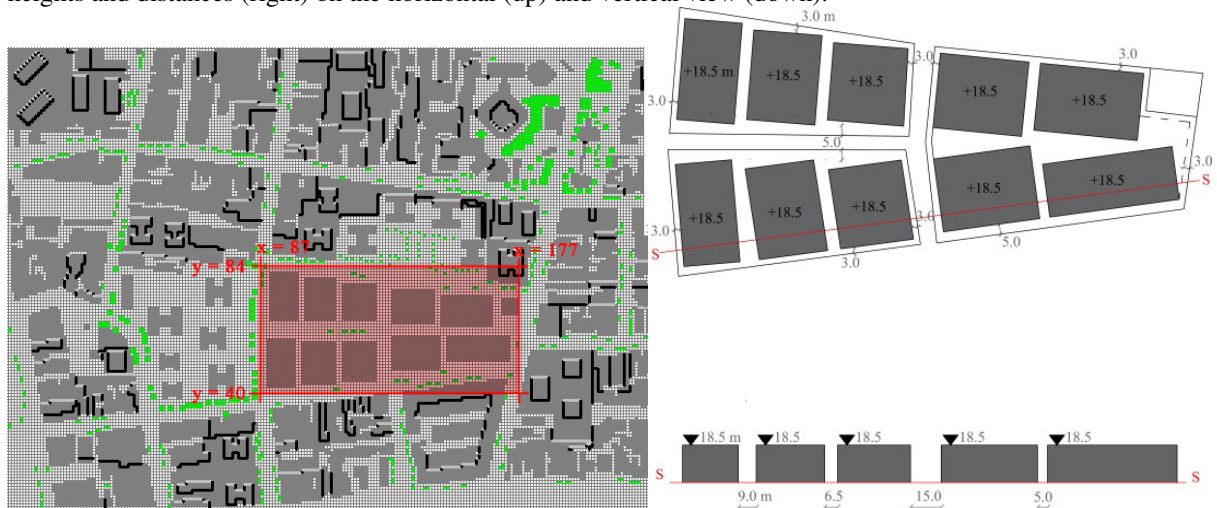
Source: Martina Pacifici (2019)

Case 2: As the previous one, the second Case adopts the maximum indexes allowed by the São Paulo Masterplan (FAR=4, BCA=80%) but distributed on 20 buildings which entail a greater fragmentation of the built mass (Figure 79). All buildings have the same height (18m that means 6 floors). Both Cases 1 and 2 represent two feasible building layouts to be implemented in the city of São Paulo; however, the builders usually prefer installing less and taller buildings surrounded by large open spaces in which recreational activities can be accommodated.

Figure 79 – Case 2: region for the analysis of results (left), detail of the new entered buildings with measures of heights and distances (right) on the horizontal (up) and vertical view (down).
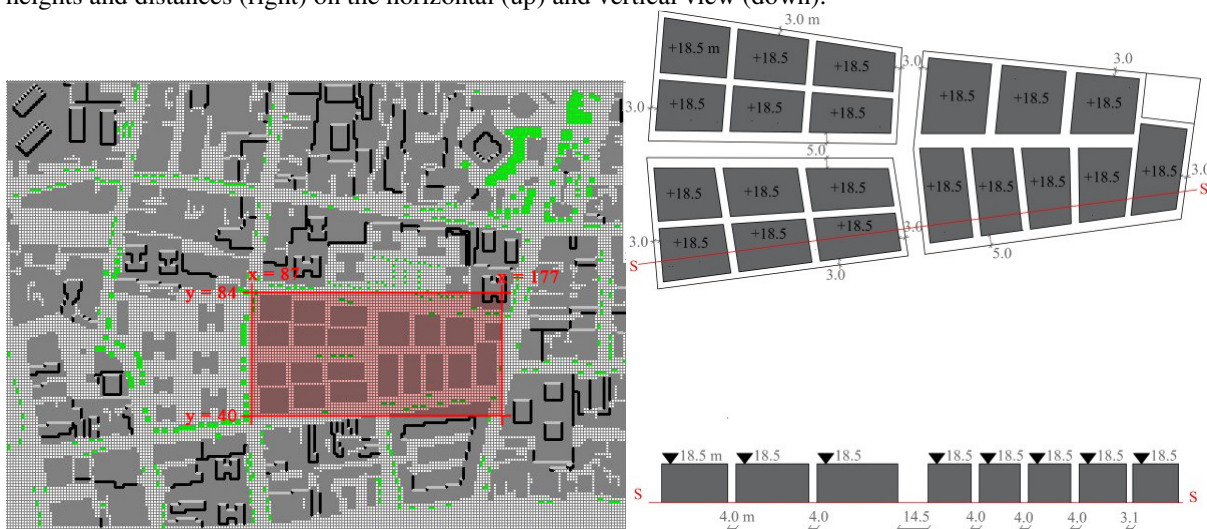
Source: Martina Pacifici (2019)

Case 3: In order to test a densified layout usually implemented by the real estate market in São Paulo, the third Case adopts a lower land coverage index (BCA = 30%), inferior to the maximal potential allowed by the São Paulo Masterplan, distributed on 10 buildings aligned on the East-West direction (Figure 80). All buildings have the same height: 40m (13 floors). FAR is maintained constant (4).

Figure 80 **–** Case 3: region for the analysis of results (left), detail of the new entered buildings with measures of heights and distances (right) on the horizontal (up) and vertical view (down).
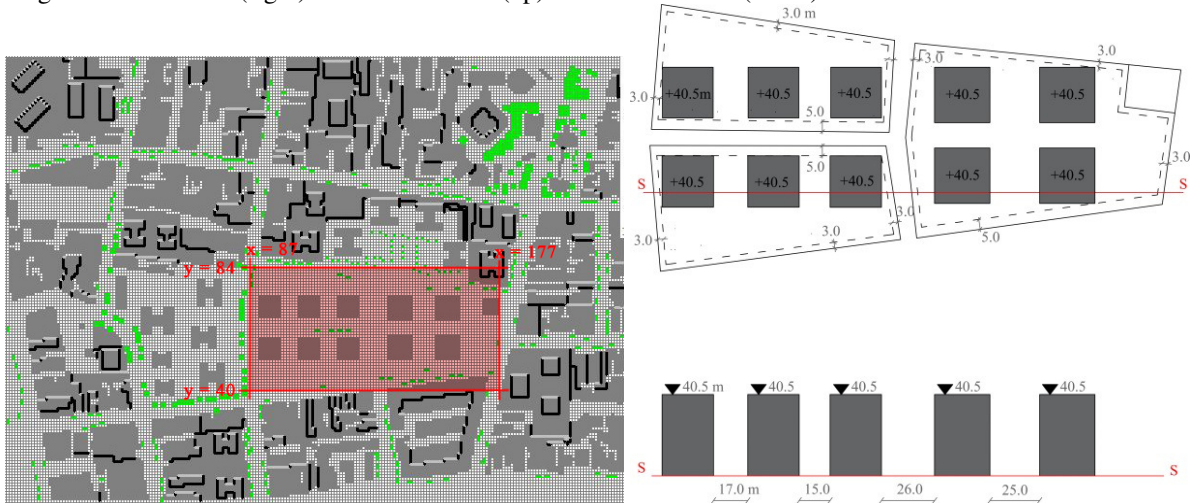
Source: Martina Pacifici (2019)

Case 4: To investigate the implications of the mutual position between buildings, Case 4 replaces the previous layout with a chessboard setting maximizing the distance between all the buildings (Figure 81). The same indexes of the previous experiment are adopted (FAR = 4, BCA = 30%), distributed on 10 scattered buildings. All buildings have the same height: 40m (13 floors).

Figure 81 **-** Case 4: region for the analysis of results (left), detail of the new entered buildings with measures of heights and distances (right) on the horizontal (up) and vertical view (down).
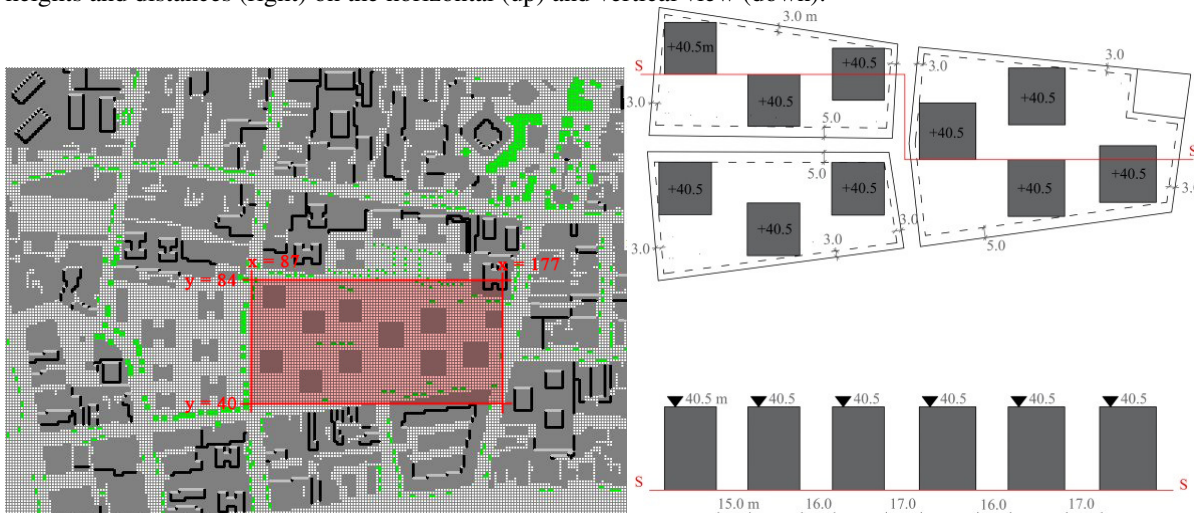
Source: Martina Pacifici (2019)

Case 5: On the same layout of Case 4, Case 5 (FAR = 4, BCA = 30%) proposes the variation of the buildings heights that decrease from the center to the borders of the low-rise studied area: 84.9 m (28 floors), 40.5 m (13 floors), 25.5 m (8 floors), 11 m (3 floors). The tallest buildings are concentrated on the block core while the shortest on the borders (Figure 82).

Figure 82- Case 5: region for the analysis of results (left), detail of the new entered buildings with measures of heights and distances (right) on the horizontal (up) and vertical view (down).
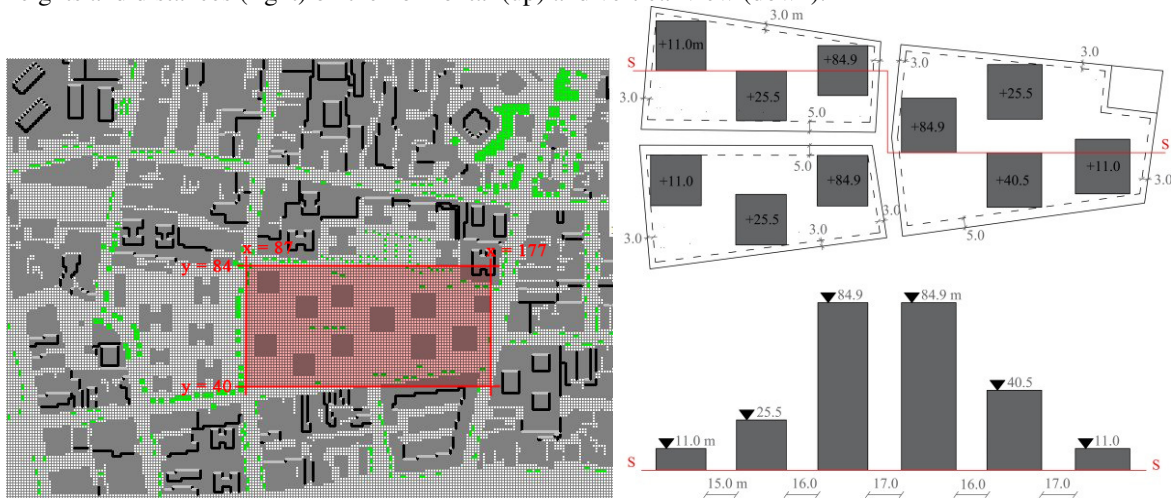
Source: Martina Pacifici (2019)

Case 6: In order to understand the impact of the heights distribution, the sixth Case scenario (FAR = 4, BCA = 30%) implements an opposite distribution, increasing the building heights from the center to the borders of the modified urban fabric: 11 m (3 floors), 25.5 m (8 floors), 40.5 m (13 floors), 84.9 m (28 floors). In this layout, the block core is occupied by the littlest buildings while the largest towers are arranged on the edges (Figure 83).

Figure 83 - Case 6: region for the analysis of results (left), detail of the new entered buildings with measures of heights and distances (right) on the horizontal (up) and vertical view (down).
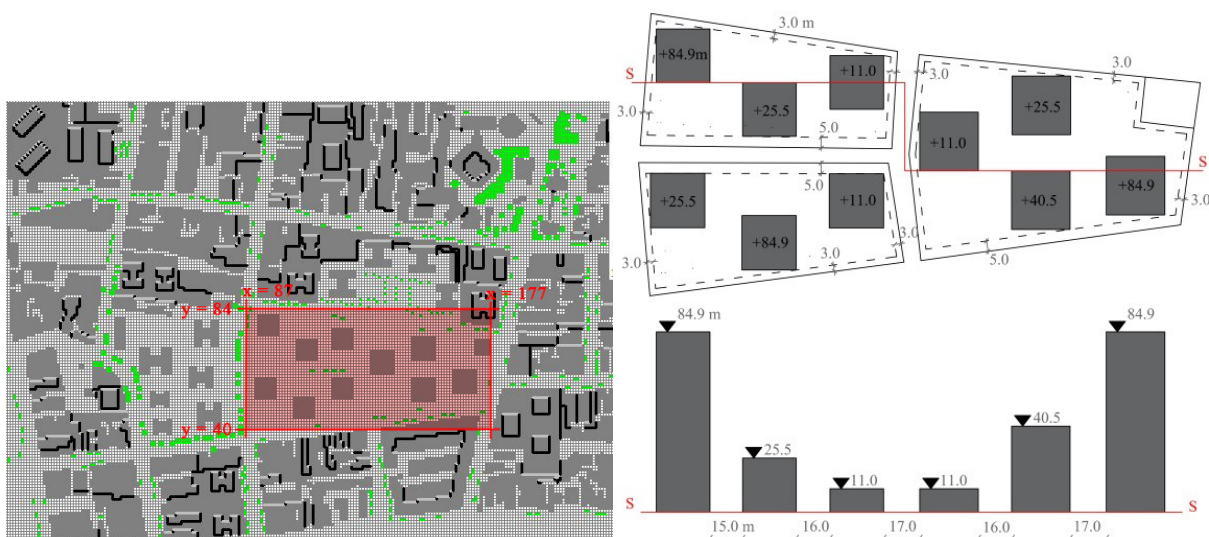
Source: Martina Pacifici (2019)

o Interpretation of scenarios

Scenarios were compared to evaluate the climate effects caused by the modification of built geometry on the climate variables. Overall, results showed variations between different scenarios in all variables selected. As expected, in the most of cases, variations were slight visible and scenarios behaved similar on average. Such findings were mainly determined by two factors. On one hand the computational code limitations observed did not favor the reactivity of certain variables (air temperature); on the other hand, scenarios applied only little changes to buildings layout. The building height and spacing were the main morphological parameter explored and attention was paid to preserve the rest of morphology. Such numerical experiments were developed within the densification limits imposed by the city of Sao Paulo and the existing context under analysis. Conversely, extremely densified and unrealistic scenarios were not functional to the model purposes. In spite of these restrictions, scenarios enhanced the insight of understanding on the climate interactions between urban forms. Unlike the complexity found at the site fieldworks, they were based on a "controlled" space of simulation, in which univariate changes had been applied. Results will be analyzed in terms of sky view factors, mean radiant temperature and surface temperature, as well as air temperature and relative humidity.

■ *Scenarios at BCA=30%*

First of all, scenarios at BCA=30% (Cases 3, 4, 5, 6) were discussed. Given the different arrangements of buildings, the obstruction of sky was observed changing at each case. The Sky view factors (usually ranging between 0 and 1) were displayed highlighting the probability of values falling within a certain range of values (Figure 84). All SVF distributions were found Gaussian, hypothesis verified by a box-cox transformation resulting in λ close to 1. Overall, scenarios presented similar distributions. This fact was reasonable, since in each scenario the amount of built mass was kept constant in terms of total heights and built areas. Cases *3* to *5* fell in the same SVF range (0.1 - 0.6), while Case *6* extended its values up to 0.7, providing opener sky views. Moreover, a substantial difference was found between the probability distribution of scenario *4* and the rest of cases *3*, *5*, *6*. Indeed, a more average-centered sky view factor was commensurated by a regular layout of equidistant and equal-height buildings (Case 4). Thus, on the totality of bins, more values around the central

position were observed in spite of a reduced amount of very low and very high SVF values. Conversely, on variable heights scenarios (Cases 5 and 6) and aligned scenario (Case 3), a greater probability of SVF extreme values was found. Furthermore, it should be noted that the probability provided by variable heights scenarios was also pretty close to the distribution of Case *3*, characterized by an aligned layout with equal-height buildings at close distance. Conversely, the simple shift of buildings between Cases *3* and *4* (increasing spacing) resulted in two different *pdf*. Thus, the sky view factor parameter was found sensitive to the variation of spacing between buildings, providing more average values for equal-spaced layout. However, when the heights of this layout were made to vary, SVF extreme values were highlighted.

Figure 84 – Sky View Factor in case 3, 4, 5, 6
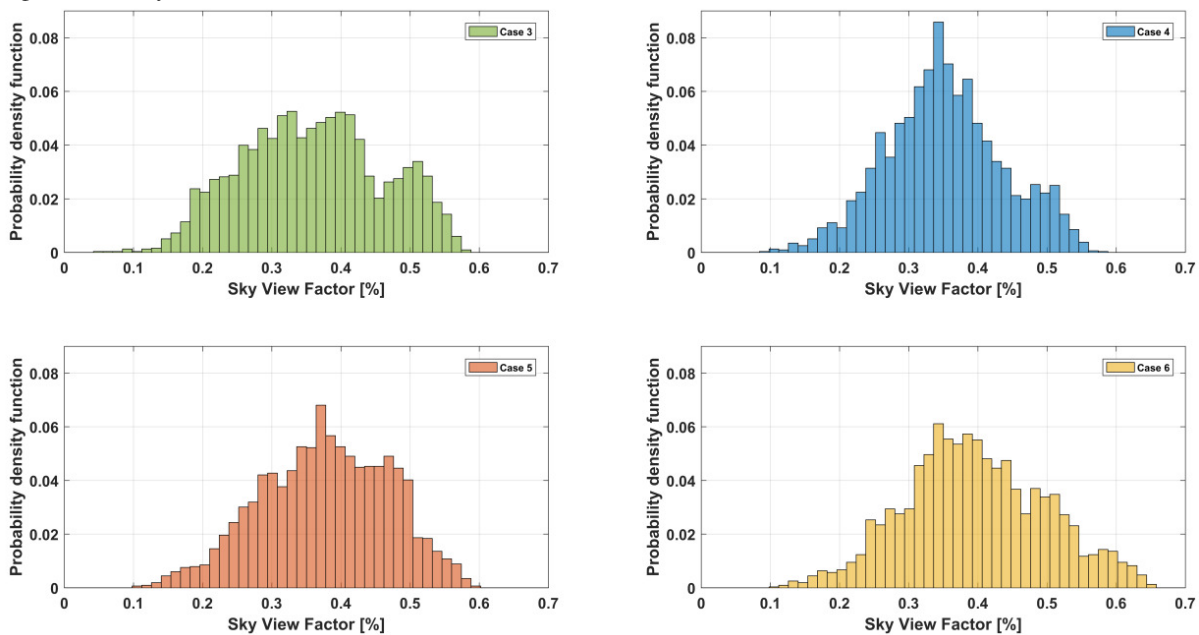
Source: Martina Pacifici (2019)

The variation of SVF through the Cases affected the budget of solar radiation on the grids, causing the heating and cooling of surfaces in certain points of domain. Implications related to the sky-view and sun-exposure were visible in the trends of surface temperatures and mean radiant temperatures. Such variables, in fact, resulted mainly driven by the shadowing and sun access. More evident gaps between Cases temperatures occurred at 8 a.m. and 4 p.m., while at 12 a.m. and 8 p.m. a decreasing of differences was observed. In these hours, in fact, shadows are not projected because sun is vertical or missing. Figure 85 makes evident this relationship, showing the percentage of domain hit by direct shortwave radiation along with the daily hours, 1 m above the ground floor. At 12 a.m. all scenarios are almost

100% irradiated and 0% shaded, regardless of the morphologic arrangement. At 8 p.m., the reversed circumstance occurs. A departure from these two extreme cases was progressively observed along with the rest of the daily hours. At 8 a.m., a "shading" gap of 12% was observed between the most irradiated Case (6) and the most shaded one (3). Scenario 6 stands out the other trends displaying the lowest percentage of shaded domain (as the highest percentage of irradiated domain). At 4 p.m., scenarios were almost equidistant; the most irradiated (3) and the most shaded (4) Cases displayed a shading gap of 10%. It should be noted that this difference was obtained only changing the spacing between buildings. As consequence of these little gaps between scenarios, greater or lower differences in temperatures were induced. In the following lines, couple of scenarios will be compared in order to explore the climate impacts related to the differences of shadow and light hitting the domain. Beyond geometrical effects, external environmental phenomena were not taken into account by model (i.e. inertia effect from Ocean).

Figure 85 – Irradiated or shaded domain percentage
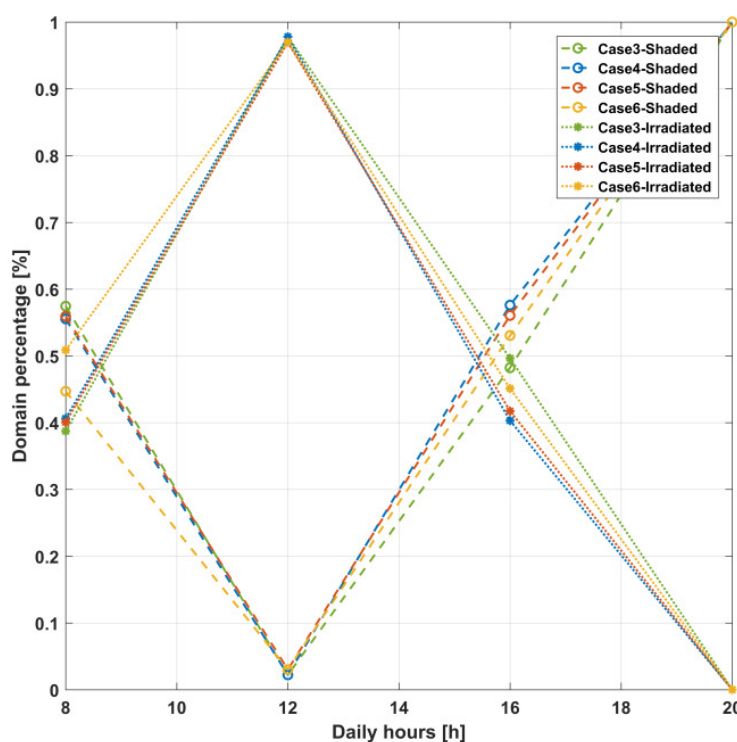
Source: Martina Pacifici, 2019

By comparing *Cases 4* and *5* other specific considerations were highlighted in terms of surface temperature (Figure 86). Positive and negative differences were observed between the two scenarios, scattered in the domain, ranging between -12.5°C and +6.95°C. The operation *Case 4 – Case 5* was displayed. Thus, negative gaps occurred when *Case 4* (same heights)

exhibited minor temperatures than *Case 5* (variable heights, higher buildings concentrated in the center), while positive values occurred vice versa. This means that, raising the same amount of built geometry (FAR=4; BCA=30), the only height variation can led to cooler or hotter temperatures. Concentrations of differences could be observed in certain points. In general, on morning, differences are mainly observed in the left side of domain. At 8 a.m., the subtraction *Case 4 – Case 5* displayed a large hotter zone, ranging between 1°C and 4°C, aligned along the shadow projection caused by one of the central towers characterizing *Case 5*. At 4 p.m. the position of the major positive differences occupied the right side of domain, since the sun had exceeded the vertical. Three hot zones could be noted nearby the three main towers, aligned to the afternoon shadows projections provided by *Case 5*. From 12 a.m. until 8 p.m., two opposite micro-climate environments could be found on the north and south exposure of one of the northern tower. Such circumstance occurred with more evidence at 12 a.m., providing hotter points on the north side ($T_{gs4} > T_{gs5}$) and cooler points on the south zone ($T_{gs4} < T_{gs5}$), as consequence of shadow projection from other buildings and proximity between them. Thus, it was showed as height variation induced the appearance of strong thermal contrasts in the middle of the buildings. Furthermore, a short distance away, a warmer zone was observed at 12 a.m. on the left side of the eastern tower of *Case 5* (84 m), probably depending on the morning shading. Its elongated shape suggests that the air corridor on the left side of the tower (Case 5) sprawled the heat concentration along the north-south direction.

Figure 86 – Difference surface temperature maps, Case 4-5, at 8h, 12h, 16h, 20h
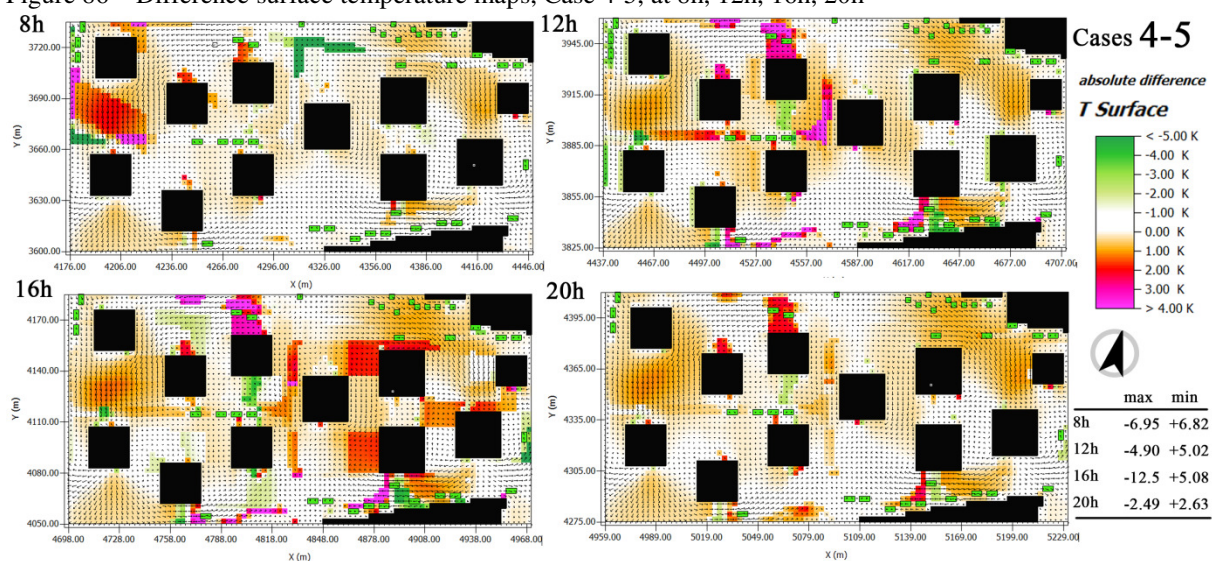
Source: Martina Pacifici, 2019

In general, the space in the middle of the central towers behaved as a controversial place, since *Cases 4* and *5* alternated hotter and cooler zones. On one hand, reciprocal shadows overlap their impact in this area, and on the other hand the increasing of tall vertical surfaces at close distance strongly reduced the visible sky view, preventing the thermal exchanges between surfaces and atmosphere, decreasing the amount of diffuse and infrared radiation from sky while enhancing reflected exchanges among surfaces.

The comparison between *Case 5* and *6* provided the greater differences ranging between -15.4°C and +13.5°C. *Cases 5* and *6* alternately showed cooler or hotter surface temperatures, depending on the time of the day (Figure 87).

Figure 87 – Difference surface temperature maps, Case 5-6, at 8h, 12h, 16h, 20h
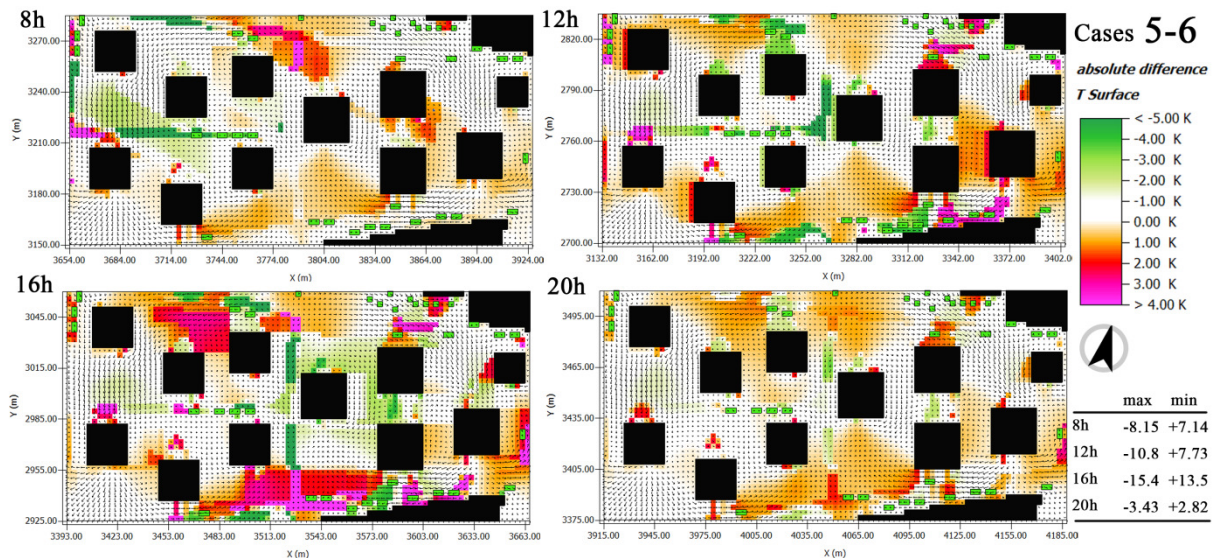
Source: Martina Pacifici, 2019

Green areas are negative values and mean higher temperature for *Case 6* (variable heights, outdistanced). Red areas are positive values and mean higher temperature from *Case 5* (variable heights concentrated in the center). However, large orange-colored areas were sprawled around the domain, showing the slight prevalence of Case 5 temperatures on Case 6 temperatures. This means that the different distribution of the heights was able to recreate different thermal reactions from ground surfaces. At 8 a.m., greater differences were seen on the north-side of the central building, where *Case 5* exhibited greater temperature than *Case 6*. This warm area is aligned with the shadow cone of the eastern tower (84 m) of scenario 5 that along this band favored cooler and shadowed areas. A similar but opposite interference, green-colored, was caused by the western tower (84 m) of *Case 5*. However, the largest contrasts were observed at 4 p.m. on the right side of the taller buildings of *Case 5* and *Case 6*. It should be noted that, at this time of the day, the extension of the hotter zones was widely

larger than the previous couple of *Cases*. At 12 a.m. and 8 p.m. slight hot differences (T_{gs5}>T_{gs6}) were also found on the north- and south-side of the central building. Such effect was distributed like a cone, dissipated by the air channels at the both sides.

The last comparison was proposed between *Case 4* (same heights) and *Case 6* (variable heights, outdistanced). Similar behaviors were found in this map (Figure 88). The warmer areas occurred at 4 p.m. along the shadow projection of tallest towers; the presence of different microclimate at the south and the north of certain buildings was again observed. At 12 a.m. and 4 p.m. green colored areas (T_{IV}<T_{VI}) were concentrated in the middle of the central three towers. In fact, in *Case 6* such buildings are characterized by really low heights (11m), strongly decreasing the probability of shading ground surfaces.

Figure 88 – Difference surface temperature maps, Case 4-6, at 8h, 12h, 16h, 20h
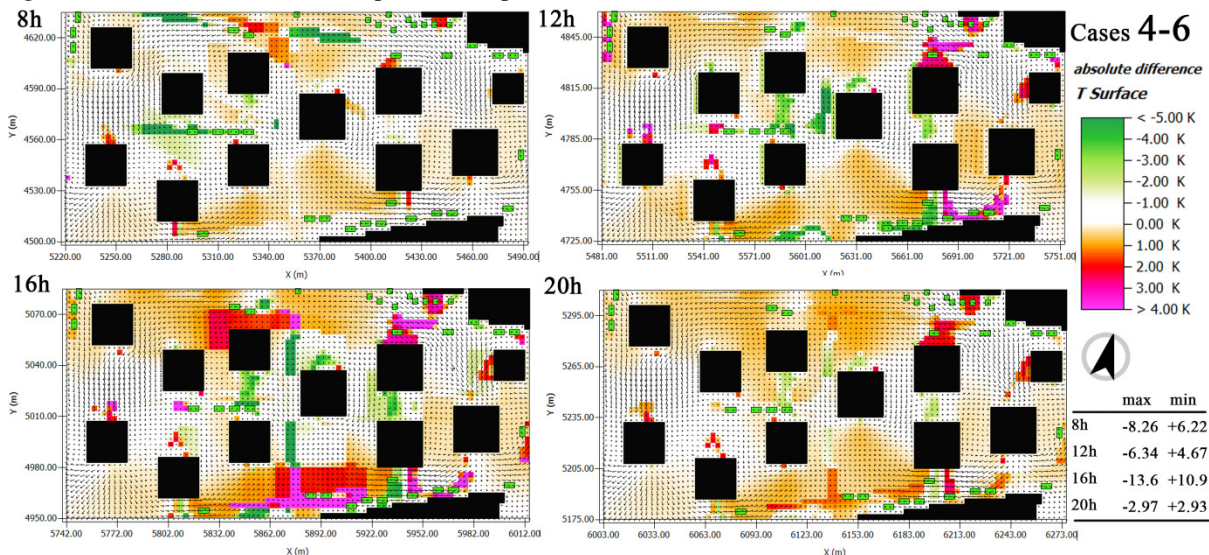
Source: Martina Pacifici, 2019

In addition to these maps, the correlation between *Cases* was also mathematically evaluated. Scatter plots of correlations were computed between all cases, at 8h, 12h, 16h (showed), 20h, and presented in combination with the histograms of each *Case* (Figure 89). Every histogram showed a not Gaussian bimodal distribution, containing two different data populations. Indeed, two ground floor materials were employed in this part of domain: *ground A,* covering the open spaces around towers, and *ground C,* covering streets. The first population (ground A) performed more moderate values (from 25°C to 35°C) while the other population (ground C) peaked close to 50 degrees. High correlations indicated similarities between *Cases*, while low correlations stood for *Cases* with few relationship between temperatures. Overall, correlations range was between 0.57 and 0.77. As an example, at 16h,

Cases 5 and *6* showed the lowest correlation (0.57), displaying a concentration of values between 30°C and 35°C; a large dispersion of data below and above this interval was observed. This means that the only modification of heights between *Cases 5* and *6*, modifying the distribution of shading and light, caused a non-correlation of 43% between temperature values at 4 p.m. Conversely, a lower non-correlation (29%) was found between *Cases 4* and *5*, more reciprocally similar than the previous couple.

Figure 89 – Correlation matrix for surface temperature, Case 4-6, at 16h
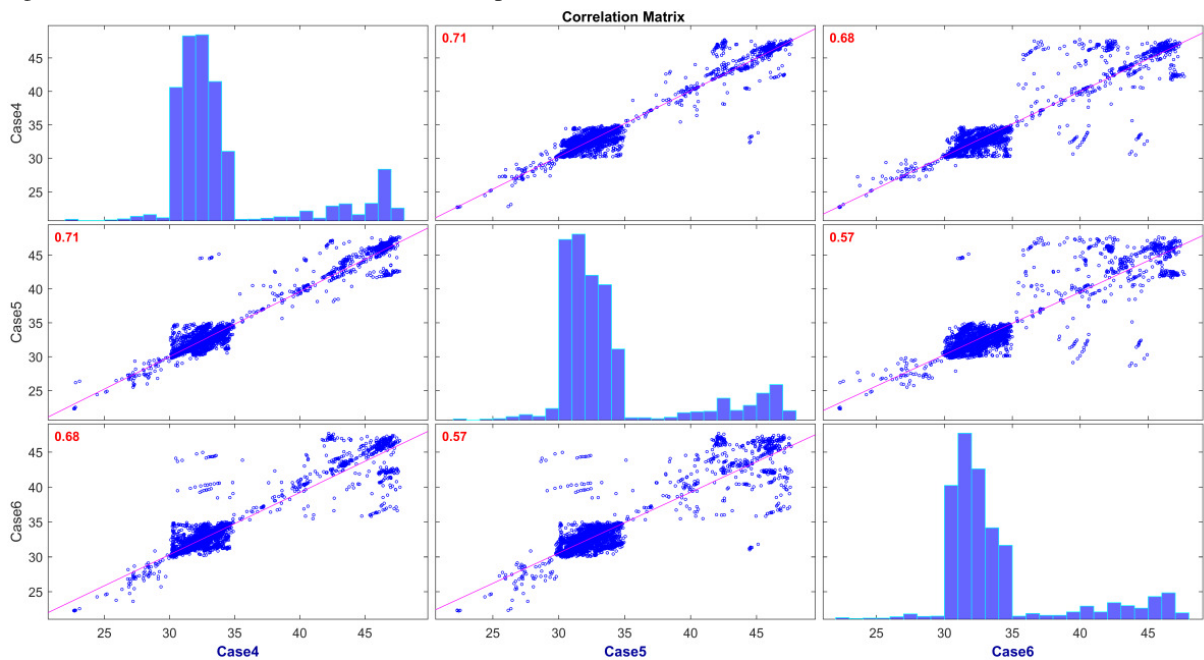
Source: Martina Pacifici (2019)

In terms of mean radiant temperature, contrasts really similar to surface temperature were observed, confirming the influence of urban morphology on this variable. Meantime, differences between *Cases* were much evident since the presence of shading was associated with strong temperature drops, while the direct exposure to short-wave radiation showed rapid increases in temperature. As consequence, *MRT* maps polarized on blue cold zones and yellow hot zones, following the shadow path projected by buildings. In the subtraction *Case 5 – Case 6* such zones carrying differences ranging between -30°C and +30°C, while in the rest of domain gaps disappeared. The contour plot (Figure 90) displays contrasting differences at 8 a.m. and 4 p.m. under the impact of tallest buildings. Blue zones ($T_{mrt5} < T_{mrt6}$) and yellow zones ($T_{mrt5v} > T_{mrt6}$) could be observed, interesting large parts of outdoor spaces. At 8 p.m., the influence of shortwave radiation is null, and the pattern of differences is totally controlled by the long-waves radiant fluxes (LW). Even if little values were observed, at this time of the day, the distribution of mean radiant temperature differences was coincident with the long-

wave radiation differences coming from the upper hemisphere. Such circumstance was noticed around the three tall central buildings that, in *Case 5*, were the tallest ones. Thus, such middle cool "island" ($T_{mrt5} < T_{mrt6}$) meant less long-wave radiant fluxes in *Case 5*, probably trapped between buildings at short distance. As consequence of less radiant losses, in this area, higher values of air temperature and absorbed heat were expected. Such findings are in agreement with the CIBSE Guide (2015) for whom the impact of longwave radiation is more obvious in the dark, when *LW* are not compensated by any incoming shortwave radiation; conversely, their impact is hidden on daylighting hours, when the absorbed incoming shortwave radiation offsets the cooling effects of long-wave radiation. On midday, the influence of long-wave fluxes also appeared in more concentrated areas, with negative differences ($LW_5 < LW_6$ and $T_{mrt5} < T_{mrt6}$) in the central zone above mentioned, as well as slight positive differences ($LW_6 < LW_5$ and $T_{mrt6} < T_{mrt5}$) on the south side of the taller buildings of *Case 6*. Actually, beside preventing direct sunshine, the shadowing on the south side of towers decreased the radiative exchange fluxes between built environment and atmosphere, implying smaller mean radiant temperatures. Since *MRT* is an important variable affecting the energy human balance, such results directly conditioned the thermal comfort of pedestrian on the outdoor spaces of domain.

Figure 90 – Difference mean radiant temperature maps, Case 5-6, at 16h
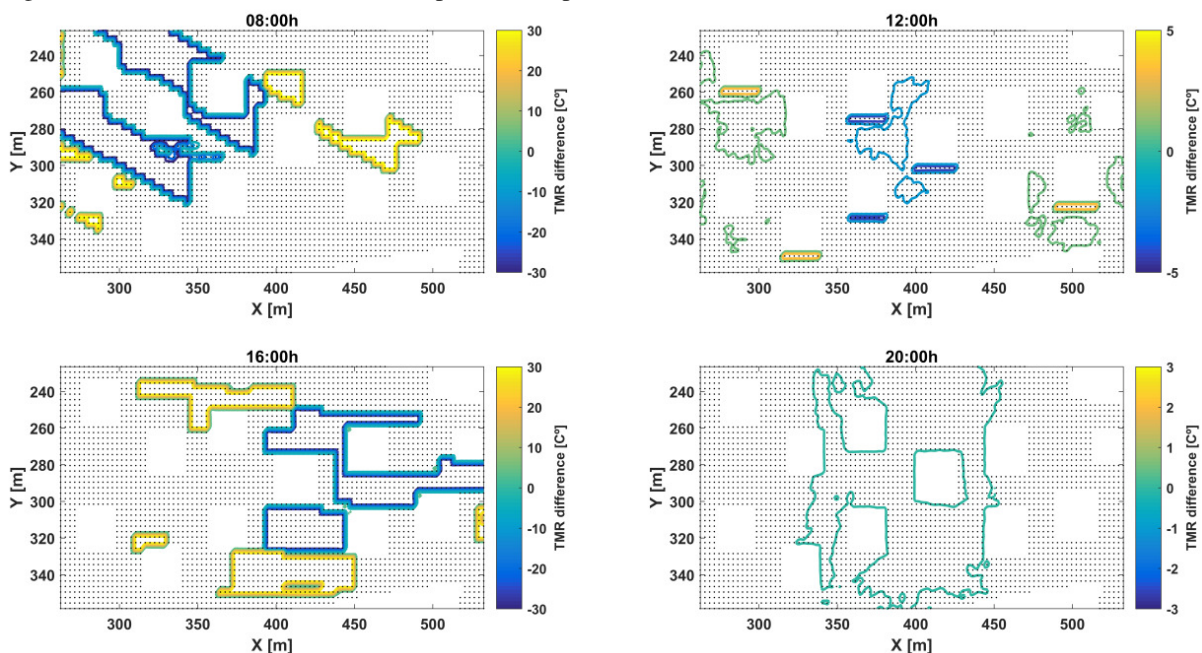
Source: Martina Pacifici (2019)

A symbolic three-dimensional surface plot of previous differences was proposed (Figure 91), with the aim to clarify the meaning of the cool and hot islands scattered on the

maps. On the horizontal plan, the domain extension, on the vertical axis *MRT* differences could be red. Temperature "mountains" indicated the intensity of *MRT* difference between two *Cases;* yellow shaded peaks meant positive difference, while blue shaded lows represented negative gaps between the two *Cases*.

Figure 91 – Three-dimensional difference mean radiant temperature map, at 4 p.m., between Case 4 and 6.
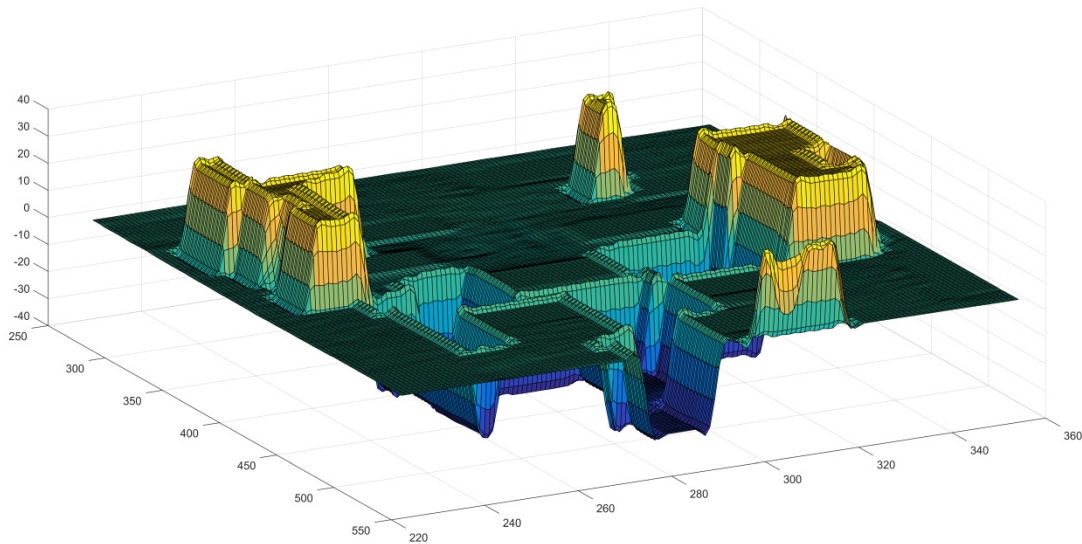
Source: Martina Pacifici (2019)

When *Cases 4* and *5* were observed, the effect related to the variation of built element height could be observed on the same buildings array (Figure 92). Actually, scenario 4, providing buildings with the same heights, projected identical shadows and ordered zones at high *MRT* (lighted) and low *MRT* (shaded). Conversely, *Case 5*, providing smaller or greater buildings heights than *Case 4*, resulted in zones with really high and really low *MRT* values. As consequence, at 4 p.m., cool and hot zones could be observed, depending on which scenario was preventing or guaranteeing more sun access. At 12 a.m. and 8 p.m. a similar distribution of long-wave radiation (and MRT) was observed, with negative values on the extremities of domain (TMR$_4$ <TMR$_5$). Indeed, on the borders, *Case 5* favored more radiant fluxes in relation to the taller domain center. Comparison between couple 4 and 6 was available on Appendix A.

Figure 92 – Difference mean radiant temperature maps, Case 4-5, at 16h
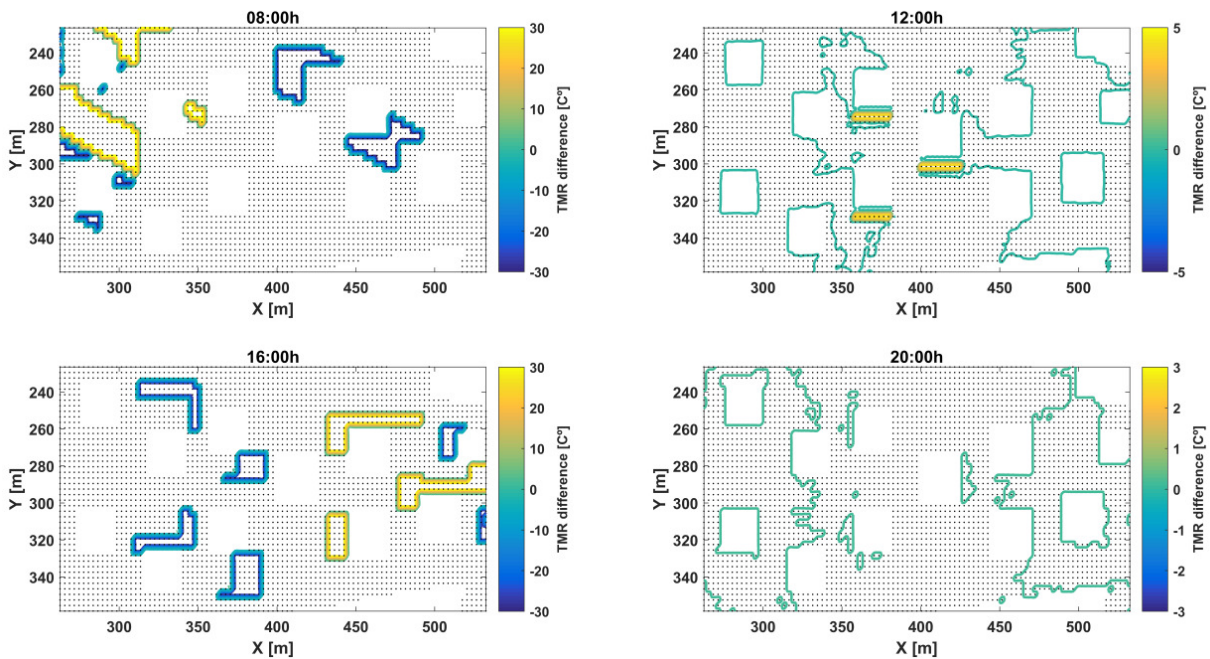
Source: Martina Pacifici (2019)

In order to explore the impact of geometry alterations on the wind distribution, a comparison between scenarios was implemented. In particular, the effects provoked on the wind pattern by variable or homogenous high buildings were investigated. From CDF findings, a perfect coincidence was found between *Cases 5* (concentrated variable heights) and *6* (outdistanced variable heights), showing that a different distribution of high buildings did not affect wind speeds at the street level on average. A slightly different pattern was instead observed at *Case 4* (same heights). On average, such *Case* displayed the lowest wind speeds (0.1-1.15m/s) when compared with the rest of *Cases*, as well as less dispersion around the average value.

Figure 93 showed the comparison between *Case 4* and *5* at 8 a.m. and 4 p.m. The greater height of blue bins (case 4) in the central interval means a higher probability of wind to fall in intermediate values. Maximum punctual differences between two simulations ranged between -0.68/+0.66 m/s. However, at greater z-grids from ground surface, increasing ranges were observed: -2.74+0.47 (18 m), -3.35+0.83 (30 m), -3.11+1.52 (34 m). At these heights, lower wind speed differences were observed ($ws_5 < ws_4$) in the middle of the three taller towers (Case 5), as well as upwind and in the downwind cavity. In the rest of domain reverse values were found ($ws_4 < ws_5$). As consequence, variable heights favored wind speeds; however, when tall buildings layout was dense, wind speeds were deflected by the building obstruction, interfering with the district flow. These findings resulted more evident far from

pedestrian level. In terms of wind direction, *Case 4* and *5* concentrated between 150° and 180°, both displaying the greater number of occurrences close to 170°.

Figure 93 – Wind speed and direction difference, case 4 and 5, at 8h and 16h.
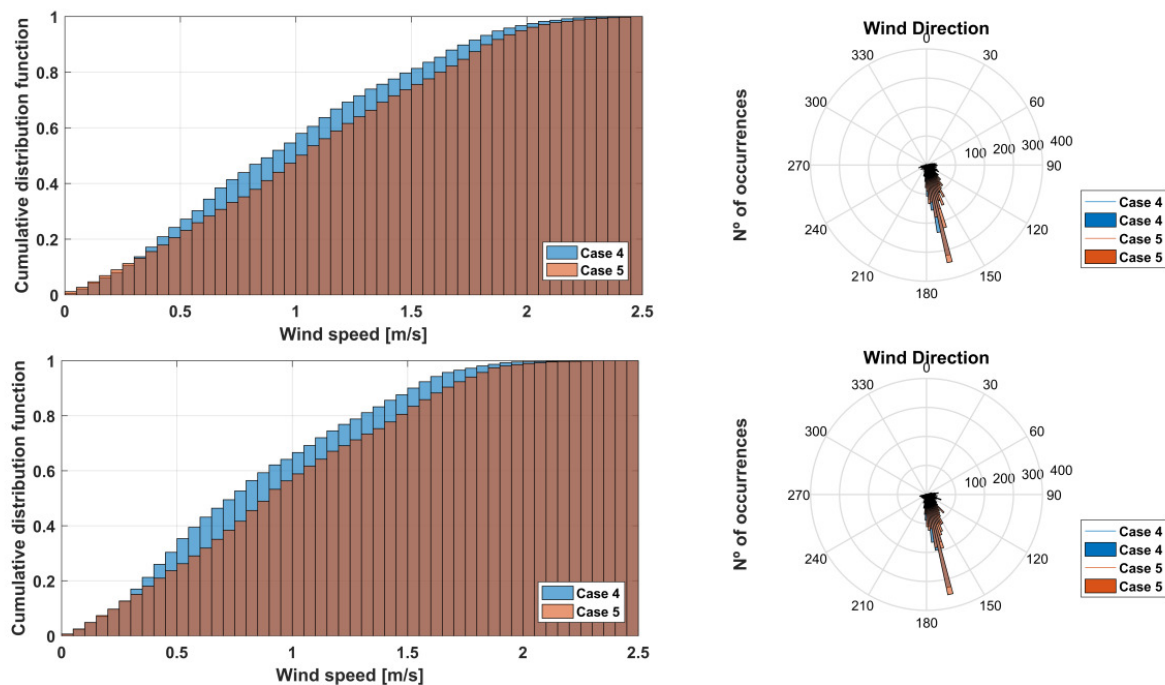
Source: Martina Pacifici (2019)

Beyond the effect of buildings height, the impact of morphology on wind pattern was also analyzed in terms of spacing between buildings. The aligned grid of *Case 3* was compared with the staggered grid of *Case 4*. Both cases counted the same amount of buildings characterized by the same heights. Wind speeds were observed at 8 a.m., 12 a.m., 4 p.m., 8 p.m., at 1m and 30 m (3/4 building height) from ground floor (Figure 94). At the hours and heights analyzed, the two scenarios showed different airflow patterns. The aligned grid channeled high speed wind along confined air corridors north-south oriented, while the staggered grid scattered the flow horizontally, affecting air velocities. A great amount of speeds and directions spread through the towers in *Case 4*. Conversely, on *Case 3*, between air channels streaming undisturbed, obstructed air zones were found. At 30 m, more contrast were observed between obstructed and windy zones then 1m height. Smoke experiments realized by Hall *et al*. (1997) demonstrated that aligned grids more deeply channeled wind through the urban morphology when compared with staggered grids. However, it could be interesting testing such different grids under other boundary windy conditions. Due to the complexity of wind flow field, more analyses would be needed, testing a large range of input speeds and directions. Further wind analyses could feed future works.

Figure 94 – Wind speed comparison between case 3 and 4, at 1m and 30 m from ground floor at 16h
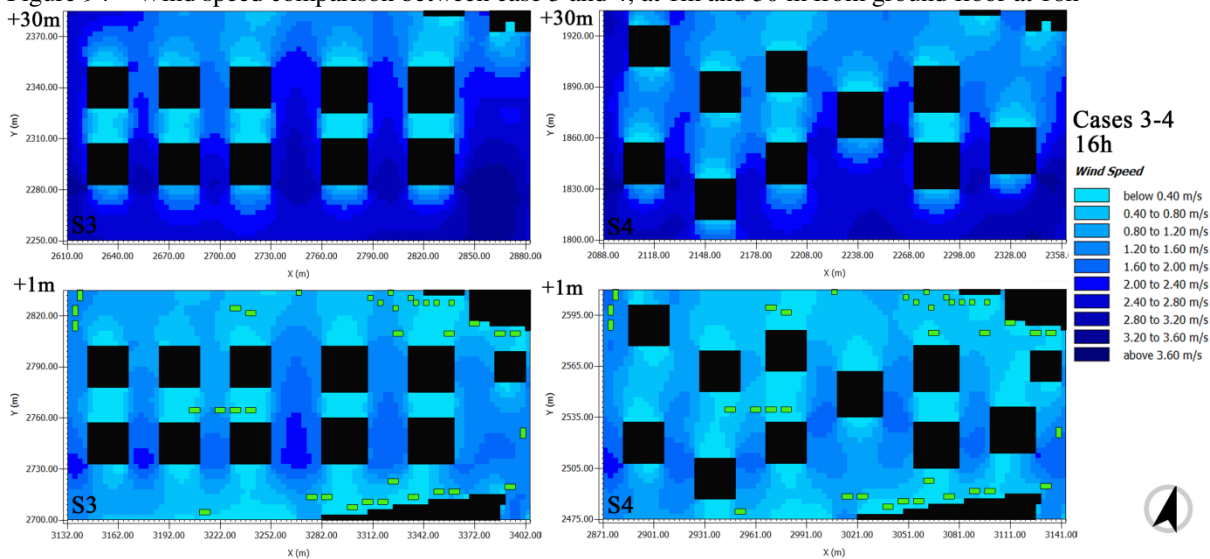
Source: Martina Pacifici, 2019

As a complementary part of previous analyses, also the reciprocal differences between *Cases* were explored in terms of air temperature and relative humidity. As mentioned at the start of this section, the modification of urban geometry between scenarios provided only slight differences on such variables. Nevertheless, the comparison 5-6 will be showed (Figure 95), but similar findings were observed in the rest of comparisons (4-5, 4-6). Overall, air temperature ranged between 20°C (8 a.m.) and 29°C (12 a.m.). Perfect coincidence between scenarios was observed at noon and after sunset. At 8 a.m., bins with greater probability exhibited a just 0.05°C difference between *Cases 5* and *6*. At 16 p.m., *Case 5* displayed its greater probability around 27.65°C, while *Case 6* around 27.80°C. In addition, *Case 5* showed with greater probability the really high values then *Case 6* which favored really low values. Relative humidity offered a slight better response at 4 p.m., even if always within the range of 1% of difference (Figure 96).

Figure 95 – Air Temperature at 8h, 12h, 16h, 20h, comparison Case 5 and 6
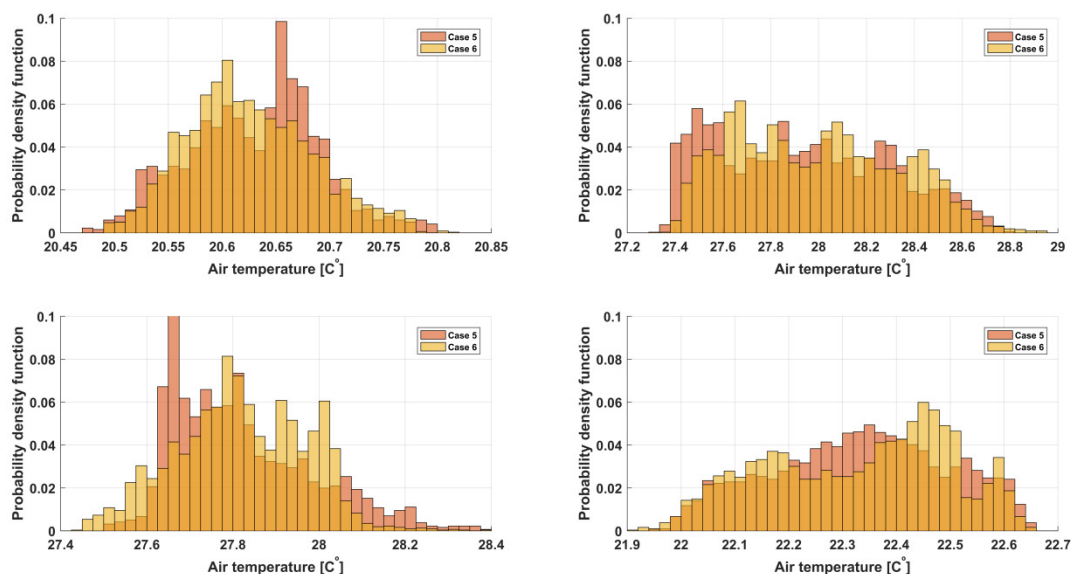
Figure 96 – Relative humidity at 8h, 12h, 16h, 20h, comparison Case 5 and 6
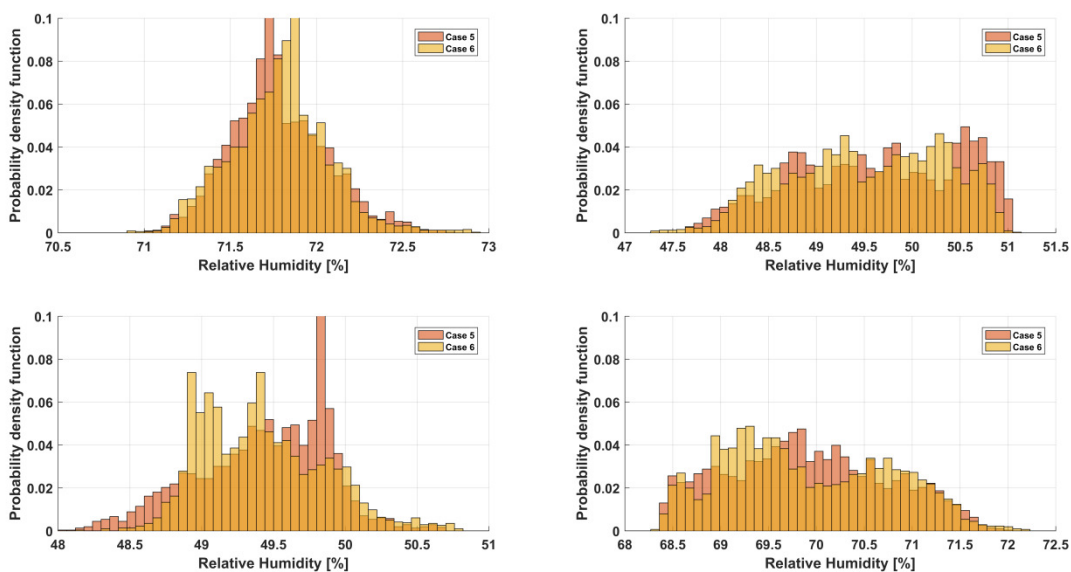
Source: Martina Pacifici (2019)

- *Scenarios at BCA=80%*

Two numerical experiments were developed at BCA=80%. *Cases 1* and *2* were designed to assess the climate impacts related to the maximum exploitation of FAR and BCA granted by São Paulo municipality. Using 80% of BCA and 4 of FAR, *Case 1* was built installing 10 buildings, while *Case 2* doubled this number. As showed on previous scenarios, a map of difference on *MRT* was presented on the 4 hours assessed (Figure 97). Again, the more contrasting daily periods occurred at 8 a.m. and 4 p.m. In both of these hours,

differences between cases were quite always positive (MRT$_1$>MRT$_2$). However, since no tall buildings or large open spaces were included, neither large shaded or irradiated areas were observed. Rather, little and concentrated micro-differences were found along with the streets crossing the blocks. At 8 a.m. and 4 p.m. differences were mainly distributed on the east-west direction, since at these hours the narrow north-south canyon did not permit the solar access. At the noon and night, instead, slight variations interested both of the directions. Such micro-islands displayed very irregular shapes, slightly shacked by the little air channels flowing through little alleys. Meantime, the most part of the domain performed as a unique whole at the same temperature.

Figure 97 – Difference mean radiant temperature maps, Case 1-2, at 8h, 12h, 16h, 20h
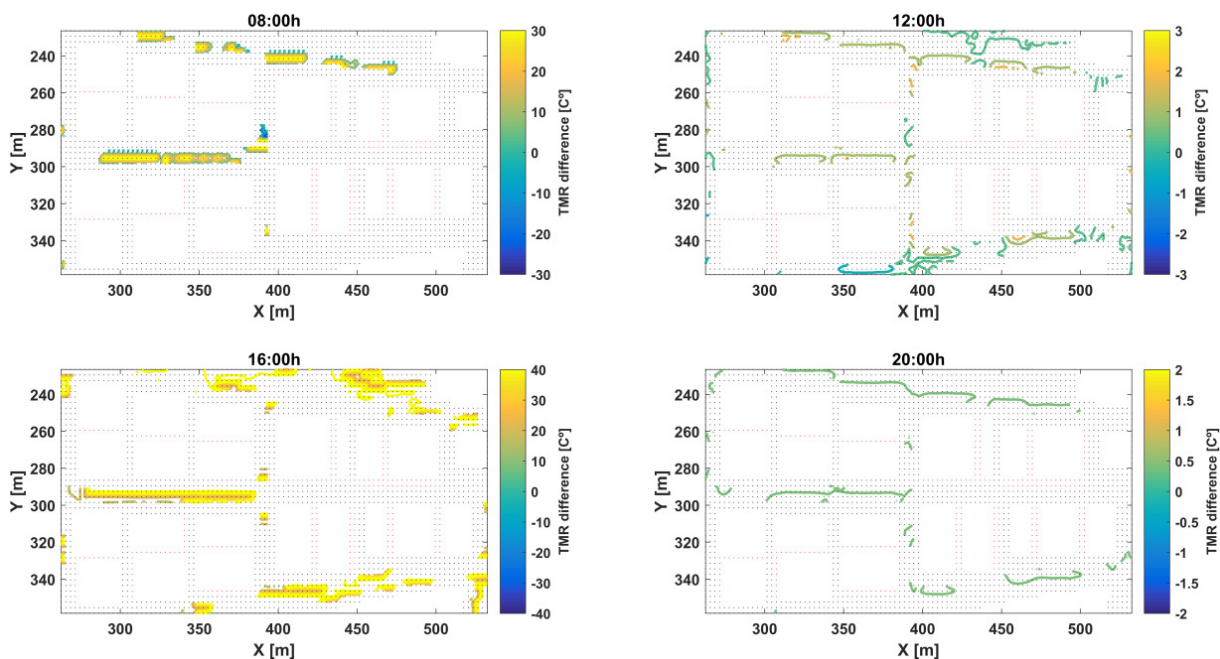
Source: Martina Pacifici (2019)

Notwithstanding, such little variations resulted quite confined, since the overall correlation between scenarios showed high values of association (0.77, 0.79, 0.77, 0.74). At 8 a.m., histograms showed similar probabilities, ranging between 19°C and 30°C. Therefore, when compact buildings arrangements were designed, using the entire built potential provided by municipality, the morphological modifications little influenced the surrounded outdoor climates, and only punctual differences were obtained. However, such typologies prevented the emergence of contrast climate micro-zones in the rest of the neighborhood (Figure 98).

Figure 98 – Correlation matrix for mean radiant temperature, Case 1-2, at 16h
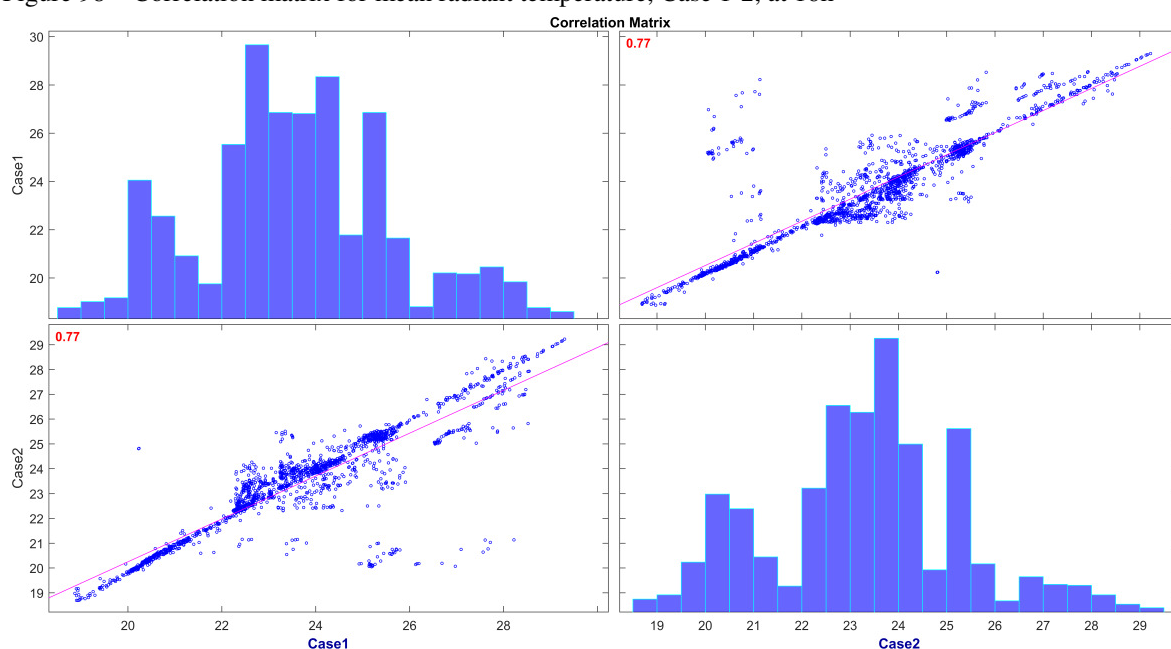
Source: Martina Pacifici (2019)

- ▪ *Comparing Scenarios at BCA=80% and 30%*

As expected, different distributions were found comparing *Case 1* (BCA=80%) with *Case 4* (BCA=30%). When distinct percentages of land coverage were implemented, the distribution of climate variables was affected considerably, exhibiting independent shapes, peaks and ranges. This occurrence is verified even if the total amount of built area is identical. The case of mean radiant temperature was displayed below (Figure 99). In general, the case of the compact scenario (Case 1) presented a smaller probability on the occurrence of high *MRT* values (12 a.m.), while a higher probability to achieve low *MRT* temperature at night (8 p.m.). Conversely, the opener scenario (4) displayed a great probability on the central position of histogram at night (14°); under these conditions, a large part of domain exhibited the same *MRT*. Lastly, during the rest of the hours, both cases concentrated their values on two populations of data: irradiated and no irradiated points. However, the open scenario (Case 4) polarized a greater amount of domain points on extreme temperatures. Conversely, in the compact scenario, a myriad of intermediate values were found, despite their little occurrence. A similar fragmented distribution had also been observed in the comparison between *Cases 1* and *2*. Indeed, in really compact scenarios (1 and 2), the abundance of little interstices and moderate heights favored the appearance of small different thermal zones. Anyway, this phenomenon is marginal, since the majority of values were concentrated on the two great thermal behaviors.

Figure 99 - Mean radiant temperature at 8h, 12h, 16h, 20h, comparison Case 1 and 4
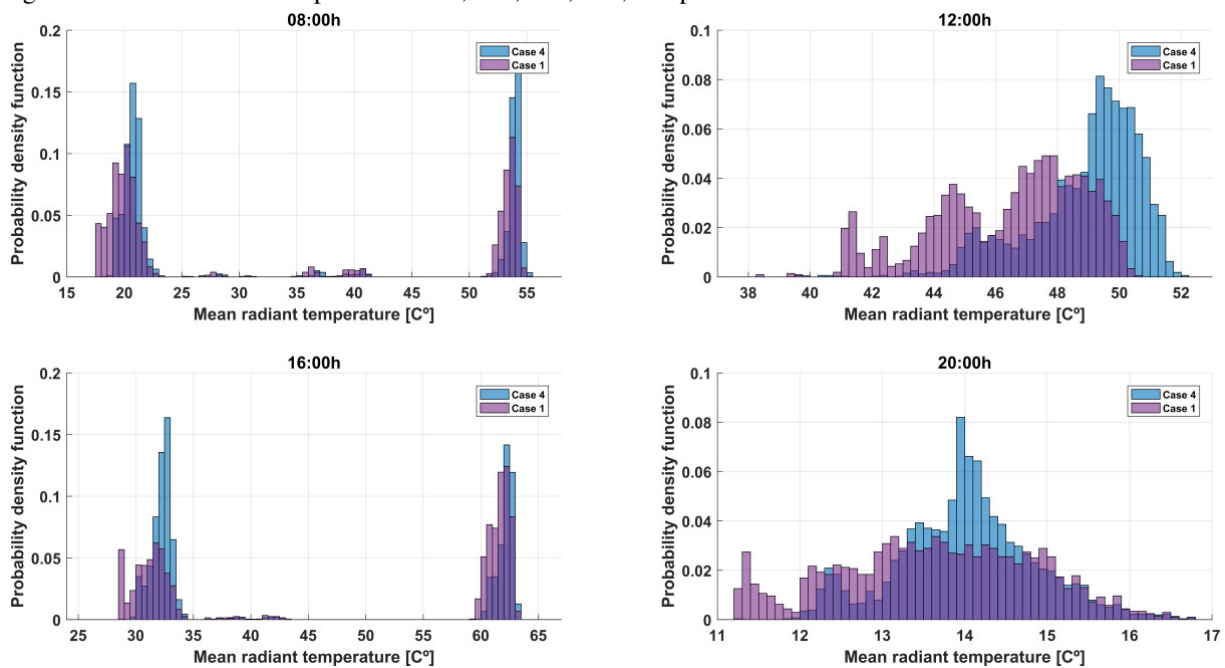
Source: Martina Pacifici (2019)

5.5 *Results from Grasshopper*

Grasshopper (G) findings aimed to integrate ENVI-met model. Moreover, another modeling technique was explored to overcome some ENVI-met limitations due to high computational costs, excessive simulation time, low reactivity of main variables (Tar, RH) and little intensity of the heating and cooling processes. The parameterization of G model was presented in Table 15. A certain amount of model parameters were related with the characteristics at the urbanized site, including the west heat from conditioning air, the anthropogenic heat from motor vehicles, the intensity of traffic depending on week days, the percentage of green areas, the properties of surfaces. Other input parameters regarded meteorological parameters (climate zone, climate variables from *epw*) and three-dimensional urban geometry features (*breps*). Through this urban morphology detailing, the extent of the heat island effect could be rightly scaled from the weather station to the urban site. This operation constituted the mathematical formulation core of Urban Weather Generator (UWG) tool, used to compute Ta and RH.

Overall, G model was much faster to run (30 - 40 minutes to run 48 hours) in comparison with ENVI-met. In particular, time simulation depended on the amount of mathematical processes included in the algorithm. While ENVI-met solved a fixed number of equations, the modular character of Grasshopper allowed modeling only relevant processes

characterizing the domain. In addition, some precautions had been adopted to enhance model performance. The initial domain was reduced to a smaller area, including low-rise and high-rise volumes (Figure 100). In this reduced area, time calculation decreased due to the smaller amount of volumes (especially towers). Low-rise housings were initially modeled individually; afterword, they were unified in few blocks and backyards canceled (section 4.4). Indeed, as ENVI-met model, Grasshopper code implements a finite-difference method (FDM) to solve partial differential equations that represent the conceptual model processes; as a consequence, a simplification of geometries was desired to well discretize the modeling space.

Table 15 – Configuration of Algorithmic Model

Urban morphology	Building Program	Midrise Apartment
	Building Age	Pre-1980's (LW), 1980's-present (HR)
	Fraction of west heat from air conditioning	0.7
	Anthropogenic heat from automobiles	8 W/m^2
	Hourly traffic pattern on weekdays	0.2, 0.2, 0.2, 0.2, 0.3, 0.4, 0.7, 0.9, 0.8, 0.6, 0.6, 0.6, 0.6, 0.6, 0.7, 0.8, 0.9, 0.9, 0.8
	Pavement (average values): albedo, thickness, conductivity, vol. heat capacity	0.2; 0.5; 1.0; 1840000
	Envelope: window surface, SHGC, wall albedo, roof albedo	0.1; 0.4; 0.2; 0.2 (LR) 0.35; 0.6; 0.4; 0.4 (HR)
Urban climate	*Epw* corollary: obstacle-height, veg coverage, temp-height, wind-height	10 m; 0.6, 1m, 1m
	Epw file	Actualized on recent data (December, 2018)
	Climate zone	2
	Time convention	UTC-3
	UBL height at daytime, nighttime, inversion height	1000m, 100m, 100m

Two different meshes were designed to simulate *MRT* and surface temperatures. *MRT* mesh is a 3 m x 3 m grid, while surface temperature mesh varied in function of the surface type and the volume: for roofs and windows, mesh coincided with the entire surface; for façades, mesh had the wall length and inter-floor height; for ground floor, a grid discretization 6 m x 6 m was applied.

Figure 100 – Grasshopper domain
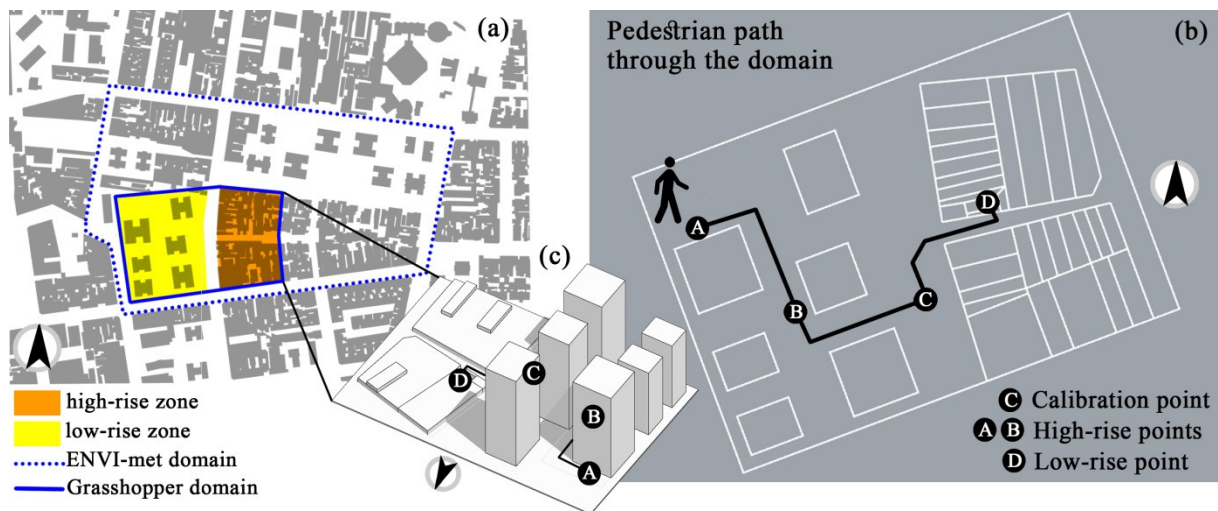
Source: Martina Pacifici (2019)

The model was calibrated comparing modeled and real values on December, 10, 2018, from 9 a.m. to the 18h (synchronized on UTC-3), when field data were collected. Air temperature, relative humidity and mean radiant temperature measured at point C were used (Figure 101). In terms of air temperature and relative humidity, the model tended to flatten the diurnal variability encountered at the field. *Ta* modeled values were rather underestimated, even if a similar trend could be recognized between the two curves. Such underestimation derived from the *Ta* input values set on the climatic station MSA. To compute the urban curve, the algorithm leveled and lowered the MSA station curve on daytime, while less affected the nighttime values. Meanwhile, other parameters characterizing the model were found less influent (ex. envelope and ground material properties). In a nutshell, the resulted urban curve was obtained by UWG model applying the urban heat island effect to the MSA values, returning lower temperature during the day and higher values in the night relative to the input station. Since MSA was not strictly rural, more similar values between urban field and weather station were found, inducing an underestimate algorithmic computation. To avoid this effect, a totally no-urbanized station should be chosen. Despite MSA was a WMO standard whether equipment, effects of urbanization were found in the close surroundings. Thus, it can be stated that suburb/not rural weather stations caused flatter trends on reproducing temperature in the urban area, worsening calibration.

With regard mean radiant temperature, a preferable correspondence between modeled and observed values was noticed. To model these variables the additional Ladybug and Honeybee plugins were employed. Plugins were interconnected, since the air temperature and relative humidity from UWG (*urban epw*) were used as input data for *Ts* and *MRT*

calculations. Notwithstanding these connections, values of *MRT* and surface temperatures were not dependent each other and their running could be performed separately. A screenshot of the graphic algorithm linking Dragonfly, Ladybug and Honeybee can be found in the appendix B.

Figure 101 – Calibration of air Temperature, relative humidity and mean radiant Temperature at the point C, from 9:00 to 18:00 (UTC-3)
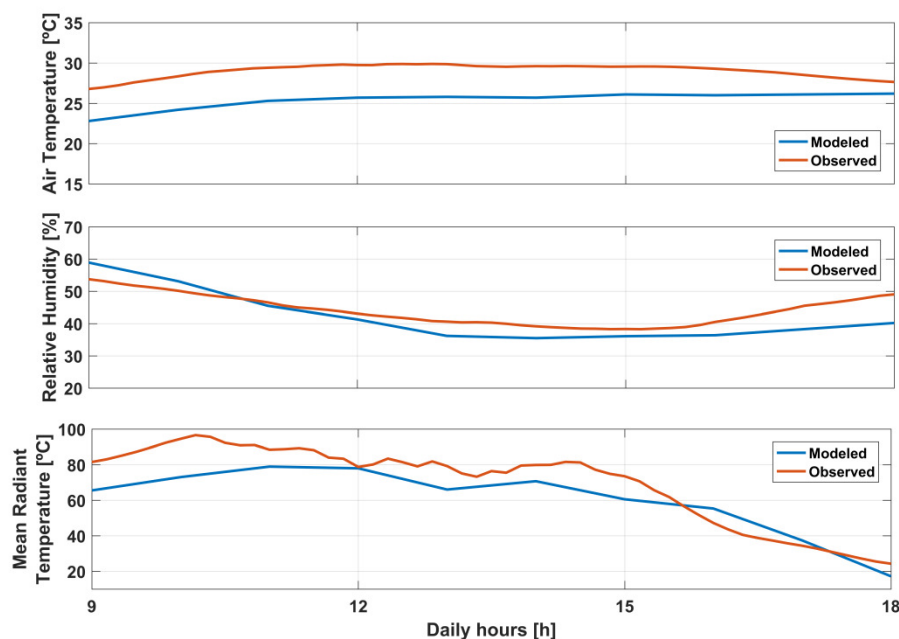
Source: Martina Pacifici (2019)

To visualizing the thermal shifting computed by UWG tool, a comparison between the input values coming from MSA station and the urban modeled curve (Belenzinho) was proposed (Figure 102). According to the UHI effect explained above, the modeled urban trend performed lower Tar values at night (from 7 p.m.to 8 a.m.) and higher values in the central hours of the day, when compared to the meteorological station MSA. At the peak a gap of almost 5 °C was simulated. The same flatten behavior was encountered in the trend of humidity. In the case of mean radiant temperature, instead, an intertwined behavior between the two curves was observed. However, a true comparison was not possible. In fact, while the input MSA mean radiant temperature was recorder at the field, the modeled *MRT* was derived by Ladybug calculator in function of the surroundings surfaces, specific shadows and materials around point C. As consequence, dips and rises were due to the specificities of each point, although around a very similar trend.

Figure 102 – Comparison between modeled (urban) and input (from MSA station) values for air temperature, relative humidity and mean radiant temperature (point c) along 24 hours
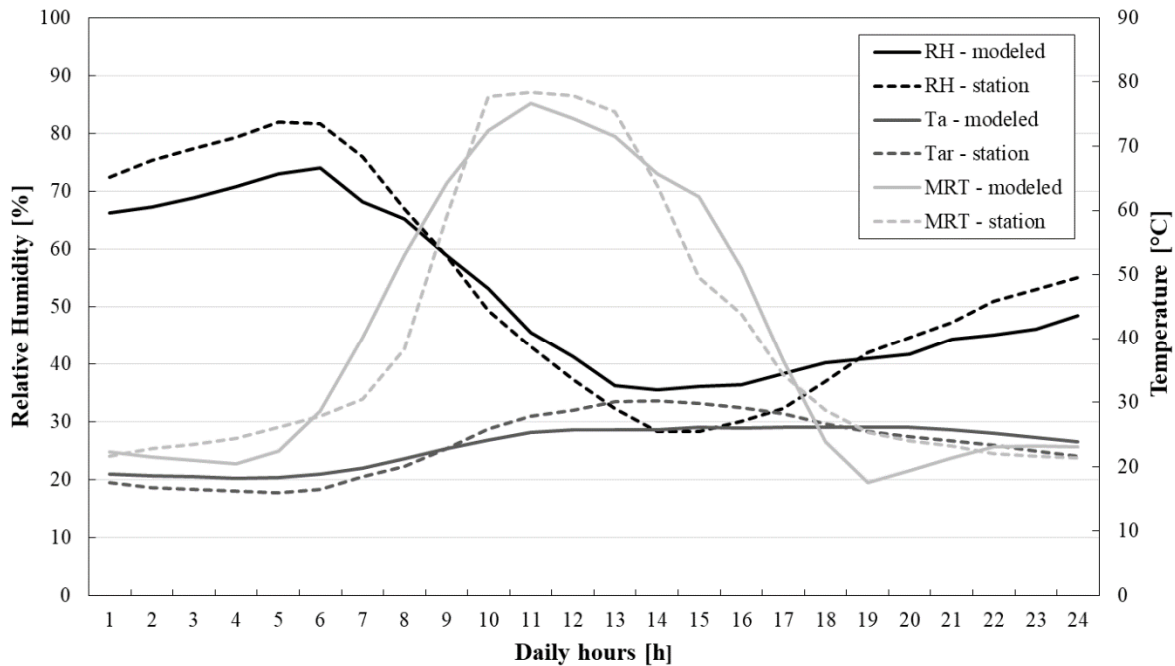
Source: Martina Pacifici (2019)

In terms of mean radiant temperature and surface temperature, findings showed the differential heating of different parts of domain at 1.5 from ground surface (Figure 103). The pedestrian path from A to D crossed the domain going from the coldest to the warmest zone. The exposure to the sun in the different daily hours favored irradiated (hot) and shadowed (cold) surfaces. *MRT* was 2D modeled; to lower computational costs, it was calculated only along the pedestrian path. The pedestrian path represents a hypothetical inhabitant walking through the different urban forms making up its neighbourhood. The pedestrian in the middle of tall buildings is subjected to variable *MRT* temperatures created by shadows. Moving towards more exposed areas, temperatures progressively increase. Sharper transitions can be observed in the central part of the day, when reciprocal position between sun and buildings created different microclimates. At 8 p.m., *MRT* fell under 22°C in all points, and the adopted legend scale could not differentiate one point from the other. At 8 a.m., the opening between low-rise and high-rise fabric let enter the morning light causing slightly warmer temperatures at the transition point C. The high-rise side of the path entails a more varied thermal assortment, with color shades indicating a rich range of values. This fact could be related to the iridescent shadow landscape, exposing or covering floors alternately. Conversely, the low-rise side showed more uniform temperatures.

Figure 103 – Mean radiant temperature on the surroundings of the pedestrian path at 8h, 12h, 16h, 20h
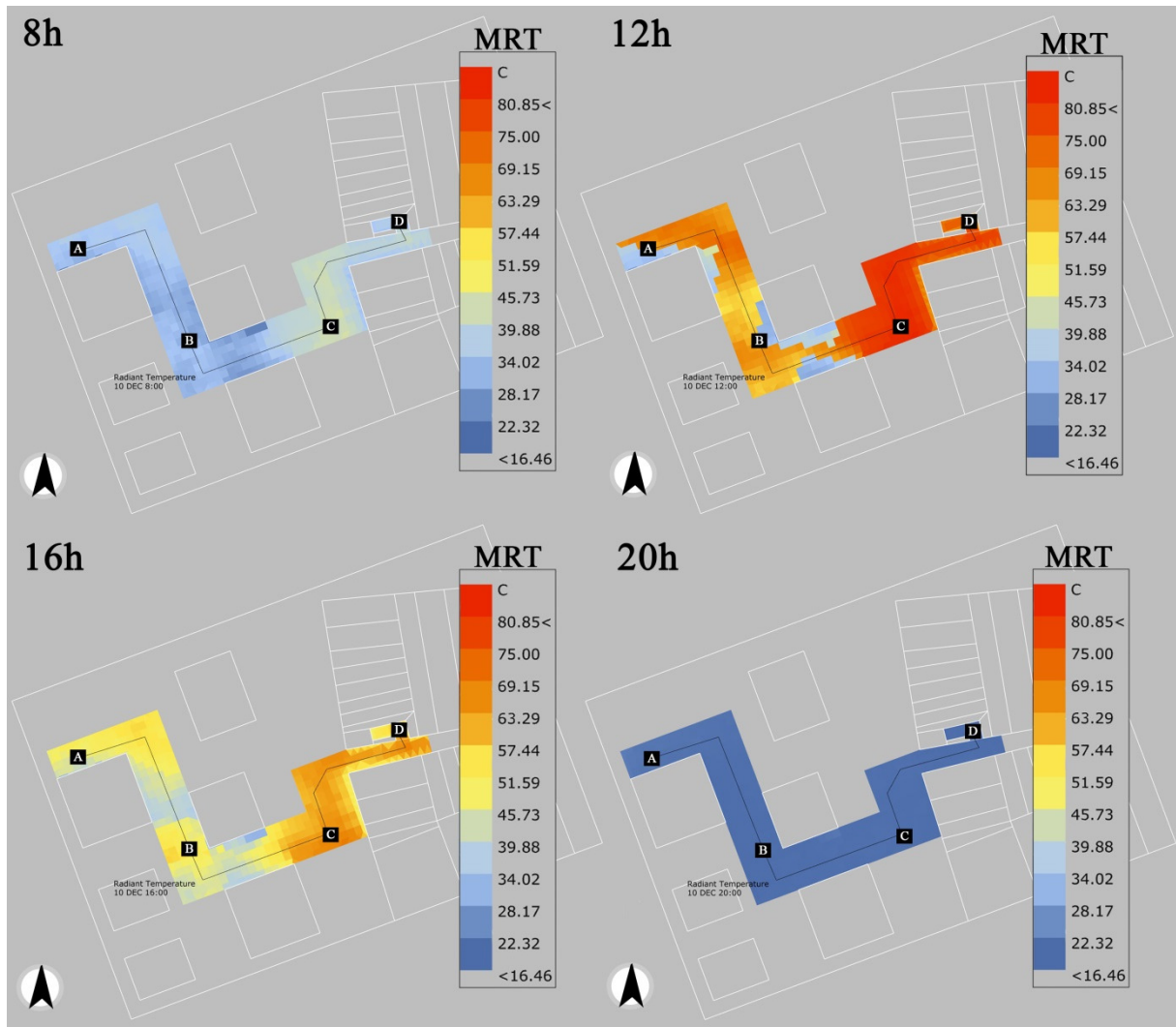
Source: Martina Pacifici (2019)

The 3D modeled scene of surface temperatures displayed a more general view of grids thermal change during the day hours (Figure 104). Similarly to *MRT* temperatures, contrast temperatures between points were visible at 12 a.m. and 4 p.m. Overall, floor surfaces returned a patchy distribution of temperatures, resulting in different micro-zones. Meantime, façades behave more uniformly and exhibited littler temperatures. These facts derived from two main reasons. On one hand, field observations revealed higher temperature values for horizontal surfaces than vertical ones, especially in the summer, when solar inclination angles are very high. On the other hand, façades were not modeled as a multitude of cells, while as single surfaces; as consequence, the mutual shading between facades on some slices of vertical surfaces remained invisible and an only averaged behavior was showed. With regard the buildings roofs, it worth stressed that at noon, when sun reaches its highest position above the horizon, low-rise and high-rise roofs belonged to the same thermal class. In the afternoon,

low-rise housings displayed higher values, probably do to the proximity with warmer ground surfaces. On the floors, once again a correspondence between cold-shaded and hot-exposed areas was noted. Besides that, additional effects were induced by the material response. The asphalted street around the low-rise fabric showed as in the hotter hours buildings are surrounded by a warm ring of high albedo surfaces. Conversely, in the middle of the towers, the light-colored concrete pavement adopted by the condominium, prevented a so accentuated heating. It also worth stressed that grass and tree canopies characterizing the open spaces around tall buildings were not modeled; thus, in reality the damping of these temperatures would be even greater.

Figure 104 – Ground surface temperature in all domain at 8h, 12h, 16h, 20h
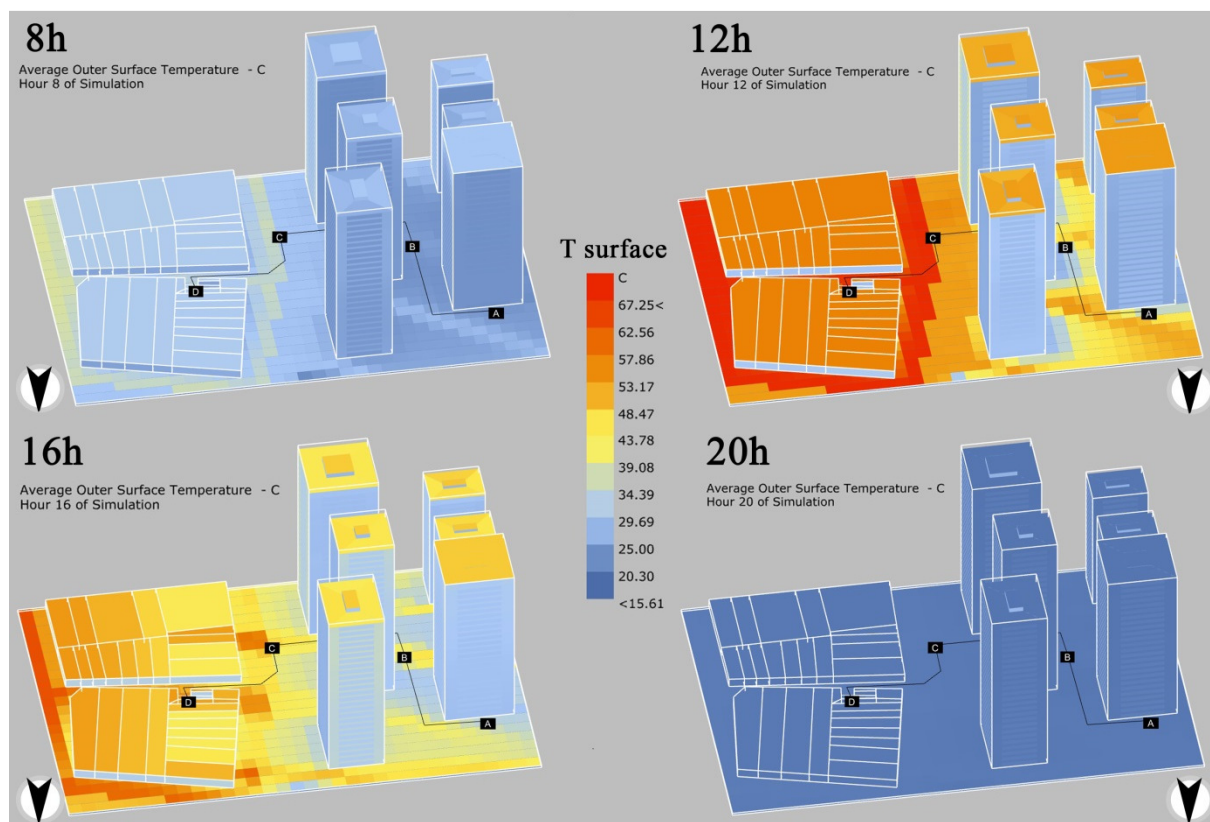
Source: Martina Pacifici (2019)

Finally, the use of UWG tools integrated in Dragonfly and combined with Ladybug plug-in allowed the modeling of thermal comfort at the urban field (Belenzinho) and meteorological station (MSA). The computation of the *UTCI index* was selected as the more reliable comfort index to be estimated by the used plugins, based on *Ta*, *MRT*, *RH* and wind speed input values. Such variables were integrated by the *UTCI* calculator (Ladybug) in a human energy balance model that allows estimating a temperature value indicative of the heat

or cold stress felt by a human body in the outdoors. *UTCI* represents the attempt of the international community to create a universal tool for the estimation of outdoor temperature sensation. The index is valid for all climates and is independent of person's characteristics, as age, gender, specific activities and clothing (http://www.utci.org/). In the case of this work, a special effort was needed to provide *MRT* at the reference MSA station. While MRT at urban site were modeled, corresponding values at the MSA station were not provided. Indeed, the reference station exists as a "fictitious" place and is not associated to a modeled environment. Thus, in order to achieve realistic *MRT* values to be entered in the model (strictly depended from the urban forms around), field data was needed. Notwithstanding, as well as many other official weather stations, MSA station did not provided *MRT* values in its measurement site. Thus, an additional field fieldwork was needed to complete the data set required by the program. This fact should be carefully taken into account by modelers that want obtain the estimation of thermal comfort, since it involved parallel measurements at the urban site (to calibrate) and at the reference station (to compute MRT). When all the input variables had been provided, the *UTCI* computation was made possible.

To verify the correspondence between modeled values and real people sensations, a comparison was proposed with the inhabitants interviews (Table 16). Votes from 150 people were collected, between 9 a.m. and 7 p.m., in the urban site of Belenzinho (point C) and on the surroundings of MSA station. People age ranged from 12 to 82 years olds. Females and males were interviewed in similar proportions. T-shirt and long trousers constituted the prevalent clothing. People's main activities were walking and staying seated. At MSA station, a good percentage of morning respondents was above 65 years and engaged in sport activity. While the first reason should favor cooler sensations, the second one should cause the opposite one; therefore, this part of respondents did not cause any particular imbalance to the samples integrity.

Overall, it was observed that the modeled UTCI values stretched the feeling of warmth over longer periods, while the opinion of the people diminished towards milder sensations. Reference station provided more stressful thermal conditions than the urban site (point C) both at modeled and real conditions, in the central hours of the day. Despite the early morning and the nightly period were not collected, some observations could be addressed to the initial and ending displayed hours. It could be noted that in the reference station the modeled hot sensations are reached (9 a.m.) and disappear (5 p.m.) an hour in advance compared to the urban site (10 and 6 p.m.). Therefore, modeled MSA station warmed up early in the morning and cooled down earlier in the evening than the urban site. At the field, the same pattern

occurred at the morning but not at the evening. This contradiction could be related to the too small sample of interviews collected, beside the heterogeneity of respondents. Therefore, interviews were used as an indicative data, while they were found little robust for a true calibration.

Table 16 – UTCI thermal comfort comparison between reference station and urban site (point C)

Hours UTC-3	Reference station UTCI-Modeled	UTCI-Interviews	Urban site UTCI-Modeled	UTCI-Interviews
9	Hot	Hot	Little hot	Little hot
10	Very hot	Hot	Hot	Little hot
11	Very hot	Very hot	Hot	Hot
12	Very hot	Very hot	Hot	Hot
13	Very hot	Hot	Hot	Hot
14	Hot	Hot	Hot	Hot
15	Hot	Hot	Hot	Hot
16	Hot	Hot	Hot	Little hot
17	Little hot	Little hot	Hot	Little hot
18	Neutrality	Little hot	Little hot	Little hot
19	Neutrality	Neutrality		

The trend of the universal thermal climate index was showed over a full day, at MSA station and at the point C of urban site (Figure 105).

Figure 105 – UTCI at reference station and urban site
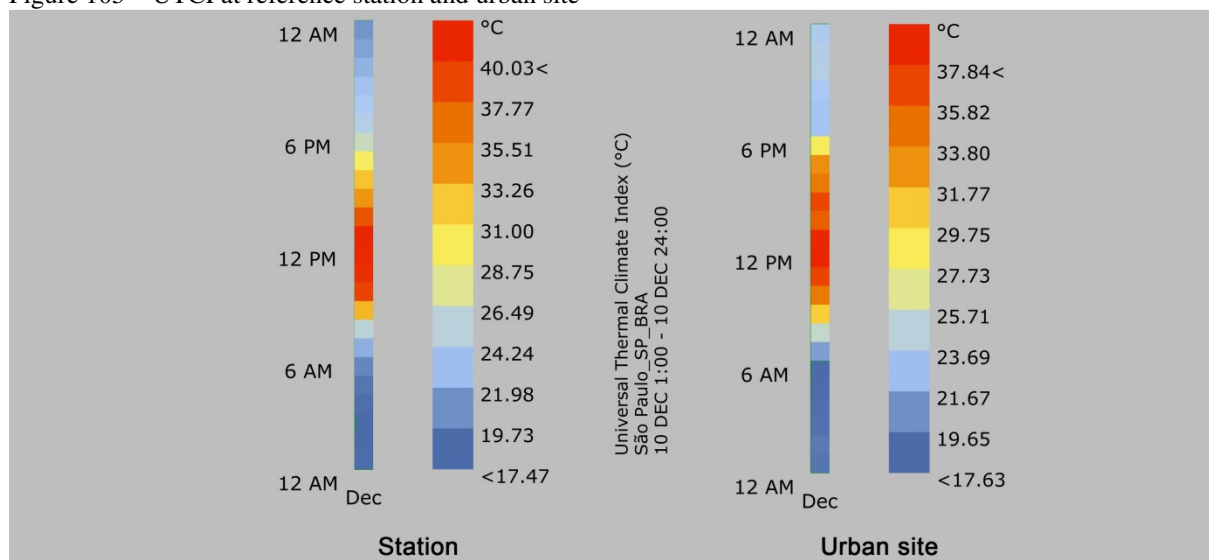
Source: Martina Pacifici (2019)

In the case of the reference MSA station (totally exposed to the sun) the *UTCI* index moved from cold to hot states more gradually, accordingly to the intensity of solar energy received. At the urban site, instead, the transition between thermal stages occurred more abruptly. This fact can make sense in the real environment, where the presence of tall

buildings prevented the gradually solar access. Additionally, it can be observed that modeled values at reference station showed the highest values; however, this intensely hot period was concentered in a 4 hours-time window, from 10 a.m. to 13 p.m. At night, according to the urban heat island "forcing", slight lower values were observed at the reference station in comparison with the urban site.

5.6   Reflections on the use of ENVI-met and Grasshopper

Overall, Grasshopper allowed investigating the case study through the implementation of other modeling techniques. The conceptual model behind the algorithm was centered on the heat island phenomenon, used as generator of urban temperatures from meteorological station. The use of a meteorological station (MSA) inside the urban heat island had led to underestimated urban site values. Since UWG worked on average values, the interconnection with Ladybug resulted very useful to simulate the thermal behavior of all domain grids, as well as to take into account more 'punctual' phenomena among which shading was once again dominant. The selection of a reduced domain was considered a convenient choice, once two representative samples of low-rise and high-rise fabrics had been included in the domain. The concurrent use of ENVI-met and Grasshopper proved how different conceptual models include some physical processes while disregard other ones, modifying their explanation of real systems. Furthermore, for each conceptual model, specific input data were required while other key-parameters were considered insignificant.

Although a comparison between models was not among the objectives and two distinct domains had been used, some considerations could be raised on the performance of the two softwares. ENVI-met simulated many interconnected processes at once, requiring a very high computational effort to solve equations. Practically, since most of the processes were simulated, a full understanding of the study area was not strictly necessary to the model design. In contrast, due to such an accurate atmospheric reproduction, ENVI-met required a simplification of built morphology and was not suitable for large urban domains. The use of forcing was found a contradictory tool. On one hand, without forcing, the urban climate conditions are far to be reproduced; on the other hand, its use causes an excessive influence of the boundary conditions on the simulated climate that practically "force" the model to assume the input values. The modular engine of Grasshopper allowed selecting the main processes characterizing the urban area, greatly reducing simulation time. Grasshopper demanded a

great clarity on the conceptual model of the field area, since the choice of processes to be simulated is set by the users. Given the lower number of simulated processes, Grasshopper allowed more complex morphologies and larger urban domains (even if a previous simplification had been applied to the domain and large dimensions had not been tested). The use of Urban Weather Generator tool permitted to simulate urban climate interaction in an urban site from external boundary inputs characterizing the city surrounding, without constrain any values. Nevertheless, the UHI was the driving force of this model, and the reproduction of other processes relied on the integration of other tools (*Ladybug*, *Honebee*). Air turbulence and radiative exchanges remained in the field of uncertainties (unexplored). For the same computational effort, ENVI-met was more adequate to deal with little domain and simplified geometries, like parametric studies, in which all the physical processes are important for the modeler and a detail scale is required. Conversely, Grasshopper was found more suitable to investigate domains in which only same physical processes were found predominant, allowing more complex geometries and long-term simulation tests. Both ENVI-met and Grasshopper showed as the proper use of modeling tool improve our ability to understand cities and enhance their future plans.

6 Summary

Goal: This last chapter aimed to convert part of results in useful urban design precepts suitable to be implemented in the areas of the city on the way of densification and verticalization, such as transport development areas (EETU). These proposals were developed to integrate some important issues to the current planning guidelines provided by the municipality of São Paulo, on the basis of fieldworks, data analysis and modeling. The proposed approach and insights concern issues shared by many other Brazilian cities, as well as abroad. Universal points were discussed and good practices were raised in support of the legislative tools. However, every city embodies a distinct climate, mainly given by its geographical location and the character of its urban development. Therefore, all the purposes should be re-discussed in each site of application.

6.1 Gaps to bridge

Findings from ENVI-met scenarios brought to light the inadequacy of current legislative precepts should guarantee the quality and effectiveness of dense urban environments in São Paulo. Within the constraints of the present planning tools, different scenarios were built and quite different responses were obtained. In other words, little detailed guidelines showed different climate impacts. Within the legislative limits, a large space of freedom was found to build a wide range of different landscapes. Such landscapes implied different levels of criticality that could be avoided if more consistent guidelines would be developed. When higher densities are implemented, issue related to less solar energy, slower ventilation and impervious surfaces have to be managed and regulated. Instead, current urban tools represent a 'comfort zone' for real estate investors and builders that foster the replication of similar urban objects in different zones of city. The insertion of new buildings is functionally planned but climatically neglected. Planning is managed at the level of plot or block-plot, while the relationship with the neighborhood and close houses is not a concern, if the minimal urban parameters are observed. Therefore, a revision of such parameters should be accomplished by planners in order to induce the design of less-impacting urban forms, suitable to be inserted in the existing built environment.

6.2   Urban design precepts

On the framework of São Paulo masterplan, points of discussion were proposed on the main precepts regulating the planning of urban areas under transformation (ZEU and ZEUP). Urban forms' attributes interfering with the open spaces climate were highlighted.

On the precept: *no limits to building height*

In the hot season of a subtropical climate, high buildings shadows contribute to keep lower surface and air temperatures in the urban open spaces, as well as they provide cooler comfort sensations. Notwithstanding, buildings heights should be regulated according to the size of surrounded elements and the distance from them. "No limits to buildings height" is a shallow precept, since buildings sizes play a central role in the district's thermal balance. In urban areas under transformation, when no limit is imposed to building height, the building vertical size only depends on the plot area, the BCA index and the FAR index. Thus, greater plot areas and FAR, together with a low BCA index, could allow really tall building. **Isolated tall buildings** in the middle of low-rise fabric can affect substantially the surroundings in terms of sunshine and wind. In the morning and evening hours, when the inclination of sun is low, as well as in the winter season, too long (but tight) projected shadow can lead to strong thermal contrasts on the ground surface, without benefitting the neighborhood as a whole. It was demonstrated that in the proximity of a tower, different micro-climates emerge between the east and west exposures, at the ground level and on the façades. Wind surface accelerations along the building lateral sides were induced. Thus, for buildings above a certain height, supplementary orientation studies should be mandatory to balance building solar gain with effects on the neighbourhood.

By means of simulations, it was also seen that **groups of tall and close buildings** strongly reduced the visible sky view, obstructing the thermal exchanges among surfaces and atmosphere. Indeed, on one hand they decreased the amount of diffuse and infrared radiation from sky; on the other hand they enhanced reflected exchanges among surfaces. A group of tall buildings at close distance increases strongly the probability of interference along with the day, inducing the appearance of strong thermal contrasts in the middle of the buildings. In terms of wind, such arrangements interfered with the surrounded flow pattern, deflecting wind speeds. In dense environments, when more buildings are arranged in groups, **height variation** should be planned. It was observed that buildings arrangements of equal or variable heights

induced different sky view factors, characterized by the prevalence of average values (equal heights) or the abundance of really high and really low values (variable heights). Equal heights arrangement projected identical shadows and favored regular zones at different *MRT*. Instead, variable heights arrangement resulted in zones with really high and really low *MRT* values. As consequence, the height variation should be softly implemented. Actually, the height variation (from 11m to 85m) adopted in ENVI-met numerical experiments led to excessive thermal gaps between buildings as regards mean radiant temperature and ground surface temperature.

In addition, special attention should be addressed to high-rise and dense zones in which few small scale buildings still persist; by the solar access study in a typical urban canyon, it was showed as the contribution of the shorter building is trivial since their shadow projection is lost in the shadow cone of the "giants". In these cases, the permanence of such littler buildings should be discussed and a moderate verticalization of their lots could work well to increase density without adding further shading to the surroundings.

Meantime, it was observed the contrasting thermal behavior between low-rise and high-rise temperature, as well as the abundance of such two typologies in the entire city of São Paulo. In Grasshopper model, the low-rise building arrangement was observed very unfavorable to the pedestrian walking. To keep the pedestrian away from high surface and radiant temperatures, arches or canopies along the road could be inserted in the low-rise fabric; even green facades would be favorable, as would the protection of interstitial spaces from the sun during the hottest hours. At a larger scale, to avoid the extreme consequences of hotter and colder environments, **midrise** zones should be required by the masterplan. Midrise zones could be a useful mean to densify meanwhile avoiding excessive sky view and sun obstruction. Buildings with intermediate heights should be located on the interface between low-rise and high-rise zones and substituting condominiums of equal-heights towers. In ZEU and ZEUP different **height subzones** could be proposed and their height limits should be defined increasing progressively the heights of the surroundings. As an example, for ZEU zones surrounding metro stations in a low-rise fabric, an increasing height could be adopted from the borders towards the core of the area.

On the precept: *maximum building coverage area (BCA ≤ 0.85) and floor area ratio (FAR≤4)*

BCA and FAR are the most important indexes regulating the process of densification in São Paulo. The combined use of such parameters determines the shape of built mass in the

plot (high & tight, low & large). The limit of 85% to building coverage ratio was observed to be a really high value, even for areas under densification and verticalization. Scenarios designed at a similar coverage ratio led to really **narrow open spaces** between buildings (3~5m). On ENVI-met, high BCAs together with minimal spacing between buildings produced really compact layouts for which a FAR equal to 4 prevented the sun access on the most hours of the days, as well as decreased wind speeds. Meantime, such compact typologies prevented the emergence of contrast climate micro-zones in the immediate vicinity, behave as unique thermal bodies. When the number of buildings was increased, the amount of alleys through the blocks increased, leading to slight temperature variations and higher wind speeds. However, such effects were of small entity. When compact buildings arrangements were designed, using the entire built potential provided by the municipality, morphological modifications little influenced the surrounded outdoor climates, and only punctual differences were obtained. The minimal distance allowed by legislative tools was found insufficient to be used in such high values of BCA. In the 3D light-hours matrix (5.3.3), for deep canyon with W=10m, a limit of houses from 1 to 3 floors was suggested as compromise to guarantee a good number of solar hours per day. Even more, limits to BCA should be defined in **couple with FAR indexes**; it follows, if high values of BCA are implemented, minor FAR should be required, especially for residential lots. Such considerations are useful in a large perspective, since all the densification possibilities offered by the master plan should be explored. However, it should be noted that entrepreneurs focus on the purchase of large lots where it is possible to install towers with a lower BCA. ENVI-met scenarios implementing low building-coverage-areas showed a larger range of thermal variability; therefore, as BCA decreases, complementary studies should be provided by builders regarding the **combined design of built and open areas**. It was showed that for larger spacing between buildings (low BCA), the distribution of the sky view factor could deeply vary its distribution, different percentages of shaded and sun exposed areas were found at different daily times and wind patterns could be affected. As a comparison, low BCA favored a prevalence of *MRT* values close to the average (night), distributed on large shaded and irradiated areas (day). For high BCA, instead, higher and lower concentrated *MRT* temperatures were observed.

On the precept: setbacks and spacing between buildings

FAR and BCA define the amount and the shape of a built mass could be constructed in a plot, once the total built area and the number of housing units were fixed. However, FAR

and BCA do not constrain neither the buildings layout, nor the **reciprocal distances** between buildings. For ZEU and ZEUP, São Paulo master plan limits the setbacks to 5m on the front side. For back and lateral sides, equation 10 (section 4.3.4) is used, D_{bor}=(H building − 6) ÷ 10, or a minimum of 3 meters is required. Between buildings of the same plot, the similar equation 11 (section 4.3.4) is used, considering the sum of contributions from each building ($D_{bld} = \sum_{Hb=1}^{n}$[(H building − 6) ÷ 10]). Equations 10 and 11 practically represent the **Height to Width factor**, defining the minimal relationship between the building height and distance. The H to W ratio is a key parameter regulating the access to sunshine radiation, the heating and cooling processes, as the radiative exchanges. In order to have control on these variables, the H to W ratio should be critically discussed in the urban design practice, exploring different urban solutions, and not simplified to an equation (Eq. 11 and 12), indistinctly applied to every circumstance.

From ENVI-met compact scenarios (1 and 2), Equations 10 and 11 were observed unsuitable to guarantee light and air in the narrow alleys of compact scenarios. In fact, for two facing buildings, 18 m-high, a minimum distance of 2.4 m was required (1.2m + 1.2m). Ensuring such low inter-distances, São Paulo master plan favor high H to W ratio that means narrow canyons. Given the considerable length of the blocks in São Paulo, such narrow canyons may involve long roads without solar access. In terms of **buildings layout**, instead, a completely freedom is granted to builders in the city of São Paulo. Consequently, the arrangement of buildings is often determined by functional exigencies, accessibility, and topography. Conversely, the orientation, combined with the reciprocal position of buildings (**H to W ratio**), contribute to the occurrence of different outdoor microclimates, affecting the thermal behavior of the urban fabric as a whole. In ENVI-met, two cases were simulated, adopting **aligned and staggered grids** of buildings. Aligned buildings layouts channeled high speed wind along confined air corridors, while left the fronts and the backs of the buildings at very low speeds. Conversely, staggered buildings scattered the flow horizontally, affecting air velocities in multiple directions. Lastly, attention should be paid to the layout of buildings at the same height. In ENVI-met, it was shown that equal-height layouts guaranteed average sky view factors when the spacing between buildings was maximized; conversely, equal-height layouts, aligned on the east-west direction, exhibited more extreme values. The only shift of buildings also affected the solar access, causing at 4 p.m., a difference of 10% on the percentage of shaded domain.

On the 'missing' precept: materials and exposures

No mentions to materials could be found in the set of precepts regulating the densification of ZEU and ZEUP. This lack should be seriously re-considered, since a densifying process implies a great amount of additional built mass to be allocated. As seen in the fieldworks, materials can retain or favor certain thermal exchanges as function of their properties, exposure and fabric. Thus, to guarantee higher people density without increasing the heat storage of the neighborhood, ground floor and façade materials should be selected considering the sun and sky exposure to which surfaces will be oriented. According to field measurements, surfaces light-colored materials should be preferred to dark-colored ones; for façade, plaster and ceramics can be applied indistinctly. For roof, concrete performs better relative to fiberglass and ceramic tiles, even if the implementation of green roofs should be strongly encouraged (not studied). As expected, the solar exposure of asphalt is dramatic at tropical latitude; out to the extent of buildings shadows, a continuous tree coverage should be provided along streets. Within the lots, when possible, concrete floors should be replaced with lawn or pervious floors, in order to decrease surface temperatures. However, as showed in site fieldwork, little effects are expected in terms of air temperature and humidity on average. Special attention has to be paid on east and west facades, subjected to intense heating and cooling phases. On these façades, shading devices are desirable.

On the 'missing' precept: green infrastructure

A more detailed planning of high and dense buildings should be combined with **suitable green coverage** precepts. Indeed, in the fieldwork, it was observed as the tree coverage (high-rise fabric) decreased notably the temperatures of certain areas in the winter, while the lack of trees (low-rise fabric) worsened considerably the heating effect during the summer. Furthermore, beneficial cooling effects were recorded under isolated tree's crown but little influences were found just out of their shadow extent. As a result, in a densely built urban area, the green fabric should be thought proportionally to the buildings sizes, and their shadings effects combined, avoiding permanent obstructed zones. In these areas, **deciduous** foliage trees are recommended. Especially in hot tropical climates, the lack of any kind of solar shelters should be escaped, especially when waterproof and dark-colored surfaces are exposed. Isolated trees can provide little micro cool islands but are insignificant at the local scale. Conversely, continuity between tree canopies should be provided in not shaded outdoor spaces and streets.

On the procedure: plot-centered planning

To build into ZEU and ZEUP areas, the set of indexes required by the São Paulo master plan are basically defined *per* lot. Conversely, there are no recommendations regarding the interrelation between lots, since each parcel is an independent exploitable unit. The entities of urban block and urban fabric are not mentioned. However, ZEU and ZEUP are large urban areas, delineated along transport lines and stations, made up of contiguous lots. The proximity between the little parcels is a **favorable condition to plan**. Meanwhile, the densification is forecasted to occur in existing lots, and their replacement will be a slow process. In the future, this circumstance could lead to semi or totally vertical dense areas, grown without the support of an in-depth climate study. The result would succeed in bringing residences closer to transport lines but would fail to ensure a better life quality, as predicted. Conversely, future urban configurations of São Paulo TOD areas (EETU) should not arise from disconnected actions of independent investors. The implementation of new oriented-transport development areas (ZEU, ZEUP) is a great opportunity of renewal. In the middle of such horizontal city as São Paulo, mainly consisting of compact and open low-rise zones, the new dense high-rise areas could become **fresh islands** across the city, contributing to decrease the local temperatures and mitigating the urban heat island effect. However, to avoid over shaded areas, low sky views and wind obstructions, as well as preventing radiated exchanges at night, the planning of such new dense zones should be managed as a whole and **local-scale criteria** introduced. This larger perspective would allow balance built and open areas within and beyond the lot boundaries, guaranteeing a continuity of the urban design and preventing conflicts between lots. A dedicated urban development department could deal with such commitment, supporting builders in the development of suitable buildings layout. A compromise between builder's capabilities and **city priorities** should be achieved in terms of buildings orientation, built and open area distributions, height of volumes, provisions of green areas, selection of trees species, application of building and surface materials. Meantime, a more general plan should be designed, involving the system of public spaces and streets around these lots, promoting walkability, slow and no-motorized transports, greenery and trees. In this perspective, the design of overall solutions involving TOD areas as recognizable wholes may support the improvement of the "environmental diversity" of such areas. New kinds of rich and varied microenvironments could be created at close distance (STEEMERS; STEANE, 2005), meanwhile avoiding the replication of identical architecture solutions that

provide a small variety of outdoors. Thus, temperature variability and diversity of urban forms should be promoted to increase the climate alternatives to all users, for all their activities.

6.3   Recommendations for planners and urban institutions

In order to make easier the understanding of thesis results and urban precepts (section 6.2), a final table 17 was proposed. The table can be consulted with a quick look by planners, urban institutions and all people interested in a climate-sensitive urban design. They particularly facilitate the TOD area design.

Table 17 – Recommendations for a climate-sensitive urban design in São Paulo; useful for other urban contexts in process of densification and transformation, at similar latitudes.

Urban element	Recommendations
Building height	To avoid the extreme consequences of hotter (low-rise fabrics) and colder environments (high-rise and compact fabrics), **midrise zones** should be required by the masterplan
	Buildings with **intermediate heights** have to be located on the interface between low-rise and high-rise zones
	In TOD areas different **height subzones** could be proposed, increasing progressively the heights of buildings from the surroundings
	Buildings heights should be **regulated** according to the size of surrounded elements and the distance from them
	For **tall isolated buildings**, supplementary orientation studies need to balance building solar gain with effects on the neighbourhood
	Groups of **tall and close buildings** should be avoided because strongly reduce the visible sky view, obstructing the thermal exchanges among surfaces and atmosphere. They also deflect wind speeds
	In dense environments, with more buildings arranged in groups, **height variation** should be planned
	Variable heights buildings groups are preferred to equal heights groups
	Small buildings close to big towers groups are climatically unimportant
Spacing between buildings and setbacks	In low-rise fabrics, to keep the pedestrian away from high temperatures, **arches or canopies** along the are desirable; even **green facades** are favorable
	The **minimal distance** between buildings allowed by São Paulo law was found insufficient to be used with high values of Building Coverage Are (80%).
	For **deep canyon** with W=10m, a limit of houses from 1 to 3 floors was suggested as compromise to give a good number of solar hours per day
	Scattered buildings should be preferred relative to aligned layouts in terms of ventilation
	About Sao Paulo legislation, **less freedom** should be grant **to builders** and more restrictions should be defined in terms of building orientations, setbacks and spacing
Materials	The matter of materials should be faced in the **masterplan**, especially in terms of TOD areas
	In high-rise and compact fabrics, surfaces **light-colored** materials are preferred to dark-colored ones; for façade, **plaster and ceramics** can be applied indistinctly. For roof**, concrete** performs better relative to fiberglass and ceramic tiles; the implementation of **green roofs** should be strongly encouraged
	The solar exposure of **asphalt** has to be avoided (use trees for example)
	Concrete floors should be replaced with **lawn or pervious floors**
Exposures	In high-rise and compact fabrics, special attention has to be paid on **east** and **west facades**, subjected to intense heating and cooling phases. Shading devices are desirable on facades
Green infrastructure	The planning of high and dense buildings should be combined with a **suitable green coverage**

	The **double obstruction** of trees and tall buildings should be avoided
	The **continuity between tree canopies** should be provided in not shaded outdoor spaces and streets
	The space between isolated trees should be fill with more trees/vegetation, in order to recreate a **continuous green path**
Planning scale	TODs should be implemented by a dedicated plan including all the area. **Lot-regulations are insufficient** to promote a good urban design. Local-scale-criteria should be introduced
	TOD areas should promote "environmental diversity". New kinds of rich and varied microenvironments should be created at close distance (STEEMERS; STEANE, 2005)
	To convert the new dense high-rise areas in **fresh islands** across the city, contributing to decrease the local temperatures and mitigating the urban heat island effect

Source: Martina Pacifici, 2019

7 Conclusion

The main objective of this thesis concerned the investigation of the interactions between climate variability and urban form features in urban areas in which processes of transformation, densification and verticalization are ongoing. To achieve this goal, a specific case study was selected in the city of São Paulo, in the neighborhood of *Belenzinho*. The case study was representative of an urban area with a prevalent compact low-rise fabric, at tropical latitude. In this area, real estate developments had been implemented and future high-rise constructive activities are forecasted, according to transit-oriented development (TOD) strategies.

The assessment of the case study highlighted the main climate effects associated with the increasing of built density and building heights in the domain. Procedures of field campaigns were applied to characterize the physical attributes of studied area, including urban forms and climate patterns. A wide range of field measurements was carried out, including climate data collection by means of transect-paths and installed meteorological stations. Moreover, thermographic assays on materials, measurements of building geometry, hemispheric lectures of sky view and tree canopy were realized. Data from municipality and meteorological stations were also integrated and updated. The interpretation of most of these investigations was condensed in two published international journals.

Through the analysis of the entire database, a conceptual model of the area was developed (Objective 1). This model provided a simplified representation of mutual effects between physical forms and specific thermal characteristics. On the basis of the conceptual model, a numerical model was built up on ENVI-met software. To facilitate the software understanding and integrate missing information about its function, sensitivity tests were implemented in a reduce domain. In this sensitivity analysis, numerical tests on the main ENVI-met parameters were implemented. Findings from conceptual model and sensitivity analysis represent useful tools for urban modelers and ENVI-met users. The modeling main contribute is related to the integration of raw data from different sources in a common framework that explains climate variations within the domain (Objective 2). On the calibrated model, different built density increases were tested on the low-rise blocks and climate effects observed. Such numerical experiments were thought within the limits of São Paulo regulation, since values under the threshold of FAR=4 and BCA=80% were applied. Findings from these scenarios highlighted different thermal behaviors between buildings arrangements, as well as

similarities on some parameters. At this stage, limitations of ENVI-met software were appointed.

However, it was showed that the insertion of high-rise areas had been able to produce thermal contrasts depending on the height distribution and spacing between buildings (Objective 3). Consequentially, the municipality of São Paulo should define very strictly these parameters if the occurrence of certain phenomena (excessive shadowing, long-wave radiation trapped, obstruction of sky view, deflection of wind, greater urban heat island effect) has to be avoided in TOD areas. Finally, a corollary model was developed on Grasshopper (using Urban Weather Generator tool) to investigate the study area under different conceptual model premises. Overall, the Grasshopper model succeeded to reproduce the field temperature variability, even if the use of reference meteorological stations inside the urban heat island was strongly discouraged. Some comparative considerations were also raised on the use of ENVI-met and Grasshopper modeling tools. In the final summary, the São Paulo urban regulation was discussed and climate-sensitive design precepts were raised to enhance the implementation of high densities in São Paulo.

7.1   Hypothesis proof

The development of an integrate procedure of analysis and modeling contributed to the physical comprehension of the São Paulo urban lands in which densification strategies are applied, and provided useful findings to plan more climate-sensitive design solutions for outdoor spaces. The impact of urban morphology variation on the distribution of climate variables in urban open spaces was proved, confirming findings achieved by several researchers around world. Verticalized and densified areas were observed to lead to contrast microclimates at the street level, affecting people comfort sensations. Moreover, the work demonstrated that São Paulo municipal regulations failed to guarantee a climate sensitive design in urban TOD areas. Indeed, by testing scenarios of urban transformation, different thermal effects could be obtained under the same building concessions (BCA, FAR, setbacks).

7.2   Highlights

The most important results are highlighted in the following points:
- The **integrated procedure** developed was found an effective urban tool for the morphological and climatic investigation of cities at multiple scales, suitable and

rather general to be replicated to different urban situations and climate conditions around the world;

- A **strong correlation** between climate variability and morphological urban forms was found within the study area, despite the smallness of domain. Thermal contrasts mainly depended on building heights and spacing between them, emphasized by the tree coverage;

- At the **local scale**, during the morning, the greater part of outdoor spaces provided similar temperatures. In the afternoon, thermal contrasts (T_a, MRT, T_{gs}) arouse between the hotter low-rise zone and the colder high-rise zone. Accordance between findings was found in the cold and the hot seasons. At this scale, LCZs were not sufficient to understand the air temperature behavior on site; thus, a integration with long-term field measurements or other investigations is strongly recommended to other researchers;

- **Buildings shadow** was pointed out as the main driving force, stressing the heating and cooling of the entire domain. The analysis of *Spearman* correlation coefficient revealed high correlation (rs = 0.741302) between the number of sun hours at the street level (not obstructed) and surface temperatures;

- At the **meso-scale**, under the same latitude and heat island effects, the São Paulo climate behaves homogeneously, as a unique climate unit, regardless of the zones. In the case of air temperature, local morphological differences between stations' sites are overcome by geographical effects and heat island influence;

- At the **microscale**, sharp air temperature variations were measured in the high-rise zone at opposite sides of an isolated tower. Greater temperature differences (T_a, T_{gs}, MRT) were observed between east and west exposures. Conversely, around the low-rise block, the exposures were less significant and did not cause air temperature gradients. Microclimate findings are invisible to a LCZ analysis;

- In terms of **materials**, dark-colored plasters displayed high peaks of surface temperature then light-colored plasters and ceramics, as expected. If dark-colored surfaces are localized in low-rise fabric, their presence exacerbates the daily heating process of urban morphology. Light-colored plaster and ceramics showed coincident thermal trends. The same coincidence was found between fiberglass and ceramic tiles;

- **Trees** under assessment were able to interfere in the microscale of domain, but unable to affect the local scale dimension, since their effect was lost in the close

surroundings. Indeed, distinct thermal behaviors between sunny and tree-shaded samples at very close distance (3-10 meters) were observed. Thus, the use of continuous tree canopies in urban areas should be preferred relative to scattered and isolated trees;

- In the **ENVI-met sensitivity** tests, air temperature and humidity were mainly found insensitive to the changes of parameters, confirming their dependence from *forcing* tool. Conversely, wind speed and directions were observed very reactive to the adjustment of several parameters;

- In ENVI-met **scenarios** differences between buildings arrangements were found as function of shading. The percentage of shaded and irradiated areas was seen of critical importance to induce temperature gradients within the domain. The **sky view factor** parameter was found sensitive to the variation of spacing between buildings, providing more average values for equal-spaced layout. However, when the heights of this layout were made to vary, SVF extreme values returned to appear. The variation of SVF through scenarios affected the budget of solar radiation on the grids, causing the heating and cooling of surfaces in certain points of domain. Implications related to the sky-view and sun-exposure were visible in the trends of surface temperatures and mean radiant temperatures.

7.3   Limitations and future researches

Future works were pointed out in order to overcome the limitations highlighted along with the manuscript.

- DATA COLLECTION - It would be interesting to reinforce the data collection in space and on time. Longer-time series should be analyzed in the different seasons, better if yearly. Complementary measurements could be developed at all the scales analyzed. At the microscale, further fieldworks should expand the database collected around isolated urban volumes, by repeating measurements around other buildings or blocks. At the local scale, more examples of high-rise and low-rise fabrics should be studied in order to consolidate our findings. Instead of supporting the mesoscale analysis by weather stations, spatially distributed climate data would improve the analysis. Similarly, to other research fields, the creation of a common urban climate

database, organized per cities and freely-accessed, would greatly enhance our understanding and description of urban climate. The study of surface materials could be complemented by collecting thermographic samples on the roof surfaces of both fabrics. In addition, the implementation of other supporting techniques of analysis (as remote sensing) could improve a lot the results obtained.

- SÃO PAULO CASE STUDY – The urban environment of São Paulo city constituted a specific case study with peculiarities and climatic mechanisms due to its location. In the research, great emphasis was dedicated to the role of the urban morphology mass and building geometry in interaction with the solar radiation. Special attention was paid to the urban heat island phenomena. However, in the daily temperature behavior the distinction between geometrical effects and inertial stresses typical of coastal cities was not investigated. Despite the relevant distance of São Paulo from the coast, the Atlantic Ocean is a high-heat-capacity water mass able to store a great amount of solar energy, later releasing it slowly, damping the peaks of temperature. In this way, the Ocean works as a thermal buffer that interferes with the heat fluxes entering and exiting the city. Conversely, in continental cities far from the sea, the study of urban morphology should guarantee more evident response due to the effect of geometry, without the damping effect of sea breeze. This could favor even more relevant differences between high-rise and low-rise fabrics. For this reason, it would be interesting to extend the research to other cities in which the influence of inertia is absent and develop comparative analyses.

- NUMERICAL MODELING - Urban Weather Generator *via* Grasshopper should be applied to other weather stations, privileging more rural reference conditions. With regard the compared urban area, the modeling process could involve other urban sites in São Paulo to verify which zones are critically affected by urban heat island effects. To calibrate such urban sites, climate campaigns should be extended to nightly hours. In the case of ENVI-met, this thesis recommends to address the code application to small domains in which the interactions between single urban elements, materials and vegetation at close distance had to been investigated. Other suitable applications could be addressed to large urban domains in which simplified parametric experiments are performed testing sharpen variations. Conversely, to model complex urban fabrics similarly to this work, software limitations should be overcome and the impact of boundaries conditions reduced, focusing on the centrality of other climate phenomena actually reproduced by the area. In agreement with field analysis, the sun access

implications would be more effectively simulated and wind influence reduced. With regards to the microscale analytical 2D model for an urban canyon implemented in Matlab, it would be interesting to estimate the real temperature increase within the canyon, including the daytime variability of the radiation energy content, as well as introducing density effects due to the closeness between neighboring buildings.

- URBAN DESIGN - It would be important to test the urban design precepts in the entire TOD area on which the domain is settled, by planning the orientations of buildings, the coverage areas and building heights of the future dense urban environment. The resulting plan could be used as reference for other TOD areas in the city of São Paulo and abroad, at similar latitudes.

References

AKBARI, H. et al. Local climate change and urban heat island mitigation techniques – the state of the art. **Journal of civil engineering and management**, v. 22, n. 1, p. 1–16, 2016.

ALEXANDER, C. **A Pattern Language**. New York: Oxford University Press, 1977.

ALLEGRINI, J.; DORER, V.; CARMELIET, J. Influence of Morphologies on the Microclimate in Urban Neighbourhoods. **Journal of Wind Engineering and Industrial Aerodynamics**, v. 144, p. 108–117, sep. 2015.

ANDERSON, M. P.; WOESSNER, W. W.; HUNT, R. **Applied Groundwater Modeling**. 2° ed. London,UK: Elsevier, 2015.

ANIELLO, C. et al. Mapping Micro-Urban Heat Islands using LANDSAT TM and a GIS. **Computers & Geoscience**, v. 21, n. 8, p. 965–969, 1995.

ARAGÃO, S. M. L. O estudo dos tipos-interfaces entre tipologia e morfologia urbana e contribuições para o entendimento da paisagem. **Geosul**, v. 21, n. 42, p. 29–43, 2006.

ARBEX, R. et al. Análise espacial da acessibilidade no município de São Paulo através de Self Organizing Maps. **Revista Brasileira de Cartografia**, v. 68, n. 4, 2016. Available in: <http://www.rbc.lsie.unb.br/index.php/rbc/article/view/1674>. Accessed: 7 mar. 2017.

ARNFIELD, A. J. Street Design and Urban Canyon Solar Access. **Energy and Buildings**, v. 14, p. 117–131, 1990.

ASHRAE 55-2017 (American Society of Heating, Refrigerating and Air Conditioning Engineers). **Thermal Environmental Conditions For Human Occupancy**. Atlanta: ASHRAE, 2017.

ASSIS, E. S. FROTA, A. B. Urban bioclimatic design strategies for a tropical city. **Atmospheric Environment**, v. 33, p. 4135–4142, 1999.

ASSIS, E. S. Critérios de acessibilidade ao sol e à luz natural para conservação de energia em escala de planejamento urbano. In: IX ENTAC Encontro Nacional de Tecnologia no Ambiente Construído, 2002, Foz de Iguaçu. **Proceedings...** Foz do Iguaçu, PR, 2002. p. 991–1000.

AUER, JR., A. H. Correlation of Land Use and Cover with Meteorological Anomalies. **Journal of Applied Meteorology**, v. 17, p. 636–643, 1978.

BARAU, A. S. et al. Urban Morphology Dynamics and Environmental Change in Kano, Nigeria. **Land Use Policy**, v. 42, p. 307–317, 2014.

BARBOSA, E.; FERNANDES, P. Formas espontâneas e induzidas: comparando São Paulo, Jacarta, Hanoi e Belo Horizonte. **Revista de Morfologia Urbana**, v. 3, n. 2, p. 85–102, 2015.

BATTY, M. The Size, Scale, and Shape of Cities. **Science**, v. 319, n. 5864, p. 769–771, 8 feb. 2008.

BATTY, M. Cities as complex systems: Scaling, interaction, networks, dynamics and urban morphologies. In: **Encyclopedia of complexity and systems science**. [s.l.] Springer, 2009. p. 1041–1071.

BERGHAUSER PONT, M. Y.; HAUPT, P. A. **Space, density and urban form.** Rotterdam: NAi Publishers, 2010.

BERTOLINI, L. Planning in the borderless city: a conceptualisation and an application to the case of station area redevelopment. **Town Planning Review**, v. 71, n. 4, p. 455-, oct. 2000.

BERTOLINI, L.; CURTIS, C.; RENNE, J. Station Area Projects in Europe and Beyond: Towards Transit Oriented Development? **Built Environment**, v. 38, n. 1, p. 31–50, 1 mar. 2012.

BLAZEJCZYK, K. et al. Comparison of UTCI to Selected Thermal Indices. **International Journal of Biometeorology**, v. 56, n. 3, p. 515–535, may 2012.

BONAN, G. B. **Ecological climatology: concepts and applications**. Third edition ed. New York, NY, USA: Cambridge University Press, 2016.

BORNSTEIN, R. D. Observations of the Urban Heat Island Effect in New York City. **Journal of Applied Meteorology**, v. 7, p. 575–582, 1968.

BOSSELMANN, P. et al. Urban Form and Climate: Case Study, Toronto. **Journal of the American Planning Association**, v. 61, n. 2, p. 226–239, 30 jun. 1995.

BOURDIC, L.; SALAT, S.; NOWACKI, C. Assessing Cities: A New System of Cross-Scale Spatial Indicators. **Building Research & Information**, v. 40, n. 5, p. 592–605, oct. 2012.

BRANDÃO, R. S. **Acesso ao Sol e à Luz Natural: Avaliação do impacto de novas edificações no desempenho térmico, luminoso e energético do seu entorno**. 2004. University of São Paulo, São Paulo, 2004. Available on: <http://www.fau.usp.br/aut5823/Acesso_ao_Sol/Me_Brandao_2004.pdf>. Accessed: 7 sept. 2016.

BRÖDE, P. et al. Predicting Urban Outdoor Thermal Comfort by the Universal Thermal Climate Index UTCI—a Case Study in Southern Brazil. **International Journal of Biometeorology**, v. 56, n. 3, p. 471–480, may 2012.

BROWN, R. D.; GILLESPIE, T. J. Estimating Outdoor Thermal Comfort Using a Cylindrical Radiation Thermometer and an Energy Budget Model. **International Journal of Biometeorology**, v. 30, n. 1, p. 43–52, mar. 1986.

BRUSE, M. Simulating microscale climate interactions in complex terrain with a high-resolution numerical model: a case study for the Sydney CBD area. In: International Conference on Urban Climatology & International Congress of Biometeorology, 1999,

Sydney. **Proceedings**... Sidney, 1999. Available on: <http://www.envi-met.net/documents/papers/CBDSimu1999.PDF>. Accessed: 29 aug. 2017.

BRUSE, M. **ENVI-met 3.0: Updated Model Overview**, 2004. Available on: <http://www.envi-met .com>. Accessed: 13 mar. 2017.

BRUSE, M.; FLEER, H. Simulating Surface–Plant–Air Interactions inside Urban Environments with a Three Dimensional Numerical Model. **Environmental Modelling & Software**, v. 13, n. 3–4, p. 373–384, oct. 1998.

BUENO, B. et al. The Urban Weather Generator. **Journal of Building Performance Simulation**, v. 6, n. 4, p. 269–281, jul. 2013.

CALTHORPE, P. **The Next American Metropolis: Ecology, Community, and the American Dream**. [s.l.] Princeton Architectural Press, 1993.

CHASKIN, R. J. Perspectives on neighborhood and community: a review of the literature. **The Social Service Review**, p. 521–547, 1997.

CHATZIDIMITRIOU, A.; YANNAS, S. Microclimate Design for Open Spaces: Ranking Urban Design Effects on Pedestrian Thermal Comfort in Summer. **Sustainable Cities and Society**, v. 26, p. 27–47, out. 2016.

CHENG, V. et al. Urban form, density and solar potential. In: PLEA 2006 - The 23rd Conference on passive and low energy architecture, 2006, Geneva, Switzerland. **Proceedings**... Geneva: Plea International, 2006, p.701-706. Available on: <http://infoscience.epfl.ch/record/84787>. Accessed: 15 aug. 2016.

COSTA, A. D. L. **Análise bioclimática e investigação do conforto térmico em ambientes externos: Uma experiência no bairro de Petrópolis em Natal/RN**. 2003. Universidade Federal do Rio Grande do Norte, 2003. Disponível em: <http://www.repositorio.ufrn.br:8080/jspui/handle/123456789/12411>. Acesso em: 6 aug. 2017.

COUTTS, A. M.; BERINGER, J.; TAPPER, N. J. Impact of Increasing Urban Density on Local Climate: Spatial and Temporal Variations in the Surface Energy Balance in Melbourne, Australia. **Journal of Applied Meteorology and Climatology**, v. 46, n. 4, p. 477–493, avr. 2007.

CURTIS, C.; RENNE, J. L.; BERTOLINI, L. **Transit Oriented Development. Making it happen**. Farnham (England): Ashgate Publishing Limited, 2009.

DAVIS, D.; PETERS, B. Design Ecosystems: Customising the Architectural Design Environment with Software Plug-Ins. **Architectural Design**, v. 83, n. 2, p. 124–131, mar. 2013.

DEPARTMENT OF ARCHITECTURE, BUILT ENVIRONMENT AND CONSTRUCTION ENGINEERING. **IMM, Integrated Modification Methodology**. [s.l: s.n.]

DUARTE, D.; BRANDÃO, R.; PRATA, A. Environmental Criteria Incorporation in a Brazilian Building Code. In: Passive and Low Energy Architecture, 21th, 2004, Eindhoven. **Proceedings…**Eindhoven: PLEA International, Technische Universiteit, 2004. v. 1, p. 543-548. Avalilable on:<http://www.fau.usp.br/aut5823/Acesso_ao_Sol/Duarte_Et_Al_2004_Coe_Mogi_das_Cruzes.pdf>. Accessed em: 20 may 2016.

DUARTE, D. H. S. Variáveis urbanísticas e microclimas urbanos-modelo empírico e proposta de um indicador. **Fórum Patrimônio: Ambiente Construído e Patrimônio Sustentável**, v. 3, n. 2, 2010. Available on: <http://www.forumpatrimonio.com.br/seer/index.php/forum_patrimonio/article/view/48>. Accessed: 13 jan. 2017.

DUARTE, D. H. S. et al. The Impact of Vegetation on Urban Microclimate to Counterbalance Built Density in a Subtropical Changing Climate. **Urban Climate**, v. 14, p. 224–239, dec. 2015.

EFFAT, H. A.; HASSAN, O. A. K. Change Detection of Urban Heat Islands and Some Related Parameters Using Multi-Temporal Landsat Images; a Case Study for Cairo City, Egypt. **Urban Climate**, v. 10, p. 171–188, Dec. 2014.

ELLEFSEN, R. Mapping and measuring buildings in the canopy boundary layer in ten US cities. **Energy and Buildings**, v. 16, n. 3, p. 1025–1049, 1991.

EMMANUEL, R. A hypothetical "shadow umbrella" for thermal comfort enhancement in the equatorial urban outdoors. **Architectural Science Review**, v. 36, n. 4, p. 25–36, 1993.

EMMANUEL, R. Performance Standard for Tropical Outdoors: A Critique of Current Impasse and a Proposal for Way Forward. **Urban Climate**, v. 23, p. 250–259, mar. 2018.

EMMANUEL, R.; ROSENLUND, H.; JOHANSSON, E. Urban Shading—a Design Option for the Tropics? A Study in Colombo, Sri Lanka. **International Journal of Climatology**, v. 27, n. 14, p. 1995–2004, 30 nov. 2007.

EPSTEIN, Y.; MORAN, D. S. Thermal Comfort and the Heat Stress Indices. **Industrial Health**, v. 44, n. 3, p. 388–398, 2006.

ERELL, E.; PEARLMUTTER, D.; WILLIAMSON, T. **Urban Microclimate. Designing the Spaces Between Buildings**. London: Earthscan, 2011.

FANGER, P. **Thermal comfort: analysis and applications in environmental engineering** New York City, NY: McGraw-Hill, 1972.

FERREIRA, L. S. et al. Mapping Local Climate Zones for São Paulo Metropolitan Region: a comparison between the local climate zone map and two other local maps. In: PLEA 2017 - Design to thrive - passive and low energy architecture, 2017, Edinburgh. **Proceedings**....Edinburgh: Plea International, 2017, p.1725-1732.

FULCO, A. H. G. **Análise exploratória do desempenho climático dos espaços urbanos livres, em quadras urbanas selecionadas em São Paulo.** Relatório de Iniciação Cientifica. University of São Paulo (USP), EEP, Department of Civil Engineering. São Paulo, 2018.

GHAFFARIANHOSEINI, A. et al. The Thermal Performance Exploration of Outdoor and Indoor Spaces Using IES & ENVI-met. In: Symposium on simulation for architecture and urban design, 2017, University of Toronto, Canada. **Proceedings**... Toronto, 2017.

GIRIDHARAN, R. et al. Urban Design Factors Influencing Heat Island Intensity in High-Rise High-Density Environments of Hong Kong. **Building and Environment**, v. 42, n. 10, p. 3669–3684, out. 2007.

GIRIDHARAN, R.; EMMANUEL, R. The impact of urban compactness, comfort strategies and energy consumption on tropical urban heat island intensity: A review. **Sustainable Cities and Society**, v. 40, p. 677–687, 2018.

GOLANY, G. S. Urban Design Morphology and Thermal Performance. **Atmospheric Environment**, v. 30, n. 3, p. 455–465, 1996.

GOWARD, S. N. Thermal Behavior of Urban Landscapes and the Urban Heat Island. **Physical Geography**, v. 2, n. 1, p. 19–33, 1981.

GRIMMOND, C. S. B. Progress in Measuring and Observing the Urban Atmosphere. **Theoretical and Applied Climatology**, v. 84, n. 1–3, p. 3–22, fev. 2006.

GUIMARÃES, L. E. et al. Acompanhamento das Variações das Temperaturas Superficiais dos Principais Materiais Utilizados em Fachadas. In: 2nd Encontro sobre pesquisas de materiais de construção, 2002, Goiânia. **Proceedings...**Goiânia, 2002.

GUSSON, C. D. S. **Efeito da densidade construída sobre o microclima urbano: construção de diferentes cenários possíveis e seus efeitos no microclima para a cidade de São Paulo**. 2014. University of São Paulo, Architecture Faculty, São Paulo, 2014.

GUSSON, C. S.; DUARTE, D. H. S. Effects of Built Density and Urban Morphology on Urban Microclimate - Calibration of the Model ENVI-Met V4 for the Subtropical Sao Paulo, Brazil. **Procedia Engineering**, v. 169, p. 2–10, 2016.

HALL, D.J., R. et al. Visualisation Studies of Flows in Simulated Urban Arrays, **BRE Client Report CR39/97**, Building Research Establishment, UK, 1997.

HARVEY, D. **A produção capitalista do espaço**. São Paulo: Annablume, 2005.

HARVEY, D. **O enigma do capital**. London: Boitempo Editorial, 2011.

HAUGHTON, G.; HUNTER, C. **Sustainable Cities**. London: J. Kingsley Publishers, 1994.

HEISLER, G. et al. **Investigation of the Influence of Chicago's Urban Forests on Wind and Air Temperature Within Residential Neighborhoods**. Radnor, PA: U.S. Department of Agriculture, Forest Service, Northeastern Forest Experiment Station: Gen. Tech. Rep. NE-186, 1994.

HÖPPE, P. The physiological equivalent temperature – a universal index for the biometeorological assessment of the thermal environment. **International journal of Biometeorology**, v. 43, n. 2, p. 71–75, 1999.

HSIEH, C.; WU, K. Climate-Sensitive Urban Design Measures for Improving the Wind Environment for Pedestrians in a Transit-Oriented Development Area. **Journal of Sustainable Development**, v. 5, n. 4, 27 mar. 2012. Available on: <http://www.ccsenet.org/journal/index.php/jsd/article/view/14384>. Accessed: 10 mar. 2019.

HUTTNER, S. **Further development and application of the 3D microclimate simulation ENVI-met**. 2012. Johannes Gutenberg University Mainz, Mainz, 2012.

IBGE (Brazilian Institute of Geography and Statistic). **Pesquisa de Orçamentos Familiares** (Family Budget Survey) 2002-2003. IBGE, 2003.
JACOBI, P. R.; VALENTE DE MACEDO, L. **Consciência dos cidadãos e poluição atmosférica na região metropolitana de São Paulo: RMSP**. Santiago de Chile: Naciones Unidas, CEPAL, 2001.

JENKS, M.; BURTON, E.; WILLIAMS, K. **The Compact City: a Sustainable Urban Form?.** Oxford, UK: Taylor & Francis e-Library, 2003.

JIANG, B.; CLARAMUNT, C. Integration of Space Syntax into GIS: New Perspectives for Urban Morphology. **Transactions in GIS**, v. 6, n. 3, p. 295–309, jun. 2002.

JOHANSSON, E. Influence of Urban Geometry on Outdoor Thermal Comfort in a Hot Dry Climate: A Study in Fez, Morocco. **Building and Environment**, v. 41, n. 10, p. 1326–1338, out. 2006.

JOHANSSON, E.; EMMANUEL, R. The Influence of Urban Design on Outdoor Thermal Comfort in the Hot, Humid City of Colombo, Sri Lanka. **International Journal of Biometeorology**, v. 51, n. 2, p. 119–133, 31 out. 2006.

KALLENDER, G. N. **Estudo do desempenho climático dos espaços urbanos livres, em quadras sujeitas a processos de verticalização no município de São Paulo.** Relatório de Iniciação Cientifica. University of São Paulo (USP), EEP, Department of Civil Engineering. São Paulo, 2018.

KNOWLES, R. L. The Solar Envelope. **Solar Law Reporter**, v. 2, n. 2, p. 263–297, 1980.

KNOWLES, R. L. The solar envelope: its meaning for energy and buildings. **Energy and buildings**, v. 35, n. 1, p. 15–25, 2003.

KNOWLES, R. L.; BERRY, R. D. **Solar Envelope Concepts: Moderate Density Building Applications**. Los Angeles, CA: National Tecnhical information Service, 1980.

KUMMU, M.; VARIS, O. The World by Latitudes: A Global Analysis of Human Population, Development Level and Environment across the North–South Axis over the Past Half Century. **Applied Geography**, v. 31, n. 2, p. 495–507, abr. 2011.

LAGIOS, K.; NIEMASZ, J.; REINHART, C. F. Animated Building Performance Simulation (ABPS) – Linking Rhinoceros/Grasshopper with Radiance/Daysim. **New York City**, p. 7, 2010.

LAMOUR, Q. **Avaliação da estratégia dos eixos de estruturação da transformação urbana, do município de São Paulo, frente à teoria do desenvolvimento orientado pelo transporte (DOT) estudo de caso: área de influência da estação Belém do metro**. 2018. São Paulo University USP, Department of Civil Engineering, São Paulo, 2018.

LAUNDER, B.E.; SPALDING, D. B. The numerical computation of turbulent flows, **Comp. Methods Appl. Mech. Eng.** v.3, p.269–289, 1974.

LOBACCARO, G. **Solar potential and microscale climate interactions in urban areas.** 2013. Polytechnic university of Milan. Department of Architecture, Milano, 2013.

LOWRY, W. P. The Climate of Cities. **Scientific American**, v. 217, n. 2, p. 15–23, ago. 1967.

LYLE, J. T. Can Floating Seeds Make Deep Forms? **Landscape Journal**, v. 10, n. 1, p. 37–47, 1991.

MACEDO, A. C.; IMBRONITO, M. I. Tipos de corredores e ruas locais no distrito da Mooca, São Paulo. **Revista de Morfologia Urbana**, v. 4, n. 2, p. 85–105, 2016.

MACEDO, S. S. et al. Os Sistemas de Espaços Livres na Constituição da Forma Urbana Contemporânea no Brasil: Produção e Apropriação (QUAPÁSEL II). **Paisagem e Ambiente**, n. 30, p. 137–172, 2012.

MARICATO, E. É a questão urbana, estúpido! Cidades Rebeldes. **Le Monde Diplomatique**, 2013. Available on: <https://diplomatique.org.br/e-a-questao-urbana-estupido/>. Accessed: 30 mar. 2019.

MARINS, K. R. C. et al. Estudo multicriterial da Forma Urbana em area de adensamento urbano, em São Paulo. In: EURO ELECS 2017, 2017, São Leopoldo, RS, Brazil. **Proceedings**... Encontro Nacional sobre Edificações e Cidade Sustentáveis, São Leopoldo: Casa Leiria, 2017, p. 1965-1975.

MARINS, K. R. C.; ROMÉRO, M. D. A. Urban and Energy Assessment from a Systemic Approach of Urban Morphology, Urban Mobility, and Buildings: Case Study of Agua Branca in Sao Paulo. **Journal of Urban Planning and Development**, v. 139, n. 4, p. 280–291, dec. 2013.

MARINS, K. R. de C. C. **Proposta metodológica para planejamento energético no desenvolvimento de áreas urbanas. O potencial da integração de estratégias e soluções em morfologia e mobilidade urbanas, edifícios, energia e meio ambiente: o caso da operação urbana Água Branca no município de São Paulo**. 2010. Universidade de São Paulo, 2010. Available on: <http://www.teses.usp.br/teses/disponiveis/16/16132/tde-09062010-155906/>. Accessed: 8 sep. 2015.

MARINS, K. R. de C. C.; ROMÉRO, M. de A. Integração de condicionantes de morfologia urbana no desenvolvimento de metodologia para planejamento energético urbano. **Ambiente Construído**, v. 12, n. 4, p. 117–137, dec. 2012.

MARINS, K. R. C.; GIROTTI, C.; PACIFICI, M.; CRUZ, R. B. C. Modelagem e comparação de efeitos simultâneos da forma urbana sobre a geração de energia fotovoltaica e o conforto dos espaços externos. o caso do Belenzinho, em São Paulo. In: XVII ENTAC 12- 14 nov. 2018, 2018, Foz de Iguaçu. **Proceedings...** XVII Encontro Nacional de Tecnologia do Ambiente Construído, Londrina: ANTAC, 2018, p. 321-331.

MARQUES, E.; REQUENA, C. O centro voltou a crescer?: trajetórias demográficas diversas e heterogeneidade na São Paulo dos anos 2000. **Novos Estudos - CEBRAP**, n. 95, p. 17–37, mar. 2013.

MATTOGNO, C. et al. **Ventuno parole per l'Urbanistica**. Roma: Aracne, 2014.

MATZARAKIS, A.; RUTZ, F. Application of the Rayman model in urban environments. In: Keystone (Colorado). In: Ninth Symposium on the urban environment. Session 13, Biometeorology and Public health in urban areas II, 6 oct. 2010, Keystone, Colorado. **Proceedings**... Available on: <https://ams.confex.com/ams/pdfpapers/169963.pdf>. Accessed: 14 out. 2016.

MATZARAKIS, A.; RUTZ, F.; BRAUNSCHWEIG, T. Application of Rayman for tourism and climate investigations. **Annalen der Meteorologie**, v. 2, p. 4, 2005.

MAYER, H.; HÖPPE, P. Thermal comfort of man in different urban environments. **Theoretical and applied climatology**, v. 38, n. 1, p. 43–49, 1987.

MCGREGOR, G. R. Special Issue: Universal Thermal Comfort Index (UTCI). **International Journal of Biometeorology**, v. 56, n. 3, p. 419–419, may 2012.

MEYER, R. M. P.; GROSTEIN, M. D.; BIDERMAN, C. **São Paulo metrópole**. São Paulo: Editora da Universidade de São Paulo: Impressa Oficial do Estado de São Paulo, 2004.

MILLS, G. An Urban Canopy-Layer Climate Model. **Theoretical and Applied Climatology**, v. 57, n. 3–4, p. 229–244, 1997.

MILLS, G. et al. An Introduction to the WUDAPT project. In: ICUC9 - 9TH International Conference on urban climate jointly with 12TH Symposium on the urban environment, 2015, Toulouse, France. **Proceedings**...

MIRZAEI, P. A. Recent Challenges in Modeling of Urban Heat Island. **Sustainable Cities and Society**, v. 19, p. 200–206, dec. 2015.

MONTEIRO, K. C. R.; OLIVEIRA, R. P. dos S. Reflexões sobre as consequências da verticalização para o clima urbano na cidade de Vitória da Conquista – BA- Brasil. In: Encontro De Geógrafos da América Latina, 14, 2013, Peru. **Proceedings**... Available on: <http://observatoriogeograficoamericalatina.org.mx/egal14/Procesosambientales/Climatologia/16.pdf>. Accessed: 15 aug. 2017.

MONTEIRO, L.M. **Modelos preditivos de conforto térmico: quantificação de relações entre variáveis microclimáticas e de sensação térmica para avaliação e projeto de espaços abertos.** p. 382. Thesis (PhD). Faculty of Architecture and Urbanism of the University of São Paulo, São Paulo, 2008.

MONTEIRO, L. M. **Conforto térmico em espaços urbanos abertos: verificações modelares como aportes à exploração de abordagens**. 2018. Faculty of Architecture and Urbanism of the University of São Paulo, São Paulo, 2018.

MONTGOMERY, D. C.; RUNGER, G. C. **Applied Statistics and Probability for Engineers**. Hoboken, NJ: John Wiley & Sons, 2011.

MOORE, D. S.; MCCABE, G. P.; CRAIG, B. A. **Introduction to the practice of statistics**. 6th ed. New York: W.H. Freeman, 2009.

MORAKINYO, T. E. et al. A Study on the Impact of Shadow-Cast and Tree Species on in-Canyon and Neighborhood's Thermal Comfort. **Building and Environment**, v. 115, p. 1–17, avr. 2017.

MORINI, E. et al. The Impact of Albedo Increase to Mitigate the Urban Heat Island in Terni (Italy) Using the WRF Model. **Sustainability**, v. 8, n. 10, p. 999, 7 out. 2016.

MOUDON, A. V. Urban Morphology as an Emerging Interdisciplinary Field. **Urban morphology**, v. 1, p. 3–10, 1997.

NABONI, E. et al. An Overview of Simulation Tools for Predicting the Mean Radiant Temperature in an Outdoor Space. **Energy Procedia**, v. 122, p. 1111–1116, set. 2017.

NEUMAN, M. The Compact City Fallacy. **Journal of Planning Education and Research**, v. 25, n. 1, p. 11–26, set. 2005.

NG, E. Policies and Technical Guidelines for Urban Planning of High-Density Cities – Air Ventilation Assessment (AVA) of Hong Kong. **Building and Environment**, v. 44, n. 7, p. 1478–1488, jul. 2009.

NICOL, F.; HUMPHREYS, M.; ROAF, S. **Adaptive Thermal Comfort. Principles and Practice.** Oxon: Routledge, 2012.

NUNES, N. Gestão ambiental urbana: planejar antes de verticalizar. **Instituto de Engenharia Arquitetura e Design – INSEAD – CEUNSP, SALTO - SP**, v. 2, n. 3, p. 5 8-6 2, 2011.

OIKONOMOU, M. The transformation of the urban block in the European city. In: 21st International Seminar on Urban Form "Our common future in urban morphology", 2014, vol.2, pp. 484-497. Available at: https://www.researchgate.net/publication/309782868_The_transformation_of_the_urban_block_in_the_European_City. Accessed: 26 jul 2017.

OKE, T. R. **Boundary Layer Climates**. 2nd. ed. London; New York: Routledge, 1987.

OKE, T. R. **Initial Guidance to obtain representative meteorological observations at urban sities**: Instruments and Observing Methods Report No. 81. [s.l: s.n.]. Available on: <https://pdfs.semanticscholar.org/d1d3/e2ffbed0e272073d73b0a3f6e55a3bdb372f.pdf>. Accessed: 19 jan. 2017.

OKE, T. R. et al. **Urban climates**. Cambridge: Cambridge University Press, 2017.

OLIVEIRA, V. **Urban morphology**. New York, NY: Springer Berlin Heidelberg, 2016.

Organization for Economic Co-Operation and Development (OECD). Effective Modelling of Urban Systems to Address the Challenges of Climate Change and Sustainability. **Global Science Forum**, 2011.

PACIFICI, M. et al. Morphological and Climate Balance: Proposal for a Method to Analyze Neighborhood Urban Forms by Way of Densification. **Sustainable Cities and Society**, v. 35, p. 145–156, nov. 2017.

PACIFICI, M.; MARINS, K. R. C. Scale analysis of the urban landscape hierarchy in vulnerable settlements in Sao Paulo. In: N-AERUS XVI - Who wins and who loses? Exploring and learning from transformations and actors in the cities of the South, 19-21 November, 2015, Dortmund, Germany. **Proceedings…** Dortmund, 2015, p.138-154.

PACIFICI, M.; MARINS, K. R. C. Análise da disponibilidade solar e cenários evolutivos em áreas urbanas sujeitas à verticalização e ao adensamento. In: SINGEURB 2017 - I Simpósio Nacional de Gestão e Engenharia Urbana - Cidades e Objetivos do Desenvolvimento Sustentável, 25 oct. 2017, São Carlos. **Proceedings**... São Carlos, 2017, p. 3002-3014.

PACIFICI, M.; RAMA, F.; MARINS, K. R. C. Analysis of Temperature Variability within Outdoor Urban Spaces at Multiple Scales. **Urban Climate**, v. 27, p. 90–104, mar. 2019.

PARSONS, K. C. **Human thermal environments: the effects of hot, moderate, and cold environments on human health, comfort, and performance.** London; New York: Taylor & Francis, 1993.

PINHEIRO, J. M. et al. Avaliação qualitativa de conforto térmico e estratégias projetuais para espaços abertos da cidade universitária da USP. In: XII SBCG - Variabilidade e suscetibilidade climática: implicações ecossistêmicas e sociais, 25-29 oct. 2016, Goiânia (GO)/UFG. **Proceedings**... Goiânia, 2016, p. 1198-1209.

RATTI, C.; RAYDAN, D.; STEEMERS, K. Building form and environmental performance: archetypes, analysis and an arid climate. **Energy and buildings**, v. 35, n. 1, p. 49–59, 2003.

REN, C.; WANG, R.; CAI, M. The Accuracy of LCZ maps Generated by the World Urban Database and Access Portal Tools (WUDAPT) Method: A Case Study of Hong Kong. In: the Fourth International Conference on countermeasure to urban heat islands (4th IC2UHI) 30 May to 1 June 2016, Stephen Riady Centre, University Town, NUS. **Proceedings**...

RIBEIRO, C. A. D. M.; DE CARVALHO, H. J. M.; DOS SANTOS, M. A. Metodologia para análise do sombreamento em centros urbanos. **III Simpósio Brasileiro de Ciências Geodésicas e Tecnologias da Geoinformação**, p. 1–9, 2010.

ROSSI, F. A.; KRÜGER, E.; NIKOLOPOULOU, M. A Influência da Configuração Urbana no Microclima e na Sensação Térmica em Ruas de Pedestre de Curitiba, Paraná. **Encontro Nacional sobre Conforto no Ambiente Construído**, v. 11, 2011.

RUTTEN, D. **1st ed. Grasshopper & Galapagos**. Seattle, WA: Robert McNeel & Associates, 2007.

SALAT, S.; BOURDIC, L. Power Laws for Energy Efficient and Resilient Cities. **Procedia Engineering**, v. 21, p. 1193–1198, 2011.

SALAT, S.; OLLIVIER, G. **Trasforming the Urban Space through Transit-Oriented Development The 3V Aprroach**. Washington, DC: World Bank Group, 2017.

SALATA, F. et al. Urban Microclimate and Outdoor Thermal Comfort. A Proper Procedure to Fit ENVI-Met Simulation Outputs to Experimental Data. **Sustainable Cities and Society**, v. 26, p. 318–343, out. 2016.

SALINGAROS, N. A.; WEST, B. J. A universal rule for the distribution of sizes. **Environment and Planning B: planning and Design**, v. 26, n. 6, p. 909–923, 1999.

SAMPAIO, C.A.P.; CARDOSO, C.O.; SOUZA, G.P. Temperaturas Superficiais de Telhas de Sua Relação com o Ambiente Térmico. **Eng. Agric.** v. 31, n. 2, pp.230-236. Jaboticabal, 2011.

SANTOS, M. **Metrópole Corporativa Fragmentada o Caso de São Paulo**. São Paulo: Livraria Nobel, 1990.

SASSEN, S. Bridging the ecologies of cities and of nature. In: The 4th International Conference of the International Forum on Urbanism (IFoU), 2009, Delft, Netherlands. **Proceedings**.... Available on: <http://portal.unesco.org/en/files/46764/12562292491Bridging_ecologogies_Sassen.pdf/Bridging+ecologogies+Sassen.pdf>. Accessed: 8 sep. 2015.

SÃO PAULO MUNICIPALITY. Law n°16.050, July 31th, 2014. **Aprova a Política de Desenvolvimento Urbano e o Plano Diretor Estratégico do Município de São Paulo e revoga a Lei nº 13.430/2002.**

SÃO PAULO MUNICIPALITY. Law n°16.402, March 22th, 2016. **Lei de Parcelamento, Uso e Ocupação do Solo - Disciplina o parcelamento, o uso e a ocupação do solo no Município de São Paulo, de acordo com a Lei nº 16.050, de 31 de julho de 2014 – Plano Diretor Estratégico (PDE).**

SÃO PAULO MUNICIPALITY. Law nº 16.642, May 9th, 2017. **Código de Obras e Edificações do Município de São Paulo – COE.**

SÃO PAULO MUNICIPALITY. Ordinance nº 57.776, July 7th, 2017. **Regulamenta a Lei nº16.642, de 9 de maio de 2017, que aprovou o Código de Obras e Edificações do Município de São Paulo.**

SÃO PAULO MUNICIPALITY. Anex. **Anexo I Integrante do Decreto n° 57.776, de 7 de julho de 2017.**

SECRETARY OF METROPOLITAN TRANSPORTS OF SÃO PAULO STATE (STMSP). **PITU 2025. Integrated Urban Transport Plan for the Metropolitan Region of São Paulo 2025.** Sao Paulo, SP: Secretaria dos Transportes Metropolitanos, 2006.

SHARMIN, T.; STEEMERS, K.; MATZARAKIS, A. Microclimatic Modelling in Assessing the Impact of Urban Geometry on Urban Thermal Environment. **Sustainable Cities and Society**, v. 34, p. 293–308, oct. 2017.

SHASHUA-BAR, L.; TZAMIR, Y.; HOFFMAN, M. E. Thermal Effects of Building Geometry and Spacing on the Urban Canopy Layer Microclimate in a Hot-Humid Climate in Summer. **International Journal of Climatology**, v. 24, n. 13, p. 1729–1742, 15 nov. 2004.

SHASHUA-BAR, L.; PEARLMUTTER, D.; ERELL, E. The Cooling Efficiency of Urban Landscape Strategies in a Hot Dry Climate. **Landscape and Urban Planning**, v. 92, n. 3–4, p. 179–186, sep. 2009.

SIMON, H. **Modeling urban microclimate. Development, implementation and evaluation of new and improved calculation methods for the urban microclimate model ENVI-met**. 2016. Johannes Gutenberg University Mainz, Mainz, 2016.

SOLEYMANPOUR, R.; PARSAEE, N.; BANAEI, M. Climate Comfort Comparison of Vernacular and Contemporary Houses of Iran. **Procedia - Social and Behavioral Sciences**, v. 201, p. 49–61, ago. 2015.

SONG, X. et al. Global Sensitivity Analysis in Hydrological Modeling: Review of Concepts, Methods, Theoretical Framework, and Applications. **Journal of Hydrology**, v. 523, p. 739–757, abr. 2015.

STEEMERS, K.; STEANE, M. A. **Environmental Diversity and Architecture**. 2. ed. Abingdon, England: Taylor & Francis e-Library, 2005.

STEINER, F. R. **The Living Landscape, Second Edition: An Ecological Approach to Landscape Planning**. [s.l.] Island Press, 2012.

STEWART, I. D.; OKE, T. R. Local climate zones for urban temperature studies. **Bulletin of the American Meteorological Society**, v. 93, n. 12, p. 1879–1900, 2012.

STEWART, I. D.; OKE, T. R.; KRAYENHOFF, E. S. Evaluation of the 'Local Climate Zone' Scheme Using Temperature Observations and Model Simulations. **International Journal of Climatology**, v. 34, n. 4, p. 1062–1080, mar. 2014.

SUAU, C.; BUGARIČ, B.; FIKFAK, A. Urban history, morphology and environmental urban design of maritime spaces in the old town of Koper. **Annals for Istrian and Mediterranean Studies**, v. 25, n. 1, p. 65–84, 2015.

SUNG, H.; OH, J.-T. Transit-Oriented Development in a High-Density City: Identifying Its Association with Transit Ridership in Seoul, Korea. **Cities**, v. 28, n. 1, p. 70–82, fev. 2011.

SUZUKI, H.; CERVERO, R.; IUCHI, K. **Transforming Cities with Transit. Transit and Land-use Integration for Sustainable Urban Development**. Washington D. C.: The World Bank, 2013.

TADI, M. et al. Transforming Urban Morphology and Environmental Perfornances via IMM® The Case of PortoMaravilha in Rio de Janeiro. **GSTF Journal of Engineering Technology**, v.3, n.2, 31 jul. 2015. Available on: <https://www.dropbox.com/home/journals/JET%20Vol%203%20No%202?preview=JET_Vo l.3_No.2_Paper+12.pdf>. Accessed: 16 fev. 2019.

TAN, Z.; LAU, K. K.-L.; NG, E. Urban Tree Design Approaches for Mitigating Daytime Urban Heat Island Effects in a High-Density Urban Environment. **Energy and Buildings**, v. 114, p. 265–274, fev. 2016.

TARIFA, J. R.; ARMANI, G. Atlas Ambiental do Município de São Paulo. Laboratório de Climatologia. Departamento de Geografia. Faculdade de Filosofia, Letras e Ciências Humanas-FFCLH Universidade de São Paulo, USP, 2000.

THOMPSON, C. W.; TRAVLOU, P. **Open Space: People Space**. [s.l.] Taylor & Francis, 2007.

TRAUTH, M. H. **MATLAB® recipes for earth sciences**. 4. ed. Berlin: Springer, 2015.

UN ENVIRONMENT. **The weight of cities. Resource requirements of future urbanization**. Paris: UNESCO, 2018.

UNGER, J. Intra-urban relationship between surface geometry and urban heat island: review and new approach. **Climate research**, v. 27, p. 253–264, 2004.

UN-HABITAT CORE TEAM. **Urbanization and development: emerging futures**. Nairobi: United Nations Human Settlements Programme (UN-Habitat), 2016.

VILLAÇA, F. **Espaço intra-urbano no Brasil**. 1ª ed. São Paulo: Studio Nobel, 2001.

VOS, P. E. J. et al. Improving Local Air Quality in Cities: To Tree or Not to Tree? **Environmental Pollution**, v. 183, p. 113–122, dez. 2013.

WALLOTH, C. et al. **Understanding complex urban systems**. New York, NY: Springer Berlin Heidelberg, 2016.

WANG, R. et al. Mapping the Local Climate Zones of Urban Areas by GIS-Based and WUDAPT Methods: A Case Study of Hong Kong. **Urban Climate**, v. 24, p. 567–576, jun. 2018.

WEGENER, M. Operational Urban Models State of the Art. **Journal of the American Planning Association**, v. 60, n. 1, p. 17–29, 31 mar. 1994.

WHITEHAND, J. W. R. British urban morphology: the Conzenian tradition. **Urban Morphology**, v. 5, n. 2, p. 103–109, 2001.

WONG, N. H. et al. Evaluation of the Impact of the Surrounding Urban Morphology on Building Energy Consumption. **Solar Energy**, v. 85, n. 1, p. 57–71, jan. 2011.

WORLD HEALT ORGANIZATION. **Ambient air pollution: A global assessment of exposure and burden of disease**. Geneva, Switzerland: WHO Press, 2016.

WORLD METEOROLOGICAL ORGANIZATION. **Guide to climatological practices**. Geneva: WMO, 2011.

XIE, X. et al. The Impact of Solar Radiation and Street Layout on Pollutant Dispersion in Street Canyon. **Building and Environment**, v. 40, n. 2, p. 201–212, fev. 2005.

YANG, X. et al. An Integrated Simulation Method for Building Energy Performance Assessment in Urban Environments. **Energy and Buildings**, v. 54, p. 243–251, nov. 2012.

YUAN, C.; NG, E. Building Porosity for Better Urban Ventilation in High-Density Cities – A Computational Parametric Study. **Building and Environment**, v. 50, p. 176–189, abr. 2012.

ZHU, J. Development of Sustainable Urban Forms for High-Density Low-Income Asian Countries: The Case of Vietnam. **Cities**, v. 29, n. 2, p. 77–87, abr. 2012.

Webpages

TRANSIT ORIENTED DEVELOPMENT INSTITUTE, http://www.tod.org/projects.html

GLOBAL SURFACE UHI EXPLORER, https://yceo.users.earthengine.app/view/uhimap

LESO-PB, https://www.epfl.ch/labs/leso/

AUTODESK CFD, https://www.autodesk.com/products/cfd/overview

GRASSHOPPER, https://www.grasshopper3d.com/

WEATHER STATION IAG-USP, http://www.estacao.iag.usp.br/seasons/index.php

IBGE CENSUS, 2010, www.ibge.gov.br/home/presidencia/noticias/notasaopaulo.shtm

ATMOSPHERIC SCIENCE - UNIVERSITY OF WYOMING, http://weather.uwyo.edu/upperair/sounding.html

BRAZILIAN NATIONAL INSTITUTE OF SPATIAL RESEARCHES INPE, http://sinda.crn2.inpe.br/PCD/SITE/novo/site/historico/index.php

ENERGYPLUS WEATHER FILE, https://energyplus.net/weather

GEOSAMPA, http://geosampa.prefeitura.sp.gov.br/PaginasPublicas/_SBC.aspx

ENVI-met official webpage, http://www.envi-met.info/doku.php?id=kb:lbc

ENVI-met old webpage, http://www.envi-met.net/documents/onlinehelpv3/helpindex.htm

Appendix A

MRT map -Difference mean radiant temperature maps, Case 4-6, at 16h
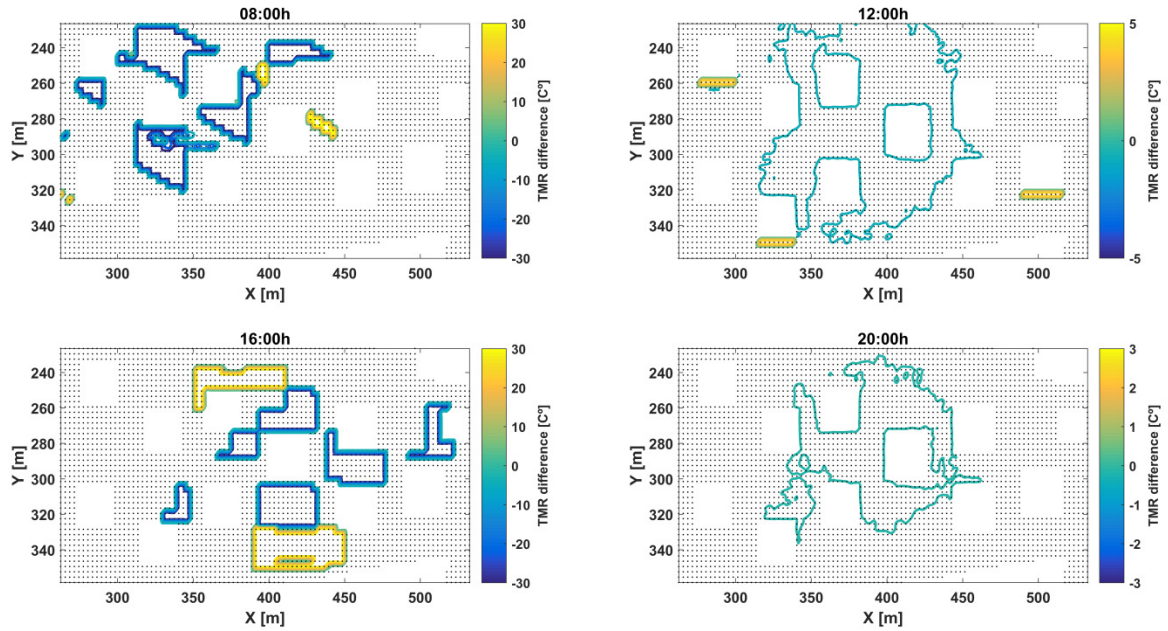
Source: Martina Pacifici, 2019

Appendix B

Grasshopper model (screenshot of the developed algorithm)

Load plugins (Honeybee, Dragonfly, Ladybug)

Urban Geometry Input for the computation of Surface Temperature and MRT values

All city parameters (urban geometry , materials, energy performance, vegetation coverage, etc.) to define Belenzinho site

Materials Input for the computation of Surface Temperature and MRT values

Climata data input (EPW + meteorological stations)

Component to run Urban Weather Generator

Computation of Surface Temperature values for Belenzinho site

Creation of outdoor microclimate maps visualizing Surface temperature in Belenzinho site

Creation of outdoor microclimate maps visualizing MRT values in Belenzinho site along with the pedestrian path

Computation of TMR values for Belenzinho site (POINT C)

Input of TMR values from field samples (Mirante Santana) for the UTCI comfort index computation

Input of EPW files for Mirante Santana and Belenzinho site (obtained from Urban Weather Generator findings)

Computation of Thermal Comfort Index (UTCI) NOT-influenced by Urban Heat Island (Mirante Santana site)

Computation of Thermal Comfort Index (UTCI) Influenced by Urban Heat Island (Belenzinho site)

For Belenzinho, MRT input values obtained by Honeybee computation)

Urban Heat Island (average and maximum values)